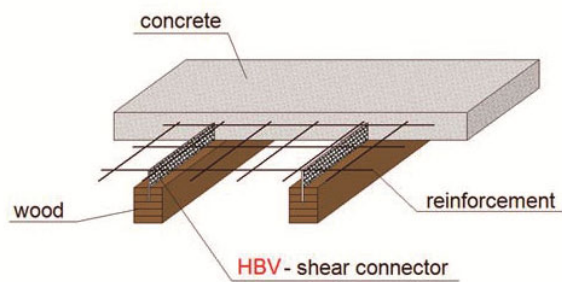


Prefabricated timber-concrete composite system



Franco Moar

Avdelningen för Konstruktionsteknik
Lunds Tekniska Högskola
Lunds Universitet, 2012



UNIVERSITÀ DEGLI STUDI DI TRENTO

Facoltà di Ingegneria
Corso di Laurea in Ingegneria Civile

Prefabricated timber-concrete composite system

Relatore
Prof. Maurizio Piazza

Laureando
Franco Moar

Correlatori
Prof. Roberto Crocetti
Dott. Tiziano Sartori

Anno Accademico 2010/2011

Report TVBK-5212

ISSN 0349-4969

ISRN LUTVD/TVBK-12/5212(209)

*If you want a happy ending,
that depends,
of course,
on where you stop your story.
(Orson Welles)*

*To my parents,
to my grandparents,
to those who stood by me,
to those who supported me
to those who helped me
during
these academic years*

Preface

Working at this master thesis has been a rich and fantastic trip for me and has taken me to many heights. The work described in this thesis was carried out at Lunds Tekniska Högskola between September 2011 and March 2012. My study permanence in Lund has been possible due to the scholarship from the European exchange student program so-called “LLP- Erasmus”. Performing my degree project here in Lund has been definitely the first and the greatest experience abroad of my lifetime. During this permanence I have got the opportunity to improve not only my English knowledge and the knowledge concerning the timber-to-concrete composite system but also the skill to live with other people. I have had the opportunity to know people of all the world, to get in contact with different cultures, habits and way of thinking. I met new friends and I have had lot of fun with them and it is so incredible how people of different countries actually are not so different at all. All of us have the same concerns, fears, but also courage, ambitions and desire to improve ourselves. I consider myself particularly lucky for this opportunity I had and I really recommend to everyone a similar experience.

Here there are some very kind people who I really would like to thank.

I would like to thank my main supervisor, *Roberto Crocetti*, professor at Lunds Tekniska Högskola, for his support over these months. He has been very kind with me, helpful, available for clarification to any questions and his advices have been invaluable to the success of this degree project. He also provided all the material for this research project and followed the experimental tests. Roberto, thank you for all this things abovementioned and also to have accepted to be my supervisor for my master thesis.

I am grateful to *Per-Olof Rosenqvist*, research engineer and laboratory technician at Lunds Tekniska Högskola, who helped me really a lot in everything concerning the preparation of the specimens, the performing of each test and for the immediate providing of everything I needed in the lab.

I would like to thank *Tiziano Sartori*, Ph.D. student at University of Trento, who constantly followed me during the development of the project, in particular in the part concerning the develop of the FE model and the test set-up.

My gratitude goes to *Maurizio Piazza*, extraordinary professor at University of Trento, who advised me this opportunity and allowed me to live this great experience in Sweden, where I never thought to come.

I would like to thank to *Anders Sjöström*, acoustics engineer at Lunds Tekniska Högskola, who helped me to perform the dynamic tests and who elaborated the data in order to get the frequencies of the composite structure.

Thanks are also expressed to *Axelsson Lennart*, designer at Moelven Töreboda AB, who gave me the six glulam beams which I used to realize the three full-scale specimens. Thank to *Albino Angeli*, rothoengineer, who gave me all the screws that I used to join the concrete slab to the glulam beams and to perform the withdrawal tests. Eventually, thanks also to *Magnus Hansson*, miscellaneous fabricated producer Bekaert Svenska AB, who gave me steel-fibres, glass-fibres and the concrete that I used to realize the concrete slab and the specimens for withdrawal tests as well.

Thanks to *Eva Frühwald Hansson*, assistant professor at Lunds Tekniska Högskola and to *Luca Costa*, research engineer, who have been my opponents during my presentation of this master thesis at Lunds Tekniska Högskola.

I would like to extend my gratitude to all my friends, especially to those who stood by me and spent lot of time with me, sharing passions, happy moments, to those who studied and have worked together with me during these accademic years.

From the depth of my heart I would like to thank all my parents, *Loris* and *Rita*, my brother *Diego* and my sister *Agata* for their support over all these years, for the continuous encouragement, the understanding, the patience, and the economical supports for each accademic year and that economically have allowed me to live this great and unique experience in Sweden.

Franco Moar

Lund, March 2012

Abstract

Timber-concrete composite structures were originally developed for upgrading existing timber floors, but during last decades, they have new applications in multi-storey buildings. Most of the research performed on these structures has focused on systems in which “*wet*” concrete is cast on top of timber beams with mounted connectors. Recently investigations on composite systems were performed at Luleå University of Technology in Sweden, in which the concrete slab is prefabricated *off-site* with the connectors already embedded and then connected on-site to the timber joists. Similar studies have been carried out also on timber-concrete composite structures with prefabricated FRC slabs at Lund University in Sweden. Two kinds of shear connectors were incorporated in the prefabricated FRC concrete slabs. These last systems can be considered globally as “*partially prefabricated structures*” because only the slabs were cast off-site with already inserted shear connectors and then the connection with the timber beams is done on the building site. An innovative composite system for floor applications is presented in this thesis. The *entire structure* is prefabricated off-side, transported and direct mounted to the building on site, that can be seen as “*full prefabricated structures*”.

Noticeable benefits of a full prefabricated structure are that the moving work from the building site to the workshop reduces construction costs, is more simple and fast of manufacture and erect, and of sure, has better quality, that means more durability.

Self-tapping full-threaded screws to connect concrete slabs to timber beam were used. Dimensions of the composite beams and the spacing between the screws has been chosen by discussing different FE model in order to reach the optimal solution.

The experimental campaign included: (i) two short-time bending tests carried out on two different full-scale specimens, (ii) dynamic tests conducted on one full-scale specimen, (iii) long-time bending test carried out on one full-scale specimen, (iv) compression tests on three cubes of concrete, (v) nine withdrawal tests of the screws with different depth in the concrete. The results of the experimental tests show that the composite beams have a very high level of resistance and stiffness and also allow to reach a high degree of efficiency.

Last, comparisons between FE results, analytical calculations and experimental values have been performed and from them it can be concluded that FE model and

theoretical calculations well interpret the behavior of the composite structure and provide reliable results.

Contents

Preface	i
Abstract	iii
1 Introduction	1
1.1 Background	1
1.2 Aims and scope	5
1.3 Outlines of the thesis	5
2 Connections for Prefabricated Timber-Concrete Composite Systems	7
2.1 Types of connector systems	7
2.1.1 Efficiency of connector systems	7
2.1.2 Shear test	11
2.1.2.1 SNP type connector	11
2.1.2.2 SM, GSP and GDF type connectors	12
2.1.2.3 SST + S and SST + S* type connectors	14
2.1.2.4 ST + S + N type connector	15
2.1.2.5 SP + N and SP + N* connector series	16
2.1.2.6 Results of Lukaszewska's shear tests	17
2.1.2.7 Discussion over Lukaszewska's connections	21
2.1.2.8 Conclusions over Lukaszewska's studies	22
2.1.2.9 Metal pipe system	22
2.1.2.10 Wooden anchor-key	26
2.1.2.11 Final values of stiffness	31
2.1.2.12 Details on materials	31
2.1.2.13 Results of shear tests on wooden anchor-key	32
2.1.2.14 Discussion over metal pipes and anchor-key connections	34
2.1.2.15 Conclusions over tube and shear anchor-key connectors	35
2.1.2.16 Summary table of connectors characteristics	37
3 Full-scale specimens with steel tubes and wooden anchor-key connections	39
3.1 Specimen details and bending tests	39

3.1.1	Residential floor type	40
3.1.2	Office floor type	45
3.2	Comparison between the two systems	49
4	Timber-to-concrete connection with inclined screws	51
4.1	Innovative connection system	51
4.2	Design of timber-concrete composite beam	53
4.2.1	Geometries and materials	53
4.2.1.1	Full-threaded screws	55
4.2.1.2	Glulam beams	56
4.2.1.3	Steel-fibre reinforced concrete (SFRC)	57
4.3	Timber-concrete composite beam assembly	58
5	Theory of composite structures with deformable connection	65
5.1	Generality	65
5.1.1	Structures and composite beams with deformable connection	66
5.1.2	Extreme case of no rigidity	68
5.1.3	Extreme case of infinite stiffness	69
5.2	Composite structures with semi-rigid connections	71
5.3	Particular solution according to the Eurocode 5	76
5.3.1	Assumptions	76
5.3.2	Approximate solution of the problem	77
5.4	Short and long term verifications	82
6	Numerical model and analytical calculations	87
6.1	Background	87
6.2	FE model for short-term analysis	88
6.2.1	Timber beam as a frame element	89
6.2.2	Concrete slab as shell elements	89
6.2.3	Shear connector as a link element	89
6.3	Load implemented in the numerical models	92
6.4	Standard model	93
6.4.1	Standard model with only dead load	95
6.4.2	Standard model without screws	95
6.5	Check of the reliability of the FE model with analytical calculation	96
6.6	Results from the FEM analysis	98
6.6.1	Models with variation of the thickness of the slab	98
6.6.2	Models with variation of the depth of the beam	100
6.6.3	Models with the variation of the spacing of the screws	101
6.6.4	Models with variation of depth of the beam and the spacing between screws.	102

6.6.5	Choice of the dimensions and of the parameters	103
7	Experimental campaign	105
7.1	Introduction	105
7.2	Dynamic test program	105
7.2.1	Experimental set-up	106
7.2.2	Results from dynamic test	107
7.2.3	Dynamic stiffness	110
7.3	Short-term bending tests program	111
7.3.1	Specimens design and construction	111
7.3.2	Bending tests	111
7.3.2.1	General procedure - Evaluation of the load P	113
7.3.2.2	Bending test set-up	124
7.3.2.3	Bending test on specimen A	127
7.3.2.4	Bending test on specimen C	134
7.4	Long-term bending tests program	141
7.4.1	Mid-span deflection after one month	141
7.5	Uniaxial compression tests program	142
7.5.1	Reason of the use of fiber reinforced concrete	142
7.5.2	Characteristics of steel-fibre reinforced concrete	143
7.6	Withdrawal tests program	147
7.6.1	Manufacturing of the specimens	147
7.6.2	Results from withdrawal tests	148
7.7	Tensile tests program	155
7.7.1	Characteristic curves force - displacement	155
7.7.2	Comparison with analytical calculations	157
7.7.2.1	Eurocode 5 approach	157
7.7.2.2	Theoretical plastic approach	158
7.7.2.3	Comparison between analytical estimation and experimental results	158
7.8	Determination of the elastic modulus of the glulam beams	159
8	Conclusions and comparison between the three approaches	163
8.1	Conclusions over the used connector system	163
8.1.1	Comparison between the mid-span deflections	164
8.1.2	Comparison between the fundamental frequencies	165
8.1.3	Comparison between the bending stiffness	166
8.1.4	Comparison between the efficiencies	167
8.1.5	Comparison between the maximum shear forces on the connector	168
8.2	Conclusions over the three different approaches	168

9	Future research	169
9.1	Experimental investigations	169
9.2	Numerical analysis	170
9.3	Industrial implementation	170
10	Example of application	173
10.1	Background	173
10.2	Materials	174
10.2.1	Steel-fibre reinforced concrete	174
10.2.2	Glulam beams	175
10.3	Load combinations	177
10.3.1	Structural permanent load	178
10.3.2	Non structural permanent load	178
10.3.3	Live load	178
10.3.4	Load combinations and external actions	178
10.4	Geometry and data	179
10.4.1	Cross-section	179
10.4.2	Connection system and its properties	179
10.5	Stiffness properties of the composite system	182
10.6	Verifications	184
10.6.1	Strength verifications	184
10.6.2	Verifications of serviceability limit states	188
10.6.2.1	Mid-span deflection check at $t = 0$	188
10.6.2.2	Mid-span deflection check at $t = \infty$	188
10.6.2.3	Vibration check at $t = 0$	188
10.6.2.4	Vibration check at $t = \infty$	190

Chapter 1

Introduction

This chapter presents a general introduction to timber-concrete composite systems and their applications, the advantages and drawbacks of the “cast-in-situ” systems. It also present the advantages of only prefabricated concrete slabs connected to the timber beams and the possibility to develop full-prefabricated composite systems. Aims and outlines of the thesis have also been described.

1.1 Background

Timber-concrete composite systems are being increasingly used for upgrading of existing timber floors in residential or office buildings as well as for new buildings and bridges. These kinds of structures consist of timber joists or beams effectively interconnected to a concrete slab cast on top of the timber members. Timber-concrete composite structures have been investigated for nearly 80 years. Floors of composite timber and concrete have been used successfully in highway bridges, hangar aprons, wharves, piers, buildings and platforms since early 1940’s (Richart and Williams). One of the first projects carried out on timber-concrete composite structures was described by McCullough (1943) who performed experimental tests (known as the Oregon tests) on timber-concrete composite beams, prompted by a desire of the Oregon State Highway Department (USA) to develop a cost-effective short-span highway bridge. In many European countries timber-concrete composite constructions are being increasingly used in upgrading and post-strengthening of existing timber floors in residential or office buildings as well as new constructions for buildings and bridges (Ceccotti 1995). In the 80’s and 90’s special attention was paid to timber multi-storey buildings. For example, Natterer et al. (1996) proposed a composite system with a timber layer made of vertical nailed planks for the floors of new residential multi-storey building. Most research on wood-concrete composite structures has been performed on various types of shear connectors, used together with standard concrete and timber/glued laminated glulam beams or wooden decks. However, a few

researchers have also explored the possibilities of using different type of concrete or other wood-based engineering materials. Most of the research performed to date and currently in progress on wood-concrete composite systems is focused on systems in which “wet” concrete is cast on top of timber beams with mounted shear connector systems (traditional or “wet” timber concrete composite systems). An example of a “wet” timber-concrete composite system with mounted shear connectors is reported in Figure 1.1.

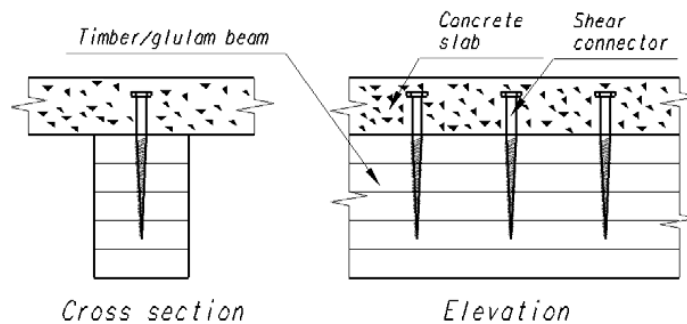


Figure 1.1: Example of “wet” timber-concrete composite system.

In timber-concrete composite structures, the concrete slab mainly resists compression, while the timber joist resists tension and bending, and the connection system transmits the shear forces between the two components. Advantages compared to wooden floors which are listed below, include:

- increased load-carrying capacity;
- higher stiffness (which leads to reductions in deflections and susceptibility to vibrations);
- improved acoustic and thermal properties;
- higher fire resistance.

There are also some advantages relative to normal reinforced concrete floors. Notably cracks in the tensile region of reinforced concrete slabs may promote penetration of moisture and corrosion of the steel rebars. Further, the lower part of a concrete slab, approximately 40-60% of the depth, is generally ineffective since it is cracked and thus non-resistant. By replacing that part with a resistant solid wooden deck, the overall depth of the concrete slab can be reduced by about 50% and, thus, the self-weight of the structure can be markedly decreased (Gutkowski 2000).

In the structure, wood resisting tensile forces, concrete slab resisting compressive forces and connectors carrying shear forces constructs. Timber-concrete system is

more competitive than either wood or concrete alone. The first principle to achieve strong, rigid and lightweight systems is to focus on the shear connector performance. The connection system is a crucial part of any timber-concrete composite system, which provide composite action in the cross-section. A range of mechanical connectors is available on the market with an extensive variety of stiffness and strength properties, which are fundamental design parameters for the composite structure. The connection needs to be stiff and strong to maximize the composite action, but its number of components and installation time should be minimal, to make the system cost effective. Evaluating the connection's stiffness is important because the behavior, both static and dynamic, of the composite concrete-wood structure is strongly influenced by the slip between the beam and the slab. Thus, the design of timber-concrete composite structures generally requires consideration of the slip occurring in the joint between the timber and concrete.

Nevertheless, despite the many advantages of timber-concrete composite structures abovementioned, the use of wet concrete has also disadvantages, notably:

- the introduction of a “wet” component in the typically “dry” construction processes applied in timber buildings;
- the time needed for the concrete to set, which adds to the time required on-site before the next scheduled action can be taken;
- low stiffness and high creep while the concrete cures, which is particularly unfavourable for unpropped composite beams, hence propping of beams at mid-span is crucial to minimize permanent deflection and enable the development of sufficient initial composite stiffness to sustain the full self-weight of the concrete slab;
- the high cost of cast-in-situ concrete slabs, mainly due to the cost of transporting fresh concrete and the use of props, formwork such as planks, particleboard or plywood sheets as composite components, which further increases the self-weight of the structure, and use of separating layer-foil between the concrete and the timber to prevent the contact between wet concrete and wood;
- potential problems of quality control.

Moreover, excessive shrinkage of concrete causes additional deflection, hence low shrinkage concrete is desirable in timber-concrete composite structures to minimize any permanent deflection.

As previously said, satisfactory strength and stiffness properties are among the most important prerequisites for timber-concrete composite structure. However, only these properties are in general not enough to guarantee the success of the structure. In fact,

besides strength and stiffness, also other aspects must be considered in the design of timber-concrete composite structures such as:

- ductility
- simplicity
- rapidity of manufacture and erection;
- higher quality;
- better working environment;
- dry bridge deck surface;
- good durability.

A notably benefit of prefabricating the concrete slab is also that most of the concrete shrinkage will occur before the slab is connected to the timber beam, markedly reducing the correlated increases in deflection and flexural stresses in the composite beam. Another advantage of the prefabrication is that moving work from the building site to the workshop reduces constructions costs.

During the last decades, several research studies have been conducted, with focus on design methods of new timber-concrete composite floor and bridges. These research works have provided a base of engineering data needed for practical applications. The competitive merit of such composite structures is borne out by several examples of successful projects decks both in Europe but also overseas.

The major part of these studies is based on the use of cast-in-situ concrete slab. Very few researches have investigated the possibility to using prefabricated concrete slabs connected to timber beams. Experience has shown that steel-concrete composite structures with prefabricated decks offer several advantages, abovementioned. Recently, some investigations have been performed at the technical University of Luleå, Sweden, focusing on the development of connector technologies for timber-concrete composite structures that are suitable only to prefabricated slabs, see [1]. Besides, another recently research, see [1], shows that the improvement perspectives of such a technique are enormous, but new possible solutions need to be tested. According to [1] and [4], the use of a prefabricated concrete slab implies several advantages such as a better material control, time saving and also, consequently money saving. To improve further the industrial process, to make prefabrication more quickly and even more cheaper, the full-prefabricated structures should be considered. This means that concrete slabs and timber beam are completely performed off-side and only mounted on-site.

1.2 Aims and scope

The purpose of this research project is to explore the mechanical performance (static short- and long-term, and dynamic) of screws as shear connectors for mounting in a prefabricated timber-concrete structure, the performance of shear connections on full-scale specimens and in such a way that the concrete slab and glulam beams can be connected off-site in a full-prefabricated point of view. Thus, such a prefabricated timber-concrete composite system can significantly reduce all the aforementioned drawbacks of the “wet” systems. It is important to remember that concrete exhibits creep and drying shrinkage. In case of only prefabricated slab these effects on the timber beams can be reduced by increasing the curing time before the assembly of the prefabricated concrete slab with the glulam beam. In such a way long-term deflection can also be reduced in comparison to traditional composite floors. To reduce the shrinkage phenomenon and reduce crack widths and control the crack widths tightly in full composite structure, it is used a fibre reinforced concrete (FRC). Particular focus was placed on the connection system, the slab and beam dimension choices, the stiffness and the mid-span deflection of two identical full-scale specimens in order to achieve the design requirements. Special attention has been paid to the development and use of connection system that is easy to produce and mount in order to speed up the construction process. Finally, the particular timber-concrete composite tested beams are reflected for a practical application such as a stand for a Swedish stadium.

1.3 Outlines of the thesis

This master thesis can be ideally divide into: *Part I* summarizes the research projects and the state of the art concerning the connections for prefabricated timber-concrete composite systems developed. It reports some examples of these kinds of connections that are studied and tested at Luleå University of Technology, see [1] and [2]. There are also represented two types of shear connectors recently studied and tested at SP Technical Research of Sweden [4]. Furthermore, *Part I* also presents the innovative connection system adopted for this research and tests realized by mean of self-tapping full-threaded screws. *Part II* reports the classical theory of composite beams with deformable connection, which is bounded by two extreme stiffness limits. In *Part II* is also described the numerical model realised for the slab and beam dimensions choices and the choice of connectors spacing. *Part III*, on the other hand, presents the experimental tests, in particular the test set up, the bending tests and the dynamic tests on both systems carried out at Lunds Tekniska Högskola. Besides, *Part III* reports also the conclusion of this research and the comparison between analytical, numerical and experimental results. Finally, there is an *Appendix* that presents a real application of these timber-concrete composite prefabricated beams. This type

of structure is adopted to renew the stands for a Swedish stadium, named Strömvalle
at Gävle in Sweden.

Chapter 2

Connections for Prefabricated Timber-Concrete Composite Systems

This chapter presents the state of the art of connectors systems for timber-concrete composite systems and some “dry-dry” connectors, already embedded into a prefabricated concrete slab, which have been recently investigated.

2.1 Types of connector systems

2.1.1 Efficiency of connector systems

Timber-concrete composite system and slabs require interlayer connectors, which provide composite action in the cross-section. A range of mechanical connectors is available on the market with an extensive variety of stiffness and strength properties, which are fundamental design parameters for the composite structure. Another crucial parameter is the cost of the connector, including the labour cost, that if too high may prevent the use of the composite system. In order to reduce the construction cost and to make timber-concrete structures more widespread on the market, it is believed that a high degree of prefabrication should be achieved. For a simple and cost effective construction process, the use of “dry” connections, which do not require the pouring and curing of concrete on site, may represent a possible solution. Here it is presented a number of different mechanical “dry-dry” connectors previously embedded into a prefabricated concrete slab. On some tests that have been performed, it was found that some of the developed connection systems for prefabricated concrete slab can perform as satisfactorily as those for cast-in-situ slabs, with the additional benefit of being relatively inexpensive.

The choice of an effective shear connection is the key to achieve strong and stiff composite systems. The efficiency of the shear connection can be measured as sug-

gested by Gutkowski, see [6]:

$$E = \frac{D_N - D_I}{D_N - D_C}$$

where

- E is the efficiency of the composite system;
- D_N is the theoretical fully composite deflection (calculated by transformed section);
- D_I is the actual deflection of the timber-concrete composite beam;
- D_C is the theoretical fully non-composite deflection (calculated as a layered beam without interlayer shear transfer).

The efficiency can vary between 0% in case of system considered without connection and 100% in the case of fully rigid connection with no interlayer slip between concrete and timber and fully composite action.

It may also be convenient to define the efficiency of a shear connection for a composite beam, using the following equation, originally proposed by Piazza in 1983 and later by Piazza and Ballerini in 2000, see [7]:

$$\eta = \frac{EJ_{real} - EJ_0}{EJ_\infty - EJ_0}$$

where

- η is the efficiency of the interlayer connection;
- EJ_∞ is the bending stiffness of the beam with a theoretical full composite action;
- EJ_0 is the bending stiffness of the beam with no composite action;
- EJ_{real} is the actual bending stiffness of the beam.

When the shear connection is very stiff EJ_{real} tends to EJ_∞ and thus η tends to 1. On the other hand, for a very flexible shear connection EJ_{real} would tend to EJ_0 and thus η tends to 0.

In order to limit the deflections in composite structures relatively rigid shear connectors should be used. However, rigidity is not the only desirable characteristic of timber-concrete shear connectors. Notably, to prevent undesirable brittle failure in the composite structure, shear connectors should also be sufficiently ductile, see [8]. Many different connectors have been proposed thus far, notably:

- steel meshes epoxy-glued into the timber;
- notched details cut into the timber part;
- steel fasteners such as nails, screws.

The last one kind of connectors are ductile and commonly used in many applications, however they are generally more flexible, and a large number of fasteners is required to achieve high efficiency. The prefabrication of concrete slab with already inserted shear connectors, and the connection with the timber beams on the building site can significantly reduce all the drawbacks of the wet systems. In this case, most of the shrinkage will develop when the prefabricated concrete slab is not yet connected to the timber beam, markedly reducing its effect in terms of increase in deflection and flexural stresses. Prefabrication also permits an improvement in the construction process achieving high quality, while saving resources and simplifying recycling of waste.

Prefabricated modular wood-concrete composite elements with a glued-in metal plate as shear connector developed in Germany resulted in a cost-effective system which can compete with contemporary reinforced concrete and steel-concrete composite systems, see [5]. The modular element can be utilized in floors, walls and roofs in both residential and commercial buildings. An example is shown in Figure 2.1.

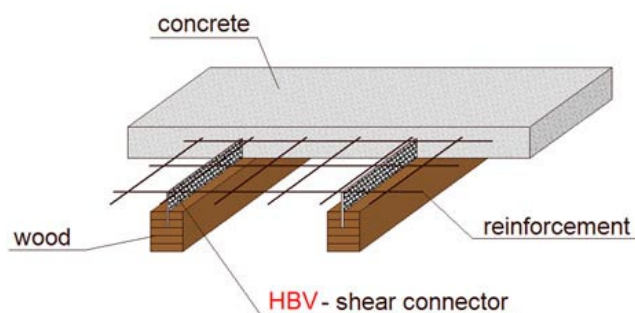


Figure 2.1: Example of a prefabricated wood-concrete composite floor panels, see [5].

The development of other mechanically effective connectors potentially leading to high efficiency is meaningless if the system is too difficult to build and/or too time consuming. This is why special attention has been paid to propose connection systems easy to produce and mount so as to speed up the construction process. The prefabrication of the concrete slab with already embedded shear connectors is believed to be a possible way to reduce the cost by moving most of the work from the building site to the factory. Here there have reported a range of connectors with either strong and stiff mechanical properties but low ductility, and with less strength and stiffness but high ductility, which were investigated by Lukaszewska, see [1] and [2]. The description of the connectors is reported in Table 2.1.

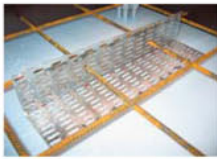



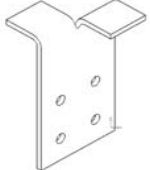
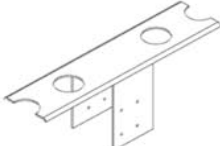
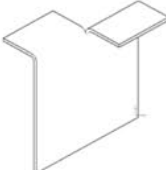
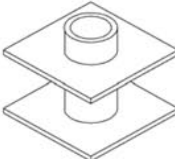
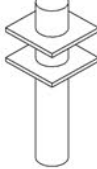
Type	Drawing	Description of the connection system
SNP		A 55 × 55 × 250 mm toothed metal plate, folded at an angle of 90°, moulded into the slab
SM		A continuous steel mesh embedded 50 mm into the slab and epoxy-glued into a 50 mm deep slot routed in the glulam beam
SST+S		A Ø 20 × 47 mm long steel tube inserted into the concrete slab with one Ø 20 × 120 mm hexagon head coach screw
SST+S*		A Ø 20 × 47 mm long steel tube inserted into the concrete slab with one Ø 20 × 160 mm hexagon head coach screw
SP+N		Two folded steel plates embedded into the slab to a depth of 50 mm and nailed to both sides of the glulam beam with eight Ø 4.5 × 75 mm annular ringed shank nails
SP+N*		U-shaped steel plates welded to a long punched metal plate embedded into the slab to a depth of 30 mm and nailed to both sides of the glulam beam with eight Ø 4.5 × 75 mm annular ringed shank nails
GSP		A 115 mm wide two-folded steel plate, embedded into the slab at a depth of 50 mm and epoxy-glued into a 70 mm deep slot milled in the glulam beam
ST+S+N		A Ø 20 × 67 mm long steel tube inserted into the concrete slab with one Ø 20 × 160 mm hexagon head coach screw and one notch cut from the glulam beam
GDF		A Ø 20 × 120 mm dowel with flanges embedded into the concrete slab to a depth of 50 mm and epoxy-glued into a 70 mm deep hole drilled in the glulam beam

Table 2.1: Descriptions of the shear connectors, which has been studied from Lukaszewska at the technical University of Luleå, Sweden.

2.1.2 Shear test

In order to investigate the performance for each type of connector shear tests were carried out. The mechanical parameters checked for the following shear connector types are: stiffness, strength and ductility. In addition to the investigation of mechanical properties, the feasibility of the proposed prefabrication process was evaluated during the manufacture of the shear test specimens.

Direct shear tests were performed on asymmetrical specimens to determine the connectors' load-slip relationships using the experimental set-up illustrated in Figure 2.2.

This type of test was chosen because asymmetrical specimens are lighter, cheaper and quicker to construct than symmetric (push-out) specimens, in which the timber beam is connected to two concrete slabs, one on the left- and the other on the right-hand side. A drawback of the asymmetrical shear test set-up is that it gives slightly higher estimation of the shear strength and slip modulus than symmetric shear tests (Van der Linden 1999). This follows the overturning moment due to the eccentricity of the axial force results in a compression force at the interface between the concrete and timber, which increase the friction and (thus) improves the apparent mechanical properties of the connection, see [1].

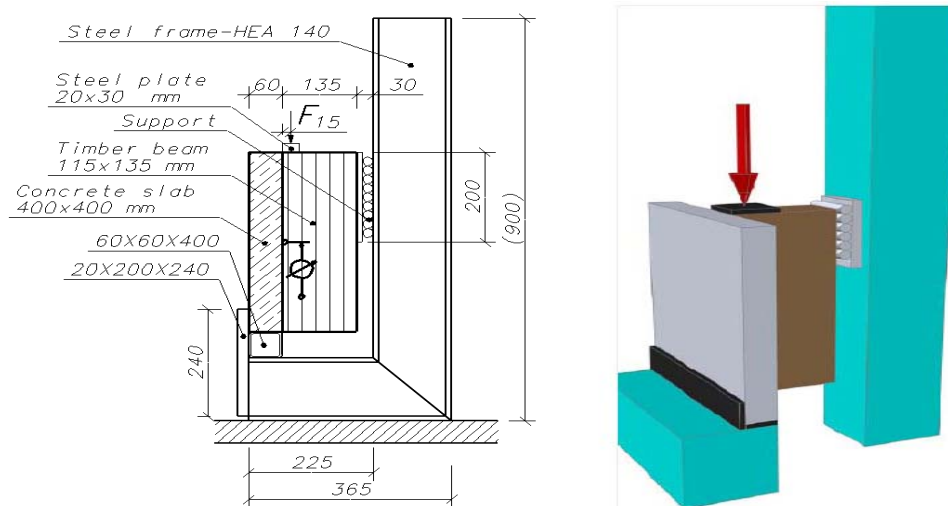


Figure 2.2: Shear test set-up.

2.1.2.1 SNP type connector

The SNP type connector is a common toothed metal plate previously investigated by Van der Linden that is characterized to have a ductile behavior. The length of the toothed plate was 250 mm and it was manufactured from common toothed plate with

8 mm long nails. A flat toothed plate was bent at an angle of 90° and the teeth were removed from the part inserted in the concrete slab to eliminate the occurrence of air pockets around the nails. The pre-cast concrete slab with the toothed plate was pressed into the glulam beam using a hydraulic jack. The pressing process created compressive stress perpendicular to grain and several cracks appeared at the mid-section of the glulam beam.



Figure 2.3: Toothed metal plate connector (Type SNP), in the moulding form on the left and the prefabricated slab with inserted the metal plate on the right.

Two drawbacks can be recognized using this connector in full-scale structures: (i) the complexity of moulding forms and concrete placement during the prefabrication process, which must be done this way to ensure that no leaking will occur on the teeth used for the connection with the timber beam, and (ii) the necessity of using specific equipment to press the glulam beam in the pre-cast concrete slab.

2.1.2.2 SM, GSP and GDF type connectors

Glued connections have been tested in previous studies by Clouston, [9] and Bathon et al. 2006, see [10], to provide almost full composite action. The following types of glued connectors were investigated by Lukaszewska and here presented: a continuous steel mesh (SM), Figure 2.4, a folded steel plate (GSP), Figure 2.5, and a $\phi 20 \times 120$ mm dowel with two welded flanges (GDF), Figure 2.6. In Lukaszewska's investigations, a two component epoxy-resin StoBPE 465/464 available on the Swedish market was used to bond the steel parts to the glulam members in all the SM, GSP and GDF series. The connection was realized by leaving a 2 mm gap around the fastener and filling the slots and holes up to $2/3$ of the depth with the epoxy. A plastic foil was placed between the concrete slab and the glulam beam to conservatively remove any bond at the interface which could increase the slip moduli for lower levels of load.



Figure 2.4: Epoxy-glued connections in the moulding forms continuous steel mesh (SM) on the left. Prefabricated concrete slab with inserted shear connector on the right, see [1].

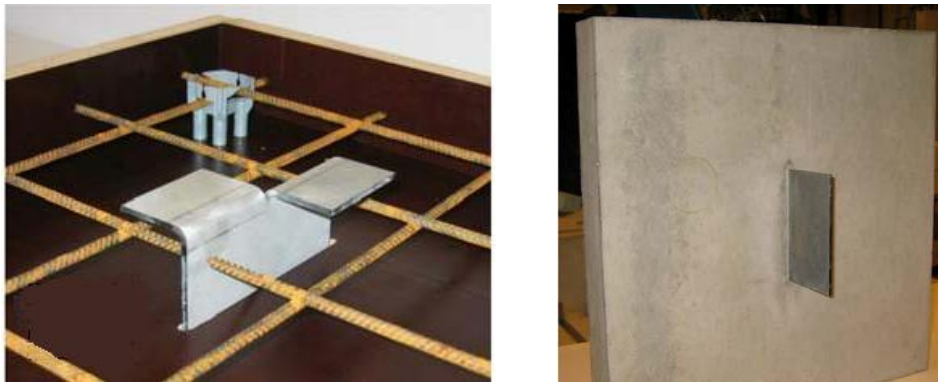


Figure 2.5: Epoxy-glued folded steel plate (GSP) the moulding forms on the left. Prefabricated slab with inserted shear connector on the right, see [1].



Figure 2.6: Epoxy-glued steel dowel with flanges (GDF), the moulding form on the left. Prefabricated slab with inserted shear connector on the right, see [1].

The SM connector was characterized by both high stiffness and strength. The shear failure was observed in the steel connector and load carrying capacity decreased once the maximum strength was reached. High degree of composite action can be achieved using this type of connection. The cost of the epoxy resin and the time needed for the glue to cure, especially for commercial buildings involving large composite sections and long beams, represent drawbacks of the system. Another shortcoming is the concrete leaking during the concrete placement in the moulding forms through the holes of the mesh used as a connector. Such a concrete leaking on the lower part of the mesh to be glued in the timber beam should be avoided and this is difficult to avoid during the construction process.

The GSP and GDF type connectors have a similar problem of the previous one as regards concrete leaking. Another drawback is the accuracy required during the prefabrication of the slab. The connectors need to be placed exactly in the right position in the moulding forms to eliminate problems during the assembling process with the timber beams on the building site. The cost of the glue and the additional time needed for the curing make these systems less attractive if compared to the other mechanical shear connectors.

2.1.2.3 SST + S and SST + S* type connectors

The SST + S connector consisted of a 47 mm long steel tube characterized by an inner diameter of 20 mm, with a welded flange embedded in the concrete slab, Figure 2.7. The connection between the concrete slab and the glulam beam was obtained with a $\phi 20 \times 120$ mm hexagon head coach screw for the SST + S series. A plastic cap was screwed on top of the steel tube to create space for the screw head during the placement of the concrete and was removed after the concrete had cured. The screw was pre-tensioned with a 130 Nm torque moment using a torque wrench.



Figure 2.7: SST+S steel tube shear connectors, the moulding form with the screw's plastic cup on the left and assembled to the glulam beam on the right [1].

For the SST+S* series the concrete slab was connected to the glulam beam using the

same kind of steel tube but with a $\phi 20 \times 160$ mm hexagon head coach screw instead of a $\phi 20 \times 120$ mm screw.

The SST + S connector was the most ductile system with, however, the lowest stiffness and strength. An increase in stiffness and strength can be obtained by using longer screws and optimizing the distance between the connectors. The prefabrication of pre-cast concrete slabs with embedded steel tubes does not require particular moulding forms. The steel tubes can be connected to the reinforcing steel mesh by spot welding and they can be placed into the moulding form. The spot welding process requires some time, however it was found to be cheaper and simpler than working with the epoxy-glue. The pre-cast concrete slab can be easily assembled to the glulam beams using pre-tensioned screws where only the pre-drilling operation is required.

2.1.2.4 ST + S + N type connector

A modified steel tube characterized by a length of 67 mm, with two welded flanges, and a hexagon head coach screw $\phi 20 \times 160$ mm was used in the ST + S + N series in conjunction with a notch cut from the timber beam, Figure 2.8. A prefabricated concrete slab with a 115×120 mm rectangular hole was placed on top of the glulam member. The hole was filled with concrete mix. The screw was pre-tensioned with 130 Nm torque moment using a torque wrench. The notch in the glulam had an inclination of 15° , a length of 100 mm, and a depth of 25 mm, Figure 2.8.

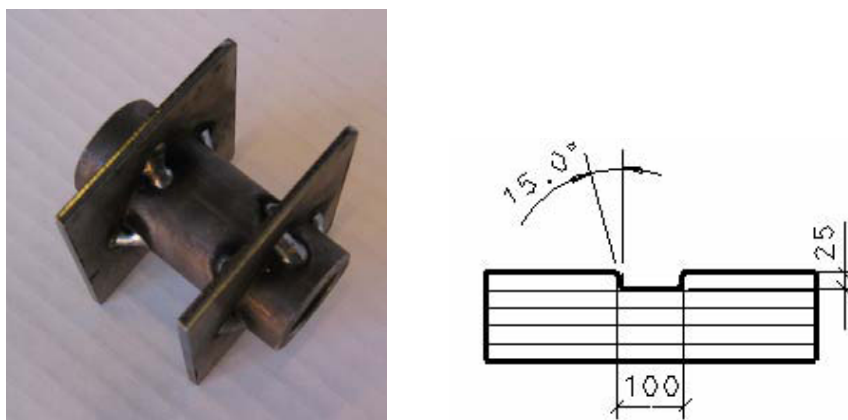


Figure 2.8: Steel tube detail of ST+S+N shear type connector on the left and notch in the glulam beam (dimension in mm) for ST+S+N connector on the right [1].

This type of connector, characterized by the highest strength among all the systems tested, high stiffness and large ductility, offers wide potentials of use in commercial applications. In order to use this type of connection in the pre-cast option, however, individual and expensive moulding forms with recesses would be needed to manufacture concrete slabs with protrusions. An alternative solution could be the prefabrication of concrete slabs with rectangular holes at the connector location, to

be filled with concrete mixture after placing the steel tubes on site as it was done for the shear specimens. Another drawback of the system is that the mix design of concrete needs to be carefully investigated to minimize the shrinkage in the notch and to achieve a tight fit between concrete and timber.

2.1.2.5 SP + N and SP + N* connector series

This type of connector consisted of a pair of folded steel plates embedded into the concrete slab and connected to the glulam beam by means of $8\phi 4,5 \times 75$ mm annular ringed shank nails (SP + N series), Figure 2.9. The two plates were placed in the moulding form so that there was a 10 mm overlap, thus the flanges folded in the steel plate acted as an anchor in the concrete slab. The plate was 160 mm long, 75 mm wide and 3 mm thick.

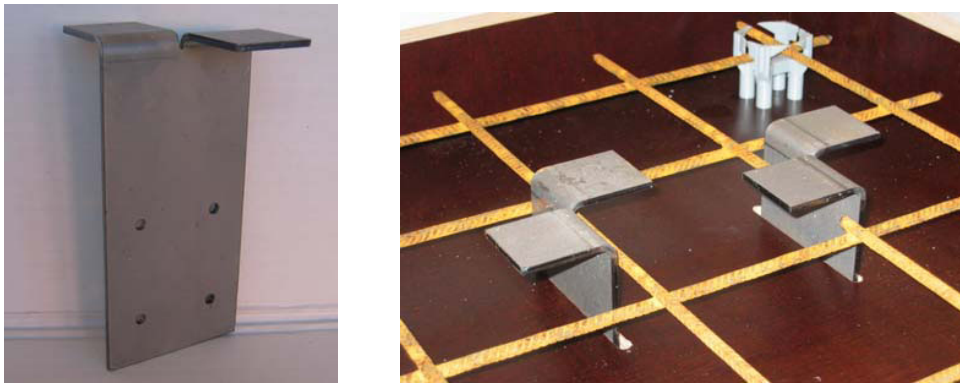


Figure 2.9: SP+N steel plate shear connector in the moulding form [1].

The connector type designated SP+N*, as showed in Figure 2.10, consisted of a U-shaped steel plate welded to a 400 mm long punched steel profile embedded into the concrete slab and nailed with eight $\phi 4,5 \times 75$ mm annular ringed shank nails to both sides of the glulam beam. The U-shaped steel plates were welded to a long steel profile running along the length of the beam to overcome the difficulty of positioning each U-shaped steel plate correctly in the moulding form individually. The U-shaped steel plates and the punched steel profile were 3 mm thick.

The SP + N is simple, economical and relatively stiff. The GSP type connector which was similar in detail achieved comparable initial stiffness but only two-thirds of the strength observed in the SP + N connector type. In addition, the complexity of the prefabrication and assembling process would make the GSP system more expensive than the SP + N. No complex moulding forms are needed to prefabricate concrete slabs with SP + N type connectors. A shortcoming in full scale beams may be the difficulty of placing every single steel plate into the right position in the moulding form.



Figure 2.10: SP+N* shear connector type in moulding form, see [1].

This problem can be overcome by welding all the connector plates to a long punched metal plates running along the length of the beam and encased in the concrete slab. Even though the use of the punched metal plate represents an additional cost, it offers significant advantages with respect to the solution without plate in terms of improved accuracy, reduces time of construction, and increases in longitudinal stiffeners of the concrete slab which is highly desirable during transportation of the panel.

2.1.2.6 Results of Lukaszewska's shear tests

The results of Lukaszewska's shear tests are reported for single shear connectors. The shear force-relative slip curves is reported over the whole range of slips in Figure 2.11 and in Figure 2.12 for low values of slips, correspond to the mechanical behavior of each type of shear connector averaged over 4 samples.

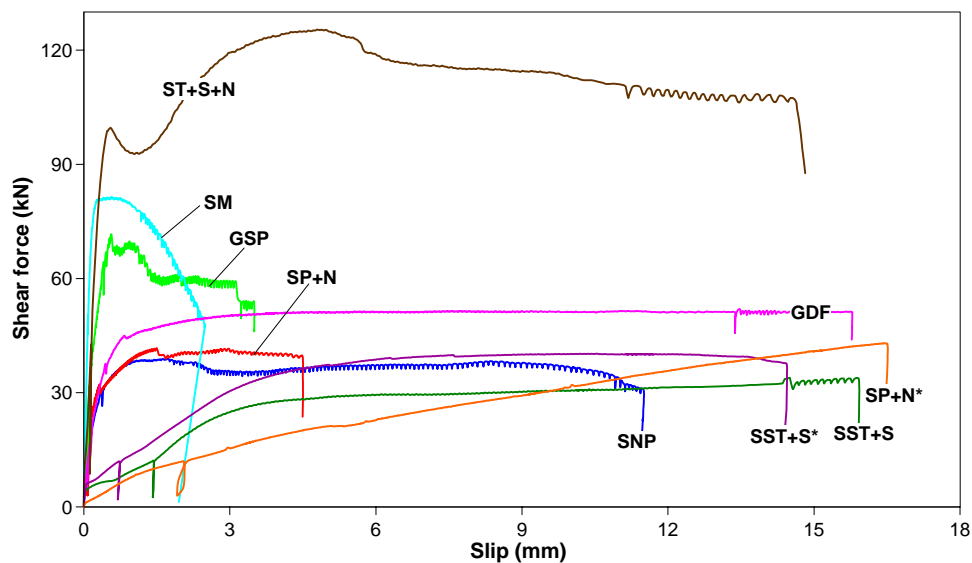


Figure 2.11: Lukaszewska's shear tests results for all previously types of connection: average shear force-relative slip curves and approximating curves, see [1].

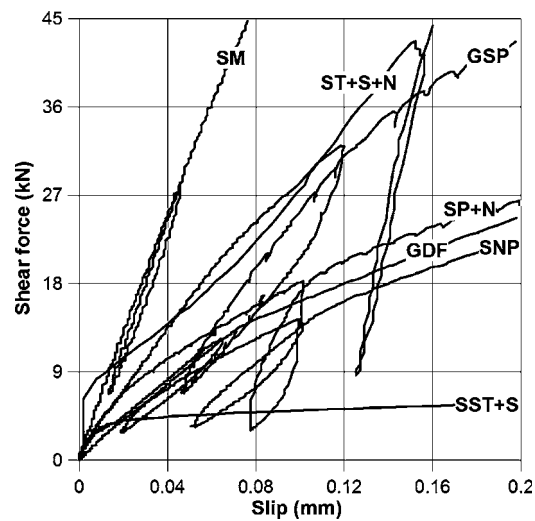


Figure 2.12: Lukaszewska’s shear test results for all types of connection: average shear force-relative slip curves for low values of slip, see [1].

The mean secant slip moduli $k_{0,4}$ at 40% of the estimated ultimate load $k_{0,6}$ at 60% and $k_{0,8}$ at 80% of the maximum ultimate load, respectively, are reported in Table 2.2 for all the test series.

Type of connection	Values	Slip moduli				Shear strength	
		$k_{0,4}$ (kN/mm)	$k_{0,6}$ (kN/mm)	$k_{0,8}$ (kN/mm)	Stiffness rank	F_{max} (kN)	Strength rank
SNP	Range	95.3–135.2	72.8–118.5	52.4–86.9	6	35.4–38.9	6
	Average	121.4	99.0	67.6		37.3	
	σ	18.0	19.3	15.8		1.6	
SM	Range	377.0–595.8	345.2–543.5	300.6–487.1	1	74.3–88.1	2
	Average	483.8	449.4	396.0		81.2	
	σ	90.8	82.7	80.0		5.7	
SST + S	Range	4.7–6.8	6.0–8.1	6.0–7.1	7	33.2–34.6	7
	Average	5.9	6.8	6.4		33.9	
	σ	0.9	1.0	0.5		0.6	
SP + N	Range	80.8–412.0	80.4–138.8	60.8–74.8	2	36.8–47.0	5
	Average	258.8	113.1	68.3		42.3	
	σ	166.6	26.2	5.8		4.3	
GSP	Range	118.2–325.9	101.4–269.0	79.7–167.9	3	43.3–73.4	3
	Average	248.5	183.4	130.9		64.4	
	σ	90.4	72.8	41.3		14.2	
ST + S + N	Range	221.3–245.6	231.6–248.2	139.6–217.9	4	99.6–126.7	1
	Average	235.7	234.4	178.0		110.6	
	σ	12.8	8.7	39.2		14.2	
GDF	Range	120.0–174.6	94.6–98.9	59.1–71.9	5	51.0–54.8	4
	Average	135.1	96.8	64.4		52.5	
	σ	26.5	2.3	5.6		1.6	

Table 2.2: Shear test results: slip moduli and shear strength.

The purpose of Lukaszewska’s research was in fact a comparative evaluation of the

performance of various connectors in order to identify the most suitable connection system for application in prefabricated composite systems.

The mean values, range of variation and standard deviations σ of shear strength and slip moduli are reported in Table 2.2 for the different connection systems tested. The connectors are also ranked in terms of slip modulus $k_{0.4}$ and strength from the highest (No. 1) to the lowest value (No. 7).

Three groups of connectors can be identified according to their average slip moduli. The SM type connector with the highest stiffness $k_{0.4} = 483,8 \text{ kN/mm}$ forms the first group. The second group contains the GSP, ST + S + N, SP + N, GDF and SNP type connectors with secant slip moduli ranging from $k_{0.4} = 258,8 \text{ kN/mm}$ for the SP + N connector type to $k_{0.4} = 121,4 \text{ kN/mm}$ for the SNP connector type. The third group includes the SST + S type connectors with corresponding secant slip modulus $k_{0.4} = 5,9 \text{ kN/mm}$, the lowest one obtained during the shear tests.

The type ST + S + N connector had the highest shear resistance $F_{max} = 110,6 \text{ kN}$, while the highest initial stiffness was observed in the SM type connector. The maximum shear load $F_{max} = 81,2 \text{ kN}$, reached by the SM connector was 25% less than that observed in the ST + S + N connector although the connector initial stiffness was more than 50% higher than that observed in the ST + S + N connector.

For all the specific test results and discussions see [1] and [2]. Here are synthesized only three type of connectors. The first one is SST + S shear connector, whose results are shown in Figure 2.13. The SST + S type connectors showed behavior different from all other connectors tested and appeared to be the most ductile system due to the ability to carry load under large deformation. The lowest maximum shear test force was displayed, about 33,9 kN, with a corresponding slip of 15 mm, while the stiffness was $k_{0.4} = 5,9 \text{ kN/m}$.

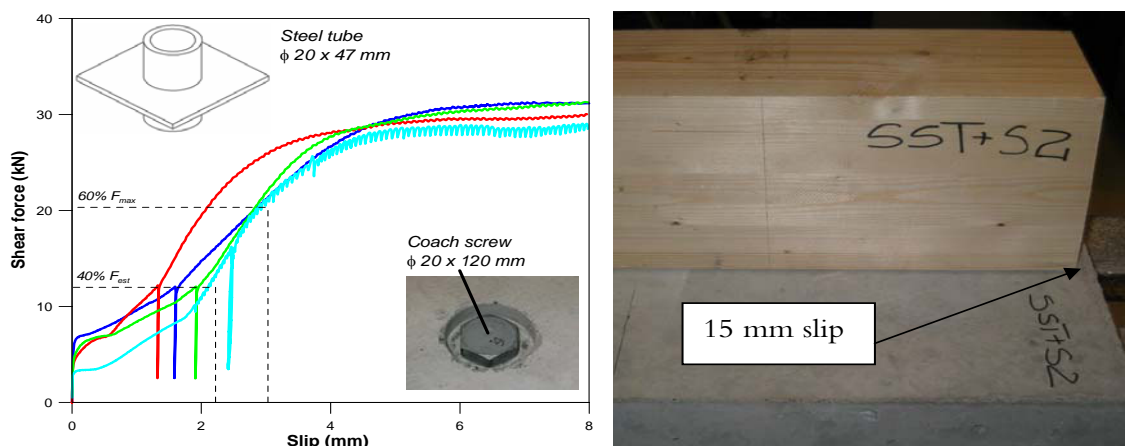


Figure 2.13: Results of the shear test for connector type SST + S.

The resistance was still increasing after 15 mm slip demonstrating significant plastic deformations from approximately 5 mm slip. The screws failed in bending due to a

plastic hinge formation into the concrete slab, and no crack appeared in the concrete slab throughout the test.

The second one is ST + S + N type connector and it is reported in Figure 2.14. The shear load vs. slip curves demonstrated consistent linear behavior of the connection up to 50% of the ultimate shear load. The secant shear moduli $k_{0.4}$ and $k_{0.6}$ are therefore very close. This type of connector displayed the highest maximum shear force, of 110,6 kN, with corresponding slip of 12 mm and stiffness $k_{0.4} = 235,7$ kN/mm.

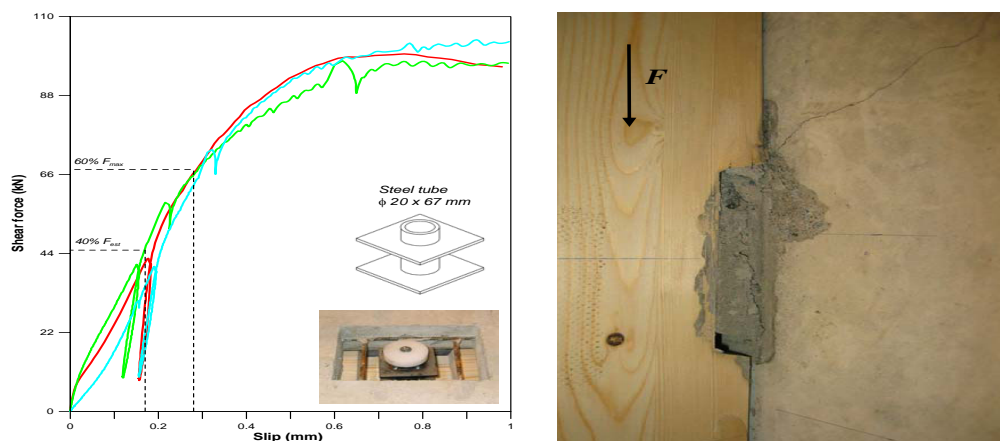


Figure 2.14: Results of the shear tests for connector type ST + S + N.

The secant slip modulus then decreased from that point up to the strength peak and farther on due to the plasticization of the connection system. The primary failure mechanism was a combination of pure shear failure at the vertical cross-section of the notch and tension in the upper part of the notch, caused by the strut-and-tie mechanism occurring in the notch due to the eccentric bearing force at the timber-to-concrete interface. The reduction in resistance gradually occurred for all tested specimens and the system was capable to carry residual shear load. The screws, in fact, acted as an anchor in tension thanks to its pull-out strength and enabled a strut-and-tie mechanism to develop into the notch.

The last one is SM type of connector. It had the highest stiffness, $k_{0.4} = 483,8$ kN/m and a maximum load of 81,2 kN with a corresponding slip of 4,0 mm, as showed in Figure 2.15. The failure of the connection system was brittle and occurred in the concrete slab due to the forming of cracks along the steel mesh line, followed by yielding and tearing of the steel mesh.

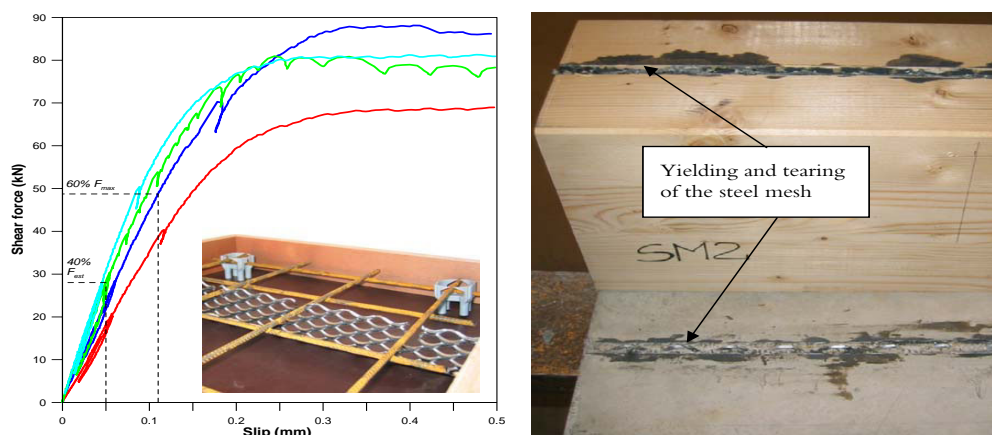


Figure 2.15: Results of the shear test for connector type SM.

2.1.2.7 Discussion over Lukaszewska’s connections

Seven series of different connector types for timber-concrete composite structures already embedded into prefabricated concrete slab were studied and different mechanical properties of the connectors such as stiffness (slip modulus), shear strength and ductility were presented and discussed.

From the results of the shear tests, it was found that some of the “dry-dry” connection systems are very stiff (SM, GSP, ST + S + N), while some other are ductile (SNP, SST + S, SP+N, GDF).

Based on the consideration reported above, it can be concluded that the most suitable connectors for prefabricated timber-concrete composite beams were the SST + S and SP + N types. The glued-in type connectors SM, GSP and GDF have a number of problems related to the use of the glue. Such problems include: (i) the need of controlled environmental conditions such as temperature and humidity to ensure a successful curing of the epoxy, and (ii) the more expensive disposal of the waste generated during the prefabrication process of the connection due to the use of the glue, which requires modification for recycling with an increase in the overall price of the system. The SNP type connector has bad mechanical properties and need a complex equipment for pressing the concrete slabs with inserted toothed plates into the glulam beams.

The connection type ST + S + N is also a promising system thanks to the excellent mechanical performance, however the prefabrication process is more complex and expensive.

As far as fire resistance of the connection systems is concerned, an overall satisfactory behavior can be achieved for SNP, SST + S and ST + S + N systems as long as suitable distance from the edge of timber beam is assumed. Connectors SM, GSP and GDF are more problematic due to the use of glue which does not perform adequately at high temperatures, as well as connector SP + N where the plates and the nails are

exposed to the fire and unprotected.

2.1.2.8 Conclusions over Lukaszewska's studies

First of all, the use of “dry-dry” shear connectors can reduce the drawbacks of the “wet” composite systems, since no time is needed for curing concrete on-site. The time required in traditional systems for placing shear connectors in timber beam on-site is eliminated when prefabricated systems are used since shear connectors are embedded in the pre-cast concrete slabs, so all that needs to be done on-site is to connect the pre-cast slab and the timber beams. Moreover, if the pre-cast concrete slab and timber beams are connected off-site too, on-site construction time can be further reduced to the time required to assemble floor elements to each other, and to vertical elements.

Avoidance of use of “wet” components during the generally “dry” process of constructing timber buildings allows to skip separating layer-foil (preventing timber from coming into contact with wet concrete) between the pre-cast concrete slab and timber, and formwork, which is often required during on-site or in traditional timber-concrete systems. Besides, the elimination of “lost” formwork also reduces the self-weight of the structure.

Another advantages of this kind of system is the realization of full stiffness timber-concrete composite structure as soon as the concrete slab and timber beam are connected (facing traditional wet systems, which require time to develop sufficient stiffness to sustain the full self-weight to the concrete slab). Finally, shrinkage of concrete can freely occur when the concrete is allowed to cure in the prefabrication plant before assembly with the timber beam, thereby reducing subsequent stresses and deflections in the composite beam.

The results of the experimental study show that it is feasible to manufacture elements, with the concrete slabs prefabricated element off-site and connected on-site on the timber beams. Advantages of the proposed systems include less cost, increase in speed of construction, and reduced effect of concrete shrinkage on the composite system compared to cast-in-situ system.

2.1.2.9 Metal pipe system

Recently studies were carried out at SP Technical Research Institute of Sweden division Building and Mechanics, to develop innovative composite structures, comprising timber beams and prefabricated concrete slab, with high prefabrication level, high performance and good durability, see [4]. For such a purpose innovative and very efficient materials, such as fibre reinforced concrete and modified wood, were used for the manufacture of the specimens and completely dry shear connection systems were investigated. The two types of shear connectors were: *special inclined steel tu-*

bes, treated in paragraph 2.1.8 and *shear anchor-key of wood*, which is introduced in paragraph 2.1.9. The entire treatment about these connectors is reported in [4]. In both cases, the connectors are incorporated in the prefabricated concrete slab, which is then easily connected to the timber sub-structure only by means of self-tapping screws.

A specimen of special steel tubes connections type is shown in Figure 2.16. They were applied in the formwork before the prefabricated concrete slab was cast. In order to achieve a better stiffness, the tubes had an inclination of 45° to the longitudinal axis of the beam. The principal dimensions of the steel parts of this connections type are shown in Figure 2.17



Figure 2.16: Steel tubes in the formwork before concrete casting.

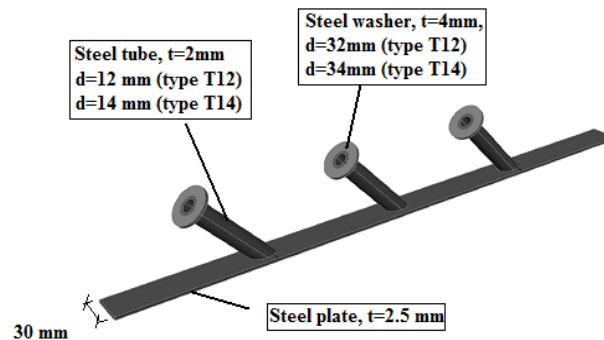


Figure 2.17: Steel tube geometry.

Inside each pipe was then inserted a 11 mm self-tapping full-threaded screw and 250 mm length, which enters the glulam and joints the slab to the beam. The screws were pre-tensioned with a torque moment of 160 Nm. Two types of configurations were adopted for this kind of connections, namely:

- connection type T12, with tube diameter of 12 mm;
- connection type T14, with tube diameter of 14 mm.

For both type of T-connections identically full-threaded screws were used. However, fast setting cement was poured into the tube for the case of connections type T14, immediately before the screw was tightened. This was done in order to fill the gap between the screw and the tube. No fast setting cement was used for connections type T12. To better understand the static principle of connections “type T” look at Figure 2.18

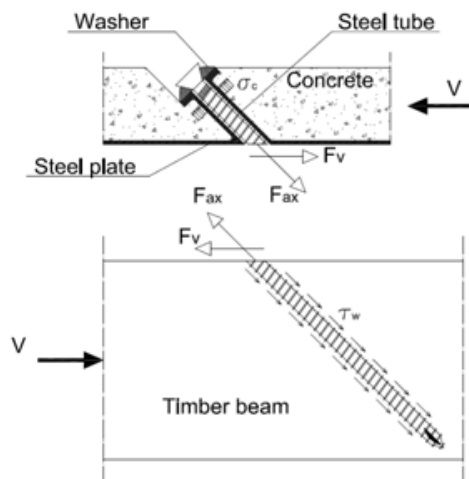


Figure 2.18: Illustration of the load path in the connection type T.

The shear force V , is transferred from the concrete slab to the timber beam both by shear action F_v , in the direction of the force V , and by tension action F_{ax} in the direction of the screw axis. In the wooden part, shear is resisted by embedment capacity of the wood, while tension is resisted by withdrawal capacity. In the concrete slab, shear is resisted by contact pressure between the screw and the internal part of the tube, while tension is resisted by axial pressure of the screw head on the top of the tube, via a steel washer. Due to the inclination of the screws, compression stresses will develop at the interlayer between timber and concrete. Such compression stresses generate friction between the two materials, which also contributes to increase the stiffness and the strength of the timber-concrete connection.

Figure 2.19 shows the trend load-displacement for the T12_1 specimen shear test. These values for the stiffness, evaluated respectively at the SLS (K_{ser}) and at the ULS (K_u) have been evaluated in agreement with the procedure described in standard reference [28]:

$$K_{ser} = \frac{0,4 \cdot F_{max}}{\frac{4}{3} \cdot (\nu_{04} - \nu_{01})} = \frac{0,3 \cdot F_{max}}{(\nu_{04} - \nu_{01})} \quad K_u = \frac{2}{3} \cdot K_{ser}$$

where:

F_{max} is the maximum load reached during the test;

ν_{04} is the values of the slip corresponding to 40% of maximum load;

ν_{01} is the values of the slip corresponding to 10% of maximum load.

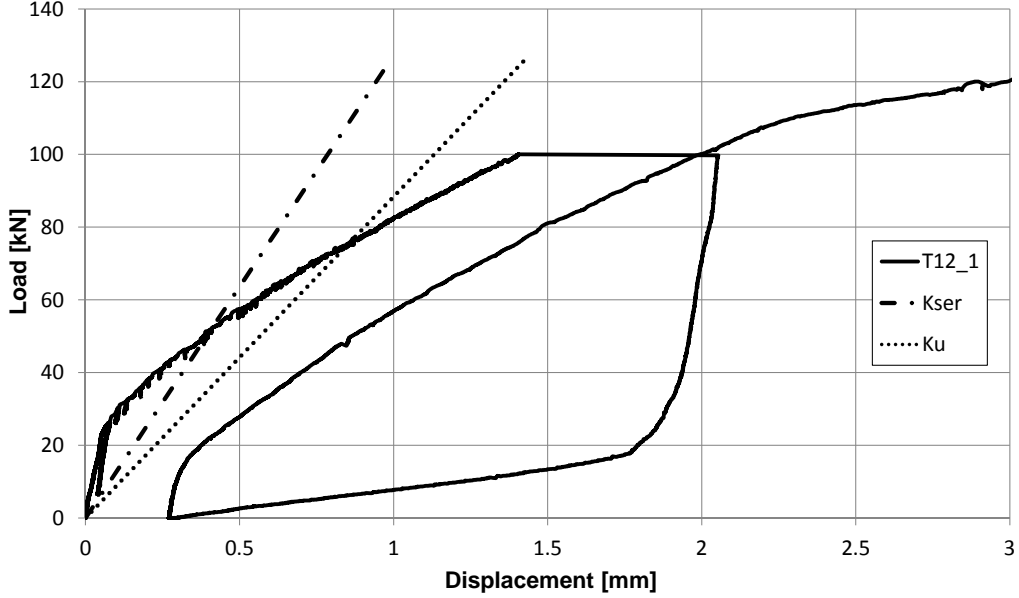


Figure 2.19: Load-displacement graph obtained for the first specimen tested with connection type T12_1.

By substituting the values obtained for T12_1 specimen it can get the stiffness:

$$K_{ser,T12_1} = \frac{0,3 \cdot F_{max}}{(\nu_{04} - \nu_{01})} = \frac{0,3 \cdot 126,2}{(0,397 - 0,029)} = 103 \frac{\text{kN}}{\text{mm}}$$

$$K_{u,T12_1} = \frac{2}{3} \cdot K_{ser,T12_1} = \frac{2}{3} \cdot 103 = 69 \frac{\text{kN}}{\text{mm}}$$

The trend load-displacement for the T12_2 specimen shear test is shown in Figure 2.20.

By substituting the values obtained for T12_2 specimen it can get the stiffness:

$$K_{ser,T12_2} = \frac{0,3 \cdot F_{max}}{(\nu_{04} - \nu_{01})} = \frac{0,3 \cdot 108,2}{(0,324 - 0,023)} = 108 \frac{\text{kN}}{\text{mm}}$$

$$K_{u,T12_2} = \frac{2}{3} \cdot K_{ser,T12_2} = \frac{2}{3} \cdot 108 = 72 \frac{\text{kN}}{\text{mm}}$$

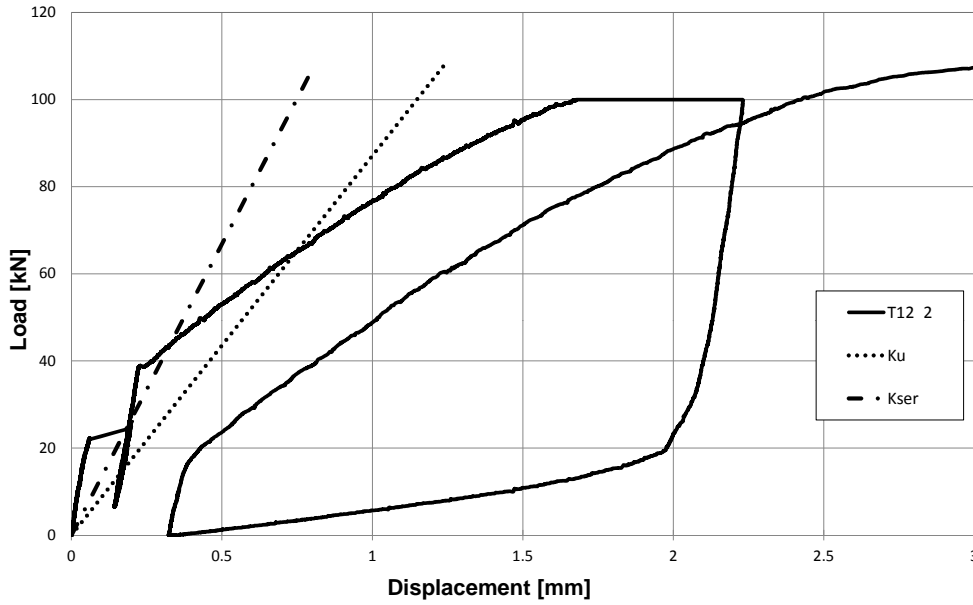


Figure 2.20: Load-displacement graph obtained for the second specimen tested with connection type T12_2.

Stiffness of connection system T12, respectively at SLS and at ULS, can be evaluated by calculating an average value:

$$K_{ser,T12} = \frac{(K_{ser,T12_1} + K_{ser,T12_2})}{2} = \frac{(103 + 108)}{2} = 105 \frac{\text{kN}}{\text{mm}}$$

$$K_{u,T12} = \frac{2}{3} \cdot 105 = 70 \frac{\text{kN}}{\text{mm}}$$

Since connection system T12 was made by three screws, stiffness for each one was thus:

$$K_{ser,T12,screw} = \frac{K_{ser,T12}}{3} = \frac{105}{3} = 35 \frac{\text{kN}}{\text{mm}}$$

$$K_{u,T12,screw} = \frac{2}{3} \cdot K_{ser,T12,screw} = \frac{2}{3} \cdot 35 = 23 \frac{\text{kN}}{\text{mm}}$$

These results are an average value of stiffness, for connection type T12, through the analysis of the result obtained from [4]. For comparison between experimental values and theoretical calculations based on Blass method see [11].

2.1.2.10 Wooden anchor-key

Wooden shear anchor-keys connection system is shown in Figure 2.21. This type of connections was applied in the prefabricated slab before concrete was cast. Self-tapping double threaded screws with diameter 6.5 and length 220 mm were driven in the anchor-keys, perpendicularly to the direction of the applied load. Such screws have two main functions:

- proper anchorage of the shear anchor-key to the concrete slab;
- reduce the risk for splitting of the anchor-key during loading of the specimen.

After the casting, 7 mm self-tapping screws with length of 180 mm were driven through the shear anchor-key to the timber sub-structure.

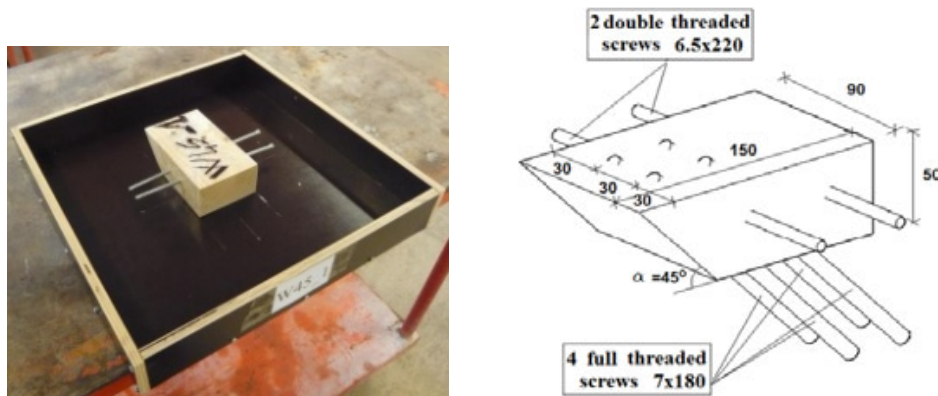


Figure 2.21: Wooden shear anchor-key type W45 before concrete casting on the left, while W45-type details are on the right.

The static principle of connection type W45 is shown in Figure 2.22. The shear force V , is transferred from the concrete slab to the timber beam both by shear action F_v , in the direction of the force V , and by tension action F_{ax} , in the direction of the screw axis. Both in the wooden shear anchor-key and in the timber member, shear is resisted by withdrawal capacity.

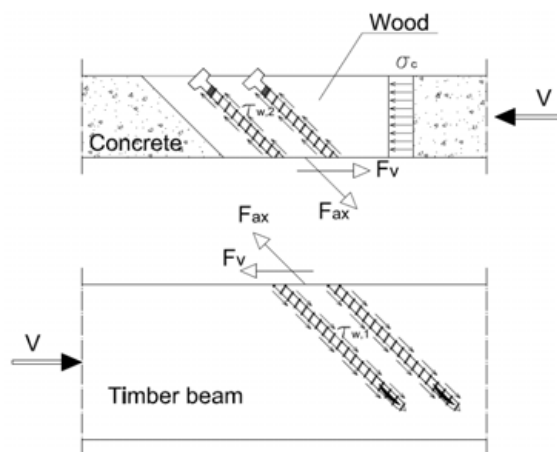


Figure 2.22: Illustration on the load path in the W45 system.

Due to the inclination of the screw, compression stress will develop at the interlayer between timber and concrete. Such compression stresses generate friction between the slab and the timber member, which also contributes to increase the stiffness and the strength of the timber-concrete connection.

The geometry of connection type W30 along with the used screws is shown in Figure 2.23.

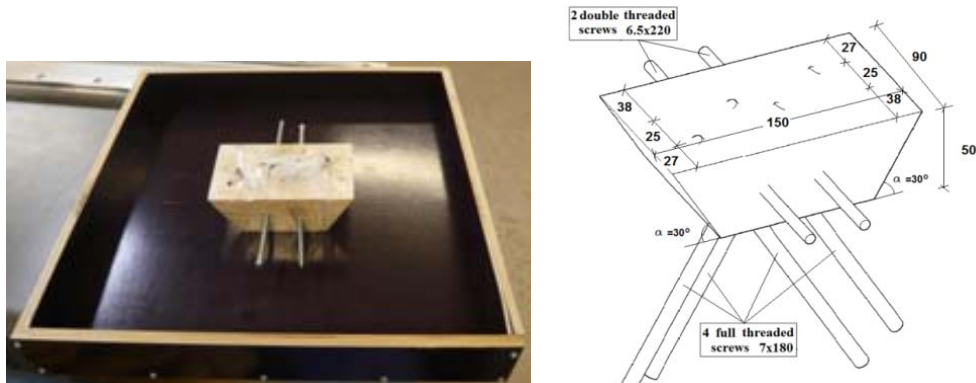


Figure 2.23: Illustration of the W30 system.

The static principle of connection type W30 is shown in Figure 2.24 and it is rather similar to the static system of connection type W45. The main difference is that, during loading, in the connection type W30 two screws act in tension while other two screws act in compression. On the other hand, in connection type W45, all screws act in tension during loading.

For two specimens, G45_1, G45_2 the shear anchor-key was connected to the timber member by means of screws and glue together, whilst for W45_A, F45_1, F45_2 and F45_3 only by screws were used, see more on [4].

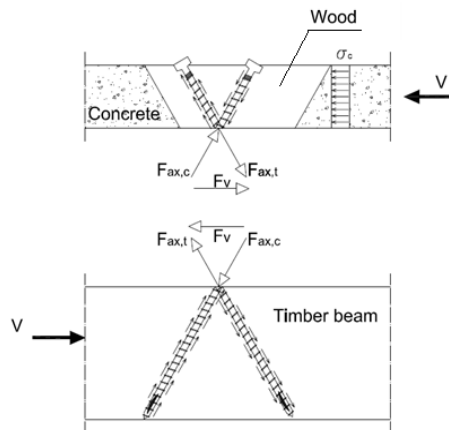


Figure 2.24: Illustration on the load path in the W30 system.

Figure 2.25 shows the trend of the load-displacement for the F45_1 specimen shear test. These values for the stiffness, evaluated respectively at the SLS (K_{ser}) and at the ULS (K_u) have been evaluated in agreement with the procedure described in standard reference [28]:

$$K_{ser} = \frac{0,4 \cdot F_{max}}{\frac{4}{3} \cdot (\nu_{04} - \nu_{01})} = \frac{0,3 \cdot F_{max}}{(\nu_{04} - \nu_{01})} \quad K_u = \frac{2}{3} \cdot K_{ser}$$

where:

F_{max} is the maximum load reached during the test;

ν_{04} is the values of the slip corresponding to 40% of maximum load;

ν_{01} is the values of the slip corresponding to 10% of maximum load.

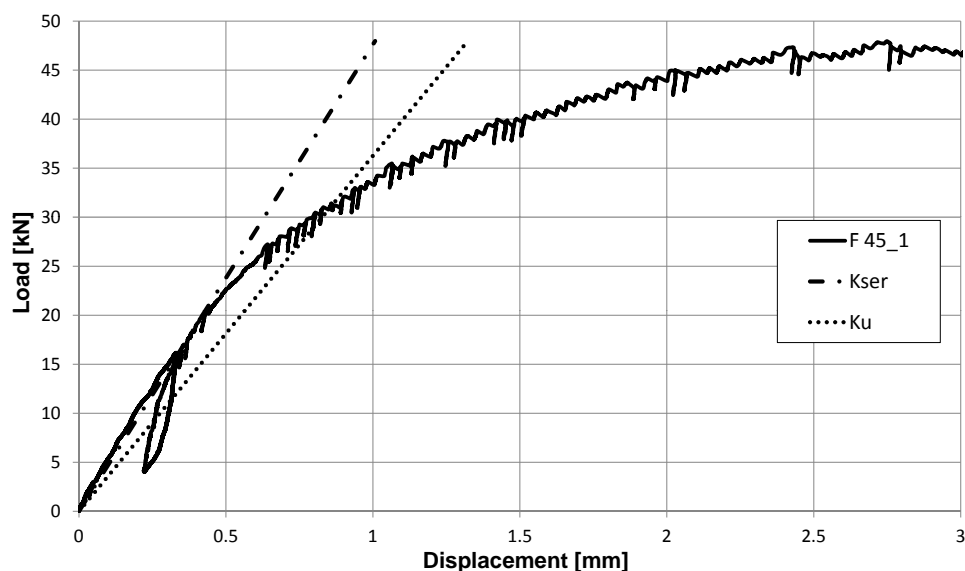


Figure 2.25: Load-displacement graph obtained for the first specimen tested with connection type F45, (specimen F45_1). In this case the shear anchor-key was connected to the timber member only by means of screws.

By substituting the values obtained for F45_1 specimen it can get the stiffness:

$$K_{ser,F45_1} = \frac{0,3 \cdot F_{max}}{(\nu_{04} - \nu_{01})} = \frac{0,3 \cdot 48,0}{(0,403 - 0,086)} = 45 \frac{\text{kN}}{\text{mm}}$$

$$K_{u,F45_1} = \frac{2}{3} \cdot K_{ser,F45_1} = \frac{2}{3} \cdot 45 = 30 \frac{\text{kN}}{\text{mm}}$$

The trend of the load-displacement for the F45_2 specimen shear test is shown in Figure 2.26.

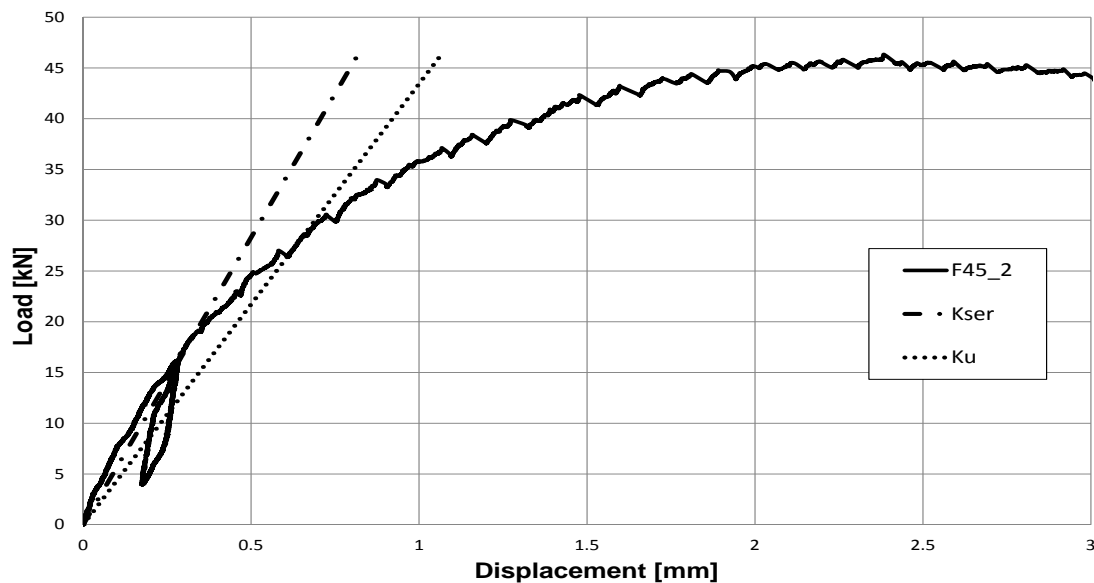


Figure 2.26: Load-displacement graph obtained for the second specimen tested with connection type F45, (specimen F45_2). In this case the shear anchor-key was connected to the timber member only by means of screws.

By substituting the values obtained for F45_2 specimen it can get the stiffness:

$$K_{ser,F45_2} = \frac{0,3 \cdot F_{max}}{(\nu_{04} - \nu_{01})} = \frac{0,3 \cdot 46,3}{(0,327 - 0,0059)} = 52 \frac{\text{kN}}{\text{mm}}$$

$$K_{u,F45_2} = \frac{2}{3} \cdot K_{ser,F45_2} = \frac{2}{3} \cdot 52 = 35 \frac{\text{kN}}{\text{mm}}$$

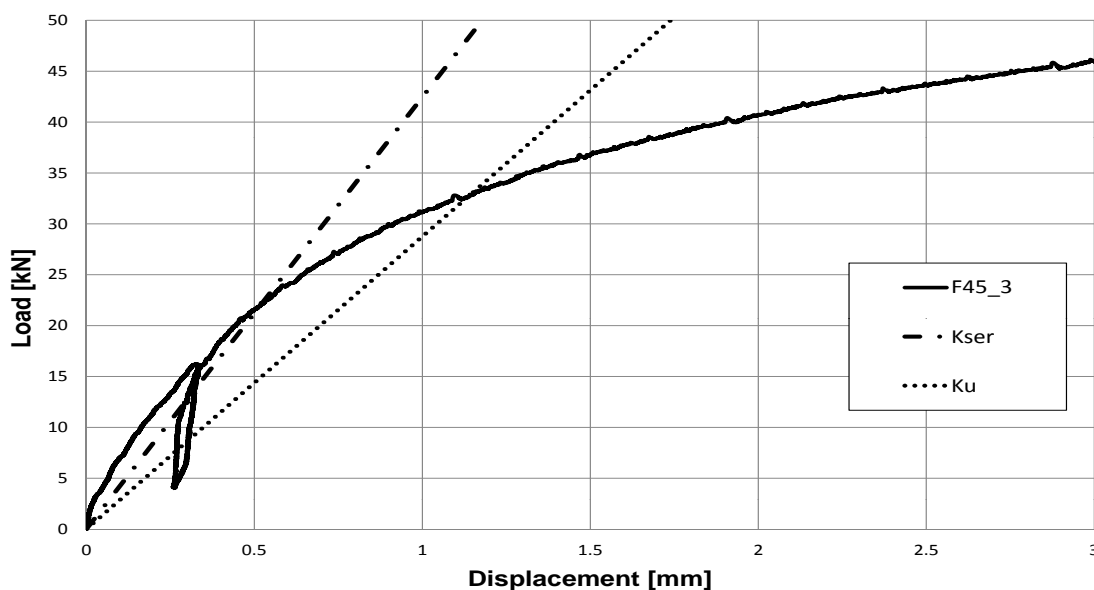


Figure 2.27: Load-displacement graph obtained for the third specimen tested with connection type F45, (specimen F45_3). In this case the shear anchor-key was connected to the timber member only by means of screws.

The trend of the load-displacement for the F45_3 specimen shear test is shown in Figure 2.27.

By substituting the values obtained for F45_3 specimen it can get the stiffness:

$$K_{ser,F45_3} = \frac{0,3 \cdot F_{max}}{(\nu_{04} - \nu_{01})} = \frac{0,3 \cdot 54,7}{(0,516 - 0,072)} = 37 \frac{\text{kN}}{\text{mm}}$$

$$K_{u,F45_3} = \frac{2}{3} \cdot K_{ser,F45_3} = \frac{2}{3} \cdot 37 = 25 \frac{\text{kN}}{\text{mm}}$$

Stiffness of connection system F45, respectively at SLS and at ULS, can be evaluated by calculating an average value:

$$K_{ser,F45} = \frac{(K_{ser,F45_1} + K_{ser,F45_2} + K_{ser,F45_3})}{3} = \frac{(45 + 52 + 37)}{3} = 45 \frac{\text{kN}}{\text{mm}}$$

$$K_{u,F45} = \frac{2}{3} \cdot 45 = 30 \frac{\text{kN}}{\text{mm}}$$

These results are an average value of stiffness, for connection type F45, through the analysis of the result obtained from [4].

2.1.2.11 Final values of stiffness

In Table 2.3 are summarized for both the examined connection systems T12 and F45 the maximum load reached and the values of the stiffness obtained by experimental tests performed and described in [4], at SLS and ULS.

Connection system	K_{ser} [kN/mm]	K_u [kN/mm]	F_{max} [kN]
T12_1	34	23	42
T12_2	36	24	36
T12_mean	35	23	39
F45_1	45	30	48
F45_2	52	35	46
F45_3	37	25	55
F45_mean	45	30	50

Table 2.3: Summarizing of stiffness and maximum shear load reached from both specimens T12 and F45.

2.1.2.12 Details on materials

Some informations about specimens and materials are given here, for more details see [4]. The amount of steel fibres used for the manufacturing of FRC slabs was 45 kg/m³. The average compressive strength of the fibre reinforced concrete was around 57,6

MPa. The aspect ratio of the fibres was $l/d = 75$ where l is the length and d is the diameter. The timber used for all specimens was glulam L40, which consists of laminations of Norway spruce with characteristic tensile strength parallel to the grain $f_{t,0,k} \geq 22$ MPa and bending strength $f_{m,j,k} \geq 39$ MPa.

The material used to manufacture the shear anchor-keys for specimens type W45 and W30 was spruce with strength class C24. The material used to manufacture the shear anchor-key of specimens type F45 was furfurylated beech. Furfurylated wood is one of those wooden materials classified as modified wood. Furfurylation is a wood modification process, using furfuryl alcohol, obtained from renewable resources of corn cobs or sugar cane residuals. Due to its polarity, furfuryl alcohol can penetrate into the cell wall, where it polymerizes. Furfurylation of wood provides a high protection level against bio-degradation. Beside the bioresistance, wood properties like dimensional stability and hardness are significantly improved by the furfurylation of wood. These wood properties depend on the amount of furfuryl alcohol that is brought into the cell wall. The mean density of the furfurylated wooden shear anchor-keys was 885 kg/m^3 . Finally, the material used for the manufacturing of the steel tubes for specimens type T12 and T14 was ordinary steel S355.

2.1.2.13 Results of shear tests on wooden anchor-key

As it can be seen in Figure 2.28, the load-slip behavior of specimens type W45 was nearly linear up to approximately 30 kN. On the other hand, the specimens type W30 exhibited almost immediately a non-linear load-slip response. The discrepancy in behavior between these two types of specimens is mainly due to the rotation of the shear anchor-key in the slab, which takes place for the case of specimens type W30.

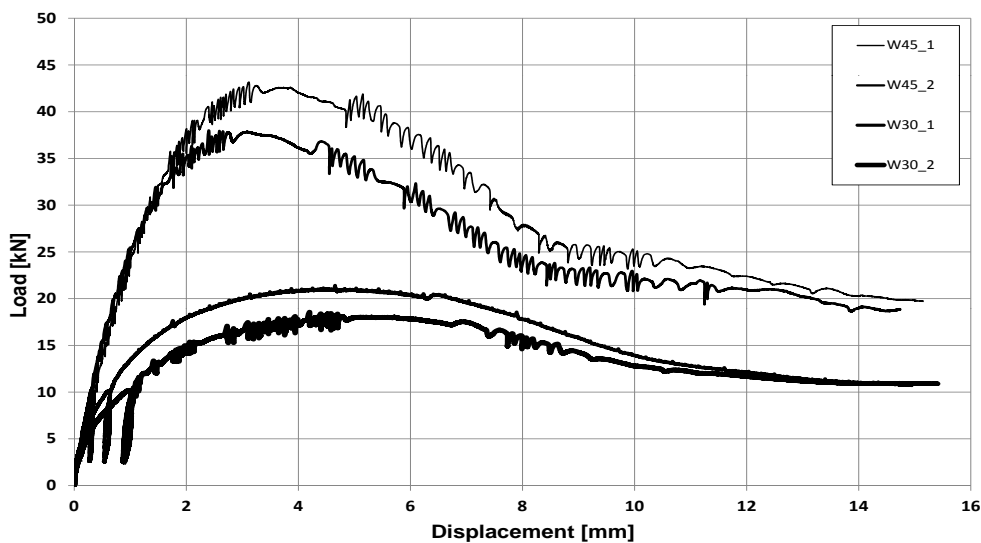


Figure 2.28: Load-slip curve for specimens type W30 and W45.

Specimens W45 showed a significant higher load carrying capacity and a higher stiff-

ness than specimens type W30. The final failure for specimens of type W45 occurred due to reached withdrawal capacity of the screws at the shear anchor-key. On the other hand, the final failure for specimens type W30 occurred mainly due to large rotation of the shear anchor-key.

Both highest failure load and highest stiffness of all tested specimens was obtained for the T-specimens, see Figure 2.29.

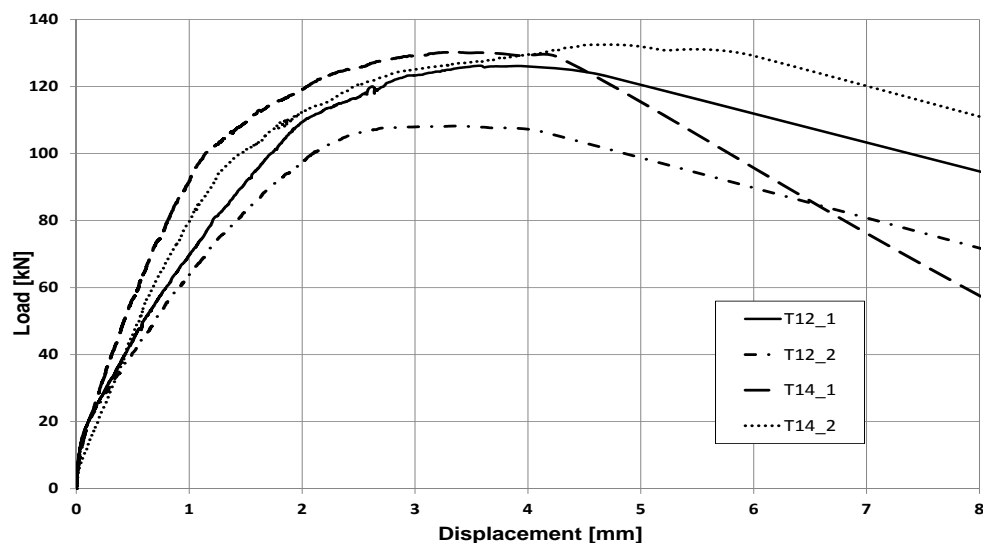


Figure 2.29: Load-slip curve for specimens type T12 and T14.

The specimens in which the tubes were filled with fast setting cement, i.e. specimens type T14, showed a slightly larger stiffness than those without fast setting cement, i.e. specimens type T12. Failure of T-type specimens occurred after rather large deformations either

- i) due to splitting of the timber member into two pieces, along the direction were the screws were driven;
- ii) due to tensile failure of the screws.

In Table 2.4, stiffness and failure load for a single connector, which was tested, are shown. For the case of W-type specimens, the values reported in the table are those for strength and stiffness of the entire system (i.e. anchor-key plus four screws). For the case of T-specimens, the values reported in the table are those for strength and stiffness of a single screw.

ID specimen #	$K_{0.4}$ [kN/mm]	$K_{0.6}$ [kN/mm]	F_{max} [kN]
F45-1	48	36	48
F45-2	57	43	46
F45-3	42	29	55
Mean F45	49	36	50
W30-1	20	14	21
W30-2	16	10	19
Mean W30	18	12	20
W45-1	27	24	43
W45-2	31	27	38
Mean 45	29	25	41
T12-1	42	29	42
T12-2	45	29	36
Mean T12	43	29	39
T14-1	49	38	43
T14-2	41	30	44
Mean T14	45	34	44

Table 2.4: Stiffness and failure load for a single connector.

2.1.2.14 Discussion over metal pipes and anchor-key connections

Anchor-key made of furfurylated wood have shown a considerably better behavior, both in terms of strength and stiffness, than anchor-keys made of spruce, as it can be seen in Figure 2.30.

The main reason for this discrepancy in behavior between the two materials is the fact that density of furfurylated wood is approximately twice the density of spruce. Consequently, the withdrawal capacity is higher for screws that are driven in furfurylated wood than for screws driven in spruce. In the case of spruce, the screws were gradually pushed-in through the shear anchor-key during loading. Eventually, the specimens failed due to complete push-in of the screw through the shear anchor-key. In the case of furfurylated wood, instead, no visible push-in of the screw through the shear anchor-key could be observed. Eventually, failure occurred in the timber member, due to reached withdrawal capacity of the screw. Furfurylated wood has a rather brittle behavior, however no tendency to split was observed during testing. After the test, this conclusion could be made:

- during loading, the screws of either W45-type specimens or T-type specimen, are taking the applied load not only to pure axial stress, but also by shear, which increase both strength and stiffness of the connection;

- in both W45-type specimens and T-type specimens, compression stresses will develop at the interlayer between timber and concrete during loading. Such compression stresses generate friction between the slab and the timber member, which also contributes to increase the stiffness and the strength of the connection.

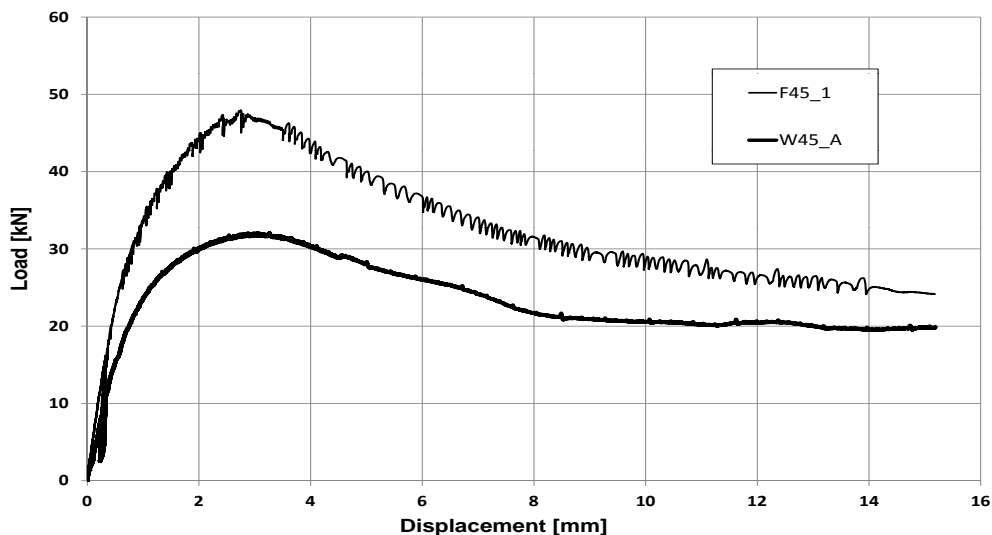


Figure 2.30: Comparison between test on the specimen made of spruce (W45_A) and specimens made of furfurylated wood (F45_1).

The very high stiffness observed at the initial stage of loading in T-type specimens can be attributed to the pre-compression generated by the applied torque moment on the screws. Such a pre-compression generates a large friction between the timber member and the concrete slab, which contributes to increase the stiffness.

2.1.2.15 Conclusions over tube and shear anchor-key connectors

In the study reported in [4], an analysis of properties of an innovative prefabricated timber-concrete composite system, with different types of shear connectors was presented. Preliminary were performed shear tests without concrete slab, i.e. consisting of solely i) a timber member and ii) a wooden shear anchor-key made either of spruce or furfurylated beech. Successively, shear tests on timber concrete specimens with different shear connectors were performed. The investigated shear connectors were:

- i) shear anchor-keys of spruce with different geometries;
- ii) special steel tubes (with and without fast setting cement filling).

On the basis of the obtained results, the following general conclusions can be drawn:

- furfurylated wood has both mechanical and physical properties that make it suitable for applications for shear anchor-key connections;

- in all shear tests where shear anchor-keys of soft wood were used, failure occurred due to reached withdrawal capacity at the anchor-key. On the contrary, withdrawal failure occurred at the timber member, when furfurylated wood was used;
- Type-W30 connections are not completely suitable as shear connectors for timber-concrete structures, mainly due to the large rotations that occur at the anchor-key during loading;
- Type-T connections have revealed to be very suitable for applications in pre-fabricated timber-concrete composite structure, due to their extremely high strength and stiffness;
- In type-T connections, the use of tubes with larger dimension and then filling the gap between the tube and the screw with fast setting cement only slightly increases strength and stiffness of the connection.

It is worth to point out that both types of connectors exhibited a great performance, both in terms of strength, stiffness and ductility. The results from this project allow to say that these shear connectors are very suitable for applications in timber-concrete composite beams. Moreover, these connectors are more effectively in large-span structures and also contribute to both simple and rapid manufacture and erection.

2.1.2.16 Summary table of connectors characteristics


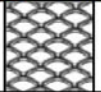












Type of connection	Drawing	Slip moduli		Shear Force
		$k_{0.4}$	$k_{0.6}$	F_{max}
		[kN/mm]	[kN/mm]	[kN]
SNP		121.4	99.0	37.3
SM		483.8	449.4	81.2
SST + S		5.9	6.8	33.9
SST + S*		8.5	8.3	38.2
SP + N		258.8	113.1	42.3
SP + N*		5.3	3.3	40.0
GSP		248.5	183.4	64.4
ST + S + N		235.7	234.4	110.6
GDF		135.1	96.8	52.5
F45		49	36	50
G45		222	188	51
W30		18	12	20
W45_A		32	28	32
W45		29	25	41
T12		43	29	39
T14		45	34	44

Table 2.5: Summary of the main properties of the above connectors.

Chapter 3

Full-scale specimens with steel tubes and wooden anchor-key connections

In 2011, at Lund University (LTH), in order to evaluate the mechanical properties and the structural behavior of a composite timber-fibre reinforced concrete system tests on two full-scale specimens have been performed. These specimens consisted, with reference to [11], of two timber-concrete composite floors with prefabricated FRC. In particular, it has been chosen to test two different types of beams with two different types of connection systems, previously presented in chapter 2. One test has been performed on the office buildings type, while the other one has been performed on the model related to apartment buildings type. The specimens tested, representing floor stripes, were built and then tested to failure.

3.1 Specimen details and bending tests

The full-scale specimens were made by two glulam GL30c beams, joined to a fibre reinforced concrete slab with 5 cm thickness, 160 cm width and length varying according to the floor type, through the connection systems previously described. The slabs were realized by fibre reinforced concrete. The fibre reinforced concrete mentioned here is referred to the one used in the experimental test described in [4]. The main reason of the use of fibre reinforced concrete is to prevent issues due to long-term actions from shrinkage of both elements, timber and concrete. To face this problem an alternative is the fibre reinforced concrete, in which the reinforcement is formed by steel fibres (it is possible to find also different types of fibres, natural and artificial), that start working when the first cracking originates in concrete. Furthermore, these fibres contribute improving strength parameters of the material with benefits on the composite system behavior. Geometrical details are reported below in Table 3.1.

Specimen type	Total length [mm]	Total width [mm]	Connection			Beam	
			type ID	spacing [mm]	width [mm]	depth [mm]	spacing [mm]
Apartment	6000	1600	F45	250	90	360	800
Office	8000	1600	T12	100	90	450	800

Table 3.1: Geometry details of the full-scale specimens.

In the bending tests, the load has been applied on four lines through steel partitioning beams; number and position of these lines have been determined in order to induce in the slab effects (bending moment, maximum shear stress and mid-span deflection) similar to those induced by a uniformly distributed load with same resultant. The supports have been realized through simple supports, of which one fixed (hinge) and the other allowing longitudinal displacements (roller).

During the experiments have been observed and monitored the total load applied to the specimen, the mid-span deflections through 2 resistive gauges, and relative slips between slab and beam at the supports through 4 inductive trasducers.

For each test have been obtained graphs load - slip at supports and load - mid-span deflection, determining also the ultimate load, slip and mid-span deflection values corresponding to fixed load levels.

3.1.1 Residential floor type

Figure 3.1 shows the formwork of one specimen before the casting of the concrete, with the connection system F45.



Figure 3.1: Formwork before the casting of the concrete with the connection system F45.



Figure 3.2: Apartment type specimen before bending test.

The failure of the composite structure was due to the failure of one timber beams, as shown in Figure 3.3.



Figure 3.3: Failure of one of the timber beams.

For a load concentrated (P), applied by the hydraulic jack, amounting to about 300 kN and thus for a q load, uniformly distributed per unit area, equal to about 31 kN/m² (the q load is obtained by dividing the P load for the total surface of the slab, 1600 × 6000 mm². This is possible only through a specific positioned partitioning steel beams in order to induce in the system the same results in terms of bending effects of the ones obtained with a uniformly distributed load per unit area with same resultant) both the glulam beams started breaking for compression perpendicular to grain at the fixed supports, see Figure 3.4. This was probably due to the indentation consequent to the high pressure and to the fact that the beams couldn't slide and slip but only rotate. These breaks did not condition the failure mode of the system. The failure of the system occurred for a P load, applied by the test machine, equal to 405 kN considering the self-weight of the system and of the steel partitioning beams, and thus $q = 42$ kN/m².

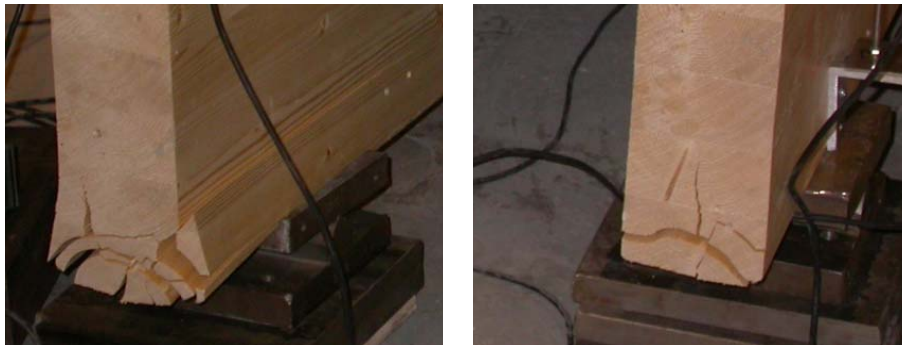


Figure 3.4: Timber beams started breaking for compression perpendicular to grain at the fixed support.

At the same time two cracks parallel to the grain appeared in one of the two beams, Figure 3.3. The lower crack was located at the interface between the second and the third lamella (or else to a depth of around 90 mm evaluated from the bottom of the timber beam), while the upper crack appeared at the same weight as the screw tips are found in the timber beam.

Figure 3.5 displays the curve load - mid-span deflection.

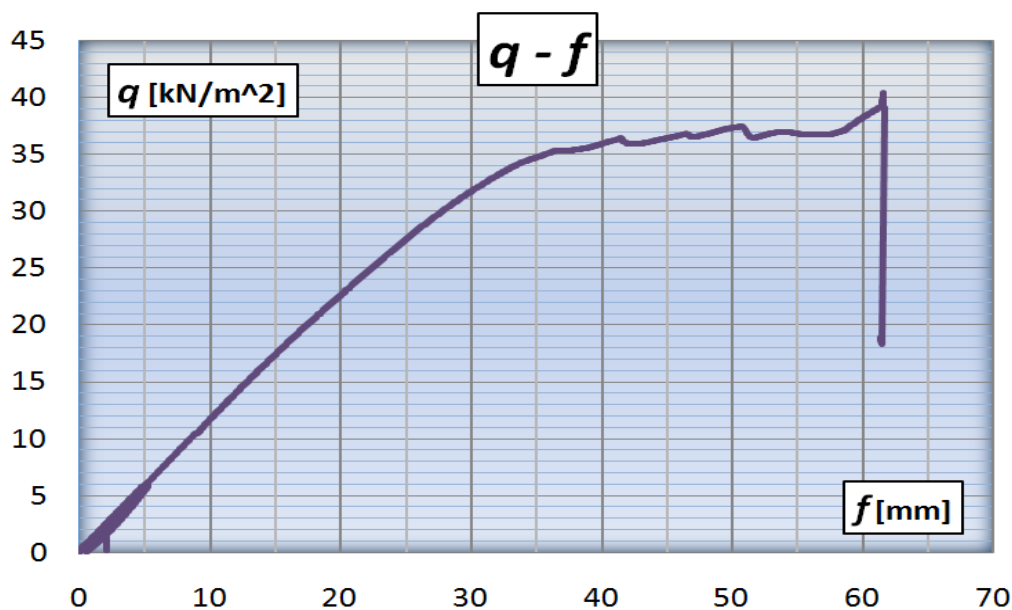


Figure 3.5: Load - mid-span deflection curve for the residential floor type.

The load-carrying capacity of the system was really high (the ultimate load is higher than 40 kN/m^2 and the service load, usually assessed as 60% of the failure load, was around 24 kN/m^2), while a normal residential or commercial floor seldom goes over $8 - 10 \text{ kN/m}^2$. It must be remembered that to this load value q it must be added weight of reply steel beams. Even if the failure was supposedly due to shear, since there is a sort of plateau clearly observable from the trend load – mid-span deflection,

the behavior of the system can be considered as ductile.

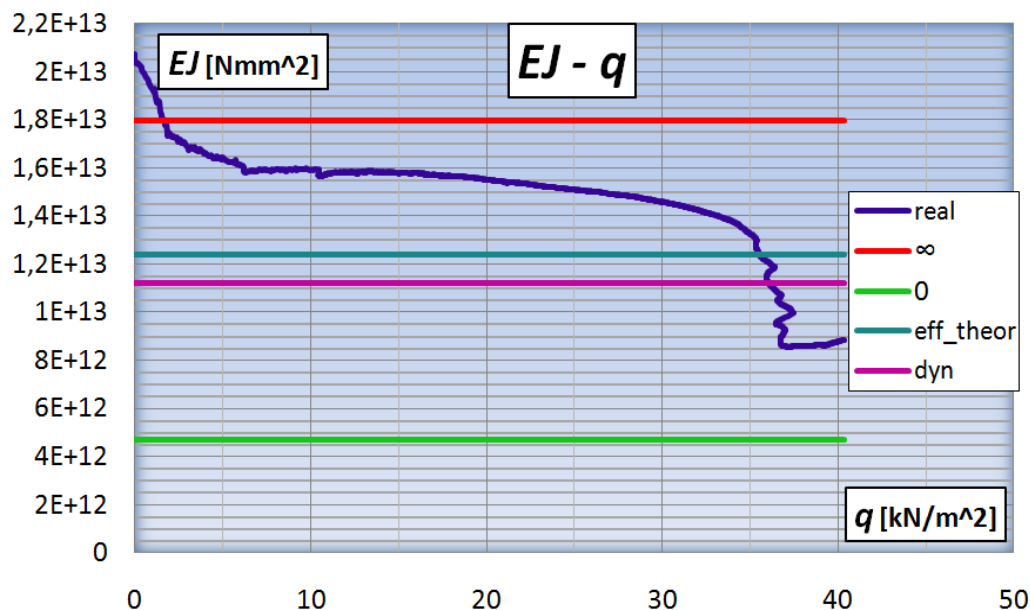


Figure 3.6: Bending stiffness of the system, compared with the theoretical cases of $EJ = 0$ and $EJ = \infty$.

Figure 3.6 shows the comparison between the real stiffness EJ_{real} in function of the applied load q , the values of the theoretical effective stiffness of the system EJ_{eff} as obtained with the theoretical method for composite sections presented in Annex B of Eurocode 5, infinite stiffness of the connection system (or else system with rigid behavior and full-composite action) EJ_{∞} , and the stiffness without the connection system (or else, stiffness of the system considered without connection, with the slab separated from the underlying timber beam) EJ_0 .

As it can see in Figure 3.6, the real stiffness was higher than the effective one. This is supposedly due to the fact that the shear tests described in [4] have been performed by using for each specimen only one piece of furfurylated wood, and also without the benefit of the surrounding concrete and the transversal screws. In this case, in addition to the transversal screws and confinement by the concrete, it can be supposed that the effective number of connections inserted was higher than the real number, and this is probably due to the high compression applied on the system and thus to the increased friction between slab and beams.

Figure 3.7 shows the comparison between the real efficiency of the connection $\eta_{real} = (EJ_{real} - EJ_0)/(EJ_{\infty} - EJ_0)$, as proposed by Piazza, in function of the load q , and the theoretical efficiency $\eta_{eff} = (EJ_{eff} - EJ_0)/(EJ_{\infty} - EJ_0)$.

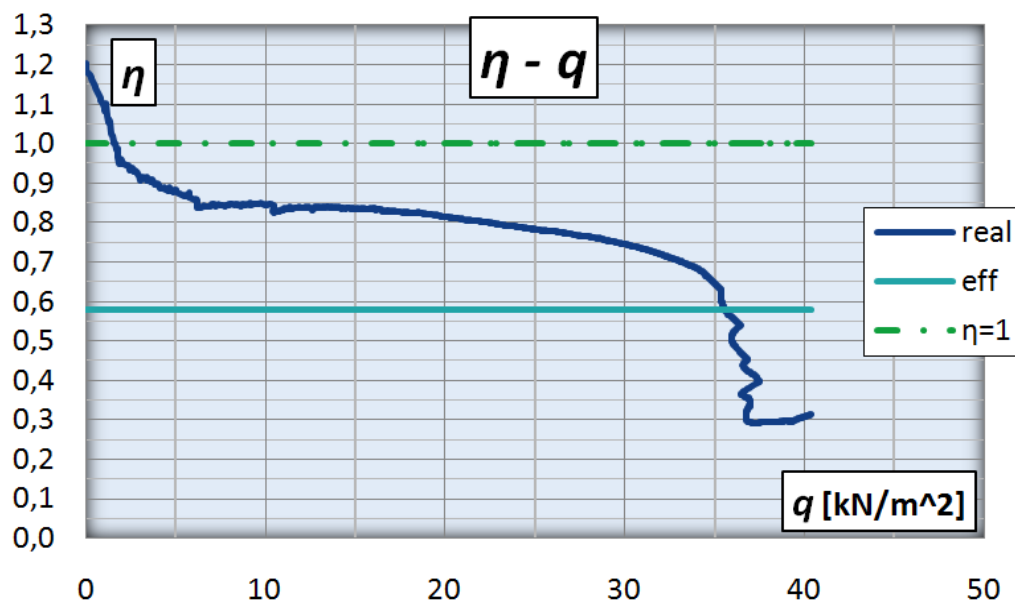


Figure 3.7: Real and effective efficiency of the system.

The real efficiency of the system, with the same trend of the stiffness, is higher than the effective one and it can be seen that, for normal service load (always lower than $8 - 10 \text{ kN/m}^2$), composite beam have almost 85% of full-composite action.

The following graph presented for the apartment type is the curve load - slip ($q - \delta$) at the supports, shown in Figure 3.8.

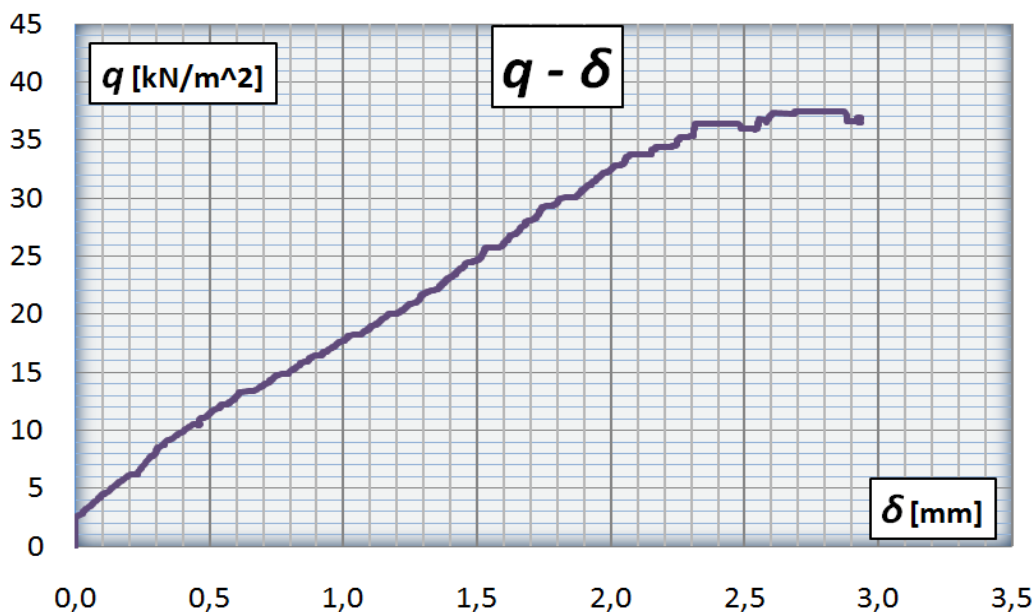


Figure 3.8: Load - slip trend of apartment type.

The graph shows the trend of the relative slip between the concrete slab and the timber beams at the support, in function of the load. At the failure load the slip was

around 3 mm, while for a normal floor load the slip is less than 1 mm.

Table 3.2 displays the real stiffness EJ_{real} and the efficiency of the system, with referring to the service load evaluated $q = 6 \text{ kN/m}^2$, and compared to analytical values obtained by using experimental researches described in [4].

Real values		Analytical values	
$EJ_{real} [\text{Nmm}^2]$	$1,60 \times 10^{12}$	$EJ_{real} [\text{Nmm}^2]$	$1,24 \times 10^{13}$
η_{real}	0,85	$\eta_{theoretical}$	0,58

Table 3.2: Comparison between real values for service load $q = 6 \text{ kN/m}^2$ and analytical calculation for the residential floor type specimen.

3.1.2 Office floor type

The second test regarded the office floor type, whose geometrical details are reported in Table 3.1. The connection typology used for this floor type was the T12-type, previously described. The spacing of the screws, which were $VGS 11 \times 250$, varies between a minimum value of 8 cm in the part from supports to a distance of 2,4 m from the supports, and a value of 10 cm in the central part. The full description of this system is presented in [11].

Before casting the concrete slab it has been provided the insertion of T12 connection system on the formwork, as shown in Figure 3.9.



Figure 3.9: Formwork before casting of the concrete with T12 connection system.

Figure 3.10 shows the office floor type before the bending tests.



Figure 3.10: Office floor type specimen before bending test.

The ultimate load has been reached by the failure at the bottom of both the wooden beams for combined tensile and bending stress. For P load amounting to about 285 kN and thus for a q load, uniformly distributed per unit area, equal to about 24 kN/m², one of the beams broke in the lowest lamella, see Figure 3.11.



Figure 3.11: First failure of the office floor due to the breaking of one finger joint in one timber beam.

After this first failure, P load decreased until a value of about 245 kN, and then has been increased until the collapse of system: for a P load amounting to about 300 kN, and thus $q \approx 25$ kN/m², in the other beam one knot broke in the lowest lamella, Figure 3.12.

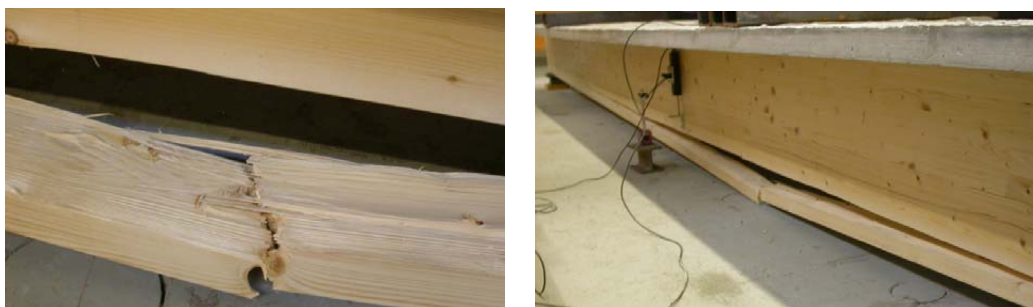


Figure 3.12: Failure of the office type specimen due to the breaking of the lowest lamella.

The load - mid-span deflection is reported in graph (Figure 3.13).

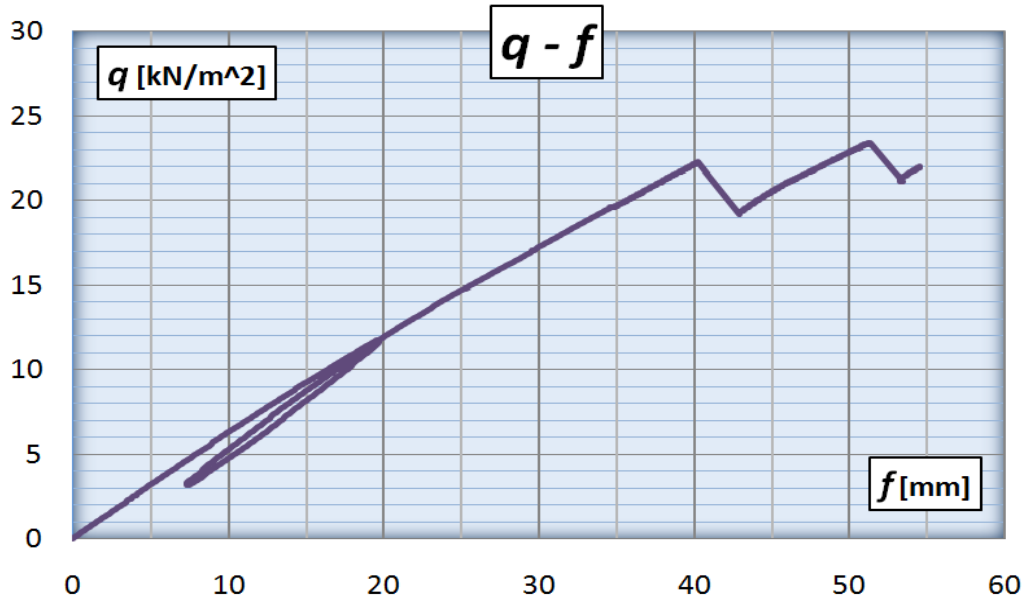


Figure 3.13: Load - mid-span deflection curve.

Also for this system load carrying capacity was really high (the ultimate load was higher than 25 kN/m² and the service load, usually assessed as 60% of the failure load, was around 15 kN/m²).

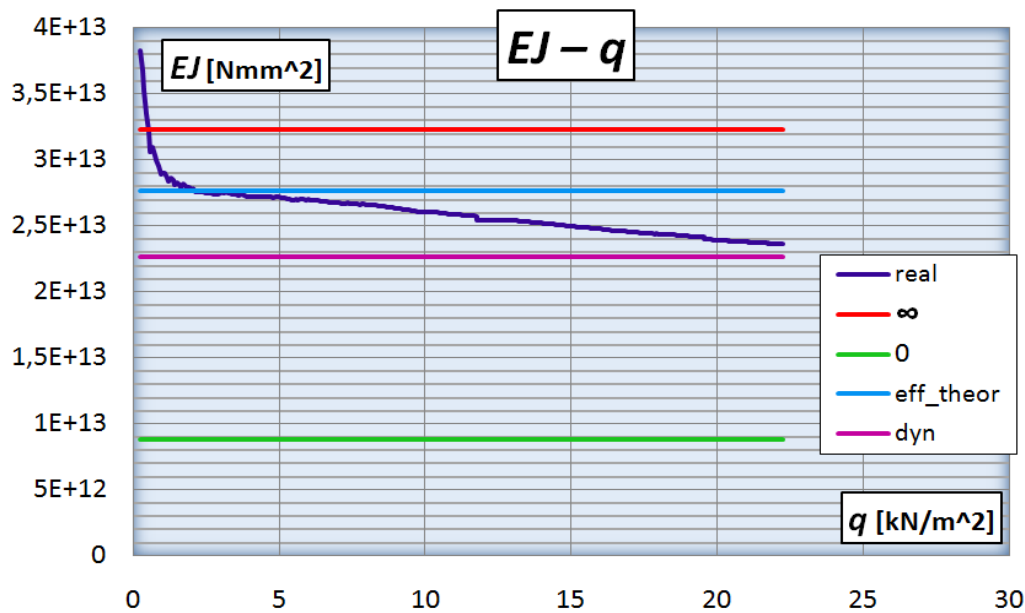


Figure 3.14: Bending stiffness of the system, compared with analytical cases of $EJ = 0$ and $EJ = \infty$ and with both effective and dynamic stiffness.

Figure 3.14 shows the comparison between the real stiffness EJ_{real} in function of the applied load q , the values of the theoretical effective stiffness of the system EJ_{eff}

as obtained with the theoretical method for composite sections presented in Annex B of Eurocode 5, infinite stiffness of the connection system (or else system with rigid behavior and full-composite action) EJ_∞ , and stiffness without the connection system (or else, stiffness of the system considered without connection, with the slab separated from the underlying timber beam) EJ_0 .

As it can see, the real stiffness was a bit lower than the effective one, evaluated on the basis of the stiffness of the shear connectors obtained from the results of the push-out test performed and described in [4] and in agreement with theoretical method of Eurocode 5 for composite sections. This was supposedly due to the fact that some screws could not be inserted because in some of the steel pipes there was stuck concrete that it has not been able to take out.

As in the previous case, the dynamic stiffness (violet line) was a bit lower than the static one, and this could be due to the fact that the connections did not lead the system to a full-composite action.

Figure 3.15 shows the comparison between the real efficiency of the connection $\eta_{real} = (EJ_{real} - EJ_0)/(EJ_\infty - EJ_0)$, as proposed by Piazza, in function of the load q , and the analytical efficiency $\eta_{eff} = (EJ_{eff} - EJ_0)/(EJ_\infty - EJ_0)$.

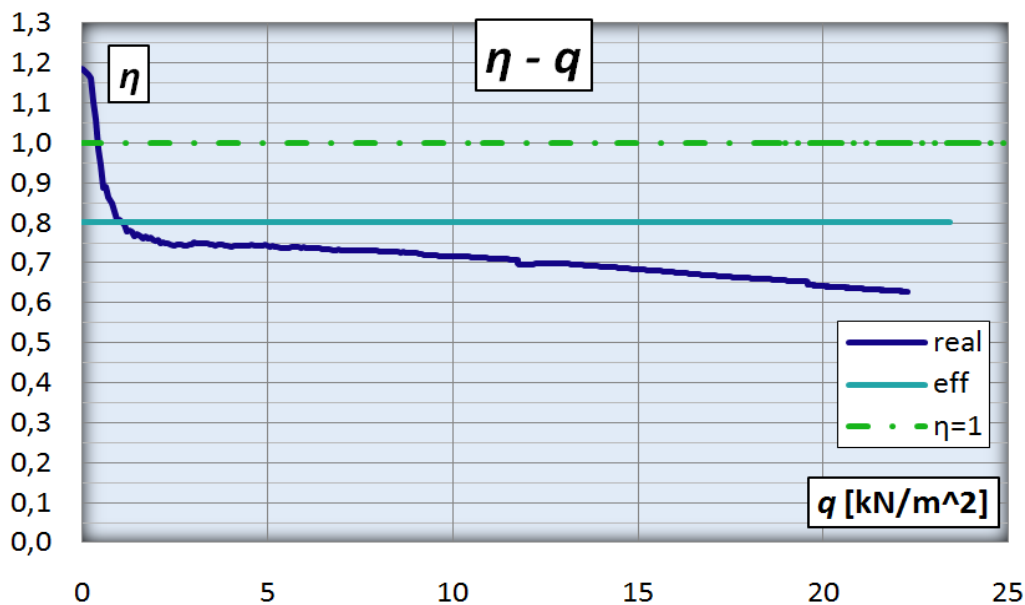


Figure 3.15: Real and effective efficiency of system.

Differently from the previous case, real efficiency for system with T12 connections, with the same trend of the stiffness, was a little bit lower than the effective, but it was anyway a high value and it can be seen that, for normal service floor-loads (always lower than $8 - 10 \text{ kN/m}^2$), it has almost 75% of the full-composite action.

The following graph presents for the office floor specimen the curve load - slip ($q - \delta$) at the supports, shown in Figure 3.16.

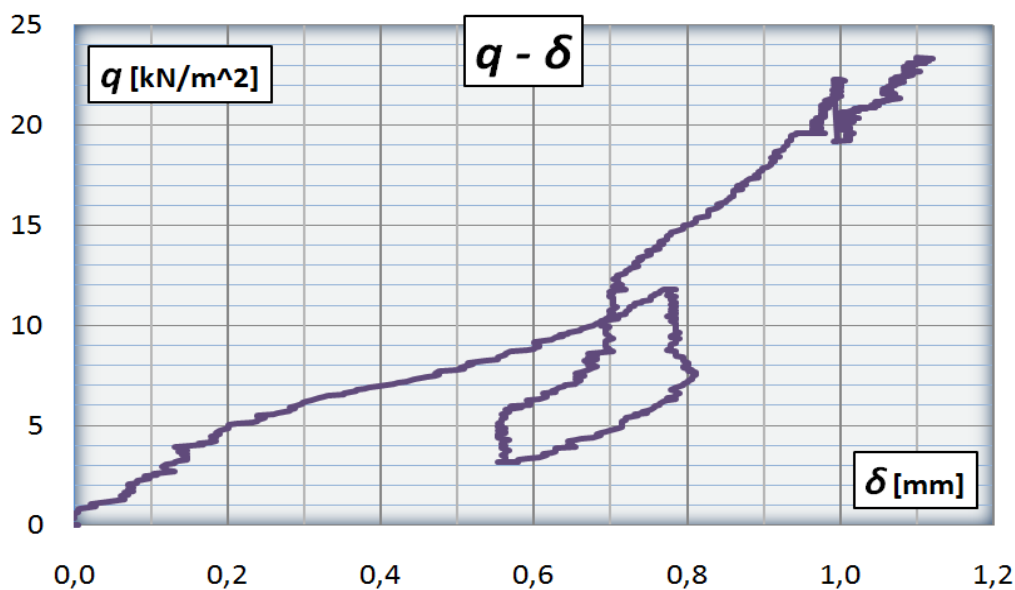


Figure 3.16: Load - slip trend for the office floor type.

The load - slip graph shows the trend of the relative slip between the concrete slab and the timber beams, in function of the load. It can be seen that, as direct consequence of rigidity of shear connectors, slip values were almost zero and always lower than 1 mm.

Table 3.3 reports the real stiffness EJ_{real} and the system efficiency, with referring to the service load evaluated $q_{Ser} = 8 \text{ kN/m}^2$, and compared with theoretical values obtained by using experimental researches described in [4].

	Real values		Analytical values
$EJ_{real} [\text{Nmm}^2]$	$2,65 \times 10^{12}$	$EJ_{eff} [\text{Nmm}^2]$	$2,76 \times 10^{13}$
η_{real}	0,75	$\eta_{theoretical}$	0,80

Table 3.3: Real stiffness and efficiency for service load $q = 8 \text{ kN/m}^2$ compared to analytical values.

3.2 Comparison between the two systems

Since the geometrical dimensions of the beams were different for the two specimens, it does not have any sense to compare the loads reached and the stiffness obtained. Figure 3.17 shows the efficiency trend related to the load q . As conclusion, it is remarked that both systems had shown a rigid behavior, if related to normal floor-loads evaluated at SLS. The most important result concerns the huge bending stiffness of the systems, whose efficiencies were near to 1.

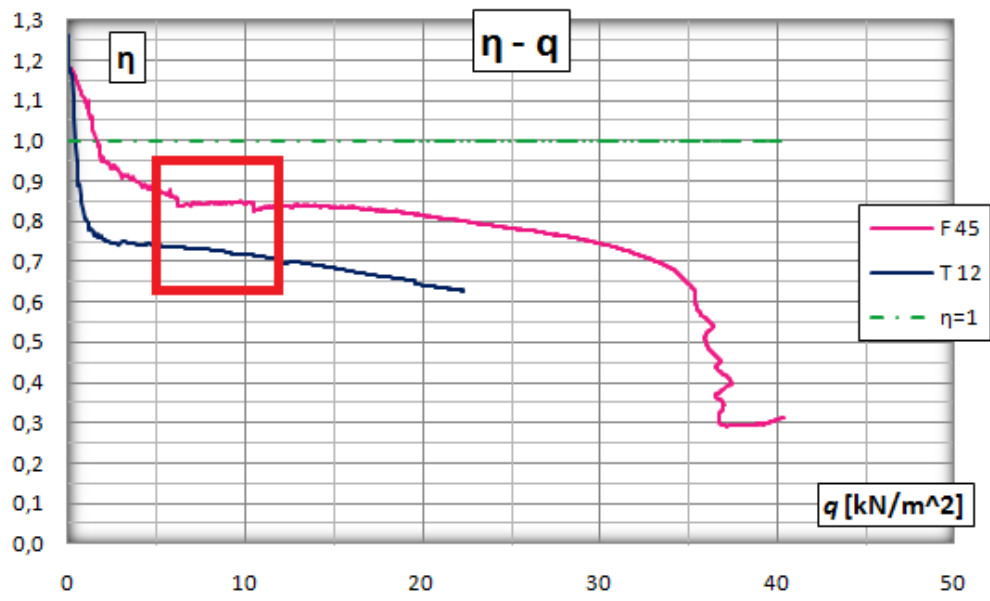


Figure 3.17: Comparison between system efficiency. The red square indicates the field of interest for an apartment or office floor.

Chapter 4

Timber-to-concrete connection with inclined screws

This chapter presents an innovative connection system for prefabricated timber-concrete composite beams. In order to investigate the behaviour of this system three nominally identical composite beams were tested at Lund University, Sweden.

4.1 Innovative connection system

An innovative connection system to connect concrete slab to timber beams has been studied at Lund University in collaboration with the University of Trento and here is presented. It regards the possibility to join timber beams to concrete slab with self-tapping full-threaded screws driven at an angle of 45° into the wood.

After the studies presented in previous chapters, it is thought that the use of only inclined screws could be enough to reach good composite action, especially looking at the results from T12 connection tests. Even if this kind of connection had special steel tubes, these were only used for support steel washers, which have the aim to spread compression stress when screws were subjected to tension. Naturally, this special steel tubes involve additional cost so it was thought to eliminate it in order to make this system more effective. In this way, it is lost the chance to join the slab to the beams on-site, which instead is required for only the prefabricated slabs with the previous types of connectors where for the industrialization point of view, especially for new buildings means save times and money.

To verify if the head of the screws used, which were $\phi 11 \times 250$, is enough to explicate the concrete cone break and to satisfy load conditions, some withdrawal tests were conducted of screws with different depths in the cubic specimens made of concrete. Withdrawal tests are reported in chapter 7. This type of connection system is not new for composite structures which use “wet” or traditional systems. On these applications there are lots of studies, experimental tests and examples. The innovation is to use it

in “full-prefabricated” composite timber-concrete structures. With “full prefabricated” word it is intended that concrete slab and timber beam are connected each other off-site, and this means that on-site it just needs to bring the composite beam and to put it in place. From an industrialization point of view, this allows to be more precise, to have more quality control, rapid manufacture and erection, saving time on-site and, of course, saving money.

Figure 4.1 shows the details of the screw in the composite structure.

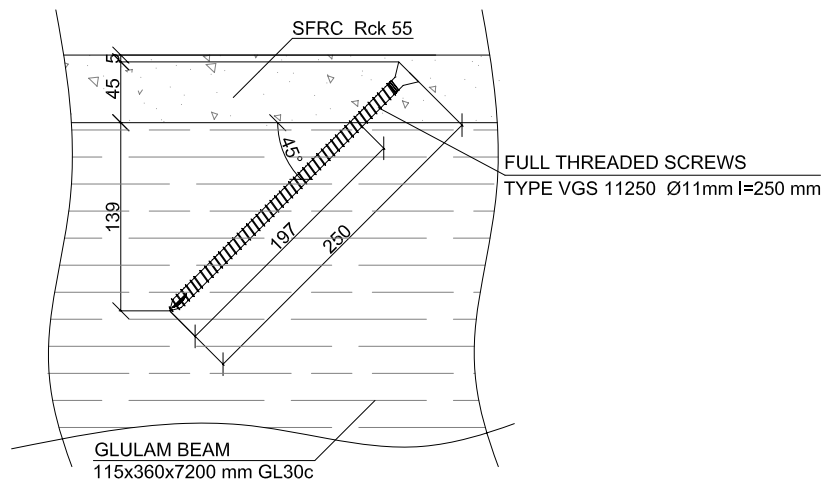


Figure 4.1: Details of inclined screw inserted in composite structures.

It has been chosen to use inclined screws at an angle equal to 45 degrees respect to the longitudinal direction of the beam because in this way the screw works in shear and tension, and more stiffness is achieved. On the other hand, if it is inserted perpendicular to the longitudinal direction of the beam, the screw carry just shear force and the connections is less stiff.

In order to better understand how the screw is working, Figure 4.2 shows the static principle of the connection. The shear force V is transferred from the concrete slab to the timber beam both by shear action F_v , in the direction of the force V , and by tensile action F_{ax} in the direction of the screw axis. In the wooden part, shear is resisted by embedment capacity of the wood, while tension is resisted by withdrawal capacity. In the concrete slab, shear is resisted by contact pressure between the screw and the concrete, while tension force in the screw is resisted by withdrawal capacity in the concrete. Due to the inclination of the screws, compression stresses will develop at the interlayer between timber and concrete. Such compression stresses generate friction between the two materials, which also contribute to increase the stiffness and the strength of the timber-concrete connection.

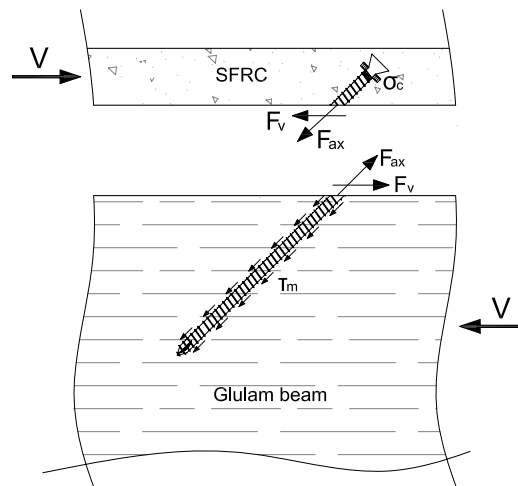


Figure 4.2: Static principle of screwed screw used.

To realize this type of connections, fibre reinforced concrete is recommended. If using normal concrete, in a long-term period it could present problems related to the shrinkage from the concrete and the creep from both timber and concrete materials. If only the slab is prefabricated, as previously presented in chapter 3, the shrinkage can occur freely and so when it is join to the timber beam on-site, it has realized the most part of its effects. Therefore, this way it will not produce significantly internal tension state in the timber beam. In this system, thus it is full prefabricated, shrinkage occurs and using normal concrete it can create an internal stress state which can crack the concrete. To avoid this, it has to use a special kind of concrete, named steel-fibre reinforced concrete (SFRC). Fibres can be realized from different materials, but in this case it was decided to use steel Fibres. In the following sections materials used to manufacture the specimens and more details will be described. Thus, when shrinkage will occur, as long as concrete has a little crack, the steel fibres will immediately act in concrete. This is the way thought to solve shrinkage effects. In fact, as it was possible to check after the curing of concrete, after around 1 month and a half from the date of the concrete casting, for the specimens which are tested to check the short-term behavior, no cracks were visible.

4.2 Design of timber-concrete composite beam

4.2.1 Geometries and materials

Figure 4.3 shows the draw which includes: longitudinal, transversal and plan views for the timber-concrete composite beam. The dimensions of the slab, are given from the particularly case study , i.e. related to the stands of a stadium,

TIMBER - CONCRETE COMPOSITE BEAM

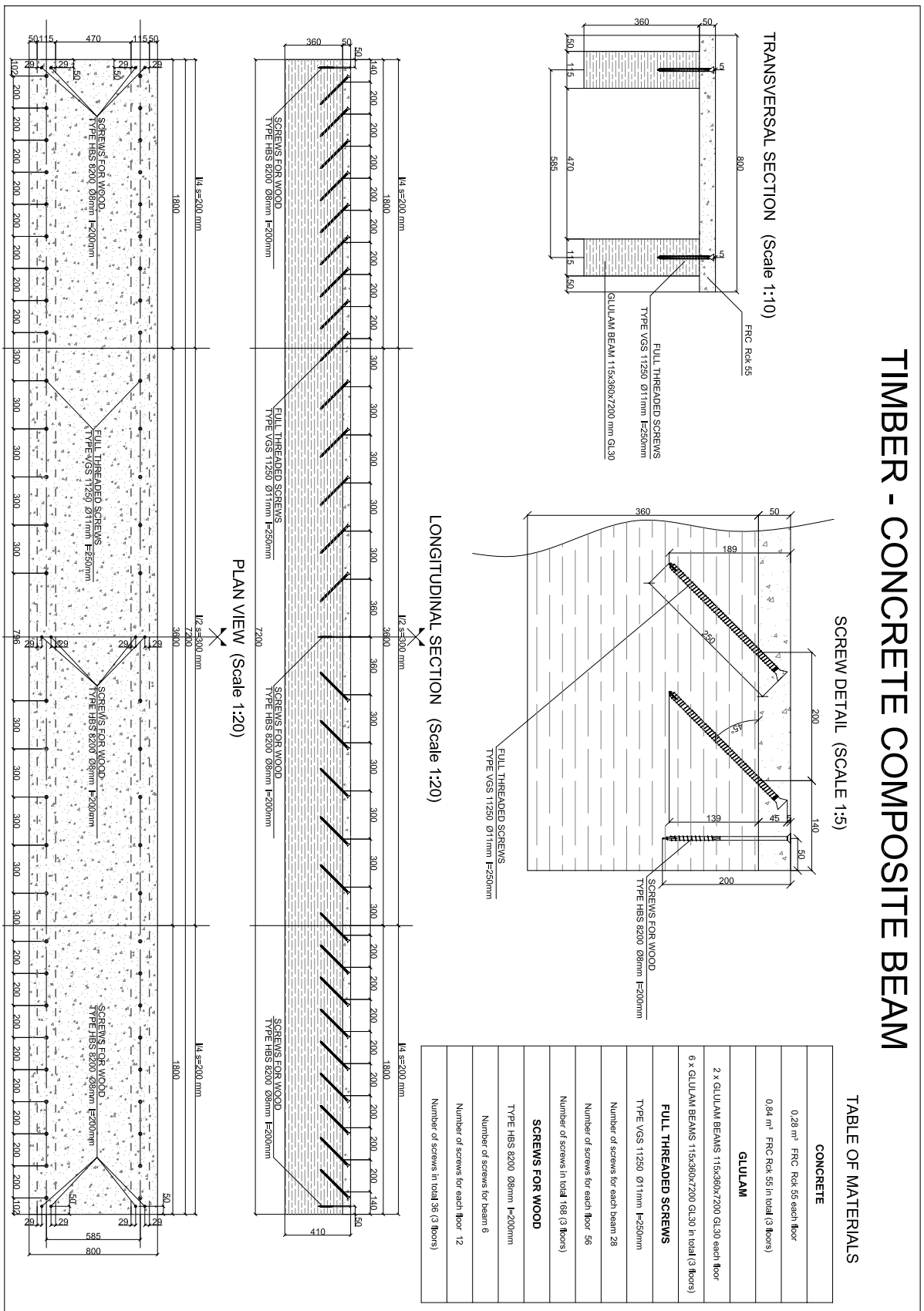


Figure 4.3: Design of the timber-concrete composite beam.

see in Appendix. In particular, width of the concrete slab is 800 mm. Width of timber beams is also given and in particular it is equal to 115 mm. As far as the thickness of the slab and the depth of the timber beam is concerning, they have been decided after an attention discussion over results from a numerical model presented in chapters 6. All discussions over these dimension choices are explained in the relative chapter as well. After FEM analysis, it has been chosen to use for the slab thickness 50 mm and for timber beam 360 mm depth. Another crucial parameter was also the spacing between the screws. This is discussed afterwards in the relative chapter 6. As results from FE model and after an accurate discussion, it has been chosen to use a spacing between screws equal to 200 mm for an extension length from the supports equal to $l/4 = 1800$ mm. In the middle part of the beam, for a length equal to 3600 mm, the spacing was equal to 300 mm, see Figure 4.3. In table of materials are summarized the quantity of materials needed to built out a single composite beam and for all of them.

4.2.1.1 Full-threaded screws

The screw used to realize the connection between the concrete slab and the timber beams are self-tapping full-threaded screws, type $VGS\phi 11 \times 250$ mm as shown in Figure 4.4. The number of screws for each single timber beam was 28, and thus, 56 screws for each floor system.



Figure 4.4: Longitudinal view of the screw.

Figure 4.5 and Table 4.1 report the details of the $VGS\phi 11 \times 250$ mm screws.

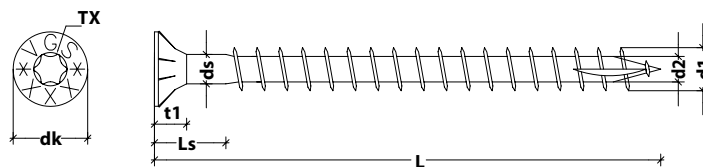


Figure 4.5: Details of VGS screws.

Description	Symbol	Dimension
Major diameter	d_1 [mm]	11
Head diameter	d_k [mm]	19, 30
Core diameter	d_2 [mm]	6, 60
Shank diameter	d_s [mm]	7, 70
Threaded length	$L - L_s$ [mm]	250 – 35
Head thickness	t_1 [mm]	8, 20
Screw length	L [mm]	250
Torx	TX	50
Characteristic yield moment	$M_{y,k}$ [Nm]	45, 90
pre-drilling hole diameter	d_p [mm]	7, 00

Table 4.1: Characteristic dimensions of the VGS screw.

4.2.1.2 Glulam beams

Structural timber used for beams is glued laminated timber GL30c. Below the characteristic values of strength, elastic moduli and density are reported, given by prEN14080:2011, see [31]. Each glulam beam consists of 8 lamellae each one characterized by a depth of 45 mm. For the manufacturing the specimens two glulam beams have been used.

Description	Symbol	Value
Bending strength	$f_{m,g,k}$	30 MPa
Tensile strength parallel to the grain	$f_{t,0,g,k}$	20 MPa
Tensile strength perpendicular to the grain	$f_{t,90,g,k}$	0, 5 MPa
Compressive strength parallel to the grain	$f_{c,0,g,k}$	25 MPa
Compressive strength perpendicular to the grain	$f_{c,90,g,k}$	2, 5 MPa
Shear strength	$f_{v,g,k}$	3, 5 MPa
Mean elastic modulus parallel to the grain	$E_{0,g,mean}$	12500 MPa
Charac. elastic modulus parallel to the grain	$E_{0,g,0,05}$	10417 MPa
Mean elastic modulus perpendicular to the grain	$E_{90,g,mean}$	300 MPa
Tangent modulus	$G_{g,mean}$	650 MPa
Mean specific gravity	$\rho_{g,k}$	390 kg/m ³
Characteristic specific gravity	$\rho_{g,mean}$	420 kg/m ³

Table 4.2: Characteristic strength and elastic moduli.

The moisture content of each timber beam was estimated. For such a purpose, two measurements were performed (at a distance approximately L/4 from each extremity side) for each beam by pushing two needles of an electrode device into the wood for a deep approximately equal to 15 mm. To estimate the moisture content it has

been calculate the average value for each beam as reported in Table 4.3. The three full-scale specimens are called A, B and C while the glulam beam used for each floor system are called A1, A2, B1, B2, C1, C2, respectively. The average value of the timber beams is reported in the last column of Table 4.3.

ID glulam beam	Moisture content		Average value [%]
	1 measurement [%]	2 measurement [%]	
A1	10,2	10,0	10,1
A2	10,9	10,1	10,5
B1	10,6	10,4	10,5
B2	9,4	10,2	9,8
C1	10,6	10,7	10,7
C2	10,5	10,8	10,7

Table 4.3: Moisture content in the glulam beams.

4.2.1.3 Steel-fibre reinforced concrete (SFRC)

The fibre reinforced concrete used in the experimental tests is classified as C45/55 with steel fibres. Compression tests on three cubic specimens of sizes 15x15x15 cm have been performed in order to check the mechanical properties of the concrete. Results of compression tests have been reported in chapter 7. It is worth to point out the reason of the use of fiber reinforced concrete. The main issues of a composite system like these in object are due to long-term actions as shrinkage of concrete and creep of both elements, timber and concrete. To face this problem a great alternative is made up by using fibre reinforced concrete, in which the reinforce is formed by steel fibres (but it is possible to find also different type of fibres) which start working when the first cracking originates in concrete. Furthermore, these fibres contribute in improving the strength parameters of the material with benefits on the composite system behavior.

The slabs of each specimens have been realized by using steel fiber reinforced concrete. The ingredients used to prepare 1 m³ of SFRC concrete are reported in Table 4.4.

Ingredients	Quantity
Fibre reinforced concrete slab	45 kg/m ³
Cement	480 kg/m ³
Water	190 L/m ³
Inert	n.d.
Fluidifying	n.d.

Table 4.4: Ingredients used to prepare 1 m³ of SFRC concrete.

As far as steel fibre is concerned, it was used steel fibres type ZP 30/0,40, where 30 means the length of the fibres in mm and 0,40 is the diameter of the fibres, and $l/d = 30/0,40 = 75$ is the aspect ratio of the fibres. Figure 4.6 shows the shape of the fibres.

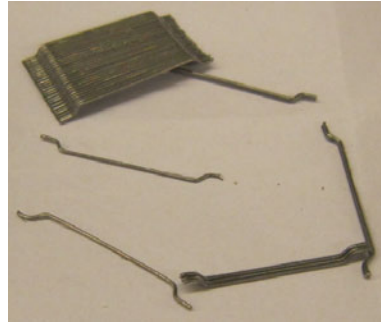


Figure 4.6: Shape of the steel fibres.

4.3 Timber-concrete composite beam assembly

In order to build out this kind of timber-concrete composite beam from an industrialization point of view and to make the production easy and fast, and also to reduce development costs a specific mount path should be followed. The construction sequence thought to achieve the aims abovementioned is here presented.

The first step, after the glulam beams have been realized with the appropriate sizes, is to tight the screws in the glulam beam with the correct inclination (in this case it is 45 degree) spacing and penetration depth that in this case it is 139 mm, as given in Figure 4.7. With regard to the spacing between screws it is not constant according to Figure 4.3.

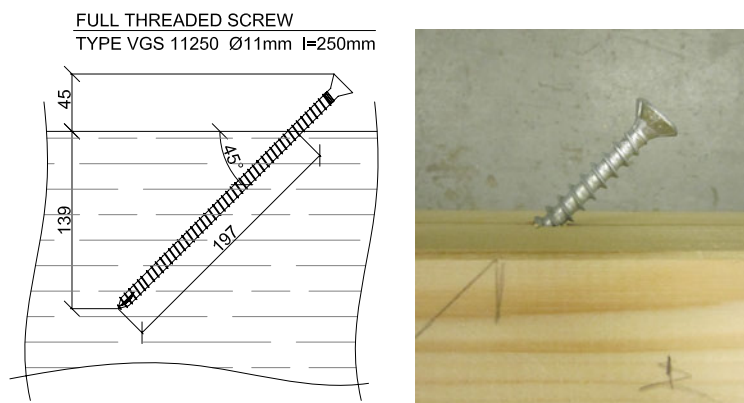


Figure 4.7: First step: screws installations in the glulam beam. Details of installation on the left and results of installation on the right.



Figure 4.8: Timber beams with inserted the screws at an angle of 45 degree.

The second step consists in preparing the formwork for casting the concrete. The internal sizes of the formwork should be the same as the slab dimensions. In this case, the width of the slab is 800 mm, the length is 7200 mm and the thickness is 50 mm. Figure 4.9 shows how the formwork for the concrete slab has been done for this case.

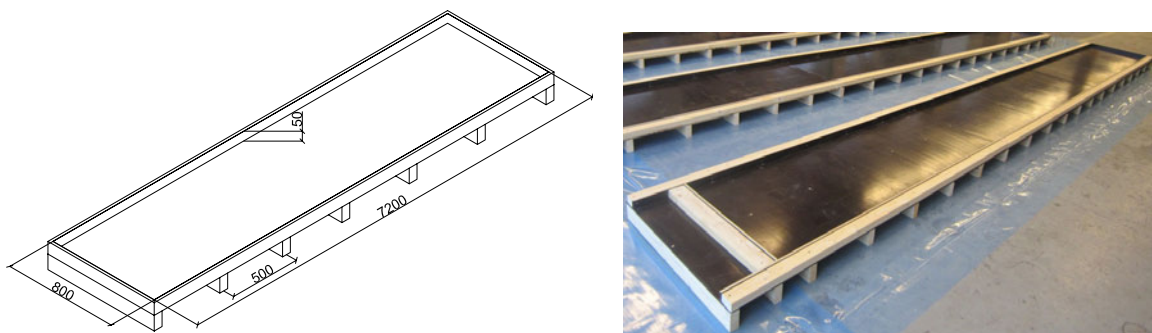


Figure 4.9: Second step: formwork before casting concrete.

In order to give strength against the self-weight during the rotation and the lifting of the slab, four rows of fibre-glass bars with diameter equal to 5 mm along the length of the system have been inserted, see Figure 4.10.

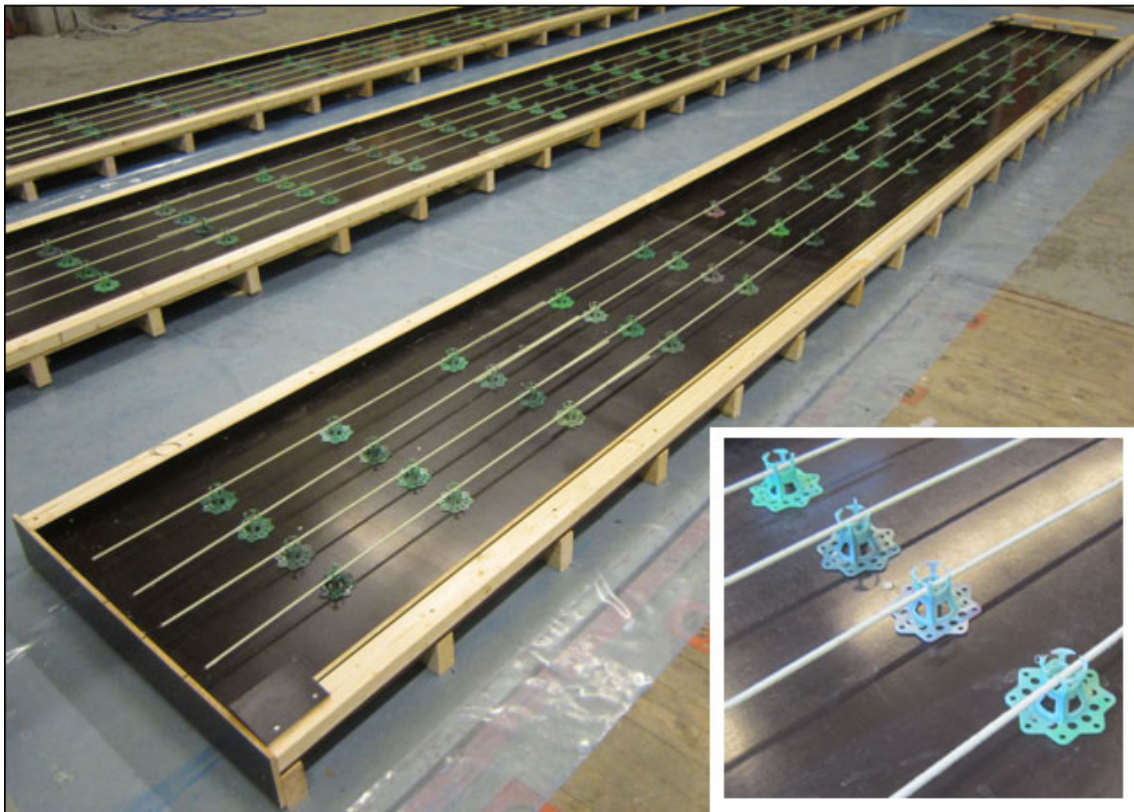


Figure 4.10: Longitudinal fibre-glass bars and final details of preparation of the formwork.

The third step consists by preparing a system composed of two glulam beams with the correct spacing and temporary connected with transversal and diagonal planks as shown in Figure 4.11, in order to lift the all system with a crane and to insert it from the top side in the formwork as soon as the concrete is cast.



Figure 4.11: Third step: system composed of two glulam beams.

The fourth step has to follows as soon as possible. In particular, immediately after the concrete casting, the system of glulam beams with screws driven on the bottom

side, has to be lifted by a crane and inserted into the concrete formwork. The screws have to be positioned in the underpart of beam as it is shown in Figure 4.12.

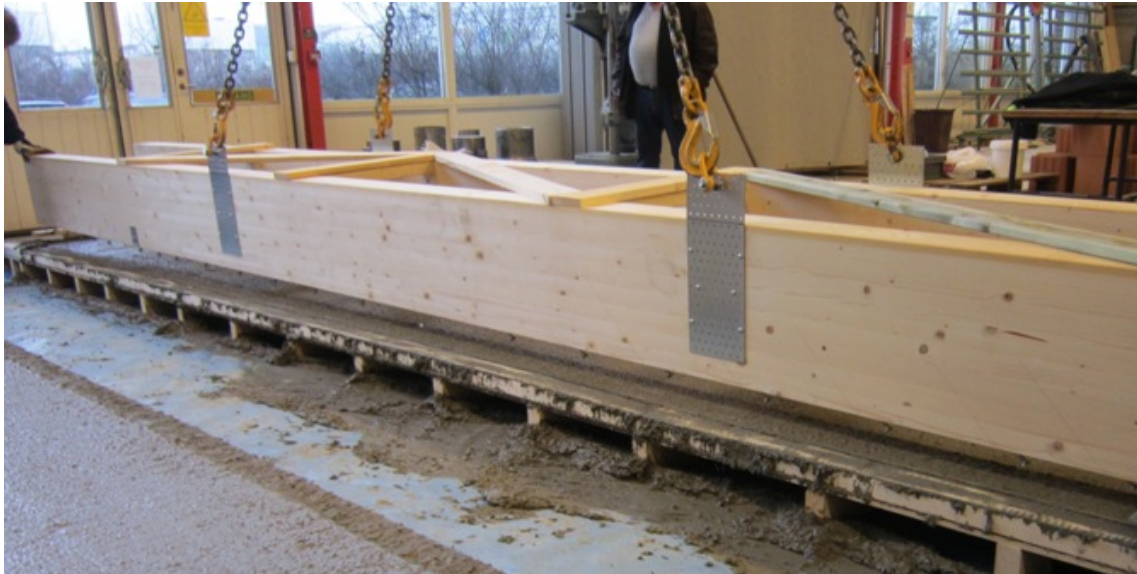


Figure 4.12: Fourth step: inserting the system of glulam beams into the fresh concrete slab.

In order to avoid that inclined screws can touch with the lower part of formwork, in the glulam beams are also screwed some different screws, type HBS 8200 with the necessary depth. In order to avoid the trouble the depth was 50 mm equal to the depth of the slab, as shown in Figure 4.3. Details about screw and penetration depth are reported in Figure 4.13

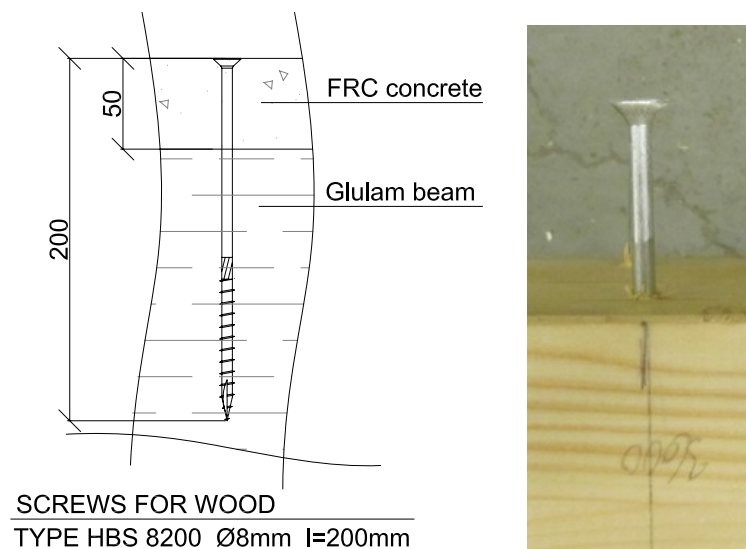


Figure 4.13: Details of service screws HBS 8200.

The fifth step, after the assembly, is to wait for the time needed by the concrete to

become hard and stiff. For usual concrete the time needed to mature is considered 28 days. The cast of the concrete has been done on December the 7th in the laboratory of the University of Lund (LTH). Figure 4.14 shows the end of the assembly phase.

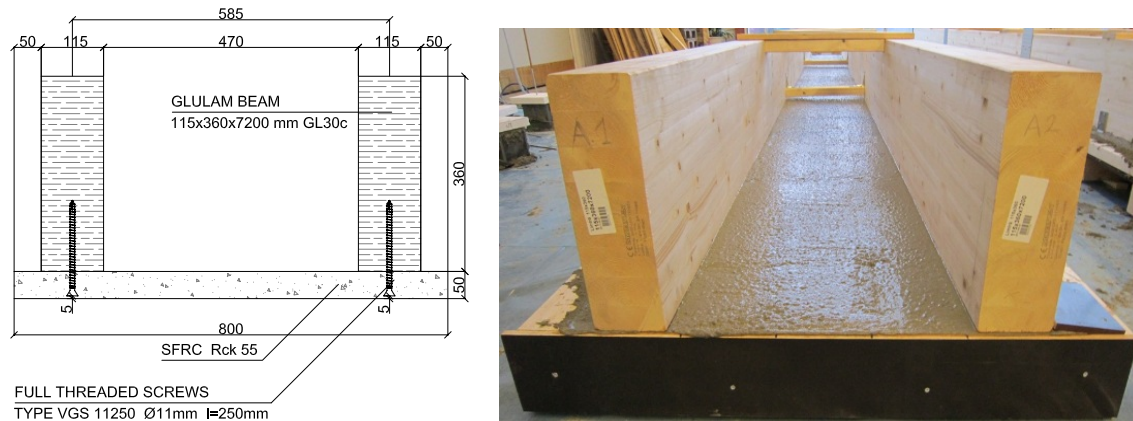


Figure 4.14: Fifth step: end of assembly phase.

The last important phase, after curing of the concrete, is to take the composite beam and to twist it for 180 degrees in order to get the right position as it is on-site, i.e. concrete slab on the top side and glulam beams at the bottom side. This is the peculiarity of the method thought for this system in order to build out timber-concrete composite beams quickly and easily. This twist has to be done with particular attention in order to not damage the composite beam. The solution which has been adopted was by using two appropriate steel frames fixed on both the extremity of the structure. Through these two special steel frames, and thanks to a crane, the beams have been lifted from their centre of gravity and rotated by hand in the air. The whole procedure is shown in Figure 4.15. The rotation of the composite beams has been done one week later the cast of concrete, precisely on December the 14th. It is worth to point out that all this movement should be done carefully and with the required safety criteria.

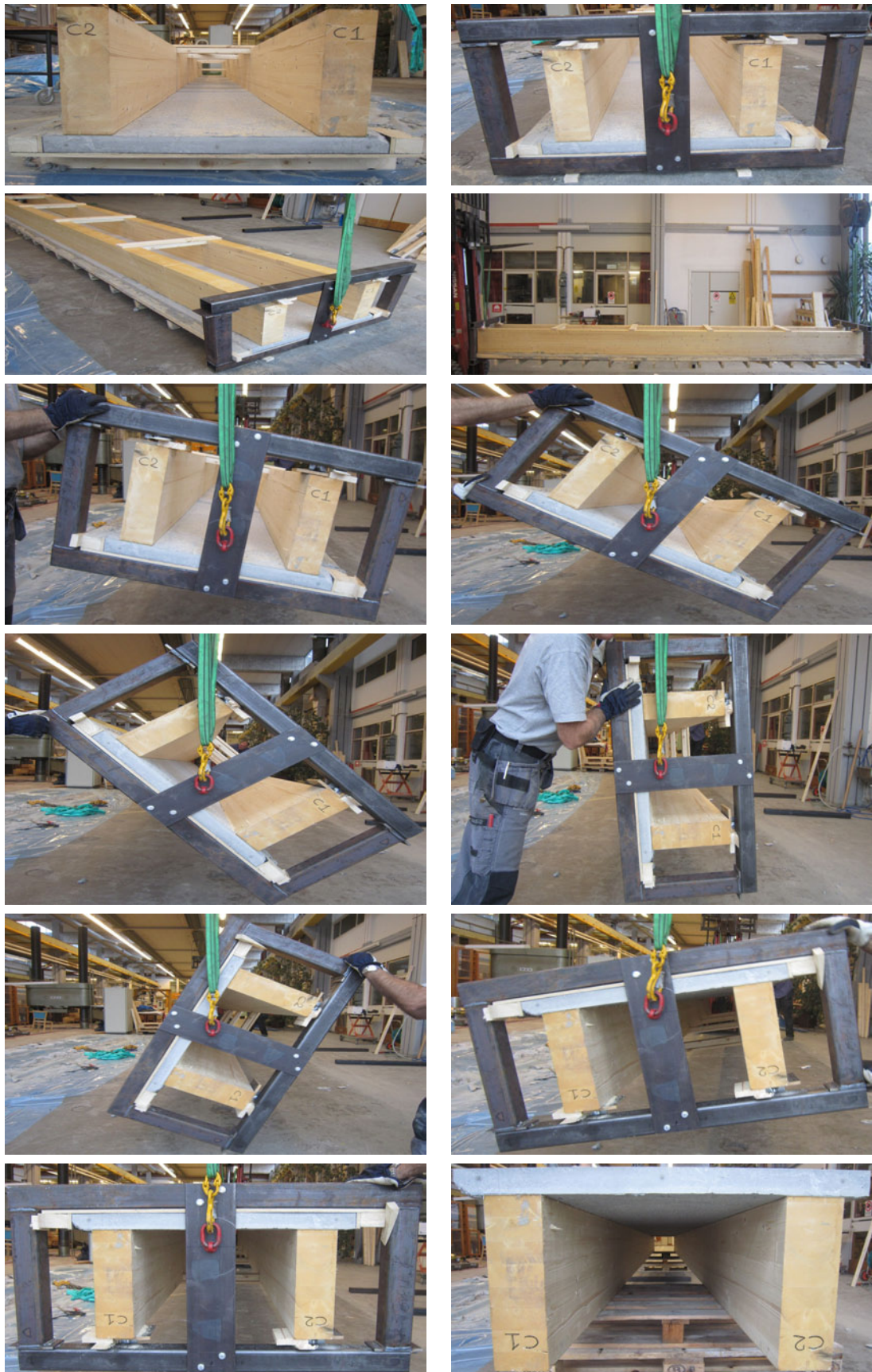


Figure 4.15: Sequence of rotation used to twist the composite structures.

Figure 4.16 and Figure 4.17 show the final position of the composite structures till the date of the experimental tests. The specimens have been maintained in this position for 41 days. The date of the first bending test was on January the 24th, and the other bending test has been performed on January the 26th. For more details see chapter 7, related to the experimental tests.

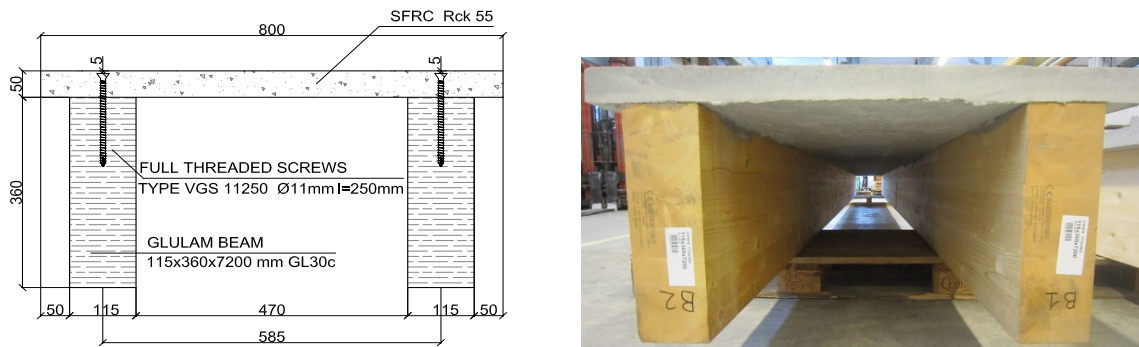


Figure 4.16: Final position of the composite beams before placing them on-site.



Figure 4.17: Composite beams stored in the laboratory of Lund.

The three equal specimens have been called as A, B and C beam (Table 4.5).

ID	Total length [mm]	Total width [mm]	Connection spacing [mm]	Width of the beam [mm]	Depth of the beam [mm]	Thickness of the slab [mm]	Beam spacing [mm]
A	7200	800	200+300+200	115	360	50	585
B	7200	800	200+300+200	115	360	50	585
C	7200	800	200+300+200	115	360	50	585

Table 4.5: Details of each specimen.

Chapter 5

Theory of composite structures with deformable connection

This chapter presents the classical theoretical model of composite structure. Particular attention is focused on composite structure with flexible connection system. This chapter also presents the γ – *method* that has been developed for predicting the behavior of composite systems with incomplete composite action between concrete and timber layers.

5.1 Generality

Considering elements with sections of increasing height, it is known that characteristics of inertia improve. In particular, the moment of inertia increase and thus the structural element behavior changes, where for same geometry and load conditions, it deforms less and resists to larger external stress. When, for a single timber element, it is not convenient to go beyond a certain height, a solution could be the coupling of two or more separate timber elements, or mating with the other material with higher stiffness and strength. In all solutions that adopt one of these strategies, the obtained result is to increase the mechanical point of view of the eccentric portions of the section than the overall centre of gravity, and therefore to increase the static efficiency of composite elements. In composite membering the connection between the various parts can be achieved by bonding (chemical adhesion between the surfaces) or implemented through the use of various types of mechanical connectors (pins, dowels, bolts, screws, nails). As it might guess, in the case of unions realized by means of gluing, the final stiffness is generally characterized by higher values (with the same geometric conditions) than it will be observed in the case of elements connected mechanically.

5.1.1 Structures and composite beams with deformable connection

The coupling of multiple structural elements operating in bending, allows to create composite structures. The efficiency of the composite structural element is much higher when the stiffness of connection systems is high (i.e. the reduced displacements between the contacting surfaces of the component element are prevented): the static behavior of real composite structure will therefore be between two extreme cases of no stiffness (i.e. no shear connections, $k = 0$) and infinite stiffness (rigid connection with prevented slip $k = \infty$). The parameter k defines the specific stiffness (per unit length) of the connection system, assuming that its effect can be thought distributed along the axis of the beam even when is used a point connection type.

To manufacture timber-concrete composite systems with high degrees of composite action, the shear between the timber beam and the concrete slab needs to be transferred effectively through the shear connector system. Therefore, the shear connectors are key elements of a composite system, which require particular attention since they determine the system's performance parameters. There are thus two bounds of composite action:

- a lower bound of fully non-composite action, displayed by timber and concrete layers that are not connected and thus work independently, with no transfer of horizontal force between the two layers via either mechanical bonds or friction. The layers have individual neutral axes and there is discontinuous flexural strain at the timber-concrete interface.
- an upper bound of fully composite action, displayed by timber and concrete components that are rigidly connected with no interlayer slip, have cross sections with a single neutral axis and identical flexural strains at the timber-concrete interface. Consequently, the transformed section method can be validly applied to analyse stress in such systems.

The timber and concrete layers are connected by mechanical fasteners in most cases (and/or in few cases by adhesives). In reality the shear connection system is deformable and most connectors generate at least some horizontal movement (“slip”) at the interface. Such behavior is referred to as “partial composite action”. The neutral axis splits and as the slip between the layers increases the two neutral axes move farther apart, hence the slip between the timber beam and the concrete slab reduces the efficiency of the cross section. It is difficult to achieve a rigid connection between timber and concrete, but a low slippage is advantageous, allowing the redistribution of shear stresses along the shear connectors.

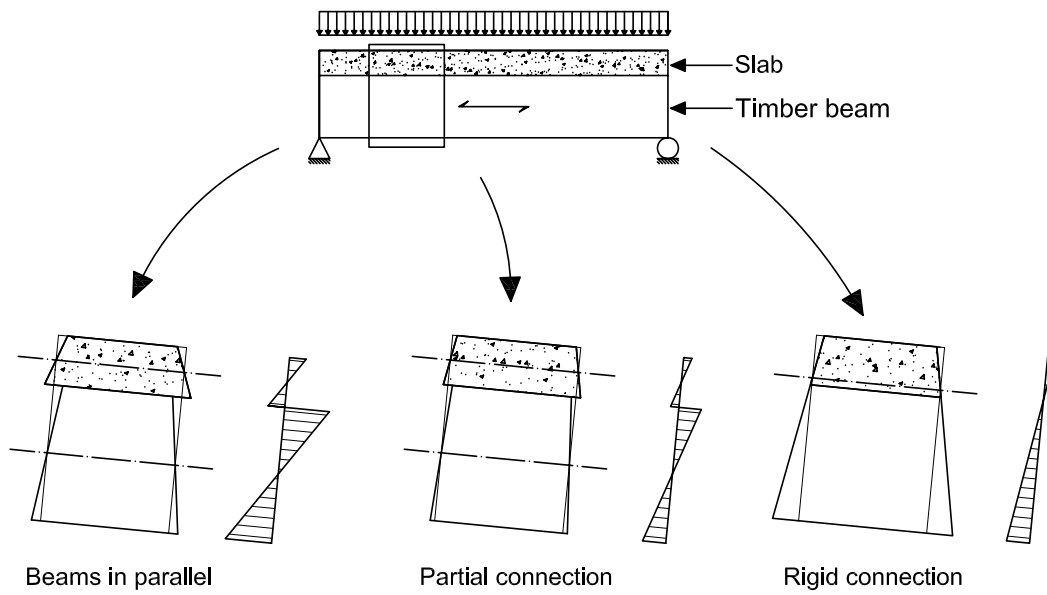


Figure 5.1: Distribution of bending deformations in a composite beam as a function of the connection stiffness (Ballerini et al. 2002).

In borderline cases of no stiffness and infinite stiffness, stress and strain states can be determined based on the classical theory of bending elements, or rather considering the hypothesis of Bernoulli on conservation of the plain section which gives rise to the well-known relationship between acting moment and curvature of the beam:

$$\chi = -\frac{M}{EJ}$$

In the extreme case of no rigidity, sections of the individual beam components are preserved, while in extreme case of infinite stiffness is the composite section which is maintained plain.

5.1.2 Extreme case of no rigidity

In the situation of no composite action, i.e. when the generic global section of beam does not remain plane, the stress and strain state of composite structures will be shown in Figure 5.2 and also in [12]. For the transversal displacement congruency, the two beams have the same curvature in the same initially sections with the same abscissa x , measured from one end of the beam, see Figure 5.3.

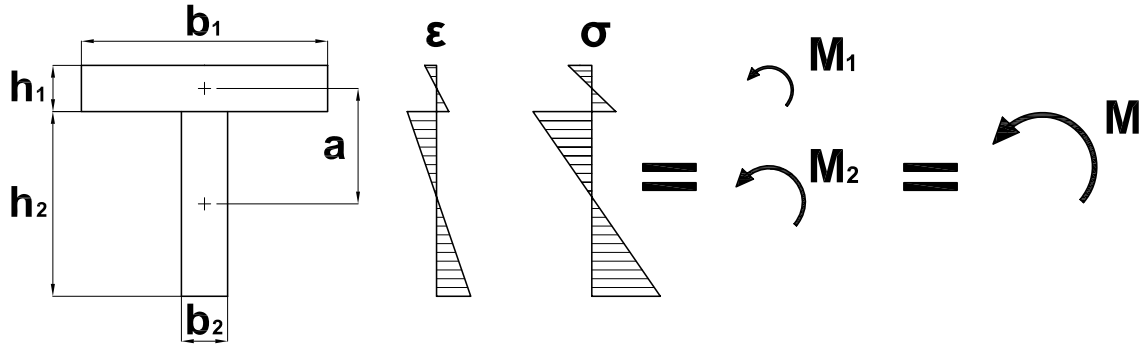


Figure 5.2: Bending strains and stresses of a composite beam with no composite action.

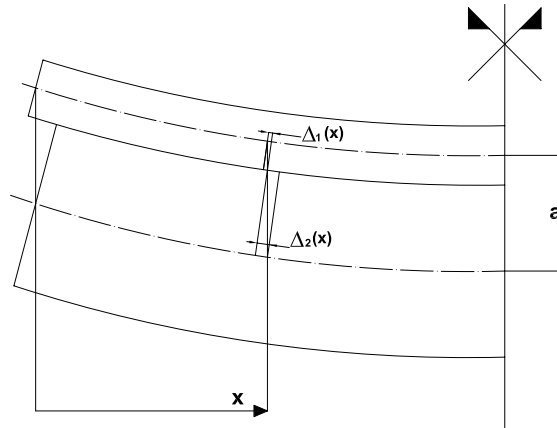


Figure 5.3: Calculation of the interface slip.

$$w_1'' = w_2'' = w'' = -\frac{M_1}{E_1 J_1} = -\frac{M_2}{E_2 J_2} = -\frac{M}{(EJ)_0} \quad (5.1)$$

Consequently, the system can be seen as two beams working in parallel, and the bending stiffness of composite beam can be calculated as follows:

$$(EJ)_0 = \sum_i E_i J_i = \frac{1}{12} (E_1 b_1 h_1^3 + E_2 b_2 h_2^3) \quad (5.2)$$

In the two beams, the external moment $M(x)$ is distributed in proportion to the stiffness. In fact, considering the assumption of congruence and considering valid the hypothesis of maintenance of the plane sections in the individual elements bending

the external moment is obtained as:

$$M(x) = M_1(x) + M_2(x) \quad (5.3)$$

Thus, it can be found easily the values of M_1 and M_2 (external moments for the two sections) in function of M (external moment):

$$M_1(x) = \frac{E_1 J_1}{(EJ)_0} M(x)$$

$$M_2(x) = \frac{E_2 J_2}{(EJ)_0} M(x)$$

From these relations it can be easily determined the stress state in the two inflected elements:

$$\sigma_{1,max} = \frac{M_1}{W_1} = \frac{E_1}{(EJ)_0} \cdot \frac{h_1}{2} \cdot M(x) \quad (5.4)$$

$$\sigma_{2,max} = \frac{M_2}{W_2} = \frac{E_2}{(EJ)_0} \cdot \frac{h_2}{2} \cdot M(x) \quad (5.5)$$

In situation of no composite action, the interface slip can be evaluated as:

$$\delta(x) = \Delta_2(x) + \Delta_1(x)$$

$$\delta(x) = \int_x^{l/2} \frac{h_2/2}{(EJ)_0} \cdot M(x) dx + \int_x^{l/2} \frac{h_1/2}{(EJ)_0} \cdot M(x) dx = \frac{a}{(EJ)_0} \int_x^{l/2} M(x) dx \quad (5.6)$$

In the special case of simply supported beam with uniformly distributed load on the entire span it is obtained:

$$\delta(x) = \frac{q \cdot a}{24(EJ)_0} (l^3 - 6lx^2 + 4x^3)$$

For symmetry reasons the slip is null in mid-span and maximum at the supports. The mid-span deflection can be calculated as:

$$\delta_{max} = \frac{q \cdot a \cdot l^3}{24 \cdot (EJ)_0}$$

5.1.3 Extreme case of infinite stiffness

In the case of fully composite action, as it can be seen in [12], the generic global section of composite beam remains plain without slips at beam-slab interface. Compared to the previous limit case, the external moment $M(x)$ turns out to be balanced, as well as the moment M_1 and M_2 , also from the couple offered by the axial action N_1 and N_2 . The stress and strain of the composite section will thus similar to the one shown in Figure 5.4.

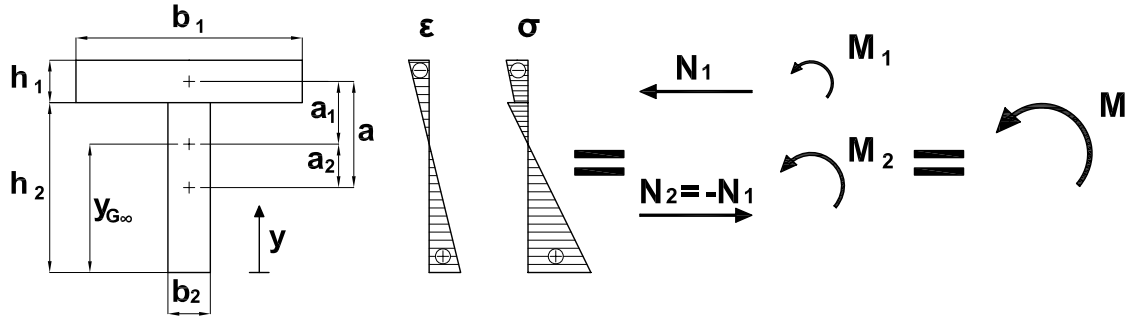


Figure 5.4: Bending strains and stresses in a composite beam with rigid connection.

It can be calculated the centre of gravity of the global section (weighted with the relative modules of elasticity of the materials), from the lower edge, as follows:

$$y_{G\infty} = \frac{E_1 A_1 \left(h_2 + \frac{h_1}{2} \right) + E_2 A_2 \frac{h_2}{2}}{\sum_i E_i A_i} = \frac{h_2}{2} + \frac{E_1 A_1}{\sum_i E_i A_i} \cdot a$$

The distance from the individual centre of gravity of single elements to that of the entire section are:

$$a_1 = h_2 + \frac{h_1}{2} - y_{G\infty} = \frac{E_2 A_2}{\sum_i E_i A_i} \cdot a = \frac{(EA)_0}{E_1 A_1} \cdot a \quad (5.7)$$

$$a_2 = y_{G\infty} - \frac{h_2}{2} = \frac{E_1 A_1}{\sum_i E_i A_i} \cdot a = \frac{(EA)_0}{E_2 A_2} \cdot a \quad (5.8)$$

where:

$$(EA)_0 = \frac{E_1 A_1 \cdot E_2 A_2}{\sum_i E_i A_i} = \frac{1}{\frac{1}{E_1 A_1} + \frac{1}{E_2 A_2}} \quad (5.9)$$

The bending stiffness of the composite section can then be calculated using the transposition theorem, where $(EJ)_0$ is the bending rigidity of the system with null connection stiffness:

$$(EJ)_\infty = \sum_i E_i J_i + \sum_i E_i A_i a_i^2 = (EJ)_0 + (EA)_0 \cdot a^2 \quad (5.10)$$

It can be therefore derived the maximum stresses using the following equation:

$$\sigma_{i,max} = \frac{M(x)}{EJ_\infty} \cdot E_i \cdot z_i = \frac{M(x)}{EJ_\infty} \cdot E_i \cdot \left(a_i + \frac{h_i}{2} \right) \quad (5.11)$$

Alternatively, the stresses in the two component elements can be derived from three distinct stresses which for equilibrium must satisfy the following relationship:

$$M(x) = M_1(x) + M_2(x) + N(x) \cdot a \quad (5.12)$$

and considering the hypothesis of congruence $w_1'' = w_2'' = w''$, it can be derived:

$$M_1(x) = \frac{E_1 J_1}{(EJ)_\infty} M(x) \quad (5.13)$$

$$M_2(x) = \frac{E_2 J_2}{(EJ)_\infty} M(x) \quad (5.14)$$

Combining the Equation (5.12) with (5.13) and (5.14), it can be obtained the following expression for the normal axial load N_1 or N_2 , unless the sign:

$$N(x) = N_\infty(x) = \frac{(EA)_{0 \cdot a}}{(EJ)_\infty} \cdot M(x) \quad (5.15)$$

and thus it can be derived the maximum stresses means the following equation

$$\sigma_{i,max} = \frac{N}{A_i} + \frac{M_i}{W_i} = \frac{M(x)}{(EJ)_\infty} \cdot \left(E_i \cdot \frac{h_i}{2} + E_i a_i \right)$$

The shear stress at the slab-beam interface is calculated by derivation of the axial force:

$$v_{s\infty}(x) = N'_\infty(x) = \frac{(EA)_0}{(EJ)_\infty} \cdot a \cdot \frac{dM(x)}{dx} = \frac{(EA)_0}{(EJ)_\infty} \cdot a \cdot V(x)$$

Alternatively, the same result is obtained with the well-known formula of Jourawsky

$$v_{S\infty}(x) = \tau \cdot b = \frac{V(x)}{(EJ)_\infty} \cdot S_1 = \frac{V(x)}{(EJ)_\infty} \cdot E_1 A_1 \cdot a_1 = \frac{V(x)}{(EJ)_\infty} \cdot (EA)_0 \cdot a$$

5.2 Composite structures with semi-rigid connections

For intermediate situations than those previously presented, where beams are mechanically jointed through a deformable connection, the bending-theory for beams is no longer applicable because of the slip in the joints. Due to the relative slip between beam and slab, the real static behavior of the composite structure can be traced back to the pattern of two parallel beams mechanically jointed. Anyway, the theory is applicable to individual components. Analytical solutions are developed by using differential equations of equilibrium (Möhler, 1956 see [13]; Heimeshoff, 1987) or energy considerations and specially developed design programs are available, see for example Kneidl (1991). The general elastic treatment of this problem was provided by Newmark et al. (1951), see [14], with the following assumptions:

- linear-elastic behavior of the material and of the connection;
- small displacements and deformations (1° order theory);
- identical curvatures for slab and beam elements;
- conservation of plain sections for each element;
- connection is uniformly distributed along the beam;
- constant cross-section and stiffness along the direction of the beam's axis.

In the general treatment the connection is considered “uniform”: in the case of punctual connector with K stiffness, assumed identical and identically spaced with spacing s , this is the equivalent to consider a specific stiffness of the system equal to $k [F/L^2] = K/s = \text{constant}$. Nevertheless, it is quite common, for simply supported beams with uniformly distributed load, to vary the spacing of connectors between a maximum value s_{max} in the mid-span and a minimum value s_{min} at the supports: it can be referring to equivalent-spacing $s_{eq} = 0,75 \cdot s_{min} + 0,25 \cdot s_{max}$.

With reference to Figure 5.5, to [15] and according to the general treatment for the mixed problem with two elements [14], imposing the equilibrium equations for an infinitesimal element of length dx of composite beam, which results to be:

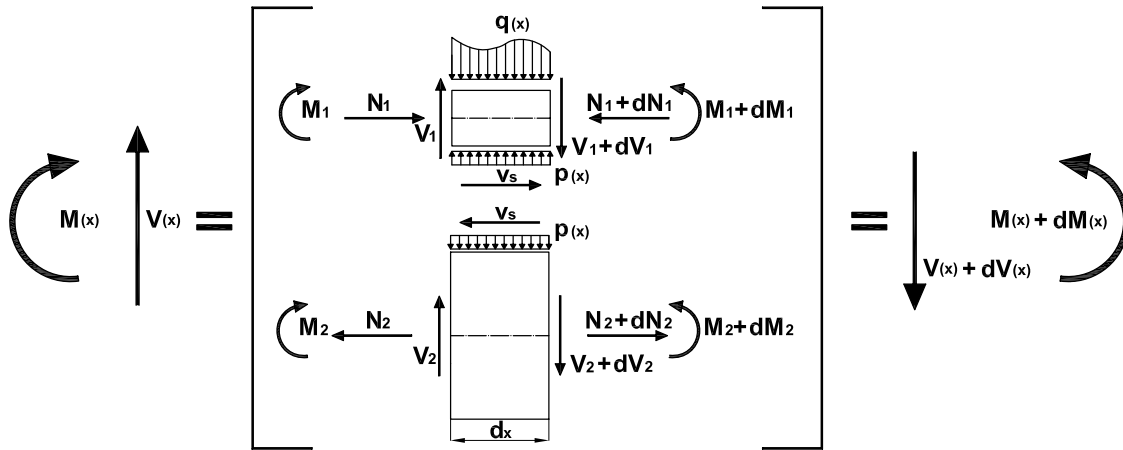


Figure 5.5: Composite beam with semi-rigid connectors. Equilibrium of an incremental element.

Equilibrium of internal actions

$$\begin{cases} N_1 - N_2 = 0 & (5.17) \\ V_1 + V_2 = V(x) & (5.18) \\ M_1 + M_2 + N_1 \cdot a = M(x) & (5.19) \end{cases}$$

Global equilibrium of the infinitesimal element

$$\begin{cases} V'(x) = -q(x) & (5.20) \\ M'(x) = V(x) & (5.21) \\ M''(x) = -q(x) & (5.22) \end{cases}$$

Equilibrium in the element 1

$$\begin{cases} N_1'(x) = +v_s(x) & (5.23) \\ V_1'(x) = (q(x) - p(x)) & (5.24) \\ M_1'(x) = V_1(x) - v_s(x) \cdot \frac{h_1}{2} & (5.25) \end{cases}$$

Equilibrium in the element 2

$$\begin{cases} N_2'(x) = -v_s(x) & (5.26) \\ V_2'(x) = -p(x) & (5.27) \\ M_2'(x) = V_2(x) - v_s(x) \cdot \frac{h_2}{2} & (5.28) \end{cases}$$

where $p(x)$ is the vertical load that the elements are exchanging.

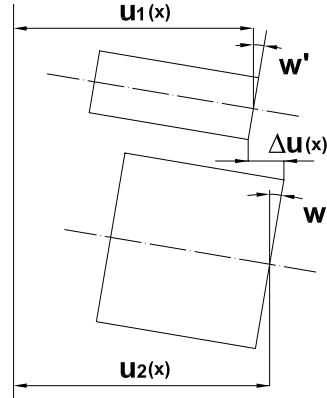


Figure 5.6: Deformation and displacement under bending moment in a composite beam.

The equations of congruence, remembering the previously assumption $w''_1 = w''_2 = w''$ (5.29) are:

$$\begin{cases} \Delta u(x) = u_2(x) - u_1(x) + w'(x) \cdot \frac{h_1}{2} + w'(x) \cdot \frac{h_2}{2} & (5.30) \\ \Delta u(x) = u_2(x) - u_1(x) + w'(x) \cdot a & (5.31) \end{cases}$$

where:

u_1, u_2 are the longitudinal displacement of the axis of cross-section 1 and 2;

w is the common bending deflection and

u is the relative displacement of the cross-section parts at the location of the joints.

The equations of elastic bond are:

for the linear behavior of the material

$$\begin{cases} w_1''(x) = -\frac{M_1(x)}{E_1 J_1} & (5.32) \\ w_2''(x) = -\frac{M_2(x)}{E_2 J_2} & (5.33) \end{cases}$$

for the linear behavior of the connections

$$v_s(x) = k \cdot \Delta u(x) \quad (5.34)$$

The exact solution

For the congruence on the displacement (5.29), the elastic behavior (5.32 and 5.33), for the equilibrium to the rotation (5.19), it can be written:

$$\begin{cases} M_1(x) = \frac{E_1 J_1}{(EJ)_0} \cdot (M(x) + N_1(x) \cdot a) & (5.34) \\ M_2(x) = \frac{E_2 J_2}{(EJ)_0} \cdot (M(x) + N_1(x) \cdot a) & (5.35) \end{cases}$$

By deriving the equation of equilibrium (5.23) and by using (5.34), it can be written

$$N_1''(x) = -v_s'(x) = -k \cdot \Delta u'(x) = -k \cdot (u_2'(x) - u_1'(x) + w''(x) \cdot a) \quad (5.36)$$

By remembering that:

$$\begin{cases} u_2'(x) = \varepsilon_2(x) = \frac{N_2(x)}{E_2 A_2} = -\frac{N_1(x)}{E_2 A_2} & (5.37) \\ u_1'(x) = \varepsilon_1(x) = \frac{N_1(x)}{E_1 A_1} & (5.38) \end{cases}$$

$$\begin{cases} w''(x) = -\frac{M_1(x)}{E_1 J_1} = -\frac{M(x) + N_1(x) \cdot a}{(EJ)_0} & (5.39) \end{cases}$$

then it can be written:

$$N_1''(x) = -k \cdot \left[-\frac{N_1(x)}{E_2 A_2} - \frac{N_1(x)}{E_1 A_1} - \frac{M(x) + N_1(x) \cdot a}{(EJ)_0} \cdot a \right] \quad (5.40)$$

$$N_1''(x) - k \cdot N_1(x) \cdot \left[\frac{1}{E_2 A_2} + \frac{1}{E_1 A_1} + \frac{a^2}{(EJ)_0} \right] = \frac{k \cdot a}{(EJ)_0} \cdot M(x)$$

which

$$N_1''(x) - \frac{k}{(EA)_0} \cdot \frac{(EJ)_\infty}{(EJ)_0} \cdot N_1(x) = \frac{k \cdot a}{(EJ)_0} \cdot M(x)$$

By placing

$$\begin{cases} \alpha^2 = \frac{k}{(EA)_0} \cdot \frac{(EJ)_\infty}{(EJ)_0} & [L^{-2}] \\ \beta = \frac{k \cdot a}{(EJ)_0} & [L^{-3}] \end{cases}$$

It can be written

$$N_1''(x) - \alpha^2 \cdot N_1(x) = \beta \cdot M(x) \quad (5.41)$$

this is the second order differential equation with constant coefficients. Note that the expression of N_1 can be determined by imposing the boundaries conditions.

The general solution of the homogeneous associated is:

$$N_1^0(x) = A_n \cdot \sinh(\alpha h) + B_n \cdot \cosh(\alpha x) \quad (5.42)$$

and the particular solution for the $q(x)$ linear loads is:

$$N_1^p(x) = -\frac{\beta}{\alpha^2} \left(M(x) - \frac{q(x)}{\alpha^2} \right) \quad (5.43)$$

The general solution is then

$$N_1(x) = A_n \cdot \sinh(\alpha x) + B_n \cdot \cosh(\alpha x) - \frac{\beta}{\alpha^2} \cdot M(x) + \frac{\beta}{\alpha^4} \cdot q(x) \quad (5.44)$$

The constants A_n and B_n are determined according to the boundary conditions. For example, for simply supported beam $N_1(0) = N_1(l) = 0$. Note $N_1(x)$ is possible to derive all the other variables except the deformed.

For the deformed it is proceed as following:

$$w''(x) = w_1''(x) = -\frac{M_1(x)}{E_1 J_1} = -\frac{M(x) + N_1(x) \cdot a}{E J_0} \quad (5.45)$$

By deriving two times and remembering that:

$$N_1''(x) = \beta \cdot M(x) + \alpha^2 \cdot N_1(x) = \beta \cdot M(x) + \alpha^2 \cdot \left(-\frac{E J_0}{a} \cdot w''(x) - \frac{M(x)}{a} \right)$$

It can get:

$$w^{IV}(x) - \alpha^2 \cdot w^{II}(x) = \alpha^2 \cdot \frac{M(x)}{E J_\infty} + \frac{q(x)}{E J_0} \quad (5.46)$$

This is the fourth-order differential equation with constant coefficients. The general solution of the homogeneous associated is:

$$w^0(x) = A_w \cdot \sinh(x) + B_w \cdot \cosh(x) + C_w \cdot x + D_w \quad (5.47)$$

The solution for linear $q(x)$ loads is:

$$w^p(x) = -\frac{1}{E J_\infty} \cdot \int \int M(x) dx + \frac{\beta \cdot \alpha}{\alpha^4} \cdot \frac{M(x)}{E J_0} \quad (5.48)$$

the total solution is

$$w(x) = A_w \cdot \sinh(x) + B_w \cdot \cosh(x) + C_w \cdot x + D_w - \frac{1}{E J_\infty} \cdot \int \int M(x) dx + \frac{\beta \cdot \alpha}{\alpha^4} \cdot \frac{M(x)}{E J_0}$$

The A_w, B_w, C_w, D_w constants are determined according to the boundary conditions. Note $w(x)$ is possible to derive all the other quantities according to the following reports:

$$\text{Axial actions} \rightarrow \begin{cases} N_1(x) = E_1 A_1 u_1'(x) = -\frac{1}{a} \cdot (E J_0 w''(x) + M(x)) \\ N_2(x) = -N_1(x) = \frac{1}{a} \cdot (E J_0 w''(x) + M(x)) \end{cases}$$

$$\text{Bending moments} \rightarrow M_i(x) = -E_i J_i w''(x)$$

$$\text{Shear actions } V_i(x) = M_i'(x) - N_1'(x) \cdot \frac{h_i}{2} = -E_i J_i w'''(x) + \frac{h_i}{2a} \cdot (E J_0 w'''(x) + V(x))$$

$$\text{Slip force at the interface [F/L]} \rightarrow V_s(x) = -N_1'(x) = \frac{1}{a} \cdot (E J_0 w'''(x) + V(x))$$

$$\text{Slip at the interface} \rightarrow S(x) = \Delta u(x) = \frac{V_s(x)}{k} = \frac{1}{k \cdot a} \cdot (E J_0 w'''(x) + V(x)).$$

5.3 Particular solution according to the Eurocode 5

5.3.1 Assumptions

The design of timber-concrete structures must satisfy both Ultimate Limit States (ULS) and Serviceability Limit States (SLS) for short- and long-term loads. The ULS are assessed by evaluating the maximum stresses in the component materials (timber, concrete and connection system) using an elastic analysis while, the SLS are checked by evaluating the maximum deflection.

Annex B of Eurocode 5 - Part 1-1, standard reference [27], provides a simplified method for calculating these parameters of mechanically jointed beams (Fig 5.8) with flexible elastic connections, under the following assumptions:

- the beam is simply supported with a span l . For continuous beams the expressions may be used with l equal to 0.8 of the relevant span, and twice the cantilever length for cantilevered beams;
- the individual parts (of wood, wood-based panels) are either full length or made with glued end joints;

- the individual parts are connected to each other by mechanical fasteners with a slip modulus k ;
- the spacing s between the fasteners is constant or varies uniformly according to the shear force, between s_{min} and s_{max} with $s_{max} \leq 4 \cdot s_{min}$;
- the load acts in the z -direction giving a moment $M = M(x)$ varying sinusoidally or parabolically and a shear force $V = V(x)$.

This method is based on an approximate solution of the differential equation for beams with partial composite action. The simplified design method, the so-called “ γ -method” is closely related to the model initially derived by Möhler (1956) and has provide excellent approximations for composite beams with closely spaced fasteners (Kenel 2000 and Frangi and Fontana 2001). The full derivation of the formulae can be found in Kreuzinger (1995).

5.3.2 Approximate solution of the problem

For the verification of composite beams with deformable connection, the Eurocode 5 offers some formulas derived from a simplified treatment in the case of simply supported beam and a distribute load q variable with sinusoidal law with maximum value q_0 in the mid-span, as shown in Figure 5.7:

$$q = q_0 \cdot \text{sen} \left(\frac{\pi x}{l} \right) \quad (5.49)$$

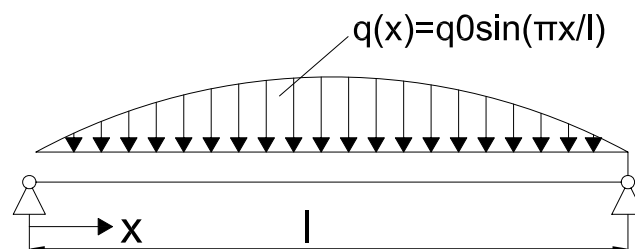


Figure 5.7: Sinusoidal load law with maximum value q_0 .

The composite section presents a symmetrical and vertical plane and it is constant along the axis of the beam: in this case the element 1 represents the slab, and the element 2 the beam. Considering equations 5.17, 5.18 , 5.21, the elastic bond and Figure 5.6 it can be written

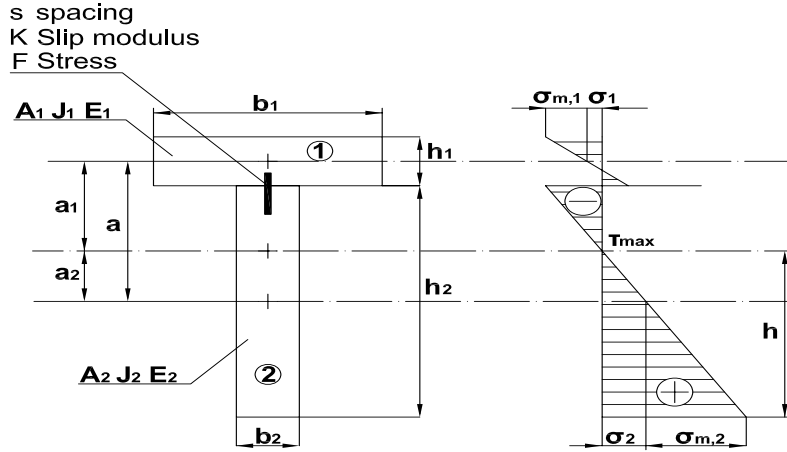


Figure 5.8: Composite beam with deformable connection.

$$N_1(x) = E_1 A_1 \varepsilon_1 = E_1 A_1 u_1'(x) \quad (5.50)$$

$$N_2(x) = E_2 A_2 \varepsilon_2 = E_2 A_2 u_2'(x) \quad (5.51)$$

$$M_1(x) = -E_1 J_1 w''(x) \quad (5.52)$$

$$M_2(x) = -E_2 J_2 w''(x) \quad (5.53)$$

$$V_1(x) = -E_1 J_1 w'''(x) \quad (5.54)$$

$$V_2(x) = -E_2 J_2 w'''(x) \quad (5.55)$$

$$v_s(x) = k \cdot u_t(x) = k \cdot (u_2(x) - u_1(x) + w'(x) \cdot a) \quad (5.56)$$

The equilibrium of the two elements in x and z direction, considering ($p_x = 0$ and $(N_1(x) + N_2(x))' = 0$) can be written as:

$$N_1'(x) + v_s(x) = 0 \quad (5.57)$$

$$N_2'(x) - v_s(x) = 0 \quad (5.58)$$

$$M_1'(x) = V_1(x) - v_s(x) \cdot \frac{h_1}{2} \quad (5.59)$$

$$M_2'(x) = V_2(x) - v_s(x) \cdot \frac{h_2}{2} \quad (5.60)$$

$$V_1'(x) + V_2'(x) = -q(x) = V'(x) \quad (5.61)$$

The sum of (5.59) and (5.60) is differentiated once with respect to x and V' is replaced by the term $-q$:

$$M_1'' + M_2'' + v' \cdot a + q = 0 \quad (5.62)$$

If the internal forces and moments are replaced using elasticity principles, the following system of differential equations results:

$$\begin{cases} E_1 A_1 u_1''(x) + k(u_2(x) - u_1(x) + w'(x) \cdot a) = 0 & (5.63) \\ E_2 A_2 u_2''(x) - k(u_2(x) - u_1(x) + w'(x) \cdot a) = 0 & (5.64) \\ (E_1 J_1 + E_2 J_2) w^{IV}(x) - k \cdot (u_2'(x) - u_1'(x) + w''(x) \cdot a) \cdot a = q(x) & (5.65) \end{cases}$$

This way three equations of equilibrium (5.57), (5.58) and (5.62) for the three deformations $u_1(x)$, $u_2(x)$ and $w(x)$ can be derived.

The variation of the elastic energy is also determined from these equations:

$$\begin{aligned} \Pi = \frac{1}{2} \int [E_1 A_1 u_1'^2(x) + E_2 A_2 u_2'^2(x) + (E_1 J_1 + E_2 J_2) \cdot w''^2(x) + \\ + k(u_2(x) - u_1(x) + w'(x) \cdot a)^2 - 2 \cdot q(x) \cdot w(x)] dx \end{aligned} \quad (5.66)$$

In an other way, it can be written the following fourth order differential equation by considering equations (5.32), (5.33) and the equations (5.18), (5.31) and (5.34), developing the expression (5.25 + 5.28) and differentiating it can be written:

$$(EJ)_0 w^{IV}(x) - k \cdot a \cdot (u_2'(x) - u_1'(x) + w''(x) \cdot a) = q(x) \quad (5.67)$$

Elastic foundation effect k_w , and the influence of second order theory effects could be taken by adding the term $k_w \cdot w(x) - N_0 \cdot w''(x)$ to equation (5.65).

For single span beams with a sinusoidal load distribution, a simple analytical solution can be given because the shape of the deformations in the direction of the axes corresponds to cos- or sin-functions. Although the derivation is based on the sinusoidal load distribution, the solution is also applicable to most other load distributions. This assumption allows to express the unknowns in the axial and vertical displacement in the following forms:

$$\begin{cases} u_1(x) = u_{10} \cdot \cos\left(\frac{\pi x}{l}\right) & (5.68) \\ u_2(x) = u_{20} \cdot \cos\left(\frac{\pi x}{l}\right) & (5.69) \\ w(x) = w_0 \cdot \sin\left(\frac{\pi x}{l}\right) & (5.70) \end{cases}$$

Under these assumptions the system resolving is reduced in a system of equations in the unknowns u_{10} , u_{20} , and w_0 . These terms, when placed in Equations (5.63), (5.64) and (5.65), give a system of equations for the constant u_{10} , u_{20} and w_0 , see also [16]:

u_{10}	u_{20}	w_0	q_0
$-\frac{\pi^2}{l^2} E_1 A_1 - k$	k	$k \frac{\pi}{l} a$	0
k	$-\frac{\pi^2}{l^2} E_2 A_2 - k$	$-k \frac{\pi}{l} a$	0
$k \frac{\pi}{l} a$	$-k \frac{\pi}{l} a$	$\frac{\pi^4}{l^4} (E_1 J_1 + E_2 J_2) - \frac{k \pi^2}{l^2} a^2$	-1

By substituting in $k = \frac{K}{s}$, $k_1 = \frac{\pi^2 \cdot E_1 A_1}{k \cdot l^2}$, $\gamma_1 = \frac{1}{1+k_1}$, it can get

$$w_0 = q \cdot \frac{l^4}{\pi^4} \cdot \frac{1}{E_1 J_1 + E_2 J_2 + \frac{E_1 A_1 \gamma_1 a^2}{1 + \gamma_1 \frac{E_1 A_1}{E_2 A_2}}} \quad (5.71)$$

$$u_{10} = w_0 \cdot \frac{\pi}{l} \cdot \frac{a \cdot \gamma_1 \cdot E_2 \cdot A_2}{\gamma_1 \cdot E_1 A_1 + E_2 A_2} \quad (5.72)$$

$$u_{20} = -w_0 \cdot \frac{\pi}{l} \cdot \frac{a \cdot \gamma_1 \cdot E_1 A_1}{\gamma_1 E_1 A_1 + E_2 A_2} \quad (5.73)$$

If it is put $EJ_{eff} = EJ_0 + (EA^*)_0 \cdot a^2$ (5.74) where

$$(EA^*)_0 = \frac{\gamma_1 E_1 A_1 \cdot E_2 A_2}{\gamma_1 E_1 A_1 + E_2 A_2} = \left[\frac{1}{\gamma_1 E_1 A_1} + \frac{1}{E_2 A_2} \right]^{-1} \quad (5.75)$$

$$w_0 = q_0 \cdot \frac{l^4}{\pi^4} \cdot \frac{1}{(EJ)_{eff}} \quad (5.76)$$

The solution of the system is

$$\left\{ \begin{array}{l} w(x) = \frac{q_0 \cdot l^4}{\pi^4 EJ_{eff}} \cdot \sin\left(\frac{\pi x}{l}\right) \end{array} \right. \quad (5.77)$$

$$\left\{ \begin{array}{l} u_1(x) = \frac{q_0 \cdot l^3}{\pi^3 EJ_{eff}} \cdot \frac{(EA^*)_0 \cdot a}{E_1 A_1} \cdot \cos\left(\frac{\pi x}{l}\right) \end{array} \right. \quad (5.78)$$

$$\left\{ \begin{array}{l} u_2(x) = -\frac{q_0 \cdot l^3}{\pi^3 EJ_{eff}} \cdot \frac{(EA^*)_0 \cdot a}{E_2 A_2} \cdot \cos\left(\frac{\pi x}{l}\right) \end{array} \right. \quad (5.79)$$

where the dimensionless factor γ_1 is like a “weight” for the area of only the element 1. The stresses are:

Axial force

$$N_1(x) = E_i A_i \varepsilon_i(x) = E_i A_i u'_i(x) = -\frac{q_0 \cdot l^2 \cdot (EA^*)_0 \cdot a}{\pi^2 \cdot (EJ)_{eff}} \cdot \sin\left(\frac{\pi x}{l}\right) \quad (5.80)$$

i.e.

$$N_1(x) = -\frac{(EA^*)_0 \cdot a}{(EJ)_{eff}} \cdot M(x) \quad (5.81)$$

where

$$M(x) = \frac{q_0 \cdot l^2}{\pi^2} \cdot \sin\left(\frac{\pi x}{l}\right) \quad (5.82)$$

Bending moment

$$M_i(x) = -E_i J_i w''(x) = E_i A_i u'_i(x) = -\frac{E_i J_i \cdot a \cdot q_0 \cdot l^2}{(EJ)_{eff} \cdot \pi^2} \cdot \sin\left(\frac{\pi x}{l}\right) \quad (5.83)$$

Shear

$$V_i(x) = \frac{E_i J_i}{EJ_{eff}} + \frac{(EA^*)_0}{EJ_{eff}} \cdot \frac{h_i}{2 \cdot V(x)} \quad (5.84)$$

$$V_s(x) = -N'_1 = \frac{(EA^*)_0 \cdot a}{EJ_{eff}} \cdot \frac{q_0 \cdot l}{\pi} \cdot \cos\left(\frac{\pi x}{l}\right) \quad (5.85)$$

$$V_s(x) = -N'_1 = \frac{(EA^*)_{0 \cdot a}}{EJ_{eff}} \cdot V(x) \quad (5.86)$$

Deformations

$$\Delta u(x) = s(x) = u_2(x) - u_1(x) + w'(x) \cdot a \quad (5.87)$$

$$\Delta u(x) = \frac{q_0 \cdot l^3 \cdot a}{\pi^3 \cdot (EJ)_{eff}} \cdot \left(1 - \frac{1}{E_2 A_2 + E_1 A_1} \cdot (EA^*)_0 \cdot \cos\left(\frac{\pi x}{l}\right)\right) \quad (5.88)$$

According to the Eurocode 5 Part 1-1, Annex B, the formulae are written in a different way and reported below. By doing the relative substitutions it can be obtained the following expressions. The effective bending stiffness $(EJ)_{eff}$ of a simply supported timber-concrete composite beam is calculated as:

$$(EJ)_{eff} = \sum_{i=1}^2 (E_i J_i + \gamma_i E_i A_i a_i^2) \quad (5.89)$$

using mean values of E and where:

$$A_i = b_i \cdot h_i$$

$$J_i = \frac{b_i \cdot h_i^3}{12}$$

$$\gamma_2 = 1$$

$$\gamma_i = \left[1 + \frac{\pi^2 \cdot E_i A_i \cdot s_i}{K_i \cdot l^2}\right]^{-1} \quad \text{for } i = 1 \text{ and } i = 2$$

$K_i = K_{ser,i}$ for the serviceability limit state calculations;

$K_i = K_{u,i}$ for the ultimate limit state calculations;

$$a_2 = \frac{\gamma_1 \cdot E_1 A_1 \cdot a}{\gamma_1 \cdot E_1 A_1 + E_2 A_2} \quad \text{where } a = \frac{h_1}{2} + \frac{h_2}{2}$$

$$a_1 = a - a_2$$

The values of K_{ser} , in absence of direct experimental evidence on the type of connector used, can be determined with referring to table 7.1 from Eurocode 5 part 1-1. Besides, the slip modulus of a connection for the ultimate limit state K_u , should be taken as $K_u = \frac{2}{3} \cdot K_{ser}$. In the case of union between timber and concrete, with reference the table 7.1 from Eurocode 5 part 1-1, the value of K_{ser} obtained should be doubled. After determining the effective stiffness of the member can be determined by means of the following expressions, the normal and the bending stresses acting on the element.

$$N_i(x) = \frac{\gamma_i \cdot E_i \cdot a_i \cdot A_i}{(EJ)_{eff}} \cdot M(x) \quad (5.90)$$

$$M_i(x) = \frac{(EJ)_i}{(EJ)_{eff}} \cdot M(x) \quad (5.91)$$

From the previous equations, it can get the stress at the centroid $\sigma_i(x)$ and the flexural component of the stress $\sigma_{m,i}(x)$ in the concrete (i=1) and timber (i=2).

$$\sigma_i(x) = \frac{\gamma_i \cdot E_i \cdot a_i}{(EJ)_{eff}} \cdot M(x) \quad (5.92)$$

$$\sigma_{m,i}(x) = \frac{0,5 \cdot E_i \cdot h_i}{(EJ)_{eff}} \cdot M(x) \quad (5.93)$$

The maximum shear stress $\tau_{2,max}(x)$ acting in the web element (element 2) and the force $F(x)$ in the shear load fastener can be obtained from the following equations

$$\tau_{2,max}(x) = \frac{0,5 \cdot E_2 \cdot h^2}{(EJ)_{eff}} \cdot V(x) \quad (5.94)$$

where $h = \frac{h_2}{2} + a_2$ and

$$F(x) = \frac{\gamma_1 \cdot E_1 \cdot A_1 \cdot a_1 \cdot s_{eq}}{(EJ)_{eff}} \cdot V(x) \quad (5.95)$$

where $M(x)$ is the bending moment, $V(x)$ is the shear force in the cross-section of interest and s_{eq} is the equivalent spacing of the fasteners as previously said in the assumptions. For the last parameter it can be therefore chosen $s_{eq} = 0,75 \cdot s_{min} + 0,25 \cdot s_{max}$.

5.4 Short and long term verifications

A general effect (such a stress and displacement), designed E^F , caused by the load combination for ultimate (ULS) and serviceability (SLS) limit states expressed in the next equations can be calculated using the formulas provided by Eurocode 5.

$$F_{d,r} = \sum_{j \geq 1} G_{k,j} + Q_{k,i} + \sum \psi_{0,i} \cdot Q_{k,i} \quad (5.96)$$

$$F_{d,f} = \sum_{j \geq 1} G_{k,j} + \psi_{11} \cdot Q_{k,i} + \sum_{i > 1} \psi_{2,i} \cdot Q_{k,i} \quad (5.97)$$

$$F_{d,p} = \sum_{j \geq 1} G_{k,j} + \sum_{i > 1} \psi_{2,1} \cdot Q_{k,i} \quad (5.98)$$

$$F_{d,u} = \sum_{j > 1} \gamma_{g,j} \cdot G_{k,j} + \gamma_{Q,1} \cdot Q_{k,1} + \sum_{i > 1} \gamma_{Q,1} \cdot \psi_{0,i} \cdot Q_{k,i} \quad (5.99)$$

These values depend on the load applied on the beam, and on the Young's modulus and slip moduli of the component materials and can be expressed in the following basic form:

$$E^{Fs} = E^{Fs}(E_{cm}(t_0); E_{0,mean}; k_{ser}) \quad (5.100)$$

$$E^{Fu} = E^{Fu}(E_{cm}(t_0), E_{0,mean}, ; k_u) \quad (5.101)$$

where in general $k_{ser} \neq k_u$.

For the serviceability limit state (SLS) three combinations: (i) characteristic, (ii) frequent and (iii) quasi-permanent are considered, while for the ultimate limit state (ULS) just one design load combination is considered, see equations (5.96), (5.97), (5.98) and (5.99). G denotes the permanent and Q the variable actions, characterized by different values of creep coefficients calculated according to the load duration class, and γ , ψ are coefficients tabulated in Eurocode 0.

The short-term verifications, at the initial state where loads are applied instantaneously and with no creep effect, can be performed according to the procedure based on the use of Young's moduli for concrete and timber, and slip modulus of the connection, as described by Ceccotti, see [17] and Ceccotti [18]. Since the load-slip relationship of the shear connection is typically non-linear, two different slip moduli are considered for design purposes, as proposed by Ceccotti (1995): k_{ser} for the serviceability limit state (SLS) and k_u for the ultimate limit state (ULS). The slip modulus k_{ser} , which corresponds to the secant value at 40% of the load-carrying capacity of the connection ($k_{0,4}$), is usually evaluated by push-out tests according to standard reference [28]. For the slip modulus k_u , use of the secant value at 60% ($k_{0,6}$) is recommended. However, if experimental data are not available, Eurocode 5-Part 1-1 suggests using the formulae for timber-to-timber connections by multiplying the corresponding values of the slip modulus k_{ser} by 2. The slip modulus k_u may then be taken as 2/3 of k_{ser} (Eurocode 5). Depending on the type of connection involved, this assumption may or may not be adequate. Ceccotti in [19], for example, reported a significant (50%) discrepancy between experimentally and analytically values of connection properties obtained from push-out tests. In the second chapter the experimental results of shear-tests performed on shear connectors are presented in terms of the slip moduli k_{ser} and k_u , which are further analysed in the short-term verifications at SLS and ULS. Thus the current procedure for short-term solutions for the serviceability and ultimate limit state can be summarized as follows:

1. For the serviceability limit state an elastic solution has been proposed where u_{inst} due to the load combination $F_{d,r}$ (Eq. (5.96) is obtained using the elastic moduli:

$$E_c = E_{cm}(t) \quad (5.102)$$

$$E_t = E_{0,mean} \quad (5.103)$$

$$k = k_{ser} \quad (5.104)$$

1. For the ultimate limit state an elastic solution has been proposed where S_{inst} due to the load combination $F_{d,u}$ (Eq. 5.99) is obtained using the elastic moduli according to Eqs 5.102 and 5.103 and:

$$k = k_u \quad (5.105)$$

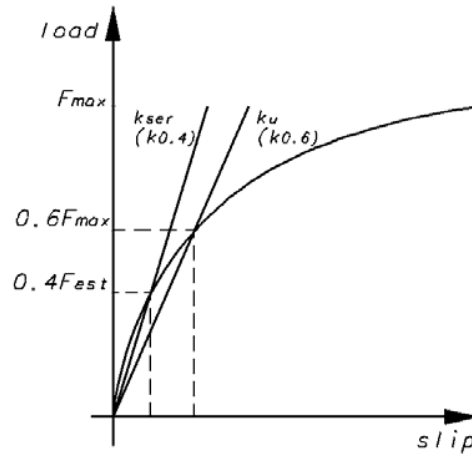


Figure 5.9: Example of load-slip behavior of shear connector and definition of slip moduli: $k_{ser}(k_{0.4})$ at 40% of the estimated load-carrying capacity, $k_u(k_{0.6})$ at 60% of the maximum load-carrying capacity.

The verification of a composite beam in the long-term is more problematic, since the concrete's creep and shrinkage, the creep and the mechano-sorption of the timber and connection, and thermal strains of concrete and timber should be considered. Numerical programs (Fragiacomo and Ceccotti 2006, Scházlin 2003) and analytical formulas (Fragiacomo and Ceccotti in [20], Scházlin and Kuhlmann in [21]) have been proposed to provide accurate solutions, but no consensus among researchers has been reached regarding methods to predict the long-term performance of timber-concrete composite structures (after Clouston 2006). Referring to Clouston for steel-concrete construction, the ACI-ASCE Joint Committee recommends using $E_c/2$ as the concrete modulus of elasticity instead of E_c when calculating sustained load creep deflection (after Clouston 2006). The AASHTO Bridge Design Specification, Section 10.38.1.4, suggests using $E_c/3$ (after Clouston 2006). The European Code recommends using creep factors developed from load duration studies to reduce the moduli of the respective materials. (Eurocode 5).

The simplified approach suggested by Ceccotti (2002) does not account for shrinkage or thermal strains and is based on the *Effective Modulus Method*, in which the creep and mechano-sorption of the concrete, timber and connection are accounted for by reducing the elastic and slip moduli according to the following expressions:

$$E_{c,fin} = \frac{E_{cm}(t_0)}{1+\phi(t,t_0)} \quad (5.106)$$

$$E_{t,fin} = \frac{E_{0,mean}}{1+k_{def,t}} \quad (5.107)$$

$$k_{fin} = \frac{k}{1+k_{def,f}} \quad (5.108)$$

For the concrete, Eurocode 2-1-1 provides some guidelines for evaluating the creep coefficient $\phi(t, t_0)$, t and t_0 being the final and loading instants, respectively. Eurocode 5-1-1 provides tables of values of the creep coefficient k_{def} for both the timber and the connection. Those moduli are then used in equations previously presented to solve the beam parameters in long-term loading.

The creep phenomenon has two types of effect on the composite beam: (i) increments with time in strains and displacements and (ii) changes in the distributions with time of stresses and internal forces in the component materials because of the differences in creep properties. Consequently, creep affects both the ultimate and serviceability limit states, and cannot be neglected in long-term verifications.

The currently proposed procedure (*Effective Modulus Method*) for calculating a long-term solution for the serviceability and ultimate limit states can be summarised as follows:

- For the service limit state an elastic solution has been proposed where u_{fin} due to the quasi-permanent part of the load combination $F_{d,p}$ (Eq. 5.98) is obtained using the effective moduli Eqs. 5.106 and 5.108.

The creep effects are due only to the quasi-permanent part of the load $F_{d,p}$ considered as acting on the structure for the entire service life. The long-term maximum vertical displacement can be calculated by substituting the long-term displacement due to the quasi-permanent part of the load for the instantaneous displacement due to the difference between the rare and quasi-permanent combinations applied at the end of the service life t :

$$\begin{aligned} u_{fin} &= u_{fin}^{F_{d,p}} + u_{inst}^{F_{d,r}-F_{d,p}} = \\ &= u^{F_{d,p}}(E_{c,fin}, E_{t,fin}, k_{ser,fin}) + u^{F_{d,r}-F_{d,p}}(E_{cm}(t), E_{0,mean}, k_{ser}) \end{aligned} \quad (5.109)$$

with $F_{d,r} - F_{d,p}$ given by the next equation

$$F_{d,r} - F_{d,p} = (1 - \psi_{2,1}) \cdot Q_{k,1} + \sum_{i>1} (\psi_{0,i} - \psi_{2,i}) \cdot Q_{k,i} \quad (5.110)$$

- For the ultimate limit state an elastic solution has been proposed where S_{fin} due to the part of load combination $F_{d,p}$ Eq. 5.98 is obtained using the effective moduli according to Eqs. 5.106 to 5.108.

In addition, for ultimate limit state verification only the quasi-permanent part of the $F_{d,p}$ of the combination $F_{d,u}$ has to be considered as acting throughout the entire service life. The effects due to the load $F_{d,p}$ can be estimated, as mentioned above, using the effective moduli E_{fin} . Moreover, the difference between the ultimate and the quasi-permanent load combination is instead applied instantaneously, therefore

for this part of the load the Young's moduli at the instant t have to be used. Consequently, the following formulation can be applied:

$$\begin{aligned}
 S_{fin} &= S_{fin}^{F_{d,p}} + S_{inst}^{F_{d,u}-F_{d,p}} = \\
 &= S^{F_{d,p}}(E_{c,fin}, E_{t,fin}, k_{ser,fin}) + S^{F_{d,u}-F_{d,p}}(E_{cm}(t), E_{0,mean}, k_u) \quad (5.111)
 \end{aligned}$$

with $F_{d,u} - F_{d,p}$ given by the next equation

$$F_{d,u}-F_{d,p} = \sum_{j>i} (\gamma_{G,j} - 1) \cdot G_{k,j} + (\gamma_{Q,1} - \psi_{2,1}) \cdot Q_{k,1} + \sum (\gamma_{Q,i \cdot \psi_{0,i} - \psi_{2,i}}) \cdot Q_{k,i} \quad (5.112)$$

Chapter 6

Numerical model and analytical calculations

This chapter presents the numerical model using FE-method for short-term analysis which has been developed. It also presents the FEM analysis and the discussions over the different models which have been considered to choose the best dimensions to realize the full-scale specimens. The reliability of the FE model was checked and compared with analytical calculations as well.

6.1 Background

In order to get the optimal dimensions of the composite beam a FE model has been developed. These make possible to take into account for effects of factors such as non-uniform connections and non-linear materials response. Unfortunately such models are neither commercially available nor user-friendly. Instead commercial FE programs can be used, based on a Vierendeel beam analogy, see Figure 6.1.

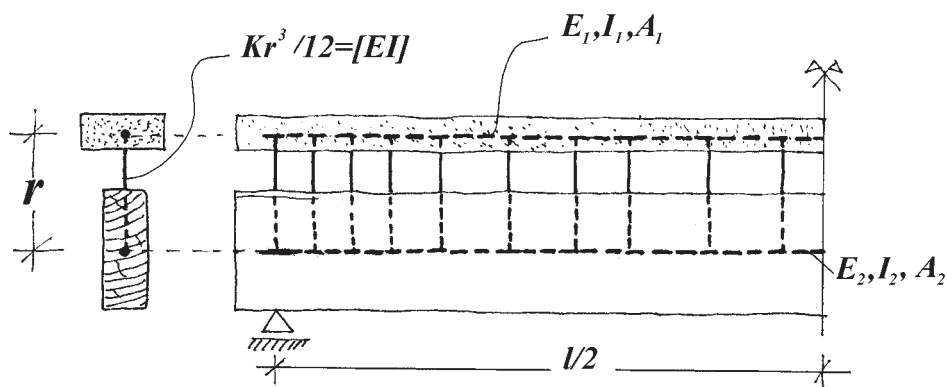


Figure 6.1: Vierendeel model.

Results for Vierendeel beam analogues are very close to those obtained with classical

formulae, except in cases where the load distribution is unusual, connection characteristics are not uniform and/or the system is hyperstatic (statically indeterminate with respect to support conditions).

The finite element (FE) program used in the analysis in the studies underlying this thesis was SAP 2000 developed by Computers and Structures, Inc. University Avenue Berkeley from California. The purpose of using FE model was to investigate the performance of the prefabricated timber-concrete composite systems for short-term conditions. In practice, in order to decide the dimensions of the components of the composite beam, in particular, regarding the depth of the beam and the thickness of the slab, some models have been developed with different geometric characteristics. Moreover, the spacing between the screws was object of study as well. After more kinds of different models and analysis, which are presented and discussed afterwards, the dimensions and the spacing of the screws for the composite structures realized have been chosen, see the design shown in Figure 4.3.

6.2 FE model for short-term analysis

The finite element model used for the short-term analysis consists of a lower timber beam, modelled as a frame element linked to an upper concrete slab modelled as a shell element, through a spring element. The following Figure 6.2 shows the adequate mechanical model in detail which has been developed. The shear connector was simulated by a non-continuous system of springs. The stiffness of the springs was derived from the shear tests, previously carried out and reported in [4], and takes into account the linear system performance. The kinematic hypothesis are: negligibility of shear strains, equal vertical displacements and planarity of the cross sections for the single component beams. If the local material behavior has to be considered, cross-sections of the two beams have to be divided in fibres.

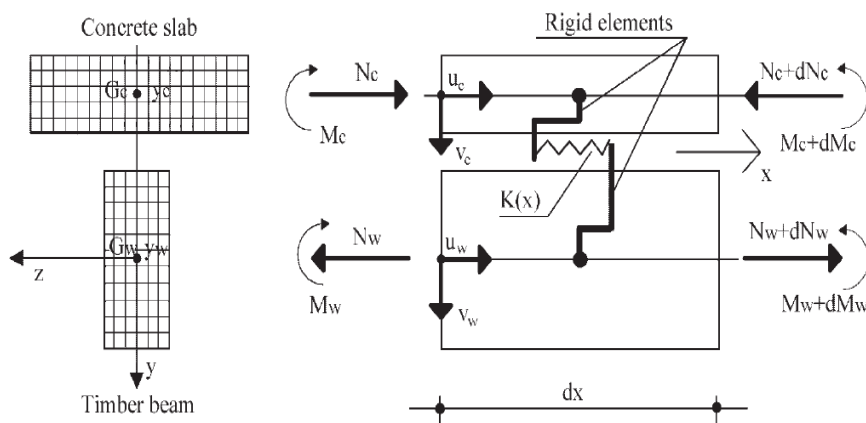


Figure 6.2: Finite element model.

6.2.1 Timber beam as a frame element

The frame element is a very powerful element that can be used to model beams, columns, braces, and trusses in planar and three-dimensional structures. A frame element is modelled as a straight line connecting two points. Each timber beam was modelled as an entire frame element with dimensions equal to $115 \times 360 \times 7200$ mm, and the material assigned was timber with specific gravity equal to 4 kN/m^3 and $E_{mean} = 12500$ MPa as elastic modulus. For this modelling, since the beams are acting only in bending, the material for simplicity was considered isotropic.

6.2.2 Concrete slab as shell elements

The shell element is a type of area object that is used to model membrane, plate and shell behavior in planar and three-dimensional structures. The shell material may be homogeneous or layered through the thickness. The shell element is a three- or four-node formulation that combines membrane and plate-bending behavior. Two distinct formulations are available: homogeneous and layered. The homogeneous shell combines independent membrane and plate behavior. These behaviors become coupled if the element is warped (non-planar). The membrane behavior uses an isoparametric formulation that includes translation in-plane stiffness components and a rotational stiffness component in the direction normal to the plane of the element. The homogeneous plate-bending behavior includes two-way, out-of-plane, plate rotational stiffness components and a translational stiffness component in the direction normal to the plane of the element. It was used a thin-plate (Kirchhoff) with four-node formulation that neglects transverse shearing deformation. Instead, if it is considered a thick-plate (Mindlin/Reissner) formulation, the effects of transverse shearing deformation will be included. In plain the displacements are quadratic while out-of-plane they are cubic. For more details about shell element it can be seen in [22]. The slab was divided in a total number of 1296 shell elements which each single element has these dimensions 88×50 mm and the material which has been implemented was a concrete with specific gravity and elastic modulus respectively equal to $\gamma_c = 24 \text{ kN/m}^3$ and $E_c = 36210$ MPa.

6.2.3 Shear connector as a link element

The link element is used to connect two joints together. Each link element may exhibit up to three different types of behavior: linear, non-linear and frequency-dependent according to the types of properties assigned to that element and the type of analysis being performed. A link element is a two-joint connecting link. Each element is assumed to be composed of six separate “springs”, one for each of six deformational degrees of freedom (axial, shear, torsion and pure bending). All linear property sets

contain linear properties that are used by the element for linear analyses as in this case. For more details about link element see [22]. The link can be seen as shown in Figure 6.2 and the stiffness of the springs was set, with reference to the limit state considered, as reported in Table 6.1.

Stiffness of the link	[N/mm]
K_{ser}	35000
K_u	23333

Table 6.1: Stiffness of the link which was set in the FE model.

Figure 6.3 reports an image of the FE model realized and in the following one, Figure 6.4, shows an extrude view of this.

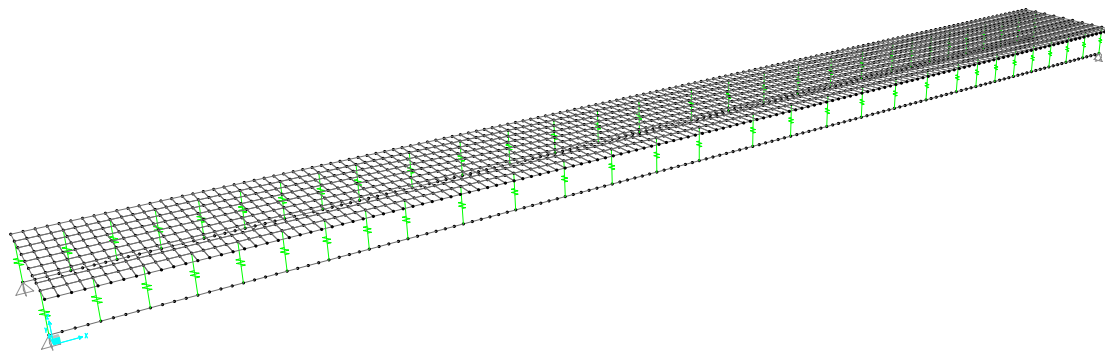


Figure 6.3: FE model.

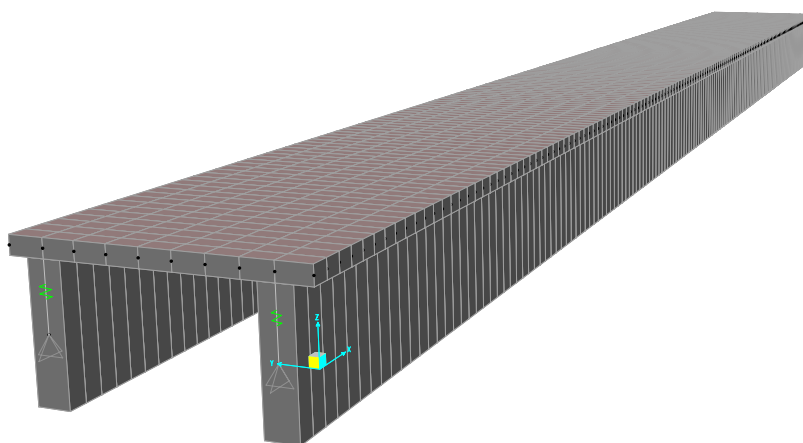


Figure 6.4: Extrude view of the FE model.

The problem of this type of modelling arises in the definition of the equivalent shear spring connector. It is not possible to define a simple spring which transmits only horizontal shear force, in fact, to satisfy the equilibrium the shear connector has to transmit moments as well, as it can be seen in Figure 6.5.

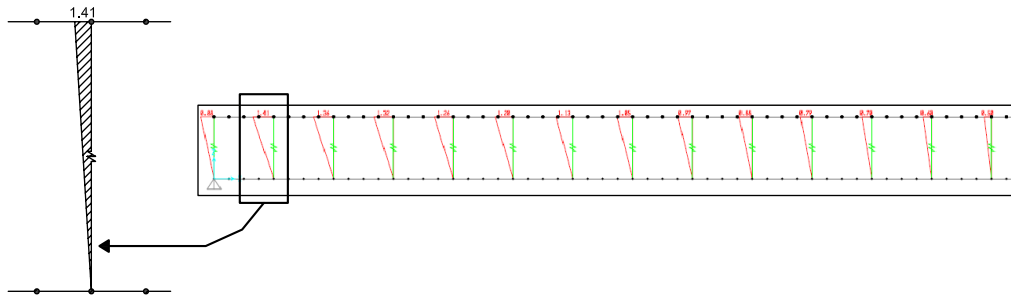


Figure 6.5: Introduction of moments in the link elements working as a shear connector.

To avoid the moments in the link connector, it must have length equal to zero and with SAP 2000 it is not possible. In the Figure 6.5, the shear force was set to pass on the axis of the timber beam, and accordingly the concrete slab was like a fixed support and a moment equal to the shear force times the distance between the axis of the beam and the slab.

As it can be seen in [23], Kneidl and Hartmann proposed different framework models. Those are the most implicit and reliable to model multi-layered beams. Each section is represented in the statical system by a beam. In order to keep into account the slip between the layers different possibilities are proposed. The model A just placed a small cantilever with the adequate hinge at the end. Model B allows running in finite model programs which do not have the possibility of hinges by adapting the stiffness of the diagonals. Hartmann combined both model to make Model C by placing the hinges at the end of a console made by diagonals to avoid the local introduction of moments (model A). The solution has a continuous development of the bending moment. These type of models are shown in Figure 6.6.

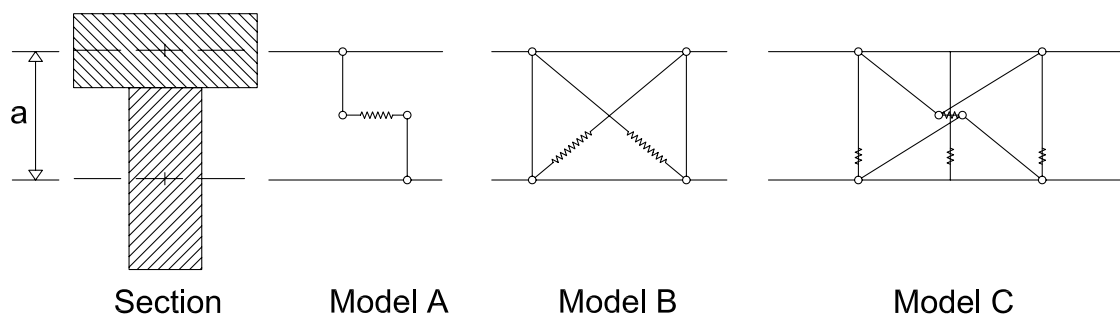


Figure 6.6: Framework models.

These systems are sensible to the inclination of the diagonals and the distance of the modelled connectors. The ratio between modelled connectors and the thickness of the planks must be smaller than 2.

Ceccotti used the same model A but schematized in a different manner, see [24]. However, by putting two rigid arms and a horizontal spring and also in this case it

creates a bending moment, see Figure 6.2. With SAP 2000 it can be done the same thing, by using the link element and specifying the distance where to apply the force. By trying to change this distance it can be found that moment, normal stress, sag, frequency and stress in the connector varies around 1-2%. Hence, it seems reasonable to schematize the structure in this last way. Furthermore, by comparing the results with the Möhler solution they are consistent. In conclusion, it was decided to use this model by setting the distance where the shear force has to pass to the timber-concrete interface how did Ceccotti. In this way, the moment on the link element has a butterfly shape, as it can be seen in Figure 6.7.

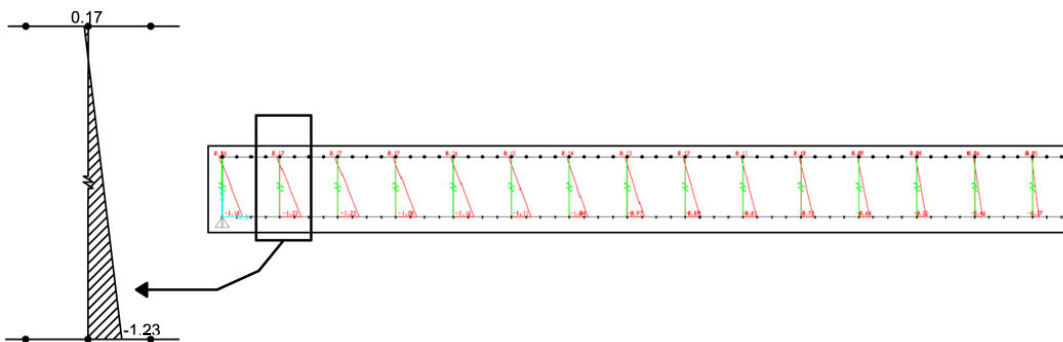


Figure 6.7: Butterfly shape of the moment in the link connector, as a modelling defect.

6.3 Load implemented in the numerical models

The load implemented in the numerical model was the same that those reported in the Appendix of this thesis. These loads concern the self-weight of the structure elements and the live load has to take into account the crowd on the beam during a demonstration in the stadium with reference to category of use C5 as reported in standard reference [30]. Table 6.2 summarizes the load used in the FE model:

Loads		
Self-weight	$G_{1,k}$ [kN/m ²]	-
Non-structural self-weight	$G_{2,k}$ [kN/m ²]	0,2
Live load	Q_k [kN/m ²]	5

Table 6.2: Summary of the characteristic loads acting on the modelled beam.

Note that the self-weight was calculated by the program. As far as the load combinations is concerned, it was considered the Swedish rules of combinations of loads which is referred to three security class reported in Table 6.3.

Security class	Description	γ_d
1	high risk of serious injury	1,0
2	limited risk of serious injury	0,91
3	no risk of serious injury	0,83

Table 6.3: Swedish security classes.

In practice the load combination considered for the choice of the dimensions of the beam are:

$$\begin{aligned}
 q_{ULS} &= \sum_{j \geq 1} \gamma_d \cdot 1,2 \cdot G_{k,j} + \gamma_d \cdot 1,5 \cdot Q_{k,1} + \sum_{i > 1} \gamma_d \cdot 1,5 \cdot \psi_{0,i} \cdot Q_{k,i} \\
 q_{SLS,rare} &= \sum_{j \geq 1} G_{k,j} + Q_{k,1} + \sum_{i > 1} \psi_{0,i} \cdot Q_{k,i} \\
 q_{SLS,frequent} &= \sum_{j \geq 1} G_{k,j} + \psi_{11} \cdot Q_{k,1} + \sum_{i > 1} \psi_{2,i} \cdot Q_{k,i} \\
 q_{SLS,quasi-permanent} &= \sum_{j \geq 1} G_{k,j} + \sum_{i > 1} \psi_{2,i} \cdot Q_{k,i}
 \end{aligned}$$

With regard to the partial safety factors γ_d , γ_{Gi} and γ_{Qi} , and the combination factors values ψ_{ij} the used values are reported in Table 6.4.

Safety factors		
Security class	γ_d	1,0
Dead load	γ_{G1}	1,2
Non-structural dead load	γ_{G2}	1,2
Live load - Areas susceptible to large crowds	γ_Q	1,5
Combination factor values	$\psi_{0,1}$	0,7
Combination factor values	$\psi_{2,1}$	0,6

Table 6.4: Partial safety factors and combination factor used.

Load combinations have been performed directly in the FEM program according to standard reference [29] and full reported in the following Appendix. As far as the geometrical characteristics is concerned see the design drawing reported in Figure 4.3

6.4 Standard model

In this paragraph, the results of the finite element analysis are shown. The models differ each other in terms of depth of the beam, thickness of the slab and from spacing amongst the screws. Combined models have also been realized. The reference model used to compare all the other models is the following one. This model is realized with a slab thickness equal to 50 mm and width 800 mm, the two beams have 360 mm depth and 115 mm width. The spacing between the screws for the standard model is equal to 200 mm. A picture of this model is reported in Figure 6.8.



Figure 6.8: Standard model used to compare with the others.

Table 6.5 reports the results from the analysis with standard model.

STANDARD MODEL							
Slab thickness	Beam depth	Frequency	QP sag	Rare sag	Axial Force in the beam	Bending Moment in the beam	Max force in the screw
[mm]	[mm]	[Hz]	[m]	[m]	[kN]	[kNm]	[kN]
50	360	13.52	0,0046	0,0065	73,96	9,61	6,41

Table 6.5: Results from analysis with standard model.

Before to explain the FEM analysis it was decided to mention the requirements that have to be satisfied, the variable parameters and the parameters monitored. This type of structures, as timber structures in general, is designed considering the serviceability limit states.

As it is reported in paragraph 7.3 from the standard reference [27], as far as vibrations is concerned, it shall be ensured that the actions which can be reasonably anticipated on a member, component or structure, do not cause vibrations that can impair the function of the structure or cause unacceptable discomfort to the users. The vibration level should be estimated by measurements or by calculation taking into account the expected stiffness of the member, component or structure and the modal damping ratio. The Eurocode 5-1-1 says also that in case of residential floors with fundamental frequency less than 8 Hz, a special investigation should be made. For residential floors with a fundamental frequency greater than 8 Hz it provides some requirements which have to be satisfied. In this case, seeing the structure is specifically addressed to realize the stands of a stadium, as it can be better seen in the Appendix of this thesis, the minimum of the fundamental frequency allowed was 10 Hz. According to the paragraph 7.2 of the standard reference [27], the limit value of the instantaneous deflections of the composite beams is $1/400$, and in this particular case, since the length of the beam is 7,2 m the maximum instantaneous deflection is 0,018 m.

The variable parameters that have been studied in order to find the best performance of the composite beam were: the thickness of the slab, the depth of the beam and the spacing between the screws. On the other hand, the monitored parameters used to compare the different numerical models are: the natural frequency, the instantaneous mid-span deflection, the maximum shear force in the shear connector, the bending moment and the axial force in the timber beam.

Finally, it is underlined that, in the FE model all the loads were combined with the safety factors and implemented with characteristic moduli of the materials in order

to decide and design the full-scale specimens. Below the following tables representing the results of the FE analysis are reported the analytical solution considering some parameters as variable. The graphs reported below, which are the solution of the “ γ – method”, displaying the trend of the shear force acting on the screw and the bending stress in the glulam beam in function of the thickness of the slab, the depth of the beam and the spacing of the screw, respectively.

6.4.1 Standard model with only dead load

It is presented the first model which has been developed. It derives from the standard model but with only the selfload, without safety factors and with $K_{ser} = 35000$ N/mm in order to compare the FE model with the analytical calculations and to ascertain the results from the numerical model are plausible. Theoretical calculations have been carried out in order to check the FE model, which have been done before studying the previous cases.

MODEL WITH ONLY DEAD LOADS WITHOUT SAFETY FACTORS							
Screw spacing	Period	Frequency	QP sag	Rare sag	Axial Force in the beam	Bending Moment in the beam	Max force in the screw
[cm]	[s]	[Hz]	[m]	[m]	[kN]	[kNm]	[kN]
20	0,08	13,31	-	0,0017	14,55	1,68	1,32

Table 6.6: Results of the analysis from the standard model with only dead load and without safety factors.

6.4.2 Standard model without screws

A simple model derived from the standard model has been developed. This model presents any kind of connections, in order to have an idea about the behavior of the composite structure with beam members working in parallel. It can be quickly seen in Table 6.7, that the bending moment in the timber beam increases a lot, while the axial force in the beam and the shear force are 0. By adopting this kind of structure, the serviceability requirements are not completely satisfied, because the natural frequency estimated is $8,41 \text{ Hz} < 10 \text{ Hz}$, while the instantaneous mid-span deflection estimated from the numerical model is $0,017 \text{ m} < 0,018 \text{ m}$. Thus, if it is wanted to satisfy the requirements it has to increase the depth of the beams and the thickness of the slab. In the last way, the materials are not used to their best characteristics.

STANDARD MODEL WITHOUT SCREWS							
Depth of beam [mm]	Period [s]	Frequency [Hz]	QP sag [m]	Rare sag [m]	Axial Force in the beam [kN]	Bending Moment in the beam [kNm]	Max force in the screw [kN]
360	0,12	8,41	0,0119	0,0169	0,25	24,32	0,00

Table 6.7: Results of the analysis from standard model without screws.

6.5 Check of the reliability of the FE model with analytical calculation

In order to check if the results from the FE model are plausible, it has been done some theoretical calculations and compared the estimate mid-span deflection and the maximum shear force acting on the connector. The whole theoretical calculations are given explicitly in the Appendix of this thesis with reference to the design of the stands of a stadium. Here, in order to check the reliability of the numerical results it was considered only the self-weight load without safety factors and the comparison was done between the instantaneous mid-span deflection and the maximum shear force in the connector as following.

The loads considered are reported in the Table 6.8.

Load expressed in [kN/m]	
$G_{1k,slab}$	0,48
$G_{1k,beam}$	0,17
G_{2k}	0,00
Q_k	0,00

Table 6.8: Self-weight load considered to check the numerical results. For the reliability check no live load has been implemented.

The axial stiffness and the bending stiffness for each component, considering just a half of the entire system, are

$$\begin{aligned}
 E_1 A_1 &= E_1 \cdot b_1 \cdot h_1 = 36210 \cdot 400 \cdot 50 = 7,24 \cdot 10^8 \text{ N} \\
 E_2 A_2 &= E_2 \cdot b_2 \cdot h_2 = 12500 \cdot 115 \cdot 360 = 5,18 \cdot 10^8 \text{ N} \\
 E_1 J_1 &= E_1 \cdot \frac{b_1 \cdot h_1^3}{12} = 36210 \cdot \frac{400 \cdot 50^3}{12} = 1,51 \cdot 10^{11} \text{ Nmm}^2 \\
 E_2 J_2 &= E_2 \cdot \frac{b_2 \cdot h_2^3}{12} = 12500 \cdot \frac{115 \cdot 360^3}{12} = 5,59 \cdot 10^{12} \text{ Nmm}^2
 \end{aligned}$$

from were it can be get the bending stiffness of the composite beam in case of no connections, the axial stiffness of the composite structure and the bending stiffness in case of rigid connection:

$$(EJ)_0 = \frac{1}{12} \cdot (E_1 \cdot b_1 \cdot h_1^3 + E_2 \cdot b_2 \cdot h_2^3) =$$

$$= \frac{1}{12} \cdot (36210 \cdot 400 \cdot 50^3 + 12500 \cdot 115 \cdot 360^3) = 5,74 \cdot 10^{12} \text{ Nmm}^2$$

$$(EA)_0 = \frac{E_1 A_1 \cdot E_2 A_2}{E_1 A_1 + E_2 A_2} = \frac{7,24 \cdot 10^8 \cdot 5,18 \cdot 10^8}{7,24 \cdot 10^8 + 5,18 \cdot 10^8} = 3,02 \cdot 10^8 \text{ N}$$

$$(EJ)_\infty = (EJ)_0 + (EA)_0 \cdot a^2 = 5,74 \cdot 10^{12} + 3,02 \cdot 10^8 \cdot 205^2 = 1,84 \cdot 10^{13} \text{ Nmm}^2$$

to determine the effective stiffness of the composite structure it was calculated before

$$s_{eq} = 200 \text{ mm}$$

$$K_{ser} = 35000 \text{ N/mm}$$

$$l = 7200 \text{ mm}$$

$$\gamma_1 = [1 + \pi^2 \cdot E_1 A_1 \cdot s_{eq} / (K_{ser} \cdot l^2)] =$$

$$= [1 + \pi^2 \cdot 7,24 \cdot 10^8 \cdot 200 / (35000 \cdot 7200^2)]^{-1} = 0,559$$

$$\gamma_2 = 1$$

$$a = 205 \text{ mm}$$

$$a_2 = \frac{\gamma_1 \cdot E_1 A_1 \cdot a}{\gamma_1 \cdot E_1 A_1 + E_2 A_2} = \frac{0,559 \cdot 7,24 \cdot 10^8 \cdot 205}{0,559 \cdot 7,24 \cdot 10^8 + 5,18 \cdot 10^8} = 90,91 \text{ mm}$$

$$a_1 = a - a_2 = 205 - 90,91 = 114,99 \text{ mm}$$

$$(EJ)_{eff} = E_1 J_1 + E_2 J_2 + \gamma_1 \cdot E_1 A_1 a_1^2 + \gamma_2 \cdot E_2 A_2 a_2^2 =$$

$$= 1,51 \cdot 10^{11} + 5,59 \cdot 10^{12} + 0,559 \cdot 7,24 \cdot 10^8 \cdot 114,99^2 + 5,18 \cdot 10^8 \cdot 90,01^2 = 1,53 \cdot 10^{13} \text{ Nmm}^2$$

The self-weight of half a composite structure per unit length is

$$q = \gamma_c \cdot h_1 \cdot b_1 + \gamma_{glulam} \cdot h_2 \cdot b_2 = 24 \times 10^{-6} \cdot 50 \cdot 400 + 4 \times 10^{-6} \cdot 115 \cdot 360 = 0,65 \text{ kN/m}$$

By considering that the bending moment in the middle and the shear force at the supports are

$$M_d = \frac{q \cdot l^2}{8} = \frac{0,65 \cdot 7,2^2}{8} = 4,18 \text{ kNm}$$

$$T_d = \frac{q \cdot l}{2} = \frac{0,65 \cdot 7,2}{2} = 2,32 \text{ kN}$$

the maximum shear force on the extreme shear connector and the instantaneous mid-span deflection was therefore:

$$F_V = \frac{\gamma_1 \cdot E_1 \cdot A_1 \cdot a_1 \cdot s_{eq}}{(EJ)_{eff}} \cdot V = \frac{0,559 \cdot 7,24 \cdot 10^8 \cdot 114,99 \cdot 200}{1,53 \cdot 10^{13}} \cdot 2,32 = 1,42 \text{ kN}$$

$$u_{g,inst} = 1,1 \cdot \frac{5}{384} \cdot \frac{(g_{1,k}+g_{2,k}) \cdot l^4}{EJ_{eff}} = 1,1 \cdot \frac{5}{384} \cdot \frac{(0,48+0,17) \cdot 7200^4}{1,39 \cdot 10^{13}} = 1,63 \text{ mm.}$$

These two results are compared with the outcomes from the analysis reported in Table 6.6, as it is reported in Table 6.9.

	Theoretical values	Numerical values	Error [%]
Mid-span deflection	1,63 [mm]	1,7 [mm]	4,12
Max shear force on the screw	1,42 [kN]	1,32 [kN]	7,04

Table 6.9: Check of the trustworthiness of the numerical results.

As it can be seen by viewing in the previous Table 6.9 the results from both the analysis were very closed. Hence, it can be concluded that the numerical model correctly describes the behavior of the short-term conditions and therefore it is possible to get from it reliable values.

6.6 Results from the FEM analysis

In this paragraph there are presented the results of the FEM analysis carried out in function of different parameters as it can be seen subsequently. Together with the numerical results there are also reported the trend of the solution in agreement with “ γ – method” presented in Eurocode 5, see standard reference [27].

6.6.1 Models with variation of the thickness of the slab

Table 6.10 reporteds the results from the analysis considering three different values of the thickness of the slab. As it can be seen, increasing the thickness of the slab, with regard to the serviceability limit states and in particular the natural frequency and the sags for the different load combinations decrease but as far as ultimate limit state is concerned, the bending moment decreases but the axial force in the beam element and the shear force acting on the connector element increase.

MODELS WITH VARIATION OF THE THICKNESS OF THE SLAB							
Slab thickness [mm]	Beam depth [mm]	Frequency [Hz]	QP sag [m]	Rare sag [m]	Axial Force in the beam [kN]	Bending Moment in the beam [kNm]	Max force in the screw [kN]
50	360	13,52	0,0046	0,0065	73,96	9,61	6,41
75	360	12,76	0,0043	0,0059	79,52	8,77	6,89
100	360	12,32	0,0041	0,0055	82,03	8,08	7,10

Table 6.10: Results of analysis from models with different depth of the slab.

In order to better understand the behavior of the composite system Figure 6.9 reports the trend of the shear force acting on the connector element and the maximum bending stress in the timber beam in function of the thickness of the slab by implementing the “ γ – method”.

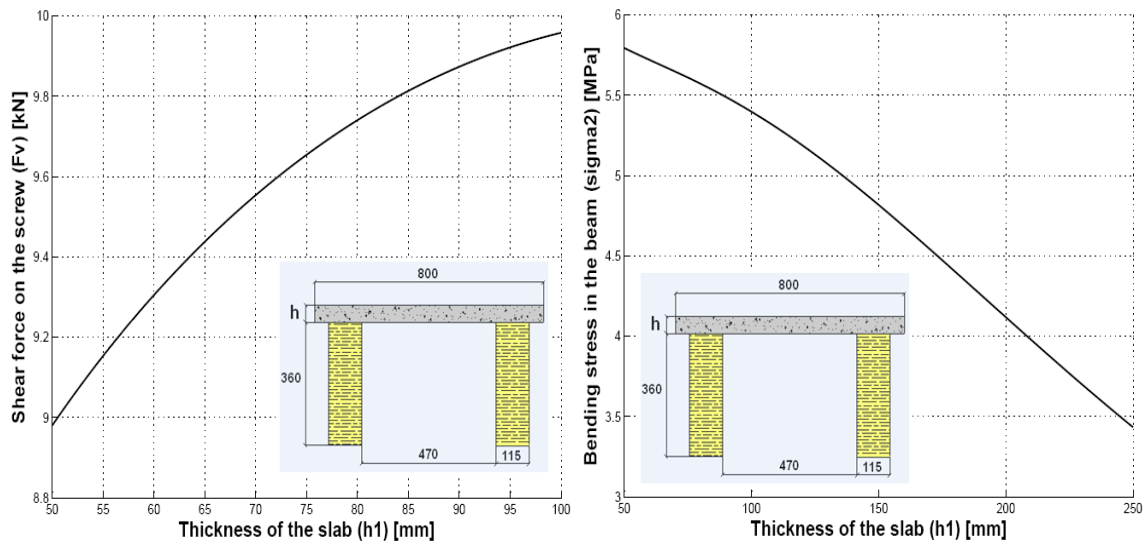


Figure 6.9: Relationship between the maximum shear force acting on the screw (Fv) and the thickness of the slab ($h1$), on the left. Relationship between the maximum bending stress ($\sigma2$) in the glulam beam and the thickness of the slab ($h1$), on the right.

By viewing the graph on the left, it is easy to see that the maximum shear force acting on the connector, considering constant the other parameters, increase with the thickness of the slab. By observing the graph on the right, it is easy to understand that more is the thickness of the slab and less is the tension in the beam at the lower edge since the composite beam is even less deflected. The neutral axis moves up and it has a migration of the compression force upwards.

6.6.2 Models with variation of the depth of the beam

Model with the variation of the depth of the timber beam has been developed. By increasing the depth of the beam, considering constant all the other parameters of course, with regard to the serviceability limit states, the natural frequency increases instead the sags for the different load combinations decrease. As far as ultimate limit state is concerned, the bending moment is increasing. On the other hand, the axial force in the timber beam decreases. Due to the increase of the depth of the beam, the inertia of the system is increased and thus the maximum shear force on the connector is decreased.

MODELS WITH VARIATION OF THE DEPTH OF THE BEAM						
Depth of beam [mm]	Thickness of the slab [mm]	Frequency [Hz]	Rare sag [m]	Axial Force in the beam [kN]	Bending Moment in the beam [kNm]	Max force in the screw [kN]
360	50	13,52	0,0065	73,96	9,61	6,41
405	50	15,34	0,0049	64,63	10,29	5,60
495	50	18,97	0,0031	50,91	11,51	4,40
585	50	22,55	0,0021	41,41	12,57	3,58

Table 6.11: Results from FE models with different depth of the timber beam.

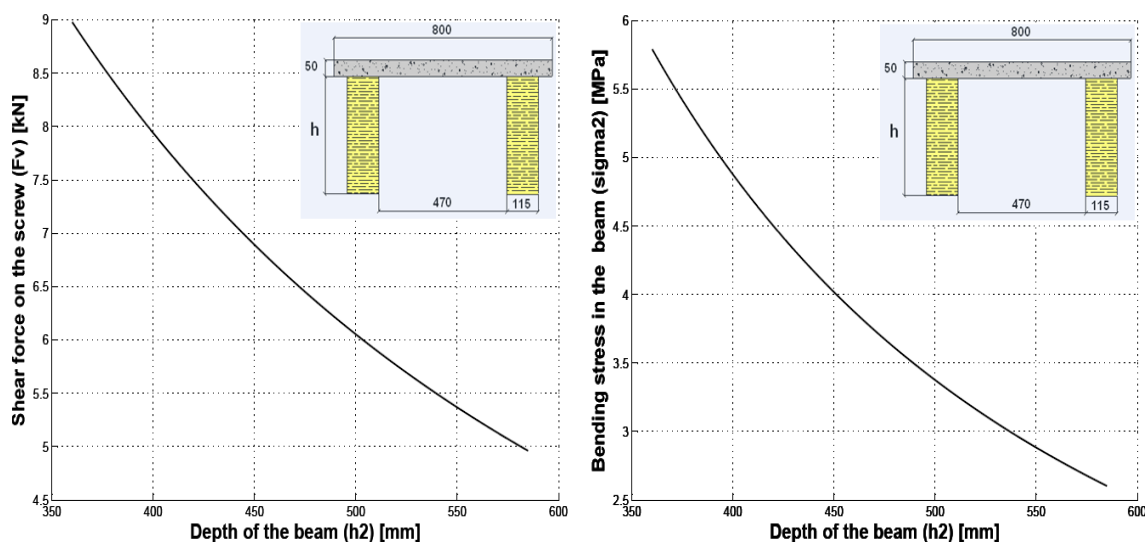


Figure 6.10: Relationship between the maximum shear force acting on the screw (F_v) and the depth of the beam (h_2), on the left. Relationship between the maximum bending stress (σ_2) in the glulam beam and the depth of the beam (h_2), on the right.

In order to see at a glance the behavior of the composite system, Figure 6.10 reports the trend of the shear force on the connector element and the maximum bending

stress in the timber beam in function of the depth of the beam by implementing the “ $\gamma - method$ ” relationship.

The trend of the maximum shear force on the connector element in function of the depth of the timber beam is shown on the left side of Figure 6.10. By keeping constant all the other parameters, the maximum shear force acting on the connector at the support, with slab thickness equal to 50 mm, decrease rapidly by increasing the height of the beam. On the other hand, on the right side it is shown the trend of the maximum tensile stress in the beam at the lower edge. By increasing the depth of the beam, the neutral axis moves upwards, the structure gains even more inertia and in this manner it deflects less and thus the lower edge of the beam is less subjected to stress.

6.6.3 Models with the variation of the spacing of the screws

These type of models consist to study the behavior of the composite structure by varying the spacing between screws. Results of these analysis are reported in Table 6.12. The first column shows the spacing adopted in the different models. Where there is a spacing expressed as, for example, 20 + 30 + 20, it means that the distribution of the screws along the beams is not uniform but there are different spacing. In particular, for this case it means that, starting from the supports for a distance equal to $1/4$ the spacing between the screws is 20 cm. On the other hand, in the middle part, for a length of $1/2$ the spacing between the screws is 30 cm. Using a non-constant spacing of the screws is very common also in “traditional system”, it allows to get better efficiency from the structure and to save screws as well. By increasing the spacing of the screws, the structure behavior is going towards the no rigid structure, like when the elements are overlapped without connections.

MODEL WITH VARIATION OF THE SPACING BETWEEN THE SCREWS						
Screw spacing [cm]	Thickness of the slab [mm]	Freq. [Hz]	Rare sag [m]	Axial Force in the beam [kN]	Bending Moment in the beam [kNm]	Max force in the screw [kN]
10	50	14,05	0,0060	78,87	8,61	3,61
15	50	13,77	0,0063	77,10	9,18	5,30
15+20+15	50	13,72	0,0063	75,21	9,50	5,35
20	50	13,52	0,0065	73,96	9,61	6,41
20+30+20	50	13,43	0,0065	71,39	10,17	6,58

Table 6.12: Results of the analysis from models with different spacing between the screws.

By increasing the spacing of the screws, the natural frequency decreases and the mid-span deflection increases according to the theoretical approach. With regard to the

ultimate limit states, the axial force in the timber beam decreases, this because the slip between the concrete slab and the timber beam will occur easily due to the total stiffness of the connection decrease. Besides, the bending moment increases according to the deflection and the connectors are even more subjected to higher shear force. The trend of the maximum shear force acting on the screw and of the maximum bending tensile stress at the lower edge in the timber beam are shown Figure 6.11 in function of the spacing of the screws.

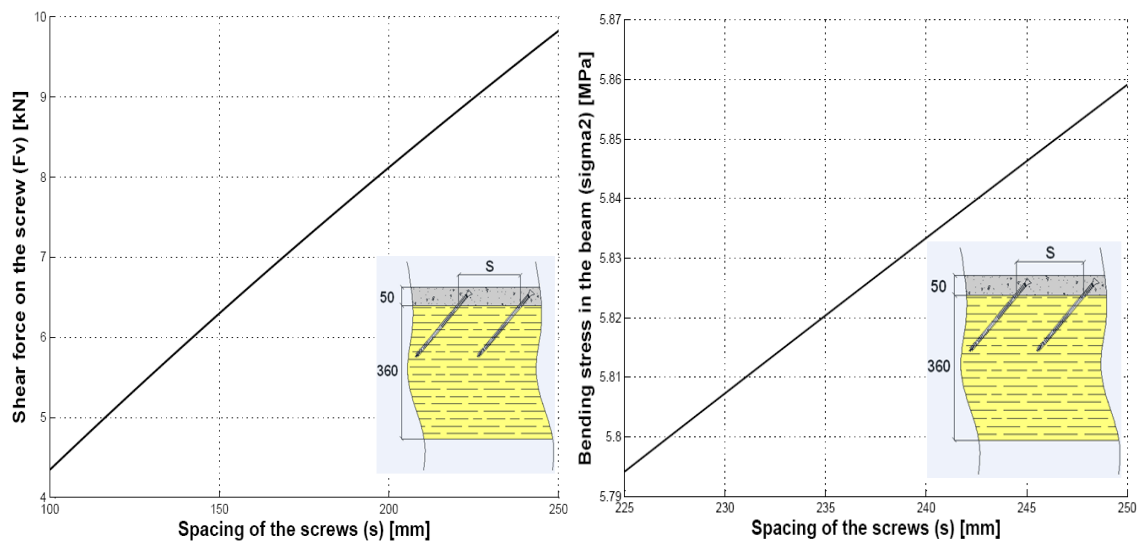


Figure 6.11: Relationship between the maximum shear force acting on the screw (F_v) and the spacing of the screws (s), on the left. Relationship between the maximum bending stress (σ_2) in the glulam beam and the spacing of the screws (s), on the right.

Both the previously graphs show a monotonous growing up trend, it means that to decrease either the number of the screws or increasing the spacing between screws the shear force acting on connectors elements and the tensile stress in the lower edge of the beam are increasing.

6.6.4 Models with variation of depth of the beam and the spacing between screws.

It was also expected to develop two different models by changing both, the depth of the beam and the screw spacing. In both the models the depth of the beam is equal to 405 mm, the thickness of the slab is still 50 mm but the spacing between the screws changed. In the first one, it was configured as 20 + 30 + 20 cm, as previously explained, whilst in the other one it was fixed constant and equal to 30 mm. All the other parameters and the loads were maintained constant. The results of these models are given Table 6.13.

MODELS WITH VARIATION OF BEAM DEPTH AND SCREW SPACING						
Screw spacing [cm]	Thickness of the slab [mm]	Freq. [Hz]	Rare sag [m]	Axial Force in the beam [kN]	Bending Moment in the beam [kNm]	Max force in the screw [kN]
20+30+20	50	15,26	0,0050	62,42	10,78	5,70
30	50	14,87	0,0053	60,45	11,24	7,58

Table 6.13: Results of the analysis from model with both depth of the beam and spacing between screws variation.

If these results are compared with the previous model with depth of the beam equal to 405 mm but with constant spacing between the screws and equal to 20 cm, it can be said that the results are almost the same. The conclusion is that to have a higher depth it is not so advantageous because the height of the entire structure will increase and efficiency of the connections could decrease to carry the same loads, and in this way the connections are not exploited but the load will be carried mostly from the timber beam. Therefore, it is cheaper to use smaller beams. Moreover, by using less screws leads to save money as well.

6.6.5 Choice of the dimensions and of the parameters

It can be concluded from the previous analysis, by maintaining constant all the other parameters, if the depth of beam is increased the mid-span deflection will reduce and the shear force on the connector will decrease as well. On the other hand, if the thickness of the concrete slab is increased, the mid-span deflection will also decrease and also the maximum shear force acting on the connector. Eventually, with the same conditions and by reducing either the number of the screws or the spacing between the screws the mid-span deflection and the shear force on the connectors increase. Actually, this is a problem of optimal solution where it has to be considered as well as the performance of the composite structure also the money saving.

After the discussion over these results, it was chosen to use for the three full-scale specimens the following dimensions, reported in Table 6.14.

Dimensions and parameters chosen for the full-scale specimens		
Depth of the beam [mm]	Thickness of the slab [mm]	Spacing between the screws [mm]
360	50	20+30+20

Table 6.14: Dimensions and parameters chosen for realize the full-scale specimens.

These dimensions allow to save material, like a lamella of wood and screws and besides to satisfy the serviceability requirements as maximum mid-span deflection

and natural frequency. In fact, with regard to the natural frequency estimated from the numerical model is 13,43 Hz more than 10 Hz which was required and for the instantaneous deflection the estimate value is 0,0065 m, less than 0,018 m as it was required. The width of the timber beam was instead fixed earlier, 115 mm and also the width of the slab, which was 800 mm in accordance with the stands for the Strömvalle stadium (see chapter 10).

Chapter 7

Experimental campaign

This chapter presents the whole experimental campaign, bending and dynamic tests program performed on full-scale specimens. It also presents the compression tests on cubes of steel-fibre reinforced concrete and withdrawal tests of screws from cubes of concrete.

7.1 Introduction

The experimental tests have been carried out at the laboratory of the Lunds Universitet (Lunds Tekniska Högskola). The experimental campaign included: (i) dynamic tests carried out on one full-scale specimen, (ii) short-time bending tests carried out on two different full-scale specimens, (iii) long-time bending test carried out on one full-scale specimen, (iv) compression tests on three cubes of steel-fibre reinforced concrete (v) nine withdrawal tests of screws with different depth in cubes of concrete.

7.2 Dynamic test program

For timber-concrete composite structures the increased stiffness and mass reduce the susceptibility to floor vibrations, which is one of the reasons why this construction technique has been extensively used to upgrade existing timber floors. However, the additional mass of the concrete topping may reduce the natural frequency of a composite floor, in particularly if the connection system is not stiff, leading to unsatisfactory dynamic performance. Remedies for this problem include increasing the stiffness of the connection system or decreasing the mass of the system. However, reducing the mass would decrease the thermal mass and acoustic separations, which are very important features of floors in multi-storey buildings. Consequently, using a stiff connection system may be the optimal way to produce timber-concrete floors with acceptable dynamic behavior and effective acoustic separation.

7.2.1 Experimental set-up

The purpose of the dynamic tests was to investigate the natural frequencies of the prefabricated composite structure, which represent the system's behavior at serviceability limit state (SLS). The measurements were performed using 24 two-axis accelerometers uniformly distributed over the floor, see Figure 7.1. The concrete slab has been divided in a mesh composed from 36 rectangles with sides 800 mm in the longitudinal direction and 200 mm in the transversal direction. This mesh has been determined to be a good compromise between the spatial resolution and the area covered by the sensor array, given the range of the frequencies which has to be investigated. An accelerometer has been positioned at each node of the mesh. An additional set of 2 accelerometers have been placed on the timber beams.

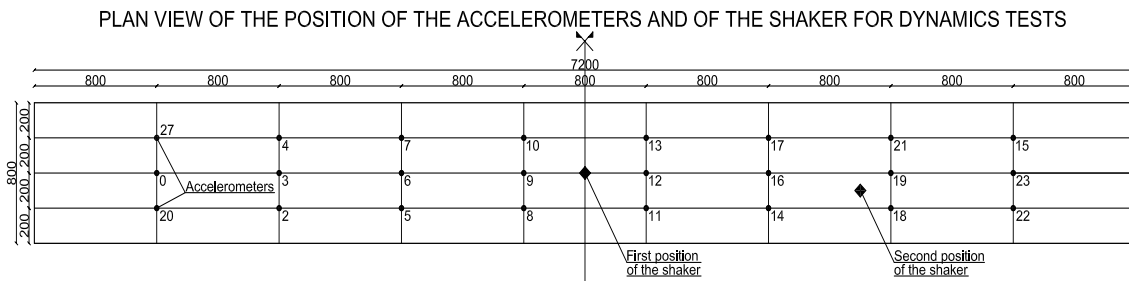


Figure 7.1: Mesh of the 24 two-axis accelerometers.

To get the force applied by the shaker (Permanent Magnetic Vibration Exciter - Type 4808) a force transducer was placed between the shaker rod and the plate attachment as shown in Figure 7.2.



Figure 7.2: The shaker and the accelerometers surrounding it.

The accelerometers and the force transducer are connected to a computer with 26-channel acquisition system. The system is capable of synchronous measuring of all

the channels up to 100 kHz sampling frequency and stores the data in a large and fast temporary buffer before it is transferred to the computer. The acquisition data is saved as Matlab.mat files for later analysis.

The very advantage of using frequency sweeps as excitation signals for the shaker is that different floor vibration modes get excited as the frequency is increased progressively. The vibration repartition over the floor is modified drastically as various modes are excited, even though the frequency is sometimes just slightly modified. Various modes of vibration have been excited, but for the purpose of this thesis, only the frequency for the first two modes has been reported with referring to both the vertical and the torsional vibration modes, respectively, see Figure 7.3 and 7.4. The first measurement campaign has been realized by positioning the shaker in the middle of the composite beam. In this way, the first mode has been well excited but the second mode has not vibrated, hence, the second measurement campaign has been conducted by positioning the shaker approximately at one-fourth the length of the beam and moved from the centreline, see Figure 7.1.

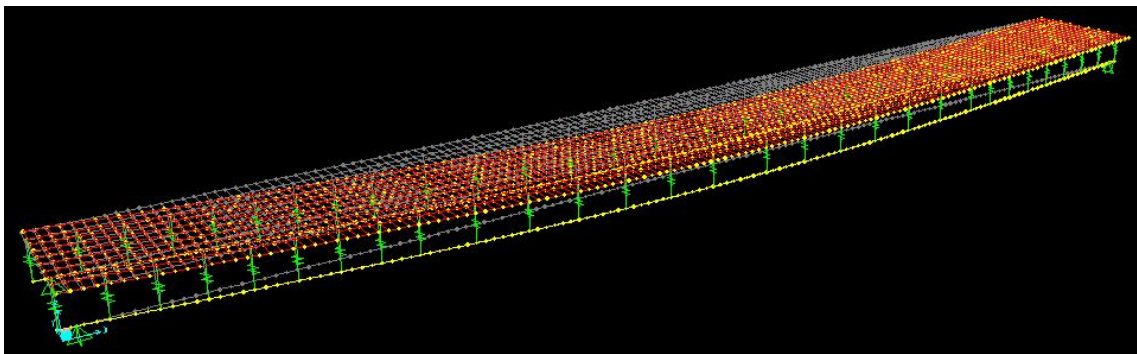


Figure 7.3: First mode of vibration of the system, related to bending.

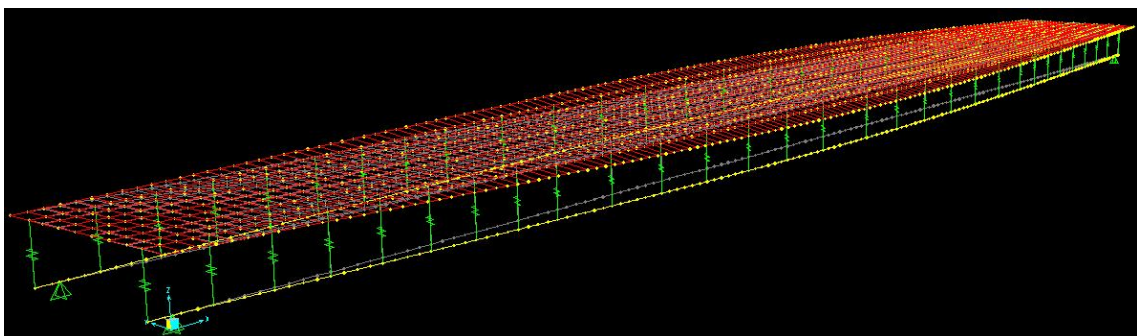


Figure 7.4: Second mode of vibration of the system, related to torsion.

7.2.2 Results from dynamic test

Frequency response functions, constructed using the fast Fourier transforms of the recorded accelerations, indicate that the fundamental frequency (f_n^I) for the specimen

B was 12,89 Hz and the second natural frequency (f_n^{II}) was 19,91 Hz. The results of the frequency response functions are displayed in Figures 7.5, 7.6, 7.7 and 7.8. Each of these figures represents the frequency response of 24 accelerometers as the excitation frequency is increased continuously between 7 Hz and 25 Hz. The modes can be easily identified here as well, and since the spatial frequency is low, all channels show their minima and maxima at roughly the same frequency.

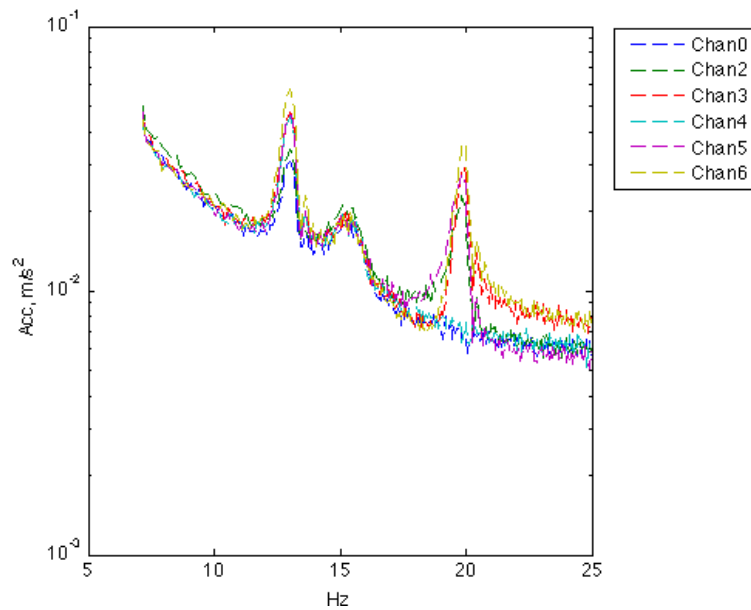


Figure 7.5: Accelerometer magnitude for a sweep between 7 and 25 Hz and for the relative channels.

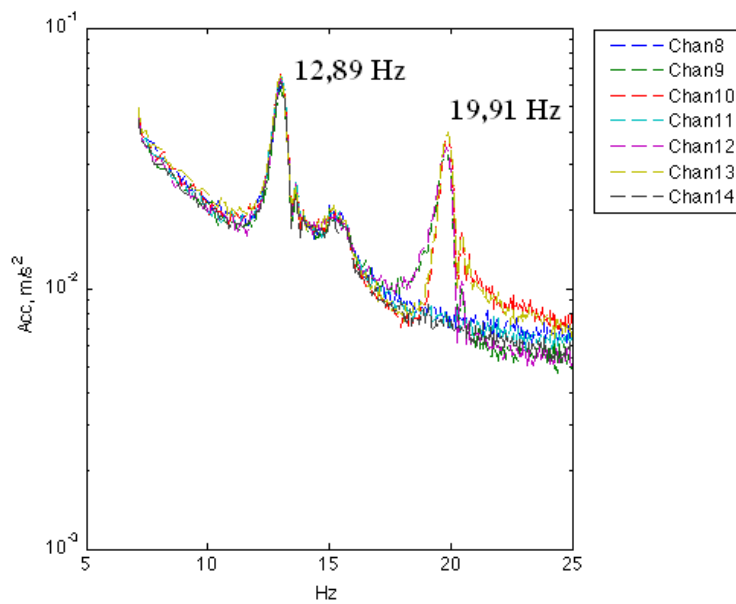


Figure 7.6: Accelerometer magnitude for a sweep between 7 and 25 Hz and for the relative channels.

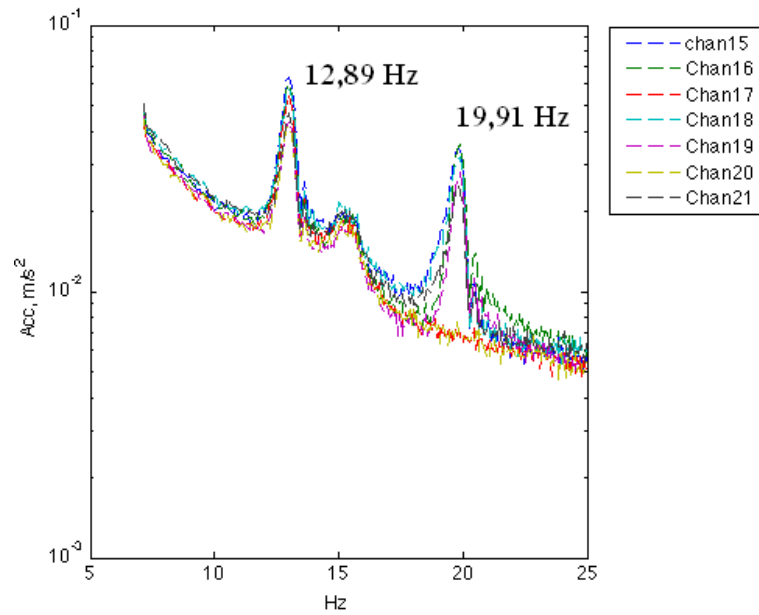


Figure 7.7: Accelerometer magnitude for a sweep between 7 and 25 Hz and for the relative channels.

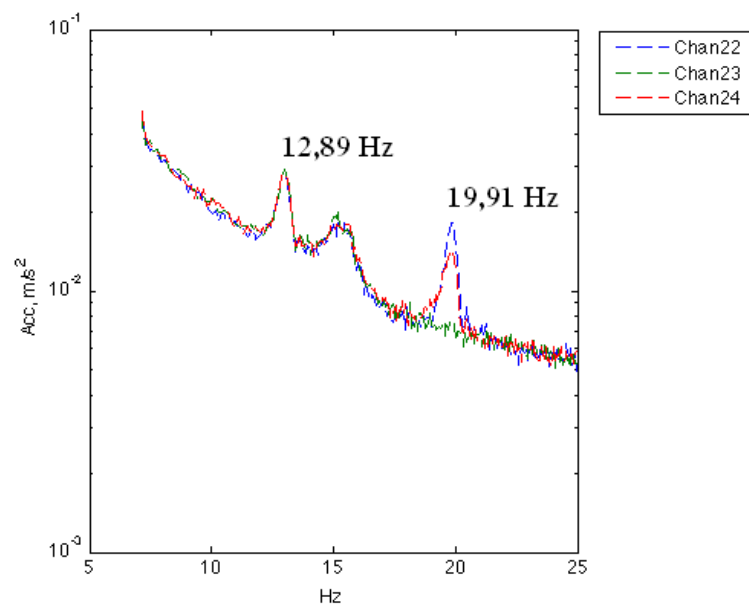


Figure 7.8: Accelerometer magnitude for a sweep between 7 and 25 Hz and for the relative channels.

The fundamental frequency is a function of the stiffness, weight and span length of the composite floor system. The fundamental frequency (f_n^I) indicate that the composite floor systems were well built from a dynamic response perspective, with natural first frequency well above 8 Hz below, which the structure may become too susceptible to vibrations. The connection system can thus be considered stiff enough and well spaced if used for a 7,2 m span system.

7.2.3 Dynamic stiffness

The dynamic stiffness has been evaluated by inverting the following expression, referred to the eigenfrequency:

$$f_n = n^2 \cdot \frac{\pi}{2} \cdot \frac{1}{L^2} \cdot \sqrt{\frac{g}{A \cdot \gamma}} \cdot \sqrt{EJ_{dyn}}$$

where

n is the number of the vibration mode;

L is the floor span, in mm;

g is the acceleration of gravity;

A is the area of the cross section;

γ is the specific gravity, in kN/m^3 ;

EJ_{dyn} is the dynamic stiffness.

Once it has been known from the FE model that the first vibration mode is the one related to the bending of the system, see Figure 7.3. The eigenfrequency of the system from the dynamic test is $f_n^1 = 12,89$ Hz, see Figures 7.5, 7.6, 7.7 and 7.8. The dynamic stiffness was then derived by inserting $n = 1$ in the previously expression:

$$\begin{aligned} EJ_{dyn} &= f_n^2 \cdot \left(\frac{2}{\pi}\right)^2 \cdot \frac{L^4}{n^4} \cdot \frac{A \cdot \gamma}{g} = \\ &= 12,89^2 \cdot \left(\frac{2}{\pi}\right)^2 \cdot \frac{7055^4}{1^4} \cdot \frac{22,95 \times 10^{-6} \cdot 50 \cdot 800 + (4,12 \times 10^{-6}) \cdot 115 \cdot 360 \cdot 2}{9,81 \cdot 10^3} = \\ &= 2,14 \times 10^{13} \text{ Nmm}^2 \end{aligned}$$

7.3 Short-term bending tests program

Bending tests are necessary to study the structural behavior and to evaluate the mechanical properties of the composite timber-concrete system. For this reason two bending tests on two full-scale specimens have been performed. The specimens tested, representing stands of a stadium, were constructed and then tested to failure.

7.3.1 Specimens design and construction

The full-scale specimens are both made by two glulam GL30c beams with dimensions $115 \times 360 \times 7200$ mm, joined to a steel fibre reinforced concrete slab with 50 mm thickness, 800 mm depth and 7200 mm length, through the inclined screws as described in chapter 4. For all the details regarding the preparation of the full-scale specimens see chapter 4. Here there are reported in Table 7.1 the geometrical details of the two composite beam tested.

ID specimen	Total length [mm]	Total width [mm]	Connection spacing [mm]	Width of the beam [mm]	Depth of the beam [mm]	Beam spacing [mm]
A	7200	800	200+300+200	115	360	585
C	7200	800	200+300+200	115	360	585

Table 7.1: Geometrical details of the composite timber-fiber reinforced concrete system.

The specimens used to perform the short-term bending tests were specifically specimen A and C. Specimen B has been used to perform the dynamic tests and also the long-term bending test.

7.3.2 Bending tests

The bending tests have been performed with the machinery and equipment shown in Figure 7.9 and in agreement with the loading pattern reported in Figure 7.10.

The load has been applied on four lines through steel partitioning beams; number and position of these lines have been determined in order to induce in the slab effects (bending moment, maximum shear stress and mid-span deflection) similar to those induced by a uniformly distributed load with same resultant. The force has been applied through an hydraulic jack jointed to a reply beam constrained to the laboratory floor, located on axis to the midpoint of the testing beams, and to the partitioning main beam.

The four loads, amounting to $P/4$ (where P is the load applied through the hydraulic jack), have to be positioned at the specific distance from one of the two supports

equal to the values carried on Table 7.2. The position of the load points is given in function of the distance (L) between the two supports.



Figure 7.9: Equipment used to perform the bending tests.

Values of the load	$P/4$	$P/4$	$P/4$	$P/4$
Distance from the first support	$0,125 \cdot L$	$0,375 \cdot L$	$0,625 \cdot L$	$0,875 \cdot L$
Distance from the previous load $P/4$	$0,125 \cdot L$	$0,25 \cdot L$	$0,25 \cdot L$	$0,25 \cdot L$

Table 7.2: Positions of the loads.

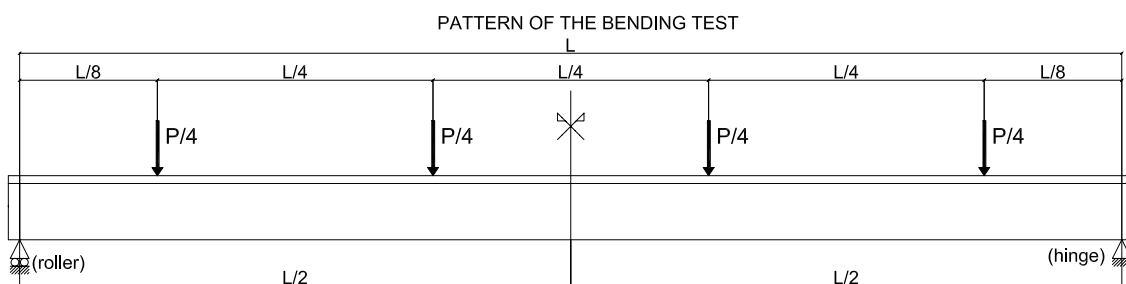


Figure 7.10: Pattern of the bending test.

The composite beams have been placed on four supports which consist in four steel plates 145 mm wide. The supports have been realized through two rollers on one side (one for each beam) and on the other side through two hinges (one for each beam). It has been chosen to reinforce the timber (compression perpendicular to the grain) at the supports with screws, in order to avoid a premature rupture of the glulam beam at the supports, as happened for the first test described in chapter 3. Besides, in order to make more rigid the area of the support it was screwed in the timber beams four screws ($VGZ \phi 11 \times 250$) with $\phi 6$ mm pre-drilled holes. The distance from the edges and the spacing between the screws are reported in Figure 7.11.

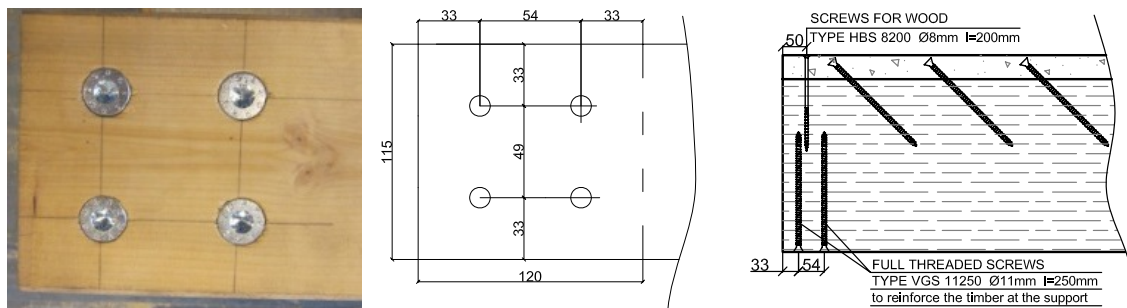


Figure 7.11: Disposition of the reinforcing screws at the supports.

7.3.2.1 General procedure - Evaluation of the load P

Experimental tests have been performed according to standard reference UNI EN 26891:1991, see [28]. For the ULS tests, once it is known the ultimate load of the specimen, P_U (initially estimated on the basis of the theoretical evaluations and eventually corrected during the test execution), the following load path is prescribed to be followed:

- Load increasing until the value of $0,4 \cdot P_U$, with an application speed of the load constant and amounting to $0,2 \cdot P_U/min$. Once it is achieved $0,4 \cdot P_U$ the specimen has to be kept in this load configuration for 30 s;
- Load has to be decreased until the value of $0,1 \cdot P_U$, and maintained constant for 30 s;
- Load is increased until the ultimate load or a slip equal to 15 mm is achieved; for $P < 0,7 \cdot P_U$ the application speed of the load has to be kept constant and amounting to $0,2 \cdot P_U/min$ ($\pm 25\%$), while instead for $P > 0,7 \cdot P_U$ the application speed of the load has to be decreased in order to reach the ultimate load, or the 15 mm slip with an extra-time varying between 3 and 5 minutes ($0,05 \cdot P_U/min$), with the total time for the test amounting to about 10 or 15 minutes.

This standard reference is calibrated on a force control test, but it has been chosen to carry out a displacement control test in order to capture with more accuracy the ultimate load. The set speed was equal to 2 mm/min up to the achievement of 40% of the estimated ultimate load and also during the decrease of the load up to 10% of the estimated ultimate load. Then, the speed has been increased to a value equal to 4 mm/min up to 70% of estimated ultimate load and after that the speed has been set equal to 2 mm/min up to the failure of the composite beam. Besides, the test has been concluded by reaching the ultimate load and not the slip of 15 mm.

It has to be remembered in the next tables and diagrams, that to the load values imposed by the hydraulic jack it must be added the self-weight of the partitioning steel beams.

The *self-weight of each one of the composite systems* are evaluable as:

$$\begin{aligned}
 P_{self-weight} &= 2 \cdot [(g \cdot \rho_{g,k}) \cdot b_{beam} \cdot h_{beam} \cdot l] + \gamma_{k,SFRC} \cdot b_{slab} \cdot h_{slab} \cdot l = \\
 &= 2 \cdot [(9,81 \cdot 420 \cdot 10^{-3}) \cdot 0,115 \cdot 0,360 \cdot 7,200] + 22,93 \cdot 0,800 \cdot 0,050 \cdot 7,200 = 9,06 \text{ kN}
 \end{aligned}$$

The load due to the *self-weight of the transversal partitioning steel beams*, which were 12 pieces of square tubular profiles with side 80 mm, thickness 5 mm and a total length of 16,52 m amounts to 1,83 kN.

The longitudinal partitioning system is made by a HEA 300 profile with length equal to 5,3 m. The *self-weight of the HEA 300 profile* amounts to 4,59 kN. The total self-weight of the entire partitioning system is therefore equal to 6,42 kN, corresponding to a uniformly distributed load amounting to 1,11 kN/m². This has to be taken into account while performing the experimental tests (the ultimate load obtained by the hydraulic jack was therefore 6,42 kN lower than the real ultimate load of the system).

7.3.2.1.1 Evaluation of the theoretical ultimate load capacity

Successively, it has been reported the discussion and the estimated theoretical ultimate load capacity of the composite system. The calculations for the theoretical ultimate load has been carried out considering half-section of the composite beam as it is shown in Figure 7.12. Here are only reported the calculations, for more informations about the method see chapter 5.

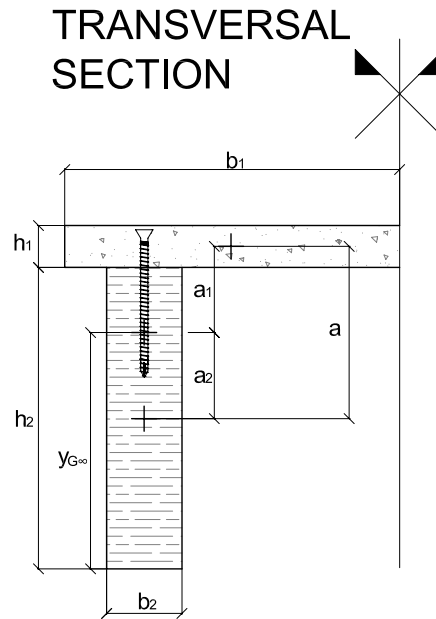


Figure 7.12: Half-section considered for the estimation of the theoretical ultimate load.

Geometric data of the slab		Geometric data of the beam	
b_1 [mm]	400	b_2 [mm]	115
h_1 [mm]	50	h_2 [mm]	360

Table 7.3: Geometric data of half a section of the composite beam.

The parameters needed to estimate the theoretical ultimate load are reported in the following lines with reference to the parameters obtained from experimental tests reported in reference [4]. The load has been assessed with referring to short-term conditions ($t = 0$), by using mean values of the parameters and without the load combinations. By assuming the same nomenclature adopted by the Eurocode 5:

$$E_1 J_1 = E_{cm} \cdot \frac{b_1 \cdot h_1^3}{12} = 36210 \cdot \frac{400 \cdot 50^3}{12} = 1,51 \times 10^{11} \text{ Nmm}^2$$

$$E_2 J_2 = E_{0,mean} \cdot \frac{b_2 \cdot h_2^3}{12} = 12500 \cdot \frac{115 \cdot 360^3}{12} = 5,59 \times 10^{12} \text{ Nmm}^2$$

$$E_1 A_1 = E_{cm} \cdot h_1 \cdot b_1 = 36210 \cdot 400 \cdot 50 = 7,24 \times 10^8 \text{ N}$$

$$E_2A_2 = E_{0,mean} \cdot h_2 \cdot b_2 = 12500 \cdot 360 \cdot 115 = 5,18 \times 10^8 \text{ N}$$

$$(EJ)_0 = E_1J_1 + E_2J_2 = 1,51 \times 10^{11} + 5,59 \times 10^{12} = 5,74 \times 10^{12} \text{ Nmm}^2$$

$$(EA)_0 = \frac{E_1A_1 \cdot E_2A_2}{E_1A_1 + E_2A_2} = \frac{7,24 \times 10^8 \cdot 5,18 \times 10^8}{7,24 \times 10^8 + 5,18 \times 10^8} = 3,02 \times 10^8 \text{ N}$$

As previously presented in chapter 3, the value of the slip modulus K_{ser} which has been obtained from push-out tests is equal to

$$K_{ser} = 35000 \text{ N/mm}$$

$$K_u = \frac{2}{3} \cdot K_{ser} = \frac{2}{3} \cdot 35000 = 23333 \text{ N/mm}$$

where K_u is the instantaneous slip modulus for the ultimate limit states.

Thus, by substituting values in the expression presented in paragraph 5.3.2, it has obtained:

$$\gamma_2 = 1$$

$$s_{min} = 200 \text{ mm}$$

$$s_{max} = 300 \text{ mm}$$

$$s_{eq} = 0,75 \cdot s_{min} + 0,25 \cdot s_{max} = 0,75 \cdot 200 + 0,25 \cdot 300 = 225 \text{ mm}$$

$$l = 7055 \text{ mm}$$

$$\gamma_1 = [1 + \pi^2 \cdot E_1A_1 \cdot s_{eq} / (K_u \cdot l^2)]^{-1} =$$

$$= [1 + \pi^2 \cdot 7,24 \times 10^8 \cdot 225 / (23333 \cdot 7055^2)]^{-1} = 0,42$$

$$a = \frac{a_1}{2} + \frac{a_2}{2} = \frac{50}{2} + \frac{360}{2} = 205 \text{ mm}$$

$$a_2 = \frac{\gamma_1 \cdot E_1A_1 \cdot a}{\gamma_1 \cdot E_1A_1 + \gamma_2 \cdot E_2A_2} = \frac{0,42 \cdot 7,24 \times 10^8 \cdot 205}{0,42 \cdot 7,24 \times 10^8 + 5,18 \times 10^8} = 75,81 \text{ mm}$$

$$a_1 = a - a_2 = 205 - 75,81 = 129,19 \text{ mm}$$

$$(EJ)_{ef} = (EJ)_0 + \gamma_2 \cdot E_2A_2 \cdot a_2^2 + \gamma_1 \cdot E_1A_1 \cdot a_1^2 =$$

$$= 5,74 \times 10^{12} + 1 \cdot 5,18 \times 10^8 \cdot 75,81^2 + 0,42 \cdot 7,24 \times 10^8 \cdot 129,19^2 =$$

$$= 1,38 \times 10^{13} \text{ Nmm}^2$$

$$(EJ)_\infty = (EJ)_0 + (EA)_0 \cdot a^2 =$$

$$= (5,74 \times 10^{12} + 3,02 \times 10^8 \cdot 205^2) = 1,84 \times 10^{13} \text{ Nmm}^2$$

$$\eta = \frac{(EJ)_{eff} - (EJ)_0}{(EJ)_{\infty} - (EJ)_0} = \frac{1,38 \times 10^{13} - 5,74 \times 10^{12}}{1,84 \times 10^{13} - 5,74 \times 10^{12}} = 0,64$$

The self-weight load of the composite beam is calculated by considering a wood density equal to $\rho_{g,mean} = 420 \text{ kg/m}^3$ as reported in paragraph 4.2.1.2 and a concrete density equal to $\rho_{c,mean} = 22,93 \text{ kN/m}^3$ with referring to the one used to built out the full-scale specimens presented in chapter 3. It has to be remembered that the load has been calculated without considering the safety factors. The self-weight load of the system floor has been summarized in the next Table 7.4.

Self-weight		[kN/m]
Concrete slab	$G_{1,slab}$	0,46
Glulam beam	$G_{1,beam}$	0,17
Non-structural weight	G_2	0

Table 7.4: Self-weight load of the composite system.

In order to estimate the ultimate load capacity of the composite system, it has been checked the failure of the connection system and the failure of the wooden beams. As regards the failure of the concrete due to the achievement of the tensile strength it has been neglected because it is not easy to estimate the tensile strength of a steel-fibre reinforced concrete through theoretical calculations and this is due to lots of parameters that come into play. Anyway, the type of concrete belongs to a high class of resistance and it has been assumed that it does not break, as it is happened. Thus, in order to give an evaluation of the ultimate load P_u it has been operated in the following order. It has been chosen a value for the variable uniformly distributed load Q to add to the self-weight of the composite beam and to the self-weight of the partitioning steel beams, in order to reach a value similar to 1 in the strength checking of the connection system and also in the strength checking of the glulam beams.

7.3.2.1.2 Failure of the connection. Approach according to Eurocode 5

The Eurocode 5 provides for screwed connections subjected to a combination of axial load and lateral load the following expression:

$$\left(\frac{F_{ax,Ed}}{F_{ax,Rd}} \right)^2 + \left(\frac{F_{v,Ed}}{F_{v,Rd}} \right)^2 \leq 1 \quad (7.1)$$

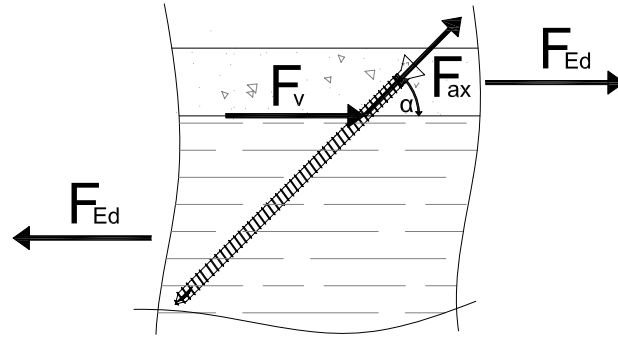


Figure 7.13: Static principle of the Eurocode approach.

where $F_{ax,Rd}$ and $F_{v,Rd}$ are the design load-carrying capacities of the connection loaded with axial load or lateral load respectively.

The mean embedment strength value in timber of screws should be estimated with mean values as

$$f_{h,0,m} = 0,082 \cdot (1 - 0,01 \cdot d_{ef}) \cdot \rho_m = 0,082 \cdot (1 - 0,01 \cdot 1,1 \cdot 6,6) \cdot 420 = 31,94 \text{ MPa}$$

The mean withdrawal strength at an angle $\alpha = 45^\circ$ to the grain has been taken as:

$$f_{ax,m} = 3,6 \times 10^{-3} \cdot \rho_m^{1,5} = 3,6 \times 10^{-3} \cdot 420^{1,5} = 30,99 \text{ MPa}$$

$$f_{ax,45,m} = \frac{f_{ax,m}}{\sin^2(45) + 1,5 \cdot \cos^2(45)} = \frac{30,99}{\sin^2(45) + 1,5 \cdot \cos^2(45)} = 24,79 \text{ MPa}$$

The mean withdrawal capacity of the connection at an angle $\alpha = 45^\circ$ to the grain has been taken as

$$n_{ef} = 1$$

$$d = 11 \text{ mm}$$

$$l_{ef} = 197 - 11 = 186 \text{ mm}$$

$$F_{ax,45,Rm} = n_{ef} \cdot (\pi \cdot d \cdot l_{ef})^{0,8} \cdot f_{ax,45,m} = 1 \cdot (\pi \cdot 11 \cdot 186)^{0,8} \cdot 24,79 = 27,59 \text{ kN}$$

The mean load-carrying capacity for screws per shear plane per fastener with referring to Eurocode 5 has been taken as the minimum value found from the following expressions

$$F_{v,Rm} = \min \left\{ \begin{array}{l} f_{h,0,m} \cdot l_{ef} \cdot d_c \\ f_{h,0,m} \cdot l_{ef} \cdot d_c \cdot \left[\sqrt{2 + \frac{4 \cdot M_{y,Rk}}{f_{h,0,m} \cdot d_c \cdot t_1^2}} - 1 \right] + \frac{F_{ax,Rm}}{4} \\ 2,3 \cdot \sqrt{M_{y,Rk} \cdot f_{h,0,k} \cdot d_c} + \frac{F_{ax,Rm}}{4} \end{array} \right.$$

$$F_{v,Rm} = \min \left\{ \begin{array}{l} 31,94 \cdot 186 \cdot 6,6 = 39,21 \text{ kN} \\ 31,94 \cdot 186 \cdot 6,6 \cdot \left[\sqrt{2 + \frac{4 \cdot 45900}{31,94 \cdot 6,6 \cdot 186^2}} - 1 \right] + \frac{27590}{4} = 23,35 \text{ kN} \\ 2,3 \cdot \sqrt{45900 \cdot 31,94 \cdot 6,6} + \frac{27590}{4} = 14,05 \text{ kN} \end{array} \right.$$

The maximum load on the fastener close to the supports can be calculated as

$$F_{Ed,connection} = \frac{\gamma_1 \cdot E_1 A_1 \cdot a_1 \cdot s_{eq}}{(EJ)_{ef}} \cdot V \quad (7.2)$$

where V is the maximum shear force acting at the supports which depends on the load applied. In order to not satisfy the equation 7.1, it has to be added a force load F amounting to 91 kN corresponding to a uniformly distributed load Q amounting to 32,25 kN/m² and 12,90 kN/m. By considering this load plus the self-weight load of the composite structure the total load used for the checking of the connection system with the Eurocode 5 approach gives a shear force at the supports equal to

$$V = (G_{1,slab} + G_{1,glulam} + Q_{variable}) \cdot l/2 = (0,46 + 0,17 + 12,90) \cdot 7,055/2 = 47,73 \text{ kN}$$

thus, the maximum load on the fastener close to the supports is estimated by substituting the values in the equation 7.2:

$$F_{Ed,connection} = \frac{0,42 \cdot 7,24 \times 10^8 \cdot 129,19 \cdot 225}{1,38 \times 10^{13}} \cdot 47730 = 30,57 \text{ kN}$$

This force is then decomposed into two components, one parallel to the axis of the screw and the other one perpendicular to the axis of the screw, respectively:

$$F_{ax,Ed} = F_{Ed,connection} \cdot \cos(45^\circ) = 21,61 \text{ kN}$$

$$F_{v,Ed} = F_{Ed,connection} - F_{Ed,connection} \cdot \cos(45) = 8,96 \text{ kN}$$

Eventually, the failure of the connection estimated with Eurocode 5 gives in this case:

$$\left(\frac{12,55}{27,59}\right)^2 + \left(\frac{8,96}{14,05}\right)^2 \simeq 1$$

Hence, the Eurocode approach provides the failure of the connection system with a load imposed from the hydraulic jack equal to $(91 - 6,42 = 84,58 \text{ kN})$ because it must be considered the load of the partitioning steel beams. This value is very low and it is unreliable. The formula does not kept the right behavior and gives value to much on the safe side.

7.3.2.1.3 Failure of the connection system by simplified approach

The simplified approach considered just the tensile strength of the screw and the contribution of friction, but this method does not consider the shear contribute which

is take into account from Johansen's approach. The present approach considers the effect resistant of the forces shown in Figure 7.14.

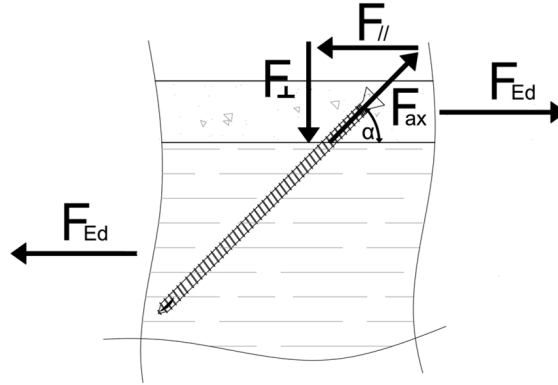


Figure 7.14: Static principle for the simplified approach.

The mean withdrawal capacity of the connection at an angle $\alpha = 45^\circ$ to the grain can be calculate considering the minimum value between withdrawal capacity and the failure of the screw in tension:

$$F_{ax,45,m} = \min \begin{cases} (\pi \cdot l_{ef} \cdot d)^{0,8} \cdot n_{ef} \cdot f_{ax,45,m} = (\pi \cdot 186 \cdot 11)^{0,8} \cdot 1 \cdot 24,79 = 27,59 \text{ kN} \\ f_y \cdot \frac{\pi \cdot d_c^2}{4} = 958 \cdot \frac{\pi \cdot 6,6^2}{4} = 32,78 \text{ kN} \end{cases}$$

The resistance force based on such approach can be evaluated by projecting $F_{ax,45,m}$ in the direction of the relative slip between the concrete slab and the timber beam and considering the contribution of the friction by assuming a coefficient of friction $\mu = 0,25$:

$$\begin{aligned} F_{v,Rd} &= F_{ax,45,m} \cdot \cos(\alpha) + \mu \cdot F_{ax,45,m} \cdot \sin(\alpha) = \\ &= 27,59 \cdot \cos(45^\circ) + 0,25 \cdot 27,59 \cdot \sin(45^\circ) = 24,39 \text{ kN} \end{aligned}$$

The strength checking of the connection system in this case is given by the following equation

$$\frac{F_{Ed}}{F_{v,Rd}} \leq 1$$

In order to get the value of the previous ratio equal to 1 and thus to unsatisfy the inequality it has to increase the variable load up to a value of $F = 72 \text{ kN}$, corresponding to a uniformly distributed load Q amounting to $25,51 \text{ kN/m}^2$ and $10,21 \text{ kN/m}$. Hence, the simplified approach provides the failure of the connection system with a load imposed from the hydraulic jack equal to $(103 - 6,42 = 65,58 \text{ kN})$ because it

must be considered the load of the partitioning steel beams. This value is still low and it is not reliable. The formula gives results on the safe side because it does not consider the shear strength of the screw.

7.3.2.1.4 Failure of the connection system by using an extension of the Johansen approach

In this section, according to paper [25], it has been adopted an extension of the Johansen's yielding theory to predict the ultimate load for timber-to-concrete joints using self-tapping threaded connectors screwed at an angle to the wood. In order to obtain the load bearing capacity of timber-to-concrete connection with inclined screws, which are principally loaded in tension, the Johansen's theory has been extended, taking into account the withdrawal capacity of fastener and friction between the contact interfaces of connected members. For more informations and for the entire derivation of the formulas see paper [25]. The study reported in this paper showed that the load-bearing capacity for connections with inclined high tensile strength screws can be predicted using the yielding theory, but this theory is unable to predict precisely the failure mode.

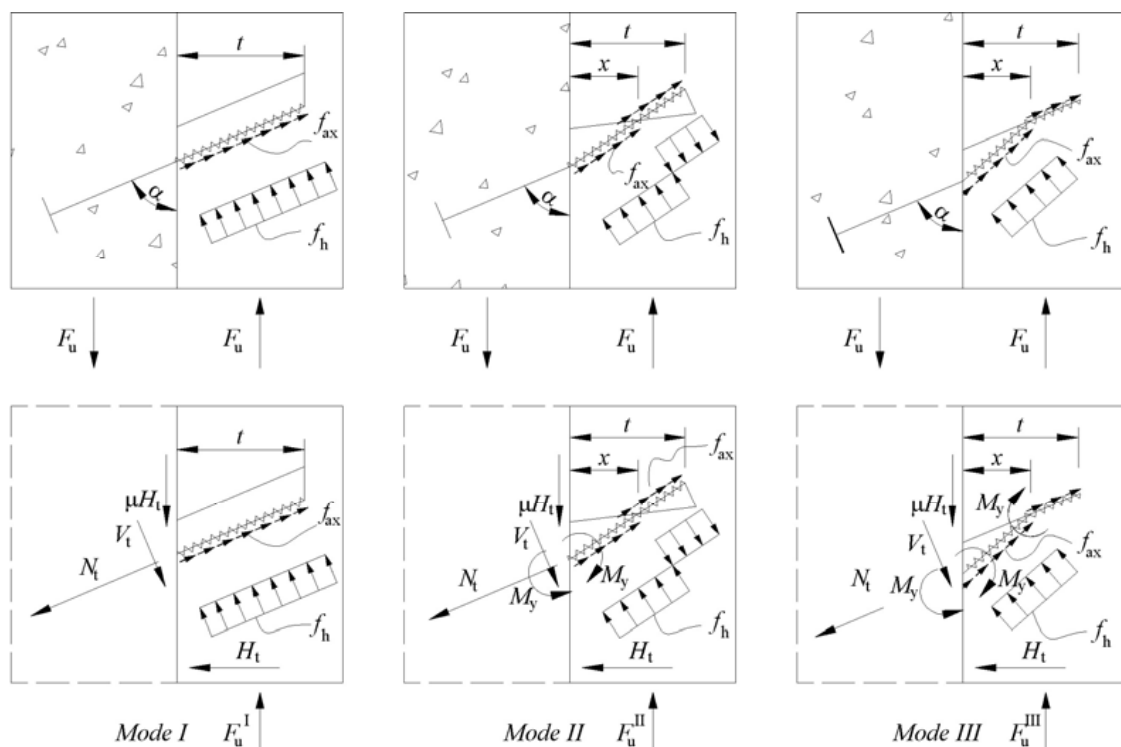


Figure 7.15: Stresses in a timber-to-concrete connection with an inclined screw for three Johansen's failure modes.

By considering this approach, the load-bearing capacity can be assumed as the minimum value of the following equations:

$$F_u = \min \begin{cases} F_u^I = f_{ax,45,m} \cdot d \cdot t \cdot (\cot\alpha + \mu) + f_{h,0,m} \cdot d_{ef} \cdot t \cdot (1 - \mu \cdot \cot\alpha) \\ F_u^{II} = f_{ax,45,m} \cdot d \cdot t \cdot (\cot\alpha + \mu) + f_{h,0,m} \cdot d_{ef} \cdot t \cdot (1 - \mu \cdot \cot\alpha) \times \\ \times \left[\sqrt{2} \cdot \sqrt{\frac{M_{y,Rk}}{f_h \cdot d_{ef} \cdot t^2}} \cdot \sin^2(\alpha) + 1 - 1 \right] \\ F_u^{III} = f_{ax,45,m} \cdot d \cdot t \cdot (\cos\alpha + \mu) + 2 \cdot \sqrt{f_{h,0,m} \cdot d_{ef} \cdot M_{y,Rk}} \times \\ \times (\sin\alpha - \mu \cdot \cos\alpha) \end{cases}$$

where F_u^I , F_u^{II} and F_u^{III} are representing the three modes of failure which could occur, $\mu = 0,25$ is the coefficient of friction between the two members and $d = 11$ mm is the outer diameter, instead $d_{ef} = 1,1 \cdot d_c$ where d_c is the core diameter of the screw and $t = 139$ mm is the depth of the tip of the screw from the interface of the two members. When the inclination angle between the screw axis and the timber plane is $\alpha = 45^\circ$ and by substituting the parameters reported before, the previous equation gives the following outcomes:

$$F_u = \min \begin{cases} F_u^I = 71,55 \text{ kN} \\ F_u^{II} = 57,57 \text{ kN} \\ F_u^{III} = 41,03 \text{ kN} \end{cases}$$

By using this approach, the failure mode awaited is the third one with a load-bearing capacity approximately equal to $F_{v,Rd} = 41$ kN.

The strength checking of the connection system in this case is given by the following equation

$$\frac{F_{v,Ed}}{F_{v,Rd}} \leq 1$$

In order to get the value of the previous ratio equal to 1 and thus to unsatisfy the inequality it has to increase the variable load up to a value of $F = 123$ kN, corresponding to a uniformly distributed load Q amounting to $43,59$ kN/m² and $17,43$ kN/m. Hence, by using the extension of the Johansen's approach it provides the failure of the connection system with a load imposed from the hydraulic jack equal to $(123 - 6,42 = 116,58$ kN) because it must be considered the weight of the partitioning steel beams. This value is not so believable because some experimental tests has shown that the load-bearing capacity for connections with inclined high tensile strength screws predicted by using the yielding theory is unable to predict precisely the failure mode. Thus, the results of this approach must be considered carefully.

7.3.2.1.5 Discussions over the failure of the connections

The calculations of the failure of the connections system has it can be seen from the previous calculations provide very different values. All of them are unreliable for predicting the ultimate load because the are on the save side and sometimes either

friction or shear capacity is neglected. Anyway, in order to check the load-carrying capacity only by shear, specific shear tests have been performed on the same screws in Borås, see [4]. Results of the tests have been presented in chapter 3. The average shear load-carrying capacity was around 40 kN, thus it has been expected that the failure of the composite structure due to bending has to happen by the failure of glulam beams.

7.3.2.1.6 Failure on the glulam beams

The strength checking of the glulam beams at $t = 0$ is given by the following inequality and it is not satisfied when gives value over 1.

$$\frac{\sigma_2}{f_{t,0}} + \frac{\sigma_{m2}}{f_m} \leq 1$$

By using a value for the variable load amounting to $F = 166$ kN, corresponding to a uniformly distributed load Q amounting to $58,82$ kN/m² and $23,53$ kN/m the strength checking of the glulam beams at $t = 0$ reaches the value similar to 1 and become unsatisfied. In particular, the normal stresses are evaluated with the following expressions, considering the maximum bending moment which for this variable load amounts to $M = 150,31$ kNm:

$$\sigma_2 = \frac{\gamma_2 \cdot E_2 \cdot a_2 \cdot M}{(EJ)_{ef}} = \frac{1 \cdot 12500 \cdot 75,81}{1,38 \times 10^{13}} \cdot 150,31 \times 10^6 = 10,33 \text{ MPa}$$

$$\sigma_{m2} = \frac{0,5 \cdot E_2 \cdot h_2 \cdot M}{(EJ)_{ef}} = \frac{0,5 \cdot 12500 \cdot 360}{1,38 \times 10^{13}} \cdot 150,31 \times 10^6 = 24,54 \text{ MPa}$$

As regards the design bending strength f_m and the design tensile strength along the grain $f_{t,0}$ for this purpose have been assumed equal to the mean values of the glulam beam without consider the partial safety factors. In Table 4.2 there are reported the characteristic values of the glulam beam. In order to estimate the mean values of them, it is enough to multiplied the characteristic values reported in Table 4.2 per 1,33. Thus, the failure of the wooden beam is reached with a value of the load $F = 166$ kN:

$$\frac{10,33}{26,6} + \frac{24,54}{40} \simeq 1$$

Hence, by considering the failure of the wooden beams, the checking formula provides a imposed load to the hydraulic jack equal to $(166 - 6,42 = 159,58$ kN) because it must be considered the load of the partitioning steel beams.

In the next Table 7.5 it has been summarized the ultimate load of the floor systems. It must be remembered that the previous ultimate load are related just to half composite system, thus for the entire composite system it has to be multiplied by two in order to get the theoretical ultimate load for each failure considered for the floor system.

Specimens A & C	P_U [kN]
Self-weight of the composite beam	9,06
Self-weight of the partitioning system	6,42
Ultimate load P_U for connection, Eurocode approach	169,16
Ultimate load P_U for connection, Simplified approach	131,16
Ultimate load P_U for connection, by using an extension of the Johansen approach	233,16
Ultimate load P_U for failure of the glulam beams	319,16

Table 7.5: Ultimate load of the floor system.

The failure of the connection system provides different values of the ultimate load based on the approach used, but they suggest that the failure of the fasteners must occur before the failure of the glulam beam. Instead, what it is expected is that one or both the two glulam beam break first, as it happened with the bending tests described in chapter 3. By considering the failure of the glulam beam, the estimated ultimate load is therefore assumed equal to $P_U = 319$ kN. The load pattern, with referring to the failure of the wooden beam for combined tensile and bending stresses is reported in the Table 7.6; to the load applied to the test machine it has to be taken off the self-weight of the system and of the partitioning steel beams (the estimated failure load becomes thus $P'_U = 319,16 - 6,42 = 312,58 \simeq 300$ kN).

Step	Path	Load level [kN]	Speed
1	Load increasing up to	$0,4 \cdot P'_U = 120$	2 mm/min
2	Load decreasing up to	$0,1 \cdot P'_U = 30$	2 mm/min
3	Load increasing up to	$0,7 \cdot P'_U = 210$	4 mm/min
4	Load increasing up to failure	$\geq P'_U = 300$	2 mm/min

Table 7.6: Load pattern with referring to the failure of the wooden beams.

It has to be remembered that between step 1 and 2 and also between step 2 and 3 it has been maintained the load level constant to the relative value for 30 seconds.

7.3.2.2 Bending test set-up

As previously explained, in order to induce in the slab effects (bending moment, maximum shear stress and mid-span deflection) similar to those induced by a uniformly distributed load with same resultant, it has been adopted for each one specimens the pattern of the bending test and the location of the test instruments which is reported in Figure 7.16.

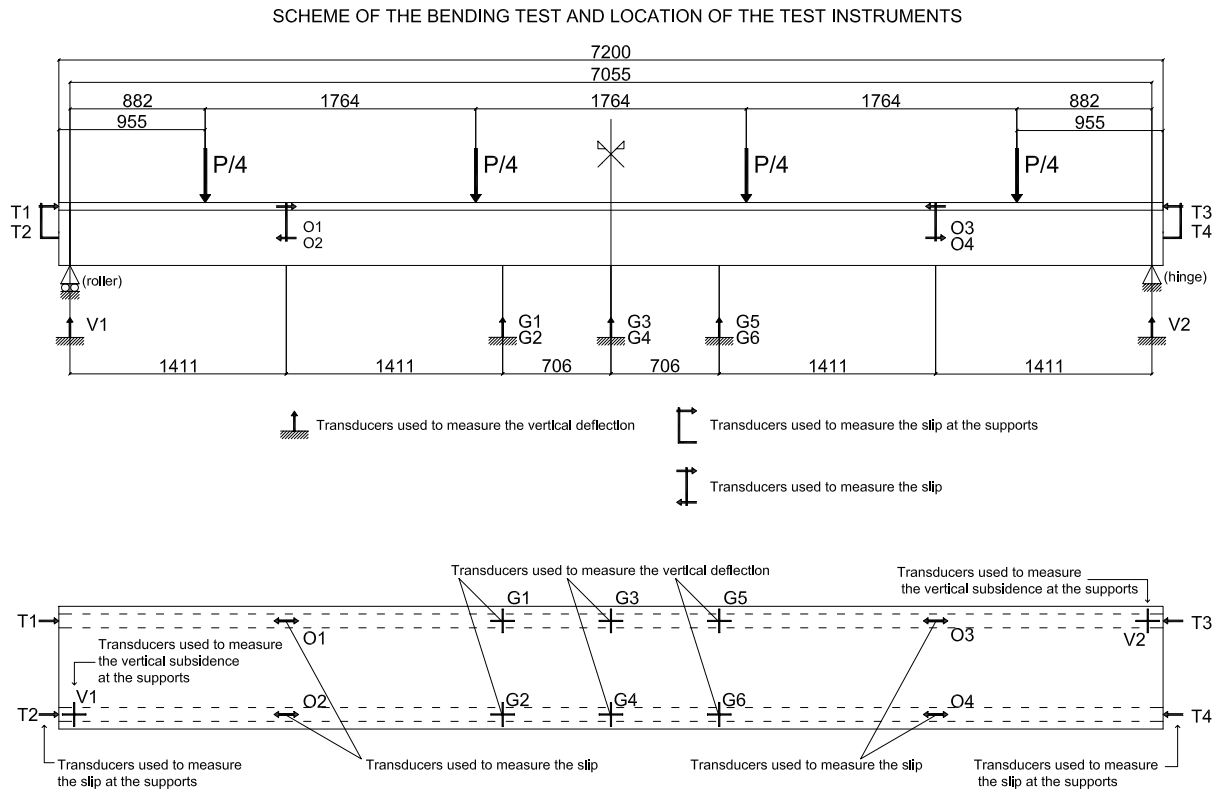


Figure 7.16: Pattern of the bending test and location of the test instruments.

The four loads amounting to $P/4$ (where P is the load applied through the hydraulic jack) have to be positioned at a specific distance from one of the two supports equal to the values carried on Table 7.7.

Values of the load	$P/4$	$P/4$	$P/4$	$P/4$
Distance from the first support [mm]	882	2646	4410	6174
Distance from the previous load $P/4$ [mm]	882	1764	1764	1764

Table 7.7: Positions of the loads for both the specimens A and C.

During the experimental tests it has been observed and monitored the total load applied to the specimen, the evolution of the mid-span deflections in the middle (channels G3 and G4) and the sags at a distance of the middle equal to 706 mm ($L/10$) for each side (channels G1, G2, G5 and G6) through 6 resistive gauges, and relative slips between slab and beam at the supports (channels T1, T2, T3 and T4) through 4 inductive transducers. It has been also monitored the relative slip between the concrete slab and the timber beam at a distance from each supports equal to 1411 mm ($L/5$) through 4 inductive transducers (channels O1, O2, O3 and O4). Eventually, in order to check the compression of the timber perpendicular to the grain at the supports it has been monitored the vertical subsidence on two supports through other 2 resistive gauges (channels V1 and V2). The imposed load has been

noted through a load cell (with maximum load set in around 500 kN) located between the hydraulic jack and the composite beam. At the load impressed by the hydraulic jack must be added the self-weight of the partitioning steel beams and joists, equal to 6,42 kN, corresponding to a uniformly distributed load amounting to 1,11 kN/m². For each test have been obtained load - slip graphs related to supports and load - deflection graph related to the middle sections, determining also the ultimate load, the slip and deflection values corresponding to fixed load levels. Furthermore, the trend of the bending stiffness and also the trend of the real efficiency have been derived in function of the equivalent uniformly distributed load.

Before performing the bending test it has been checked if the test was well prepared. In particular, it has been checked if the HEA 300 profile is stiff enough in order to obtain four equal forces to the respective load points previously determined. For such a purpose, a FEM model has been performed. For the four point has been assumed four transversal beams infinitely rigid. These transversal beams have been connected from the centre of gravity of each elements with the centre of gravity of the HEA profile through links which are assumed as springs. To all the springs have been given the same axial stiffness. The longitudinal steel profile has been loaded in the middle from a point load with a value equal to 400 kN. After the analysis it has been checked if the force acting on each spring is approximately the same and close to 100 kN. Figure 6.9 shows the result from the FEM analysis.

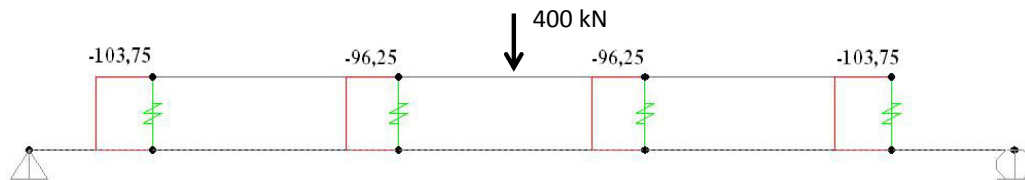


Figure 7.17: Check of the relative stiffness between the HEA profile and the composite system.

The important thing is not the absolute stiffness of both the profile and the composite structure, but the relative stiffness and that the steel HEA profile is more stiff than the underlying composite structure, because this way the force move to the bottom structure through four equal forces.

As it can be seen from the previously Figure 7.17, the four forces are almost the same, so it is correct to assume that the HEA profile is more stiff than the composite structure. Another check has been done with theoretical calculations. The stiffness of the HEA 300 profile is easy to calculate and is equal to $3,83 \times 10^{13}$ Nmm², while the stiffness of the floor system has been calculated in paragraph 7.3.2.1.1. Actually, the value calculated in this paragraph refers to half a section so it is worth to double its value in order to get the theoretical stiffness of the timber-concrete composite structure, and thus it is $EJ_{ef} = 2,76 \times 10^{13}$ Nmm². Eventually, it is considered the

ratio $(EJ_{HEA}/EJ_{ef}) = 1,4$ thus the steel profile is 40% stiffer than the composite floor and thus it is correct to assume this beam enough stiff to distribute uniformly the point load to four equal forces.

7.3.2.3 Bending test on specimen A

The bending test on the full-scale specimen A has been performed on January the 24th, exactly 48 days after the casting of the concrete. Figure 7.18 shows the full-scale specimen A before the bending test.



Figure 7.18: Floor system A before the bending tests.

The ultimate load has been reached by the failure at bottom of one of the two glulam beams (beam A2), instead the other one is intact (beam A1), Figure 7.19. The ultimate P load, applied by the test machine, amounts to about 482 kN, and thus for a q load, uniformly distributed per unit area, equal to about 84 kN/m² (the q load is obtained by dividing the P load for the total surface of the slab, 800 × 7200 mm²). The evaluating of the q load is possible only because it has been positioned the partitional steel beam in the exact positions in order to induce in the system the same results in terms of bending effects of the ones obtained with a uniformly distributed load per unit area with the same resultant. The failure of the composite floor A occurs

by the failure of the timber beam A2 due to breaking of one finger joint located close to the centre of the lowest lamella, Figure 7.20. After this failure, the test has been stopped because if it have been continued the composite beam could have only rotated. To the load applied from the hydraulic jack, it must added the self-weight of the composite beam and the one of the partitioning system, thus the failure load is $P_{Failure} = 482 + 9,06 + 6,42 \simeq 498 \text{ kN}$, corresponding to a uniformly distributed load equal to $q \simeq 86 \text{ kN/m}^2$.



Figure 7.19: Cracks along the failure beam A2.



Figure 7.20: Failure of the floor system due to the breaking of one finger joint in one timber beam.

In the next graphs are shown the following curves:

- $q - f$ (load - mid-span deflection) in Figure 7.21;
- $q - \delta$ (load - slip at the supports) in Figure 7.22;
- $q - \delta'$ (load - slip to an intermediate point) in Figure 7.23;
- the trend of the real stiffness EJ_{real} related the applied load q in Figure 7.24;
- the real efficiency of the connection $\eta_{real} = (EJ_{real} - EJ_0) / (EJ_{\infty} - EJ_0)$, as proposed by Piazza, in function of the applied load q in Figure 7.25;

- $q - v$ (load - subsidence at the rollers (supports)) in Figure 7.26;
- $q - v$ (load - subsidence at the hinges (supports)) in Figure 7.27.

The parameters needed to define these curves are evaluated and reported in the section 7.3.2.1.1 - Evaluation of the theoretical ultimate load capacity.

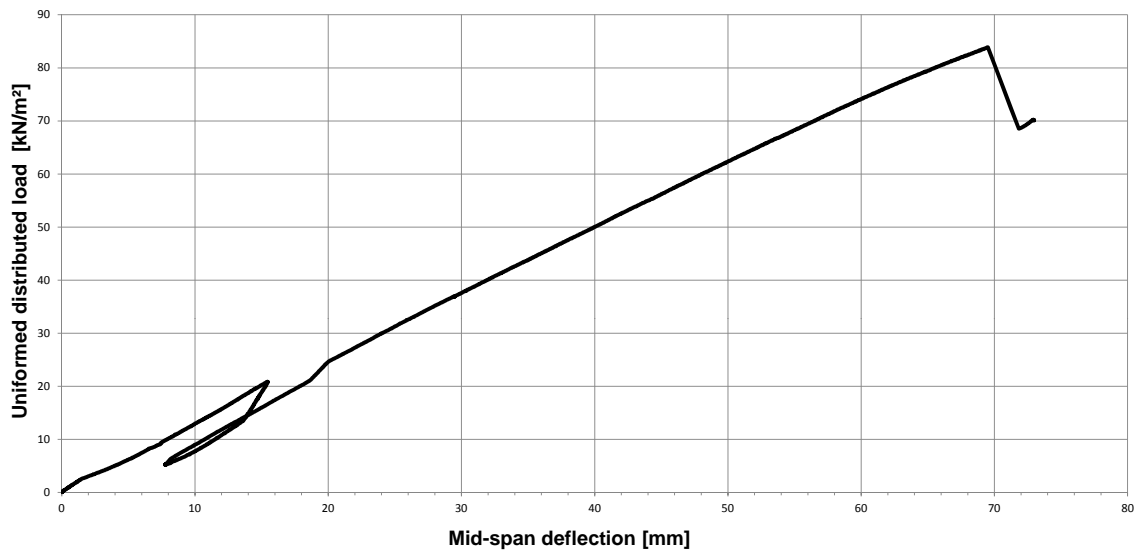


Figure 7.21: Load - mid-span deflection curve for specimen A.

The load-carrying capacity of the composite system is really high (the ultimate load is almost 84 kN/m^2 usually assessed as 60% of the failure load, while the serviceability load (40%) is around 49 kN/m^2 . The combined design load of the stands is around $8,46 \text{ kN/m}^2$ and the design service load provided from the Eurocode 1 is only 5 kN/m^2).

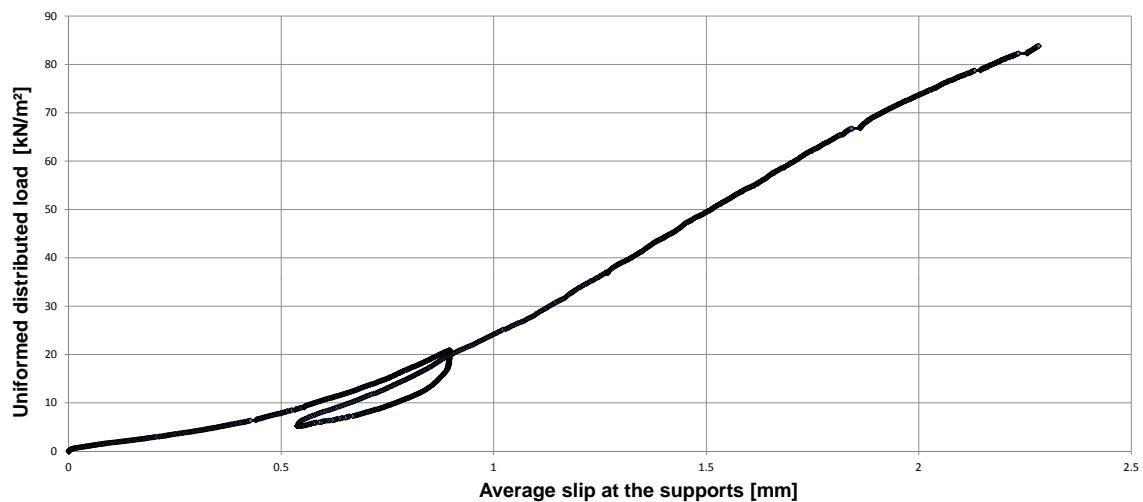


Figure 7.22: Load - slip trend at the supports for specimen A.

It must be remembered, that to these value of load q it must added both the self-weight of the composite system and partitioning system.

Figure 7.21 shows the behavior of the full-scale specimen A is really linear up to the failure and even if the good design requires a ductile failure, here the failure is brittle, but it is far from the usual service conditions so it may be considered highly unlikely to occur. Eventually, the maximum mid-span deflection corresponding to an instant just before the failure of the finger joint was close to 70 mm.

Figure 7.22 shows the trend of the relative slip between the concrete slab and the timber beams at the supports, in function of the equivalent uniformly distributed load. It can be seen that, as direct consequence of the very rigid shear connection, the values of slip are almost null (at the failure load it has registered a value of 2,3 mm, while for the design service load it is about 0,5 mm). It must be remembered, that to these values of load q it must added both the self-weight of the composite system and of the partitioning system.

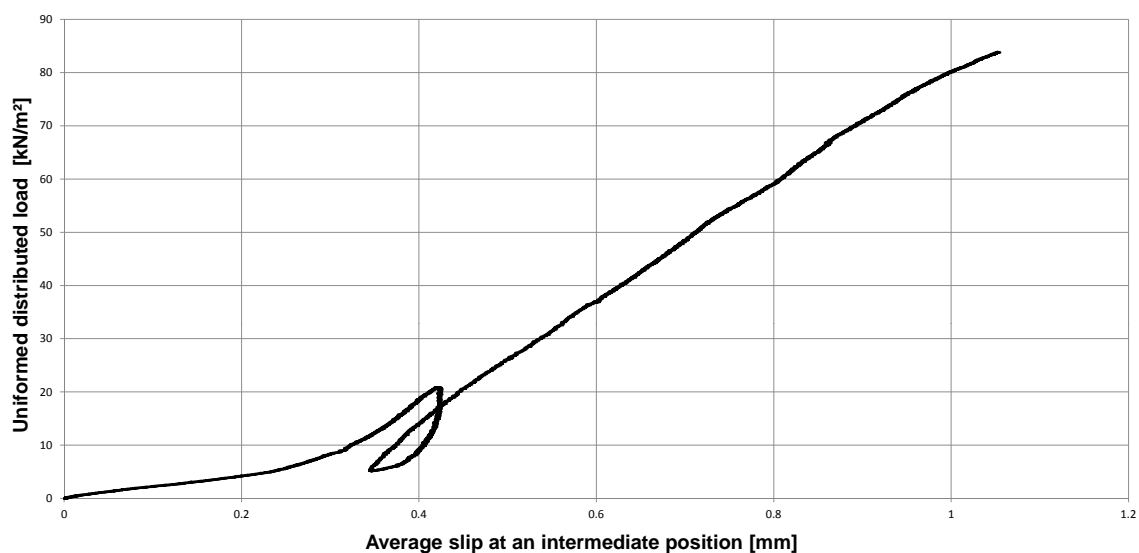


Figure 7.23: Load - slip trend to an intermediate point for specimen A.

The graph reported in Figure 7.23 shows the trend of the relative slip between the concrete slab and the timber beams at an intermediate point between the middle of the beam and the supports, in function of the equivalent uniformly distributed load. For a $q = 84 \text{ kN/m}^2$ load corresponding to the failure of the beam, at the intermediate point the average slip between the concrete slab and the timber beams are around $\delta = 1,1 \text{ mm}$. It must be remembered, that to these value of load q it must added both the self-weight of the composite system and partitioning system. This consideration allows to say that the deformable connection which has been realized throughout inclined screws actually shows a very rigid behavior besides to not show any sign of abating. No cracks appear around the screws during the test.

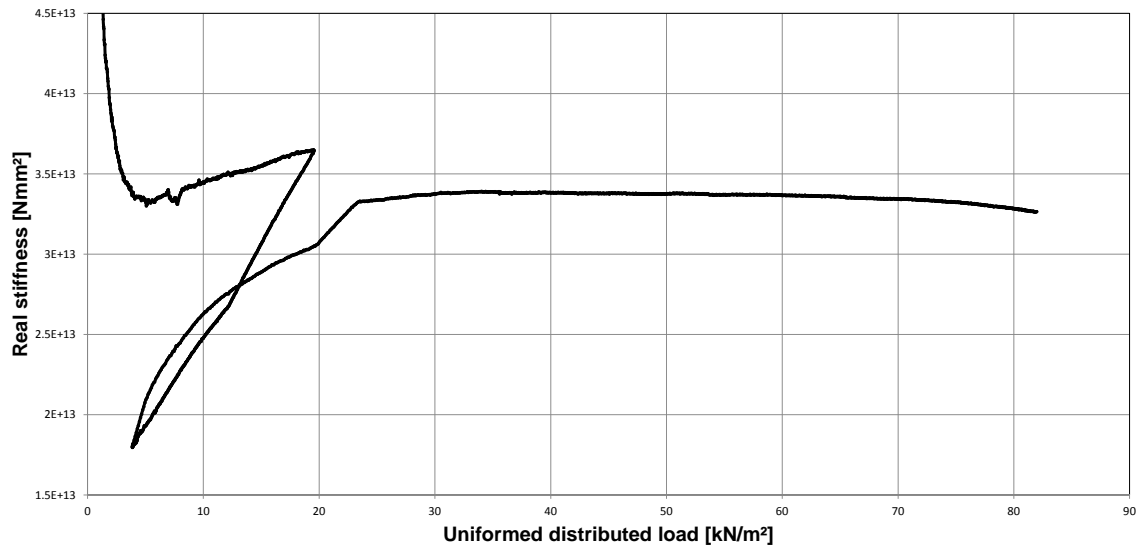


Figure 7.24: Bending stiffness EJ_{real} of the specimen A in function of the applied load q .

Figure 7.24 shows the trend of the real stiffness, after the setting phase of the test, has a constant value equal to $3,38 \times 10^{13} \text{ Nmm}^2$ and only close to the failure there is a very small decrease. It can thus concluded that the connection realized by self-tapping inclined screws is very stiff and maintains its value almost up to the failure.

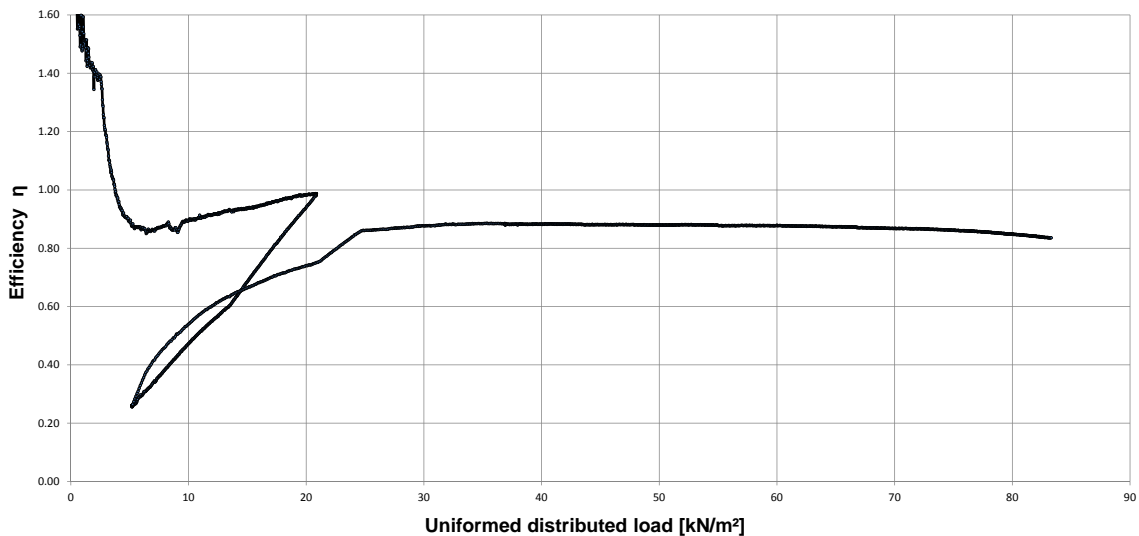


Figure 7.25: Real efficiency η_{real} of the connection system of specimen A in function of the applied load q .

Figure 7.25 shows the trend of the efficiency of the connection which is closely related to the trend of the real stiffness. Such efficiency has been evaluated using the formula proposed by Piazza considering the values of stiffness related to a full-composite action EJ_{∞} and no-composite action EJ_0 evaluated at paragraph 7.3.2.1.1. Precisely, it must be considered the double of these stiffness since they are related only to half

a section. The efficiency assumes a constant value equal to 0,88 of the full-composite action after the setting phase of the test up to almost the failure.

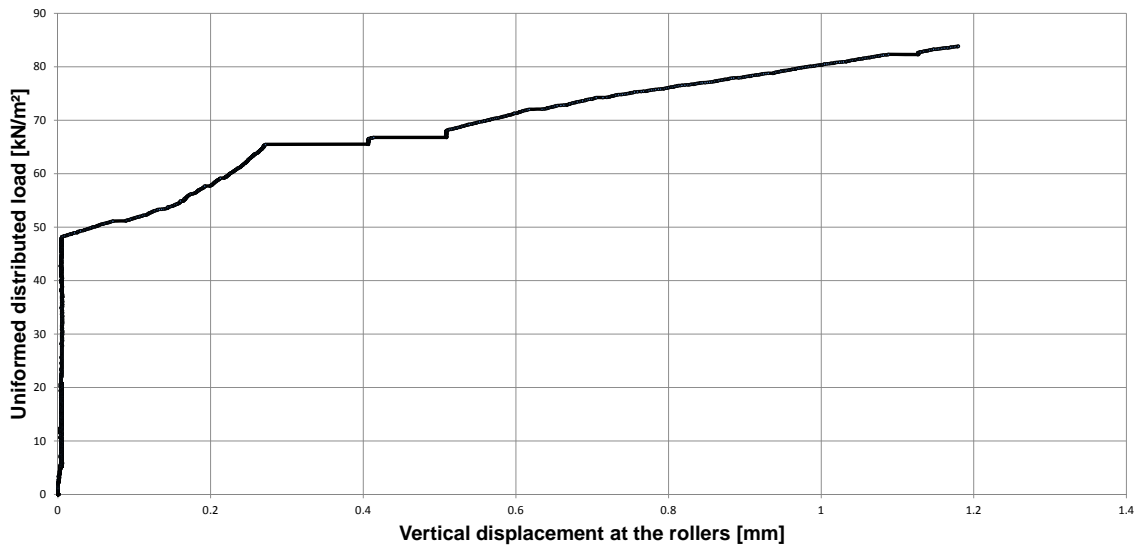


Figure 7.26: Load - subsidence at the rollers for specimen A due to compression perpendicular to the grain.

The graph reported in Figure 7.26 shows the subsidence of the timber beam at the two supports realized by two rollers. It has to be noted that the contact surface has been reinforced through four screws in order to avoid a possible premature breaking of the timber beam due to compression perpendicular to grain.

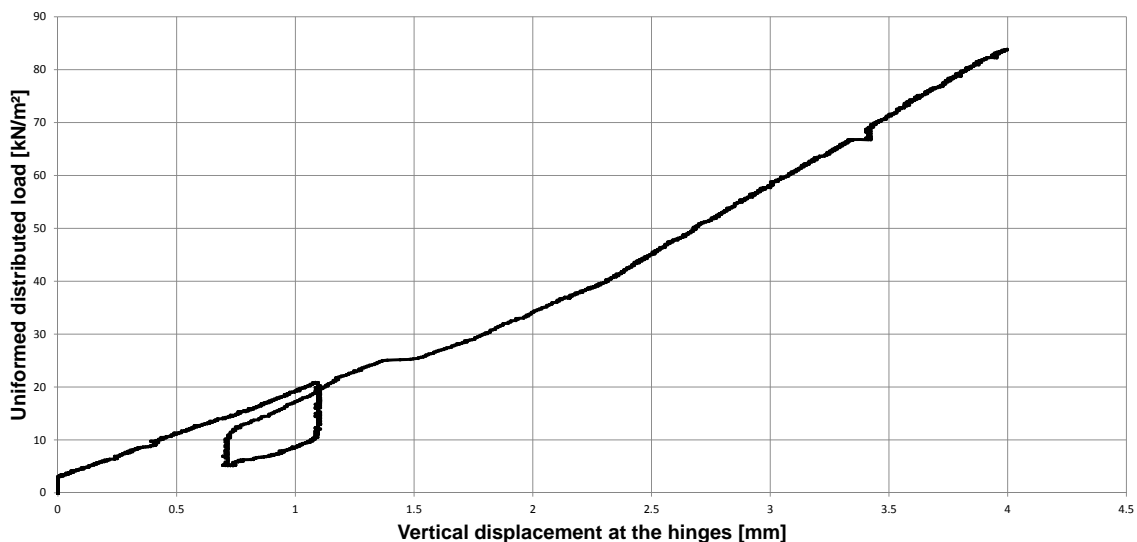


Figure 7.27: Load - subsidence at the hinges for specimen A due to compression perpendicular to the grain.

As it can be seen from the Figure 7.27 up to an equivalent uniformed distributed load amounting approximately to 48 kN/m² no subsidence has been registered. After this

load level, the subsidence increase and at the failure of the composite beam its value was less than 1, 2 mm.

The reported graph in Figure 7.27, shows the subsidence of the timber beam at the two supports realized by hinges. It has to be noted that, since the residential background type of floor, presented in chapter 3, has shown a premature breaking for compression perpendicular to grain at the these supports, before testing it four screws were inserted in the timber beam at the contact surface in order to stiff the, see section 7.3.2. In fact, in this bending test no premature failure at the contact surface has been occurred. Anyway, the graph shows the trend of the vertical displacement with the increasing of load. The compression perpendicular to the grain increase fairly linear with the equivalent load applied. To the failure, the maximum subsidence registered at the hinges has had a value of 4 mm.

In Table 7.8 are summarized the main value of the variables measured.

Variable	values
Maximum load P	498 kN
Uniformly equivalent distributed maximum load q	86 kN
Maximum mid-span deflection f	70 mm
Average slip at the supports δ	2, 28 mm
Average slip at an intermediate point δ'	1, 1 mm
Constant value of real stiffness EJ_{real}	$3, 38 \times 10^{13}$ Nmm ²
Constant value of the real efficiency η_{real}	0, 88
Maximum subsidence at the supports (hinges) $v_{,h}$	4 mm
Maximum subsidence at the supports (rollers) $v_{,r}$	1, 2 mm

Table 7.8: Main value of the variables measured for the full-scale specimen A.

7.3.2.4 Bending test on specimen C

The bending test on the full-scale specimen C has been performed on January the 26th, exactly 50 days after the casting of the concrete. Figure 7.28 shows the full-scale specimen C before the bending test.



Figure 7.28: Full-scale specimen C before the bending tests.

The ultimate load has been reached by the failure at one of the two glulam beams (beam C2) while the other one is intact (beam C1), Figure 7.29. The ultimate P load, applied by the test machine, amounts to about 462 kN, and thus for a q load, uniformly distributed per unit area, equal to about 80 kN/m² (the q load is obtained by dividing the P load for the total surface of the slab, 800 × 7200 mm²). The evaluating of the q load is possible only because it has been positioned the partitional steel beam in the exact positions in order to induce in the system the same results in terms of bending effects of the ones obtained with a uniformly distributed load per unit area with the same resultant. The failure of the composite floor C occurred by the failure of the timber beam C2 due to the sudden appearance of two huge crack parallel to the grain. The lowest crack is located in the second lamella, at a position approximately 70 mm from the lower edge. The second huge crack is located in the fifth lamella, approximately 250 mm from the lower edge of the glulam beam, see

Figure 7.30. Such a failure seems to be quite common in timber-concrete composite structures, since also the residential background floor presented in chapter 3 has shown the same type of failure. The failure can be supposedly due to either shear or tensile stress perpendicular to the grain.



Figure 7.29: Cracks along the failed beam C2.



Figure 7.30: Failure of the floor system due to the sudden appearance of two cracks. It can be supposedly due to either shear or tensile stress perpendicular to the grain.

After this failure, the test has been stopped because if it have been continued the composite beam could only rotate.

To the load applied from the hydraulic jack, it must added the self-weight of the composite beam and the one of the partitioning system, thus the failure load is $P_{Failure} = 462 + 9,06 + 6,42 \simeq 477$ kN, corresponding to a uniformly distributed load equal to $q \simeq 83$ kN/m².

In the next graphs are shown the following curves:

- $q - f$ (load - mid-span deflection) in Figure 7.31;
- $q - \delta$ (load - slip at the supports) in Figure 7.32;
- $q - \delta'$ (load - slip to an intermediate point) in Figure 7.33;

- the trend of the real stiffness EJ_{real} in function of the applied load q in Figure 7.34;
- the real efficiency of the connection $\eta_{real} = (EJ_{real} - EJ_0) / (EJ_{\infty} - EJ_0)$, as proposed by Piazza, in function of the applied load q in Figure 7.35;
- $q - v$ (load - subsidence at the rollers (supports)) in Figure 7.36;
- $q - v$ (load - subsidence at the hinges (supports)) in Figure 7.37.

The parameters needed to define these curves are evaluated and reported in the section 7.3.2.1.1 - Evaluation of the theoretical ultimate load capacity.

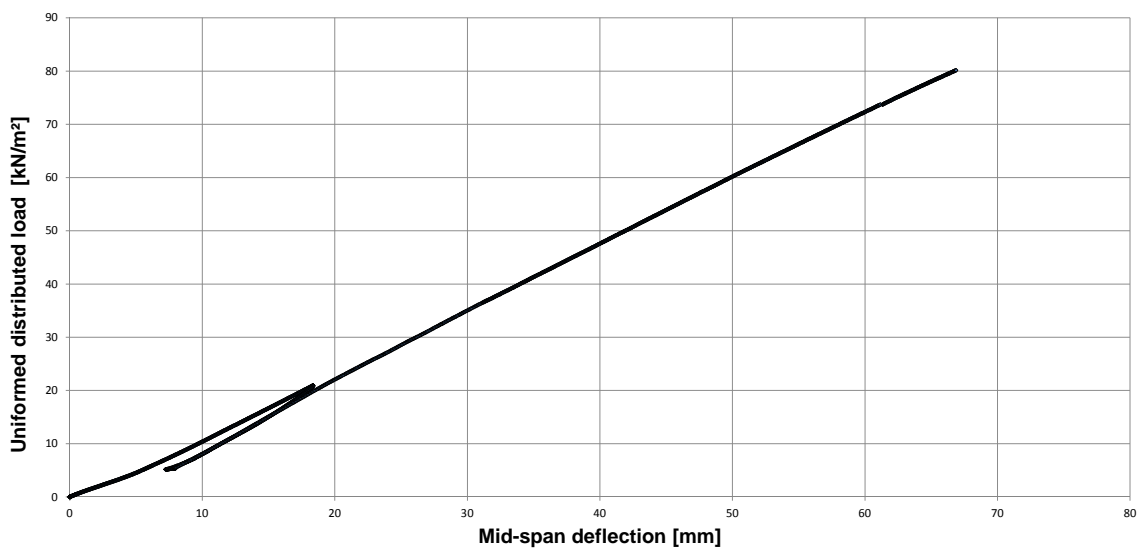


Figure 7.31: Load - mid-span deflection curve.

The load-carrying capacity of the composite system is also in this case really high (the ultimate load is almost 80 kN/m² usually assessed as 60% of the failure load, while the serviceability load (40% of the failure load) is around 48 kN/m². The combined design load of the stands is around 8,46 kN/m² and the design service load provided from the Eurocode 1 is only 5 kN/m²). It must be remembered, that to these value of load q it must be added both the self-weight of the composite system and the partitioning system. As it can be seen from Figure 7.31, the behavior of the full-scale specimen C is really linear up to the failure and even if the good design requires a ductile failure, here the failure is brittle, but it is so far from the usual service conditions that it may be considered highly unlikely to occur.

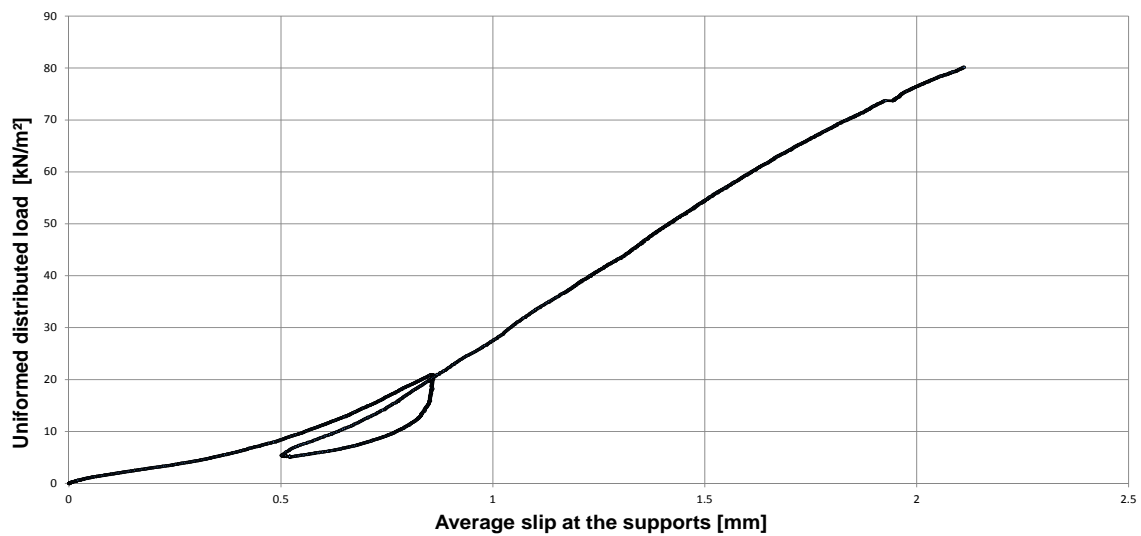


Figure 7.32: Load - slip trend at the supports for specimen C.

Eventually, the maximum mid-span deflection corresponding to only an instant before the failure of one of the two glulam beams is very close to 67 mm.

The graph reported in Figure 7.32 shows the average trend of the relative slip between the concrete slab and the timber beams at the supports, in function of the equivalent uniformly distributed load. It can be seen that, as direct consequence of the very rigid shear connection, the values of slip are almost null (at the failure load it has registered a value of 2,1 mm, while for the design service load it is about 0,5 mm). It must be remembered, that to these value of load q it must be added both the self-weight of the composite system and the partitioning system.

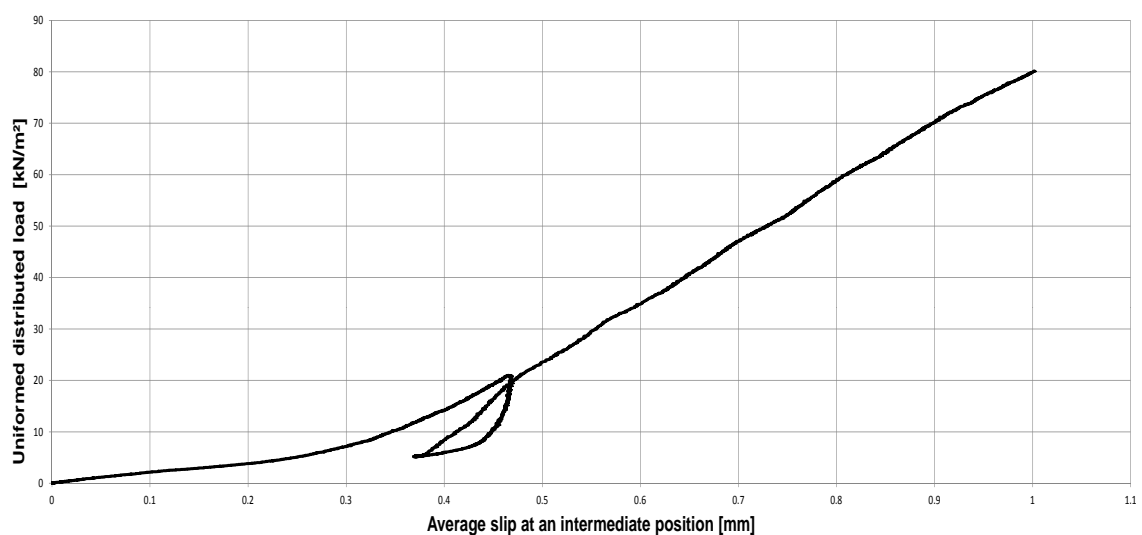


Figure 7.33: Load - slip trend to an intermediate point for specimen C.

The graph reported in Figure 7.33 shows the trend of the relative slip between the concrete slab and the timber beams at an intermediate point between the middle

of the beam and the supports, in function of the equivalent uniformly distributed load. For a $q = 80 \text{ kN/m}^2$ load corresponding to the failure of the beam, at the intermediate point the average slip between the concrete slab and the timber beams are around $\delta = 1 \text{ mm}$. It must be remembered, that to these value of load q it must be added both the self-weight of the composite system and the partitioning system. This consideration allows to say that the deformable connection which has been realized throughout self-tapping inclined screws actually show a very rigid behavior and does not show any sign of abating. No cracks appear around the screws during the test.

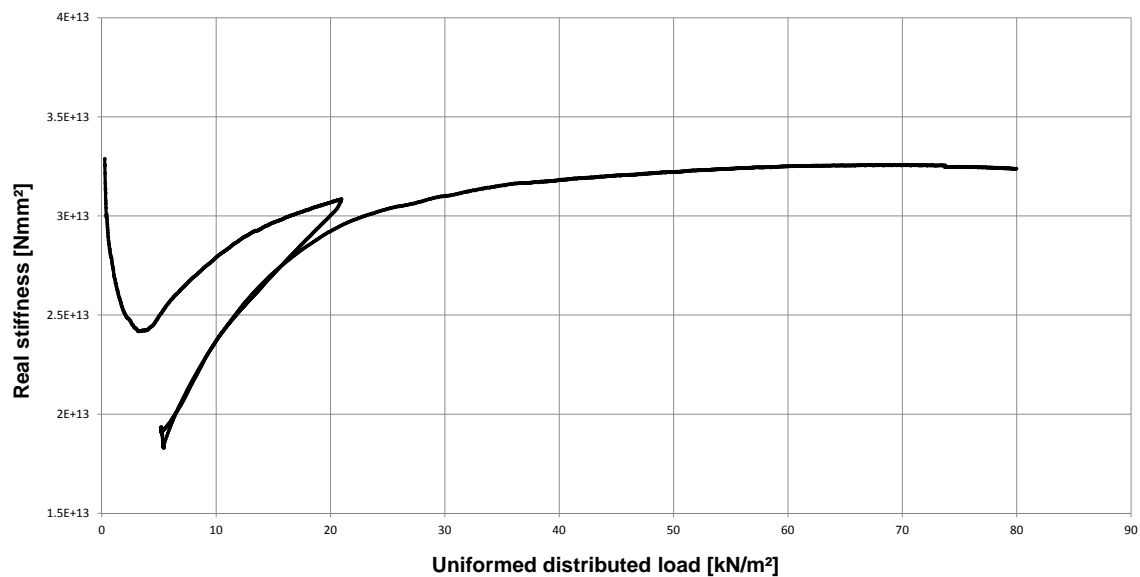


Figure 7.34: Bending stiffness EJ_{real} of the system C in function of the applied load q .

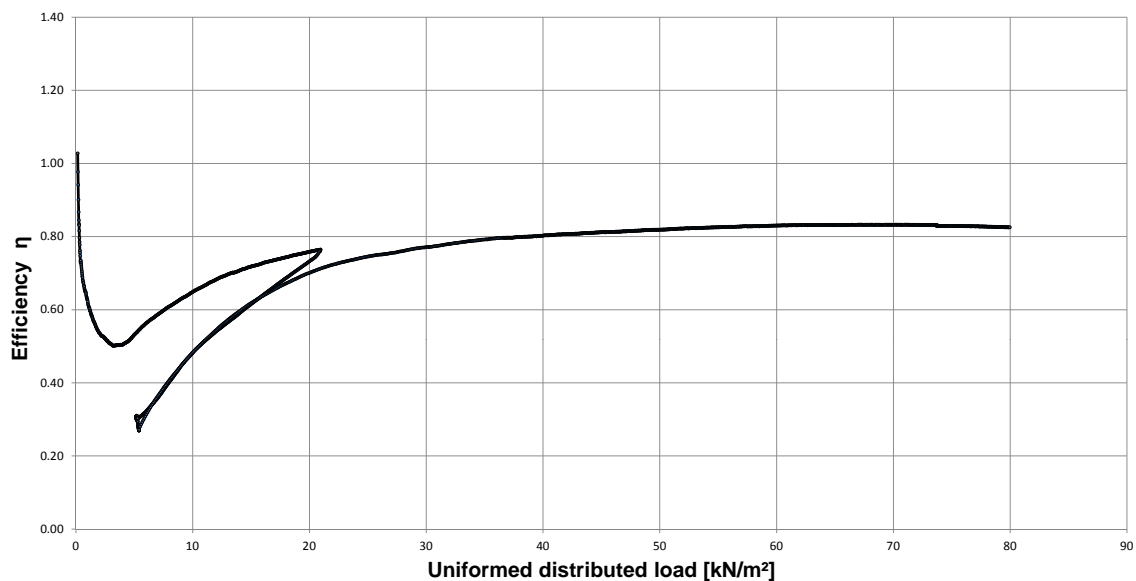


Figure 7.35: Real efficiency η_{real} of the connection system of system C in function of the applied load q .

Figure 7.34 displays the trend of the real stiffness.

After the setting phase of the test the real stiffness shows slowly increases almost up to a corresponding 70 kN/m^2 and has an average value equal to $3,24 \times 10^{13} \text{ Nmm}^2$ between 50 and 80 kN/m^2 levels of load. Such bending stiffness, only when close to the failure shows a very small decrease.

It can thus conclude that the connection realized by self-tapping inclined screws is very stiff and increase the bending stiffness with the grow of the applied load almost up to the failure.

Figure 7.35 shows the trend of the efficiency of the connection which is closely related to the trend of the real stiffness. Such efficiency has been evaluated using the formula proposed by Piazza considering the values of stiffness related to a full-composite action EJ_∞ and no composite action EJ_0 evaluated at paragraph 7.3.2.1.1. Precisely, it must be considered the double of these stiffness since they are related to only half a section. The efficiency assumes an average value equal to $0,82$ of the full-composite action in a range of load included between 50 and 80 kN/m^2 . Such efficiency shows actually a slow increasing with the grow of the load applied almost up to the failure.

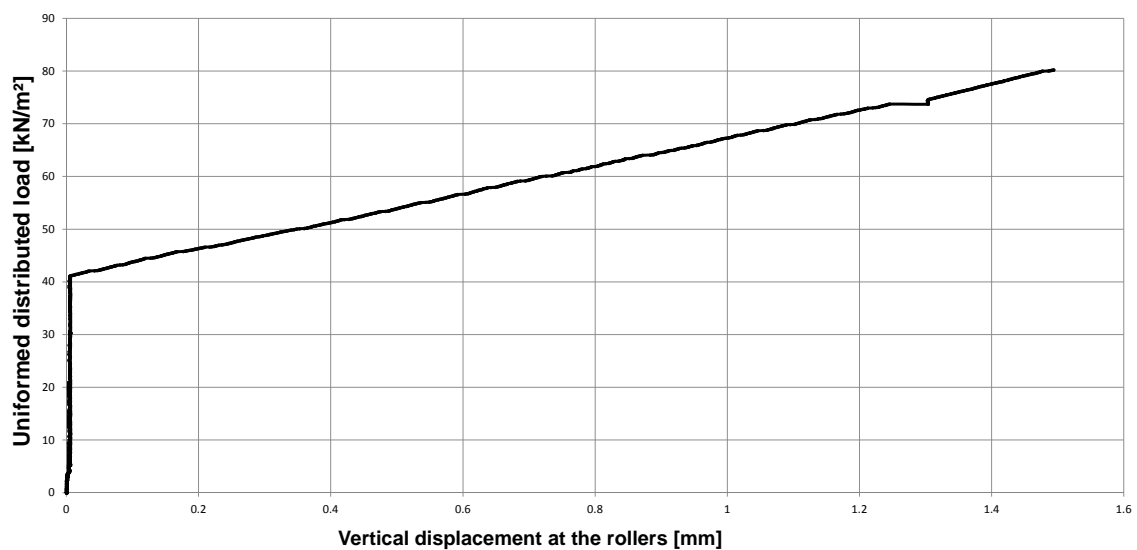


Figure 7.36: Load - subsidence at the rollers for specimen C due to compression perpendicular to the grain.

The reported graph in Figure 7.36 shows the subsidence of the timber beam at the two supports realized by two rollers. It has to be noted that the contact surface has been reinforced through four screws in order to avoid a possible premature breaking of the timber beam for compression perpendicular to grain. As it can be seen from the graph, up to an equivalent uniformed distributed load amounting approximately to 41 kN/m^2 no subsidence has been registered. After such a load level, the subsidence increases and at the failure of the composite beam its value was around $1,5 \text{ mm}$.

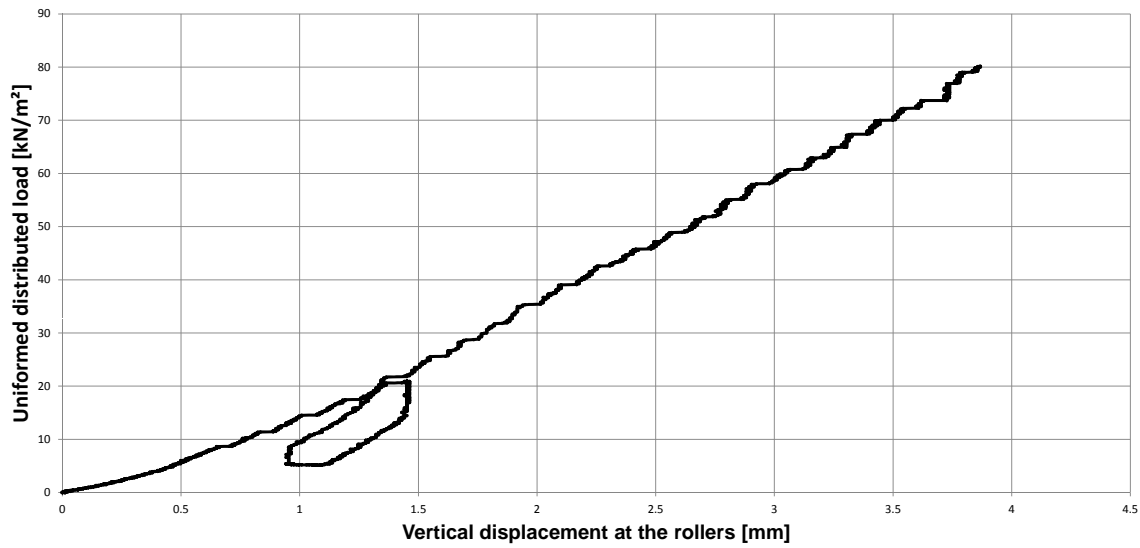


Figure 7.37: Load - subsidence at the hinges for specimen C due to compression perpendicular to the grain.

Figure 7.37 shows the subsidence of the timber beam at the two supports realized by two hinges. It has to be noted that, since the residential background type of floor, presented in chapter 3, has shown a premature breaking for compression perpendicular to grain at the these supports, before testing it four screws were inserted in the timber at the contact surface in order to reinforce the supports, see section 7.3.2. In fact, in this bending test no premature failure at the contact surface occurred. Anyway, the graph shows the trend of the vertical displacement with the increasing of the load. The compression perpendicular to the grain increases fairly linear with the equivalent load applied. To the failure, the maximum subsidence at the hinges has been registered a value less than 3,9 mm.

Table 7.9 summarizes the main value of the variables measured.

Variable	values
Maximum load P	477 [kN]
Uniformly equivalent distributed maximum load q	83 [kN]
Maximum mid-span deflection f	67 mm
Average slip at the supports δ	2,1 mm
Average slip at an intermediate point δ'	1 mm
Constant value of real stiffness EJ_{real}	$3,24 \times 10^{13}$ Nmm ²
Constant value of the real efficiency η_{real}	0,82
Maximum subsidence at the supports (hinges) v	3,9 mm
Maximum subsidence at the supports (rollers) v	1,5 mm

Table 7.9: Main value of the variables measured for the full-scale specimen C.

7.4 Long-term bending tests program

The purpose of the long-term test was to investigate the time-dependent behavior of the prefabricated timber-concrete composite system at the serviceability limit state. For such a purpose one full-scale specimen (specimen B), representative of a stand of a stadium, see the following Appendix, was constructed and tested under sustained loading for at least six months. Actually, since the composite structure has been loaded on February the 3rd and the master thesis has been discussed at University of Trento on March the 30th successively there are reported only the results for the first month, precisely till on March the 3rd. However, the test goes on at least until July the 3rd. The full-scale specimen has been loaded with 24 bags of cement whom weighing approximately 25 kg each. The bags have been distributed on the slab in order to induce on the composite structure an uniformly distributed load equal to 100 kg/m² which represents an usual serviceability load. It is worth to point out that the value according to the Eurocode 1, see paper [30], is 5 kN/m², i.e. approximately equal to 500 kg/m². Such a value of the serviceability load is so high firstly because it is used in a designing phase and secondly because it includes in a easy way the dynamic effects by increasing the static load. Figure 7.38 shows the full-scale specimen B loaded with the 24 bags of cement.



Figure 7.38: Full-scale specimen B loaded by 100 kg/m² for long-term test.

7.4.1 Mid-span deflection after one month

The long-term test results, after one month loading for the specimen B is presented in this section in terms of mid-span deflection. The variables monitored during the

entire test (here are reported only the results for the first month of test) were the mid-span deflection through 2 inductive transducers, positioned under the middle section of each glulam beams.

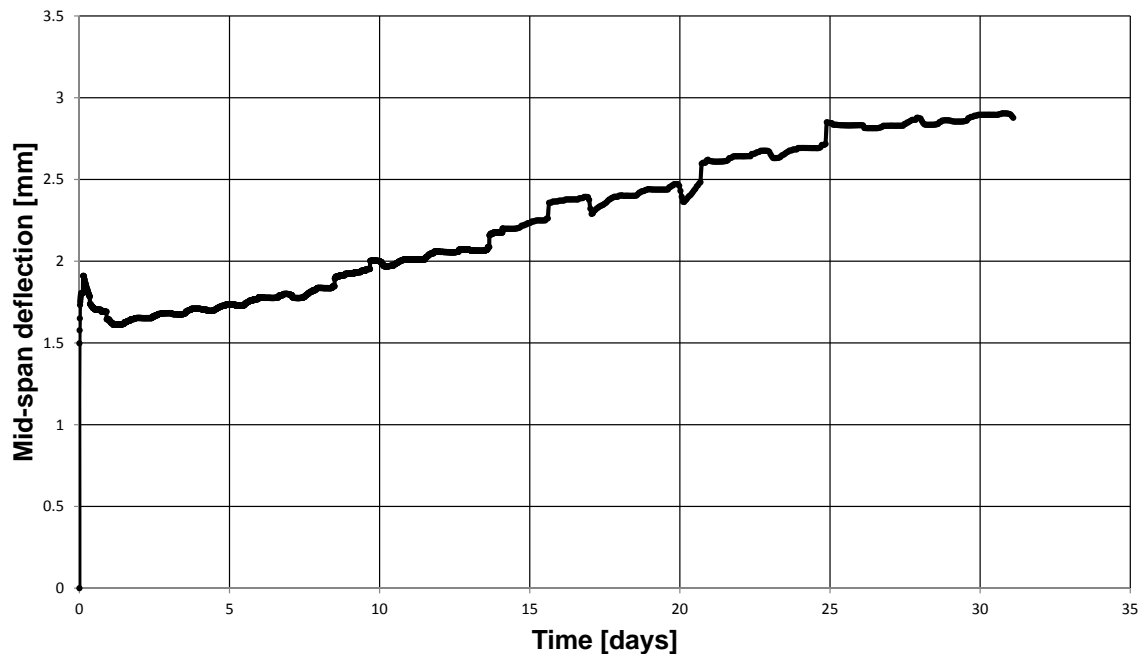


Figure 7.39: Mid-span deflection of specimen B during the long-term test.

The experimental results are presented in Figure 7.39. The elastic deflection w_{el} after the live load application was 1,54 mm. After on month test (31 days after the load application) the mid-span deflection $w_{el,31}$ of the specimen B was 2,90 mm.

7.5 Uniaxial compression tests program

In order to evaluate the mechanical characteristics of the steel-fibre reinforced concrete used to build out the three full-scale specimens, uniaxial compression tests have been performed at the laboratory of the Lunds Universitet (Lunds Tekniska Högskola).

7.5.1 Reason of the use of fiber reinforced concrete

Fibre-reinforced concrete (FRC) is currently used in wide range of applications, including bridge decks, airport pavements, tunnels and others. FRC is concrete primarily made from hydraulic cements, aggregates and discrete reinforcing fibers. Steel-fibre reinforced concrete (SFRC) has advantages over traditionally reinforced concrete in civil engineering. Steel-fibres are added to the concrete mix and become an integral part of the wet concrete. Reinforcement using steel fibres can improve the resistance

to shrinkage cracking and durability of the reinforced concrete structures. The main issues of a composite system like the one which is analyzed in this thesis, firstly due to long-term actions, are the shrinkage of the concrete and the creep of both elements, timber and concrete. To face this problem it has been decided to use a steel-fibre reinforced concrete (but it is possible to find also different types of fibres, natural and artificial), whose fibres that start working when the first cracking originates in concrete. Furthermore, the addition of steel fibres to concrete has been shown to increase both ductility of the concrete and its fatigue strength and also contributes improving the strength parameters of the material with particular benefits on the composite system behavior.

In general the properties of this kinds of concrete depend on more parameters than normal concrete, as fibre volume fraction, aspect ratio and orientation of the fibres. The specific study of the steel-fibre reinforced concrete is beyond the purpose of this thesis. Uniaxial compression tests on three cubic specimens has been carried out just to check the strength of the concrete used to build out the full-scale specimens.

7.5.2 Characteristics of steel-fibre reinforced concrete

The details of the steel fibre reinforced concrete have been reported in chapter 4, precisely in paragraph 4.2.1.3. Fibre reinforced concrete used to built out the three full-scale specimens is made of 480 kg/m^3 of cement and 45 kg/m^3 of steel fibres type ZP 30/0,40 (Dramix).

Characteristic strength R_{ck} is defined according to values obtained by uniaxial compression tests on 150 mm wide cubic specimens, matured 54 days, since the casting of the three full-scale specimens have been carried out on December the 7th while the uniaxial compression tests have been performed on January the 30th at the laboratory of the Lunds Universitet (Lunds Tekniska Högskola).



Figure 7.40: Uniaxial compression failure test and cubic specimens before the compressive test.

The three concrete cubes have been demolded after twenty four hours and submerged

in a curing water tank till the date of the uniaxial compression tests.

Characteristic strength f_{ck} is instead defined using cylindrical specimens with 300 mm depth and 150 mm diameter. The relation between the two values is following one:

$$f_{ck} = 0,83 \cdot R_{ck}$$

The concrete strength class is based upon cubic characteristic compression strength (R_{ck}), defined as the value beneath which lies only 5% of the whole samples resistance value (lower fractile at 5%). By using normal Gauss distribution (the most common statistic distribution), lower fractile 5% can be calculated according to following expression:

$$R_{ck} = R_m - 1,64 \cdot sqm \tag{7.3}$$

where:

R_m is the average specimens resistance;

sqm is the standard deviation, computable as

$$sqm = \sqrt{\sum_{i=1}^{n=3} \frac{(R_i - R_m)^2}{n - 1}} \tag{7.4}$$

where

R_i is the resistance of each specimen;

n is the number of the specimens tested.

In this case the test to determine the compression strength of the concrete have been provided leading to rupture three cubic specimens. The strength of each specimen have been reported in the following Table 7.10.

ID	Side	Side	Depth	Area	Weight	Density	Failure force	Compression strength
#	a	b	h	A	m	ρ	F_m	σ_m
	[mm]	[mm]	[mm]	[mm ²]	[kg]	[kg/m ³]	[kN]	[N/mm ²]
A	150	150	150	22500	7,908	2343	1150	51,11
B	150	150	150	22500	7,890	2338	1145	50,89
C	150	150	150	22500	7,886	2337	1150	51,11

Table 7.10: Mechanical parameters of the concrete specimen tested after 54 days.

By substituting the values given in the last column of Table 7.10 in the equations 7.3 and 7.4 it is possible to get first the standard deviation and then the compressive

characteristic strength:

$$R_m = \sum_{i=1}^{n=3} \frac{R_i}{n} = \frac{51,11 + 50,89 + 51,11}{3} = 51,04 \text{ MPa}$$

$$sqm = \sqrt{\frac{(51,11 - 51,04)^2 + (50,89 - 51,04)^2 + (51,11 - 51,04)^2}{3 - 1}} = 0,13 \text{ MPa}$$

$$R_{ck} = R_m - 1,64 \cdot sqm = 51,04 - 1,64 \cdot 0,13 = 50,83 \text{ MPa}$$

Mechanical characteristics of concrete can be deduced by formulations reported in Eurocode 2, see [32]:

Description	Equations	Value [MPa]
Characteristic compressive cylinder strength of the concrete	$f_{ck} = 0,83 \cdot R_{ck}$	42,19
Mean value of concrete cylinder compressive strength	$f_{cm} = f_{ck} + 8$	50,19
Mean value of axial tensile strength of the concrete	$f_{ctm} = 0,3 \cdot (f_{ck})^{2/3}$	3,64
Characteristic value at 5% fractile of tensile strength of the concrete	$f_{ctk,0,05} = 0,7 \cdot f_{ctm}$	2,54
Characteristic value at 95% fractile of tensile strength of the concrete	$f_{ctk,0,95} = 1,3 \cdot f_{ctm}$	4,73
Mean value of tensile strength of the concrete due to bending	$f_{cfm} = 1,2 \cdot f_{ctm}$	4,36
Secant modulus of elasticity of the concrete	$E_{cm} = 22000 \cdot \left(\frac{f_{cm}}{10}\right)^{0,3}$	35695

Table 7.11: Mechanical characteristics of concrete according to Eurocode 2.

It has to be taken into consideration the fact that these formulas provide reliable values for usual concrete belonging up to class C50/60, but here it has been reinforced with steel fibres so as regards the elastic modulus and the tensile strength the values reported in Table 7.11 are lower than the real. The specific study of the properties of the steel fibre reinforced concrete gets beyond the purpose of this thesis. In particular, the estimation of the tensile strength of this type of concrete requires to take into account lots of parameters like aspect ratio, volume fractions of steel fibres and orientation. For the purpose of this thesis the important characteristic which the concrete must have is enough tensile strength in order to avoid the rupture of its before the failure of the glulam beam due to combined bending and axial tension or the failure of the connection due to shear force.

As far as the elastic modulus of this steel-fibre reinforced concrete is concerned it can be estimated taking into account the steel fibres by using an empirical formula proposed for the overall elastic modulus with randomly orientated fibres as reported in [26]. It has been demonstrated that the equivalent elastic modulus \tilde{E} is insensitive to the aspect ratio of the steel fibres for $30 \leq l/d \leq 150$, where the aspect ratio l/d in this case is equal to 75. The equivalent elastic modulus \tilde{E} of the steel-fibre reinforced concrete can thus be estimated with the following formula:

$$\tilde{E} = E_m \cdot \frac{1 + \xi \cdot \eta \cdot V_f}{1 - \eta \cdot V_f}$$

where E_m is the original elastic modulus of the concrete matrix. The values of η is given by:

$$\eta = \frac{E_f/E_m - 1}{E_f/E_m + \xi}$$

and E_f is the elastic modulus of the fibers. The empirical parameters ξ for a volume fractions of steel fibres V_f less than 0,3 can be assumed equal to 2,5, for more information see [[26]]. In this case, the volume fractions of steel-fibres can be calculated as:

$$V_f = W_f \cdot \frac{\rho_c}{\rho_f}$$

where the density of the concrete $\rho_c = 2339 \text{ kg/m}^3$ has been calculated as the mean value of the density of each specimen tested; the density of the steel fibre has been assumed equal to $\rho_s = 7800 \text{ kg/m}^3$, instead W_f is the weight ratio fibre/concrete, in particular, for 1 cubic meter of concrete reinforced with 45 kg of steel-fibres produced this value amounts to

$$W_f = \frac{45}{2339} = 0,019$$

thus the volume fractions of the steel-fibres is:

$$V_f = 0,019 \cdot \frac{2339}{7800} = 0,0057 = 0,57\%$$

and especially less than 0,3 and it can be assumed $\xi = 2,5$. Therefore, the values of η amounts to:

$$\eta = \frac{200000/35695 - 1}{200000/35695 + 2,5} = 0,57$$

eventually, the equivalent elastic modulus of the steel-fibre reinforced concrete can be estimated as:

$$\tilde{E} = 35695 \cdot \frac{1 + 2,5 \cdot 0,57 \cdot 0,0057}{1 - 0,57 \cdot 0,0057} = 36105 \text{ MPa}$$

It is worth to point out that the cubic specimens after the compressive test have not

shown the classical hourglass shape as normal concrete usually shows, but as it is reported in Figure 7.41. Due to the steel-fibre reinforcement the specimens preserve the cubic shape and presents only cracks. The concrete has brittle behavior but with steel fibre it presents a good ductile compressive failure and does not crumble so much.



Figure 7.41: Concrete cubes after the compressive test.

7.6 Withdrawal tests program

On January the 30th withdrawal tests of screws from concrete cubes have been performed in order to understand if the screws used for the full-scale specimens develop enough compressive strength on the concrete without needing washers. In fact, when the full-scale specimens are submitted to vertical load, at the interface between concrete slab and timber beam slip occur and the screws are subjected to tensile and shear force, as previously shown in chapter 4. The screws work mean shear and tensile force. The tensile force has to be opposed by the concrete compression strength. In this connection system which consists just in screws without special steel tubes or metal washers as presented in chapter 3, it has been investigated if the screws with their own head can involve a good portion of concrete and transfer the tension stress to the concrete. Another purpose of these tests was to investigate the optimum depth of anchor of the screws in the concrete matrix.

7.6.1 Manufacturing of the specimens

For such a purpose, it has been prepared three kinds of specimens with three different depth of the screws in the concrete cubes. The specimens have been prepared on December the 7th with the same steel-fibre reinforced concrete used to build out the full-scale specimens. The concrete belongs to the class C45/55. The screws used were the same used for the full-scale specimens, type $VGS\phi 11 \times 250$ mm, and the three different depth of anchor were, 50 mm, 75 mm and 100 mm. Figure 7.42 shows the

samples for the withdrawal tests.



Figure 7.42: Samples for the withdrawal test with three different depth of anchor.

The nine concrete cubes with screws inserted have been demolded after twenty four hours from the casting of the concrete and placed to mature in nylon bags in order to maintain constant the humidity. They have not been submerged in a water tank because it was thought that maybe the screws could be subjected to corrosion.

Since the head diameter is wider than the major diameter when the screw is submitted to tensile strength, it involves a great part of concrete and it is expects that to the failure point it develops a cone of rupture (in case of normal concrete without fibre reinforcement).

7.6.2 Results from withdrawal tests

The machine used for the withdrawal tests is shown in Figure 7.43. In particular, it was necessary to build a special steel frame in order to perform the tests. Every specimen has been placed under two steel profiles which are designed to hold the concrete cube while the piers of the machine pulled up the screw.

Next figures report the curve force-displacement for each test. In the same figures it has been also reported a picture with the failure modes of each test. The purpose of the test is to measure the withdrawal capacity of each specimen and to check the optimal depth of insertion. The tests have been conducted till the total removal of the screws in order to check the behavior of the concrete. The test has been performed in displacement control and the speed used in the test was 0,02 mm/sec till the maximum load and after speed has been increased up to 0,08 mm/sec till the total removal of the screws.



Figure 7.43: Machine and steel frame used to perform of the withdrawal test.

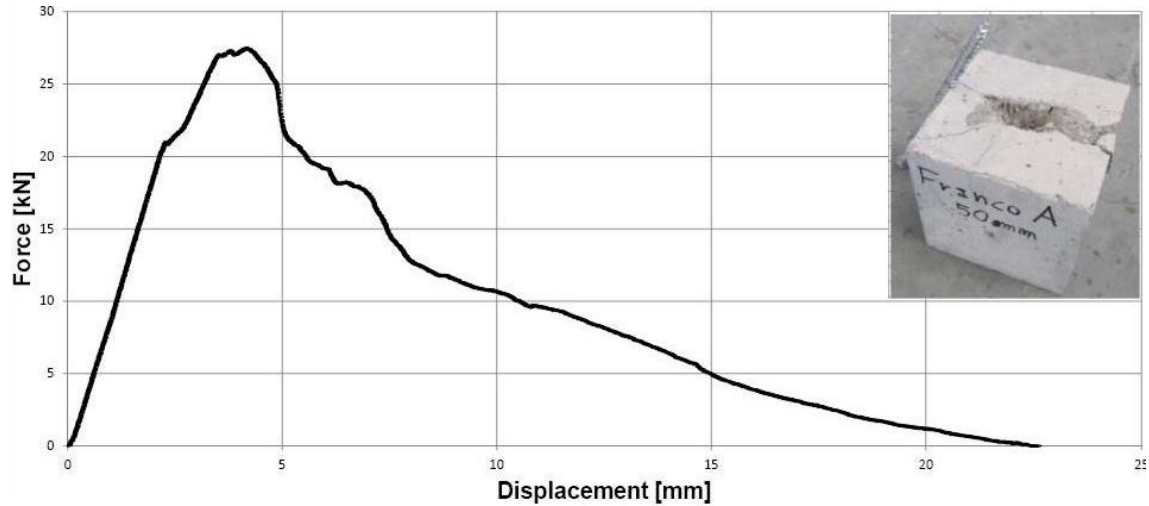


Figure 7.44: Curve force - displacement of the specimen A with the depth of insertion of the screw equal to 50 mm in the concrete.

The curve force-displacement of the specimen A with a depth of insertion equal to 50 mm shows a linear behavior till a force equal to 21 kN. The peak of the force has been reached with 4 mm of displacement and the value amounted to 27,49 kN. The screw has been removed from the concrete and the failure has developed cracks just in the half upper part of the specimen.

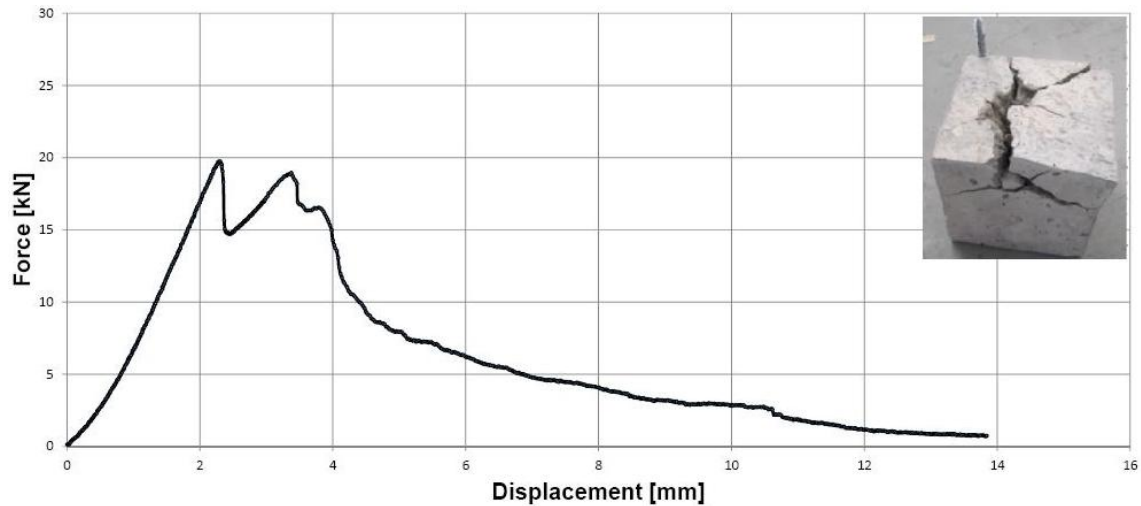


Figure 7.45: Curve force - displacement of the specimen B with the depth of insertion of the screw equal to 50 mm in the concrete.

The curve force-displacement of the specimen B with a depth of insertion equal to 50 mm shows a less linear behavior than the previously one. The maximum force is equal to 19,75 kN. After this peak value, the force decreased suddenly till a value of approximately 15 kN. Successively the tensile capacity increased again but till a value less of the previously one. This behavior may be due to the presence of a stone close to the screw. The peak of the force has been reached with 2,2 mm of displacement. The screw has been removed from the concrete and the failure has developed huge cracks just in the half upper part of the specimen.

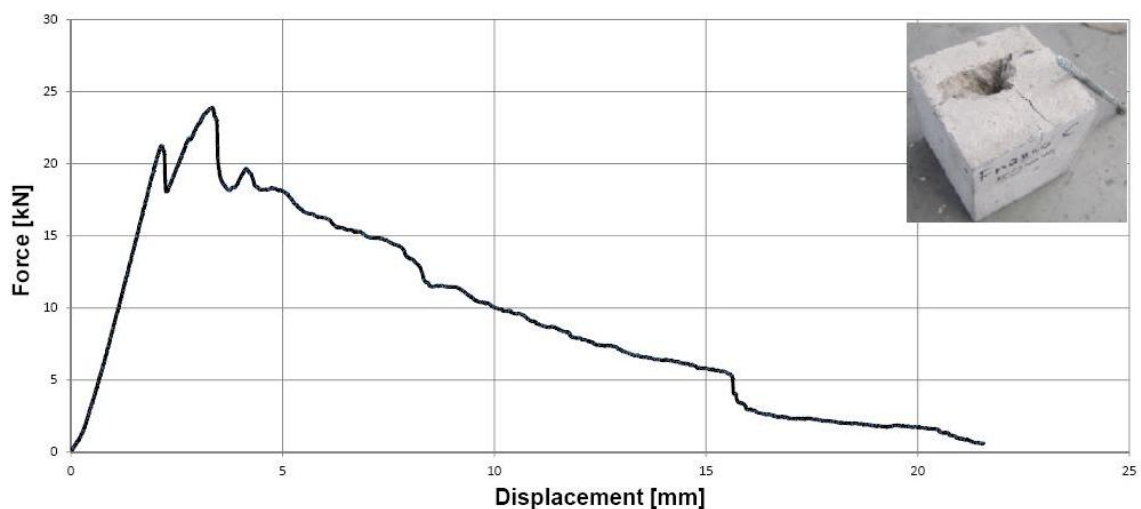


Figure 7.46: Curve force - displacement of the specimen C with the depth of insertion of the screw equal to 50 mm in the concrete.

The curve force-displacement of the specimen C with a depth of insertion equal to 50 mm shows a linear behavior till a force approximately equal to 21 kN. After this value,

the force decreased suddenly till a value of approximately 18 kN. Successively the tensile capacity increased again till the peak value equal to 23,90 kN. This behavior may be due to the presence of a stone close to the screw. The peak of the force has been reached after 3 mm of displacement. The screw has been removed from the concrete and the failure has developed small cracks just in the half upper part of the specimens and it shows a good defined hole where the screw was placed.

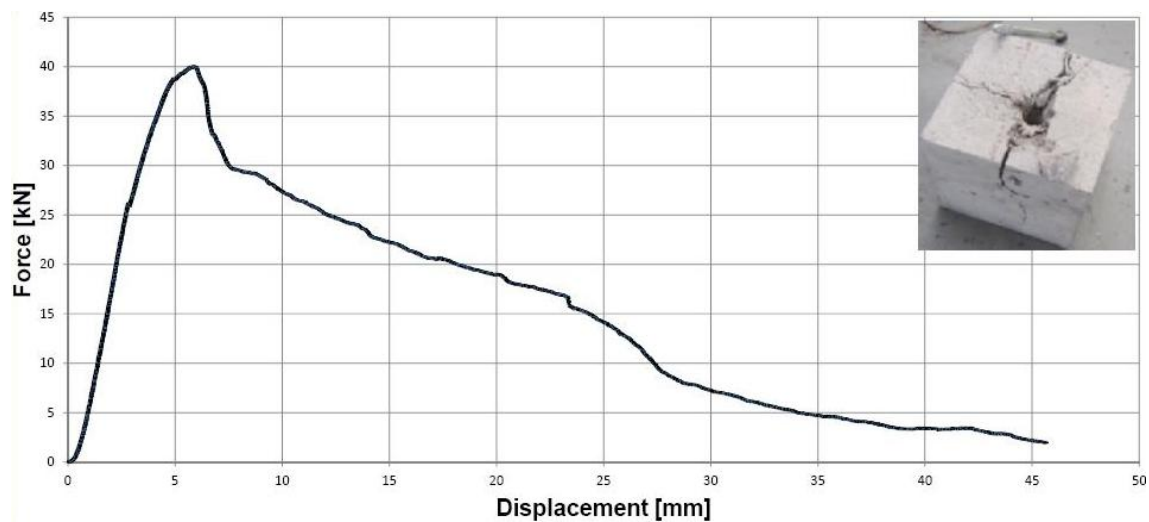


Figure 7.47: Curve force - displacement of the specimen A with the depth of insertion of the screw equal to 75 mm in the concrete.

The curve force-displacement of the specimen A with screw depth of insertion equal to 75 mm, Figure 7.47, shows a linear behavior till a force equal to 26 kN. After that, the force still increased and the peak has been reached with 6 mm of displacement and the value amounted to 40,03 kN.

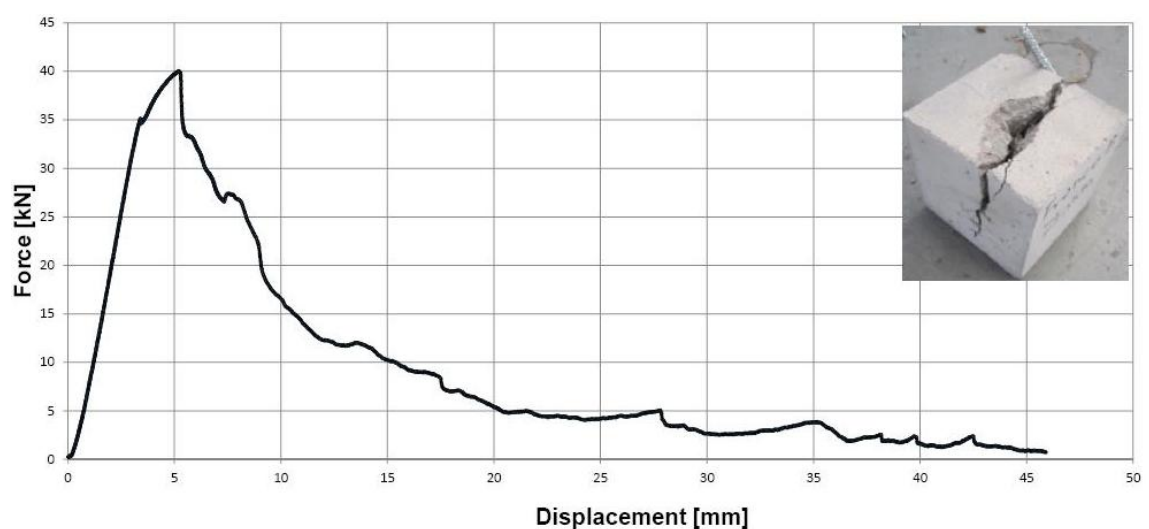


Figure 7.48: Curve force - displacement of the specimen B with the depth of insertion of the screw equal to 75 mm in the concrete.

The screw has been removed from the concrete and the failure has developed cracks that propagated up to the lower part of the specimen.

The curve force-displacement of the specimen B with the screw with 75 mm depth of insertion, Figure 7.48, shows a very linear behavior till a force equal to 35 kN. After that, the force still increase but more slowly and the peak has been reached approximately with 5 mm of displacement and the value amounted to 40,04 kN. The screw has been removed from the concrete and the failure has developed two huge cracks that propagate up to the lower part of the specimen.

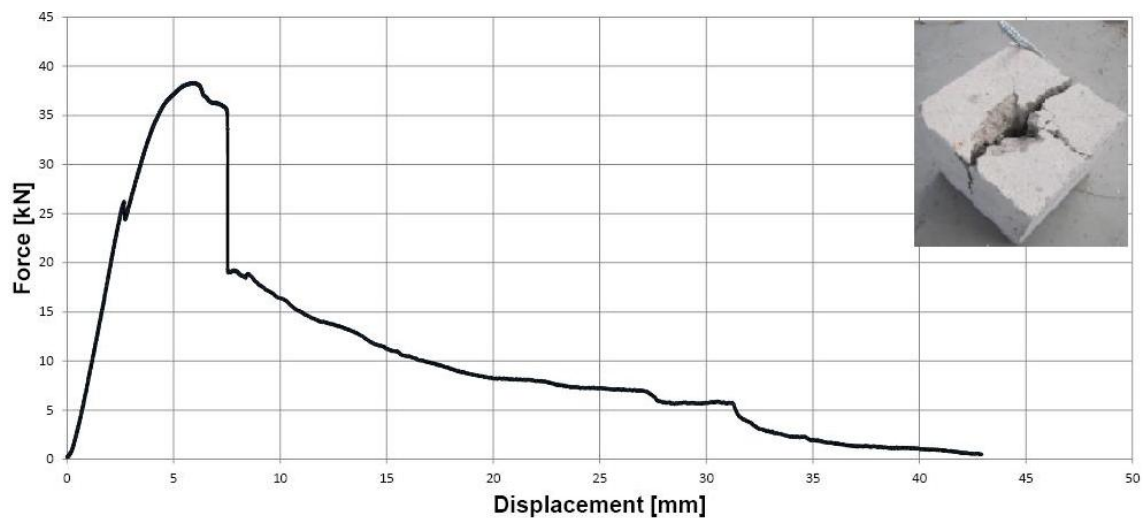


Figure 7.49: Curve force - displacement of the specimen C with the depth of insertion of the screw equal to 75 mm in the concrete.

The curve force-displacement of the specimen C with screw depth of insertion equal to 75 mm shows a linear behavior till a force equal to 26 kN.

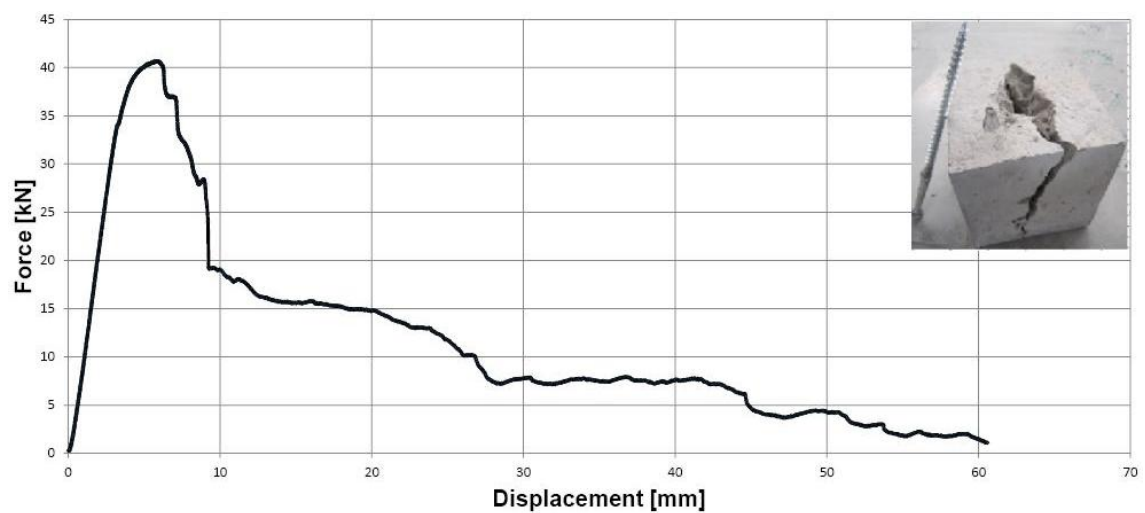


Figure 7.50: Curve force - displacement of the specimen A with the depth of insertion of the screw equal to 100 mm in the concrete.

After that, a short decrease maybe due to the presence of a stone happened and then the force still increased to the maximum value reached with 6 mm of displacement, amounting to 38,32 kN. The screw has been removed from the concrete and the failure has developed two huge cracks that propagate up to the lower part of the specimen.

The behavior of the specimen A with 100 mm depth of insertion is presented in Figure 7.50 shows a linear trend till a force approximately equal to 34 kN. The force still increased to the maximum value reached with 6 mm of displacement, amounting to 40,68 kN.

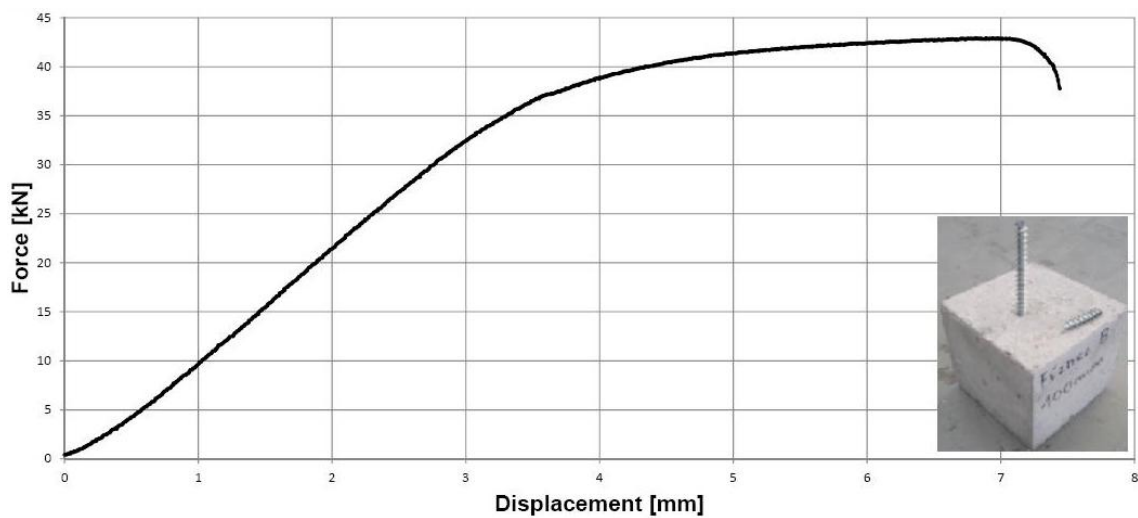


Figure 7.51: Curve force - displacement of the specimen B with the depth of insertion of the screw equal to 100 mm in the concrete.

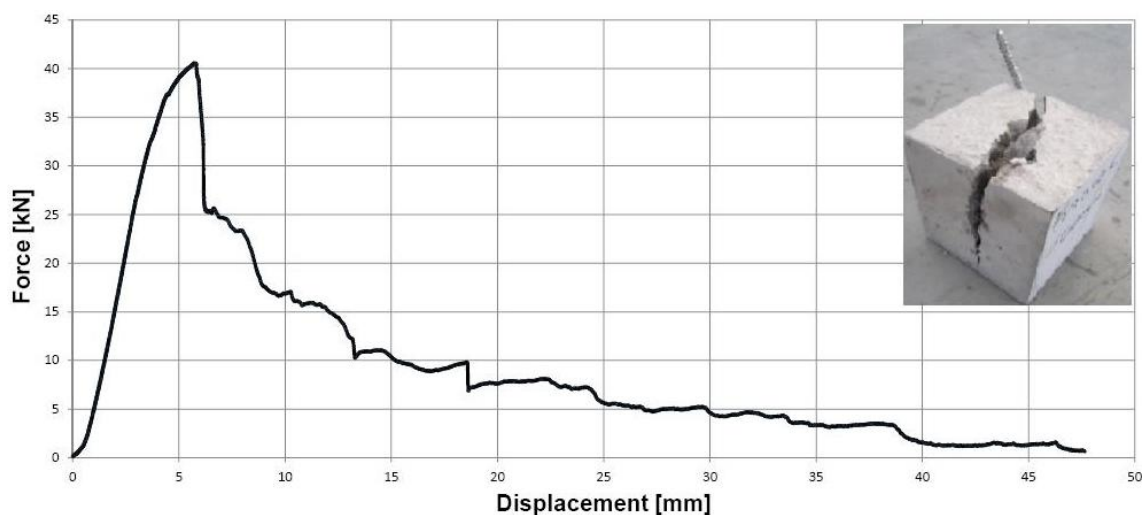


Figure 7.52: Curve force - displacement of the specimen C with the depth of insertion of the screw equal to 100 mm in the concrete.

The screw has been removed from the concrete and the failure has developed two

huge cracks that propagate up to the lower part of the specimen. The two main pieces of the concrete cubic have not separated from each other due to the action of the steel fibres.

The curve force-displacement of the specimen B with 100 mm depth of insertion, Figure 7.51, shows a linear behavior till a force equal to 26 kN. The force increased linearly with the displacement till approximately 35 kN. After that, the force still increased till the failure of the screw occurred. This was an unexpected break maybe due to the defectiveness of the screw. However, the maximum value reached is 42,92 kN. The failure of the screw occurred at a displacement equal to 7,9 mm, while the concrete cubic shows very little cracks just in the upper part around the screw.

The behavior of the failure of the specimen C with screw depth of insertion equal to 100 mm is presented in Figure 7.52. The force increased linearly with the displacement till approximately 33 kN. After that, the force still increased till the peak value equal to 40,58 kN. The ultimate tensile capacity occurred at a displacement equal to 6 mm. The concrete cube shows two very huge cracks that propagate up to the lower part of the specimen.

In Table 7.13 are summarized the ultimate tensile capacity for each specimen and it has been calculated the average values for each type of samples.

ID specimen	Depth of insertion [mm]	Ultimate tensile capacity [kN]
A	50	27,49
B	50	19,75
C	50	23,90
Mean value		23,71
A	75	40,03
B	75	40,04
C	75	38,32
Mean value		39,46
A	100	40,68
B	100	42,92
C	100	40,58
Mean value		41,39

Table 7.12: Ultimate tensile capacity of the screws inserted into the concrete with different lengths.

By looking at the results from the withdrawal tests, which are reported in Table 7.12, it can be seen that for a depth of insertion equal to 50 mm, the ultimate tensile capacity is around 24 kN. For a depth of insertion equal to 75 mm the ultimate tensile capacity is approximately 39 kN while for the last depth of insertion considered, 100

mm, the ultimate tensile capacity is around 41 kN. First of all, it can be concluded from these results that using a depth of insertion over 75 mm gives not much greater performance, while compared to the ultimate tensile capacity of the specimens with 50 mm depth of insertion, the resistance is almost the double. Secondly, if it is considered that the screws inserted in the full-scale specimens have an inclined depth of insertion approximately equal to 55 mm, and considering not only the connector axial strength but also the shear component and the contribution of friction, screws develop a total resistance much greater.

7.7 Tensile tests program

Tensile tests on three screws has been performed in order to have an estimation of the failure load of the only screws when acting in tension. It is known that, in order to have a real good estimation of the tensile failure it must be conducted lots of tensile tests with statistical consideration, but this goes beyond the purpose of this thesis. Figure 7.53 displays the machine and how the tensile tests have been performed.



Figure 7.53: Tensile tests on the three screws.

7.7.1 Characteristic curves force - displacement

However, it has been reported in Figures 7.54, 7.55 and 7.56 the characteristic curves of the three screws.

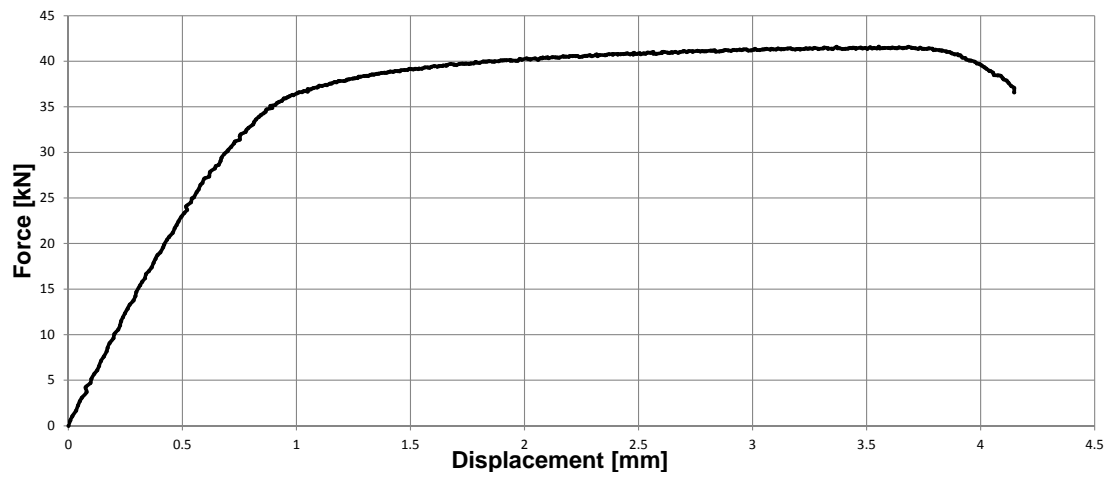


Figure 7.54: Characteristic curve force - displacement of the first screw.

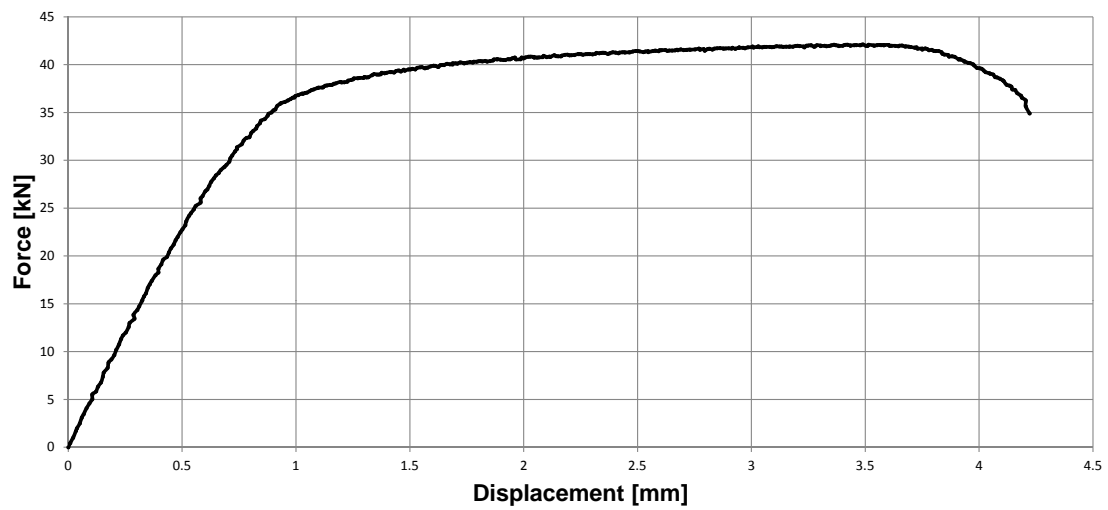


Figure 7.55: Characteristic curve force - displacement of the second screw.

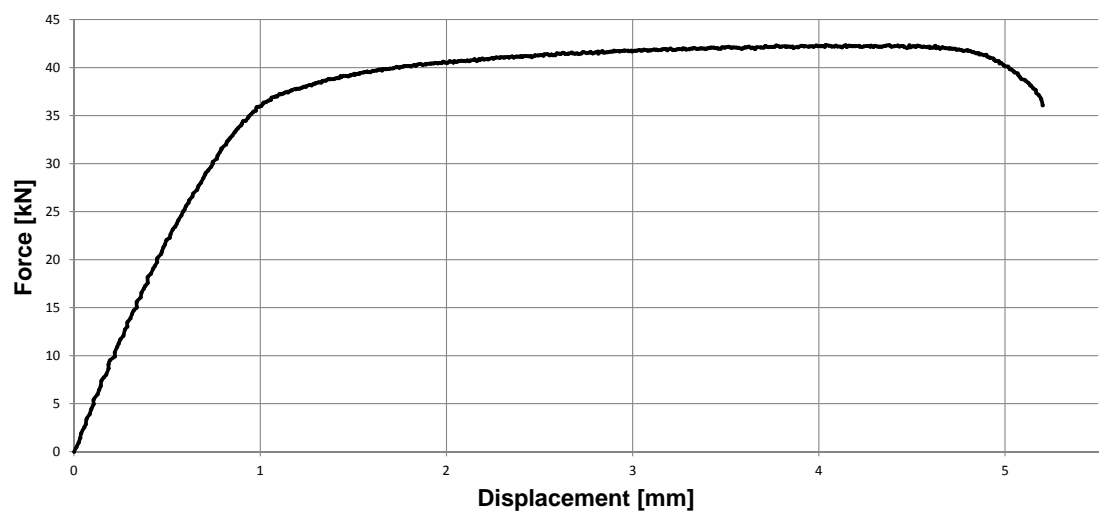


Figure 7.56: Characteristic curve force - displacement of the third screw.

From the previous figures it can be seen that the three curves have the same behavior. They show a good plateau which means ductile behavior. The ultimate tensile capacity reached before the curve of softening for each screws is reported in Table 7.13.

ID	Type of screw	F_u [kN]
1	$VGZ\phi 11 \times 250$ mm	41, 60
2	$VGZ\phi 11 \times 250$ mm	42, 12
3	$VGZ\phi 11 \times 250$ mm	42, 35

Table 7.13: Ultimate tensile capacity of the three screws $VGZ\phi 11 \times 250$ mm.

7.7.2 Comparison with analytical calculations

7.7.2.1 Eurocode 5 approach

With reference to standard reference [27], to the part relative to the screw connections the following formula is reported

$$M_{y,Rk} = 0,3 \cdot f_{u,k} \cdot d^{2,6}$$

where

$M_{y,Rk}$ is the characteristic value for the yield moment, in Nmm ;

$f_{u,k}$ is the characteristic tensile strength, in N/mm^2 ;

d is the core diameter of the screws, in mm .

Since the characteristic tensile strength $f_{u,k}$ is not given from the manufacturer of screws, it has been derived by reversing the previous formula and considering that the characteristic value for the yield moment is declared from the manufacturer and is equal to $M_{y,Rk} = 45900$ Nmm. For the diameter d it has been assumed the core diameter of the screw which is equal to $d = d_2 = 6,6$ mm. Hence, the characteristic tensile strength can be evaluated as

$$f_{u,k} = \frac{M_{y,Rk}}{0,3 \cdot d^{2,6}} = \frac{45900}{0,3 \cdot 6,6^{2,6}} = 1132 \text{ MPa}$$

Eventually, the ultimate tensile capacity can be estimated as

$$F_u^{EC5} = f_{u,k} \cdot \frac{\pi \cdot d^2}{4} = 1132 \cdot \frac{\pi \cdot 6,6^2}{4} = 38,73 \text{ kN}$$

7.7.2.2 Theoretical plastic approach

Another possible manner to predict the characteristic tensile strength of the screw is by considering the plastic moment of a circular section which can be estimated as

$$M_{pl} = M_{y,Rk} = f_y \cdot \frac{d^3}{6}$$

by reversing this formula it is possible to evaluate the characteristic yielding strength

$$f_{y,k} = M_{y,Rk} \cdot \frac{6}{d^3} = 45900 \cdot \frac{6}{6,6^3} = 958 \text{ MPa}$$

thus, by considering a ratio $f_{u,k}/f_{y,k} = 1,2$ the characteristic tensile strength of the screw can be estimated as

$$f_{u,k} = 1,2 \cdot f_{y,k} = 958 \cdot 1,2 = 1150 \text{ MPa}$$

eventually, the ultimate tensile capacity of the screw can be evaluated as

$$F_u^{theoretical} = f_{u,k} \cdot \frac{\pi \cdot d^2}{4} = 1150 \cdot \frac{\pi \cdot 6,6^2}{4} = 39,34 \text{ MPa}$$

7.7.2.3 Comparison between analytical estimation and experimental results

Table 7.14 summarizes the experimental values of the ultimate tensile capacity of the screws, the calculations according to the Eurocode 5 and the theoretical calculations.

Method	Ultimate capacity [kN]
Experimental test screw 1	41,60
Experimental test screw 2	42,12
Experimental test screw 3	42,35
Eurocode approach	38,73
Theoretical approach	39,34

Table 7.14: Comparison between the ultimate tensile capacity of the screws.

By viewing the previous table, it can be said that the theoretical calculations, the Eurocode formulations and the experimental outcomes are very precise and give values very close to each other. The mean value of the ultimate tensile capacity of the screws is 42,02 kN and the percentage error of Eurocode approach is 8,5% to the safe side instead the percentage error of the theoretical approach is 6,8% to the safe side as well. It must be also remembered that the values calculated from the theoretical approach and from the Eurocode 5 approach are characteristic values, while instead

the values obtained from the tensile tests are mean values, thus in reality the manual estimation are a little bit higher and hence even closer to the tests values.

It can be concluded that the design formulae give realistic values which can be used during the design phases.

7.8 Determination of the elastic modulus of the glulam beams

Since one of the glulam beams for each specimens have not been broken during the short-term bending tests, it has been decided to conduct bending tests on these integral timber beams (A1 and C1) in order to investigate the modulus of elasticity of the glulam beam. At the same time it has also been investigated the global density of the wood. Actually, timber beam C1 has been damaged at one side during the short-term bending test of the full-scale specimen C, so it has been cutted a piece. In the next Table 7.15 are reported the geometrical properties of the two glulam beam used to investigate the modulus of elasticity.

ID beam	Length [mm]	Depth [mm]	Width [mm]	Mass [kg]	$\rho_m [kg/m^3]$
A1	7198	355	112	136,60	477,30
C1	6595	356	111	117,23	449,83

Table 7.15: Geometric data of the timber beams used to investigate the modulus of elasticity.

It is know that in order to have a good estimation over both the specific gravity and the modulus of elasticity it has to make these non-destructive tests before the preparation of the full-scale composite specimens on all the timber beams. Anyway, these investigations have been conducted only on timber beam A1 and C1 after the bending tests. The average value of the specific gravity for this case is thus 491,20 kg/m³.

As the elastic modulus is concerned, with reference to UNI EN 408:2004, see paper [33], two bending non-destructive tests have been carried out on the two glulam beams. The non-destructive bending tests have been performed with same machinery used for the short-term bending tests and the equipments shown in Figure 7.57 and in agreement with the loading pattern reported in Figure 7.58. The load has been applied on two lines through a partitioning IPE profile, whose weight was 1,52 kN. The force has been applied through an hydraulic jack jointed to a reply beam constrained to the laboratory floor, located on axis to the midpoint of the testing beams, and to the partitioning beam. The maximum load applied has been less than the 40% of the estimated failure load of the glulam beam in order to not damage the

beam. The tests have been carried out with a displacement control test with speed equal to $0,003 \cdot h = 1,1 \text{ mm/s}$ and in order to estimate the ultimate limit capacity of a single timber beam, mean values without safety factors have been used as done for the previous bending test. The distance of the supports (one hinge and one roller) and the position of the two lines has been reported in Table 7.16. The distance between the two supports is equal to $18 \cdot h = 6480 \text{ mm}$. The calculations can be easily done and are not here reported, but with reference to Figure 7.58 the value estimate of the force F was equal to 92 kN . Thus, the maximum load applied by the hydraulic jack has been $F = 37 \text{ kN}$.

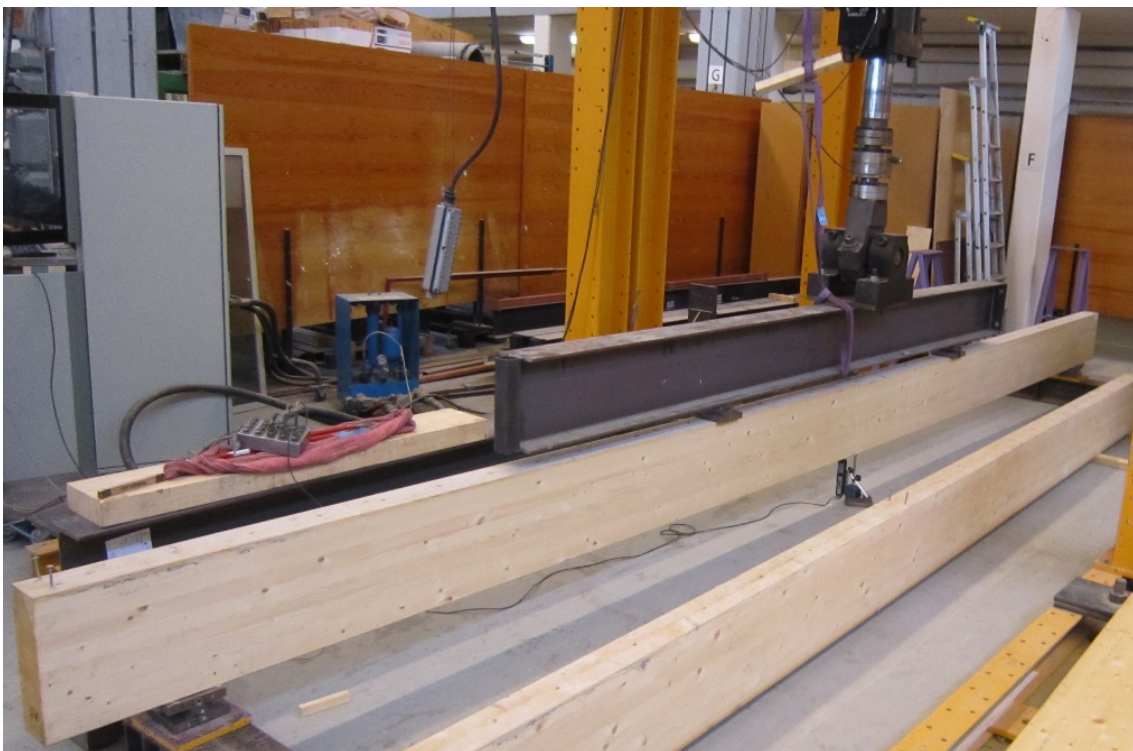


Figure 7.57: Equipment used to perform the bending non-destructive tests.

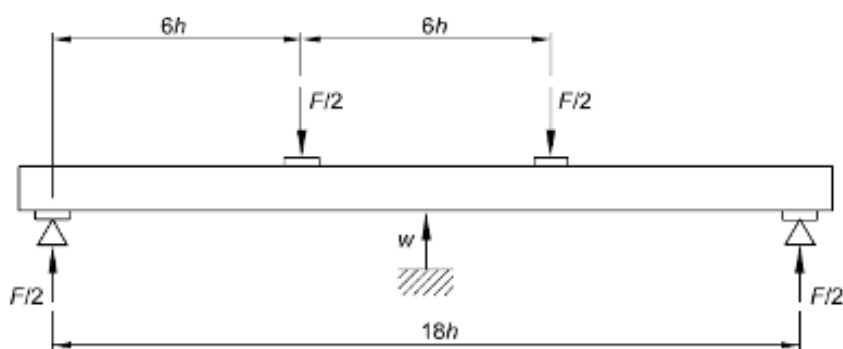


Figure 7.58: Pattern of the bending non-destructive tests.

Values of the load	F/2	F/2
Distance from each supports	2160 [mm]	2160 [mm]

Table 7.16: Distance and positions of the loads for the non-destructive tests.

During the experimental tests it has been observed and monitored the total load applied to the specimens, the evolution of the mid-span deflections in the middle through one resistive gauge. From this test the following load-strain curves have been obtained, see Figures 7.59 and 7.60.

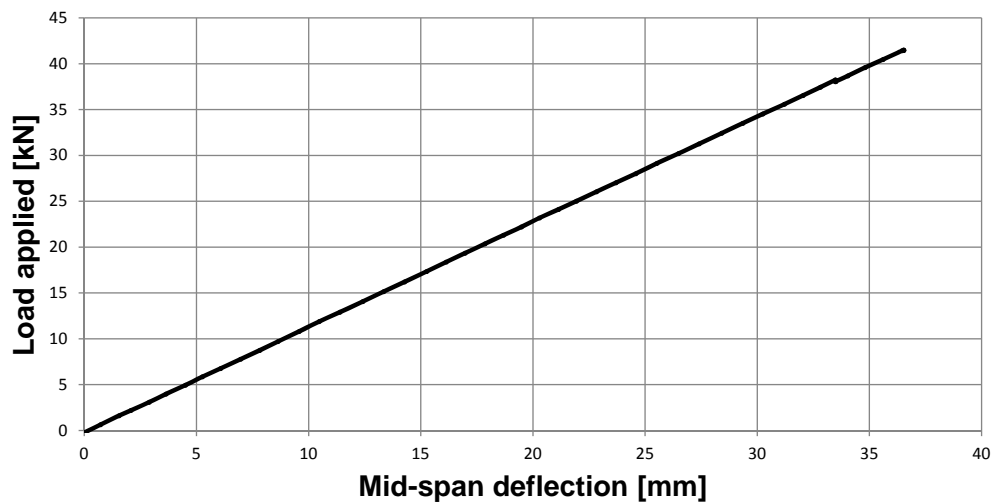


Figure 7.59: Load-strain curve for beam A1 up to 40% of the ultimate load.

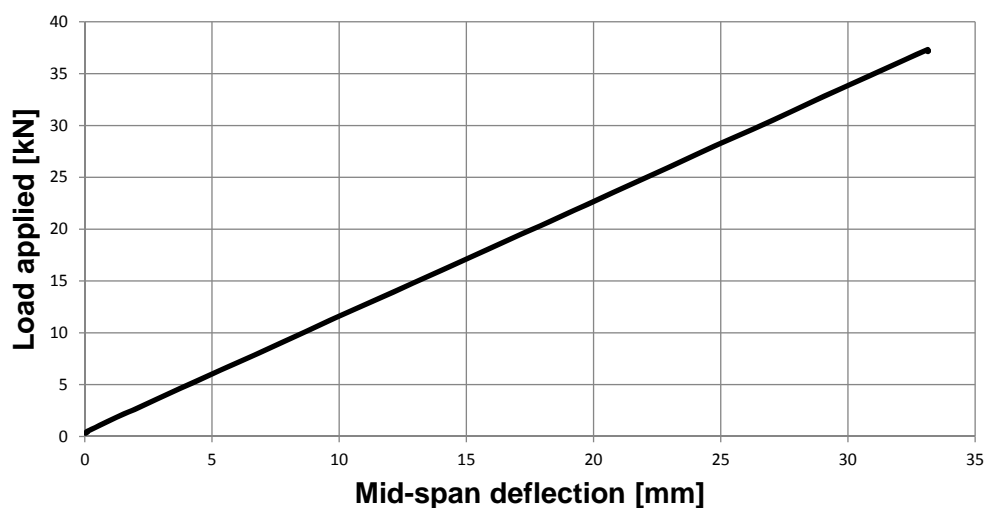


Figure 7.60: Load-strain curve for beam A1 up to 40% of the ultimate load.

It has to be remembered that to the load given from the hydraulic jack it has to be added the self-weight load of the partitioning steel IPE 300 profile, whose weight is 1,52 kN.

By using the following formula, reported in the paper [33], the global modulus of elasticity $E_{m,g}$ has been evaluated for both the beams:

$$E_{m,g} = \frac{l^3 \cdot (F_2 - F_1)}{b \cdot h^3 \cdot (w_2 - w_1)} \cdot \left[\left(\frac{3 \cdot a}{4 \cdot l} \right) - \left(\frac{a}{l} \right)^3 \right]$$

where

$F_2 - F_1$ is the increase load on the straight stretch of the load-strain curve, in N;

$w_2 - w_1$ is the increase deflection corresponding to $F_2 - F_1$, in mm;

a is the distance between the application point of the load and the support;

l is the distance between the two supports.

Table 7.17 reports the modulus of elasticity of the two glulam beams and the average value is equal to 12334 MPa, a little bit lower than the design value assumed which was 12500 MPa. The value given from the specific legislation for designing phase is reported in Table 4.2 which is derived from paper [31] and gives average values based on a statistical analysis of many samples. The modulus of elasticity depends a lot on the beam, on its dimensions, on the seasoning, on the amount of nodes and so on, thus is reasonable to expect fluctuating values between 12000 and 13000 MPa.

ID	$F_2 - F_1$	$w_2 - w_1$	$E_{m,g}$
A1	35,91 – 8,18 kN	33 – 9 mm	12480 MPa
C1	35,70 – 7,48 kN	33 – 8 mm	12189 MPa

Table 7.17: Elastic modulus of the glulam beams.

Chapter 8

Conclusions and comparison between the three approaches

This chapter presents the conclusions over all the research project and the comparison between results from numerical model, analytical calculations and experimental results.

8.1 Conclusions over the used connector system

For an industrial perspective, joining concrete and timber through self-tapping screws as shear connectors in a full-prefabricated system offers several advantages, including:

- (i) Reduction of construction times, since no time is needed for curing concrete on-site and for joining prefabricated slabs with timber beams. The time required in traditional systems for placing shear connectors in timber beams on-site and needed for curing concrete on-site is eliminated when prefabricated systems are built out moving work from the building site to the workshop. Thus, all that needs to be done on-site is to lift and to put the composite structure in place.
- (ii) Avoidance of use of “wet” components during the generally “dry” process of constructing timber buildings. The elimination of “lost” formwork also reduces the self-weight of the structure.
- (iii) Realization of the full stiffness of the timber-concrete composite structure before to put the composite system in place on-site (in contrast to traditional wet systems, which require time to develop sufficient stiffness to sustain the full self-weight of the concrete).

- (iv) The shear connectors are quite cheap and need only to be screwed in the wood. As it has been shown from the bending tests, the efficiency of this kind of shear connectors is very high, around $\eta = 0,85$. It means that also if the connection used is classified as deformable, in reality it shows a very highly stiff behavior. The full prefabricated system is very convenient for new buildings, especially it allows to get more simplicity and rapidity of erection, better quality that means more durability as well. It can be also used for rehabilitate floors for old buildings. For this last case also only prefabricated slab and connected to timber beam on-site may be considered.

To predict the behavior of the composite structure a finite element model has been realized and also to support and to compare the theoretical calculations which are reported in Eurocode 5 for the design of the timber-concrete composite structure. Furthermore, three full-scale specimens have been performed where on two of them bending tests have been carried out. On the other hand, on the last one dynamic and long-term test have been carried out.

In the next sections are reported the comparison of the results from the three approaches related to the most important variable which needs to be checked during the designing phase.

8.1.1 Comparison between the mid-span deflections

In this section it has been compared the mid-span deflection obtained with analytical calculation, FE result and registered from the two bending tests. For the analytical calculations, in order to get the necessary parameters to evaluate the mid-span deflection, see paragraph 7.3.2.1.1. Therefore, Table 8.1 reports the deflection obtained by applying a uniformed distributed load Q equal to 80 kN/m^2 , which is close to the ultimate load on both the specimens. It has been also reported the deflection for a live load $Q = 5 \text{ kN/m}^2$. Analytical mid-span deflection for ultimate limite load can be estimated as:

$$u_{g,inst} = 1,1 \cdot \frac{5}{384} \cdot \frac{(Q \cdot b_1) \cdot l^4}{EJ_{eff,SLU}} = 1,1 \cdot \frac{5}{384} \cdot \frac{(80 \cdot 0,4) \cdot 7055^4}{1,38 \times 10^{13}} = 82 \text{ mm}$$

and the estimation for the live load load is

$$u_{g,inst} = 1,1 \cdot \frac{5}{384} \cdot \frac{(Q \cdot b_1) \cdot l^4}{EJ_{eff,SLS}} = 1,1 \cdot \frac{5}{384} \cdot \frac{(5 \cdot 0,4) \cdot 7055^4}{1,49 \times 10^{13}} = 5 \text{ mm}$$

Uniformly distributed load Approach	Failure load $Q = 80 \text{ kN/m}^2$ Mid-span deflection	Live load $Q = 5 \text{ kN/m}^2$ Mid-span deflection
FEM model	77 mm	5 mm
Analytical calculation	82 mm	5 mm
Results from Specimen A	65 mm	4 mm
Results from Specimen C	67 mm	3 mm

Table 8.1: Comparison of the mid-span deflection between the three approaches.

From the Table 8.1 it can be concluded that the mid-span deflection predicted for the ultimate load from the “ γ -method” is greater than the one which results from the FE model. For live load it has been obtained the same result. By comparing theoretical calculation and FEM result with bending test results it can be seen that for live load, the discrepancy is less than for ultimate load. Thus using the “ γ -method” during designing phase allows to get results on the safe side.

8.1.2 Comparison between the fundamental frequencies

This section shows the comparison between the fundamental frequencies obtained from the dynamic test with the one given from the FE model and from analytical calculations. The values are summarized in Table 8.2. As far as analytical calculations is concerned, the fundamental frequency has been evaluated referring to Eurocode 5 by the following expression

$$f_1^{theoretical} = \frac{\pi}{2 \cdot l^2} \cdot \sqrt{\frac{g}{A \cdot \gamma} \cdot EJ_{eff}} =$$

$$\frac{\pi}{2 \cdot 7055^2} \cdot \sqrt{\frac{9,81 \times 10^3}{22,95 \cdot 50 \cdot 800 \times 10^{-6} + 2 \cdot (420 \cdot 9,81) \cdot 115 \cdot 360 \times 10^{-9}} \cdot 2,98 \times 10^{13}} =$$

$$= 15,21 \text{ Hz}$$

where the parameters used have been reported in the previous chapter 7.

Approach	Frequency [Hz]
FE model	14,80
Analytical calculation	15,21
Experimetal value gets from static stiffness, specimen A	16,19
Experimetal value gets from static stiffness, specimen C	15,86
Results from dynamic test on specimen B	12,89

Table 8.2: Comparison of the fundamental frequency between the three approach.

By viewing the Table 8.2 it can be concluded that the fundamental frequencies ob-

tained by FE model and analytical calculation give fairly results and a higher value than the frequency measured by the dynamic test performed on the specimen B. It is common that FEM programs give higher frequencies than the one measured and it means that the FE models are usually more stiff. On the other hand, frequencies derived by using the real stiffness from the bending tests provide higher values of frequency.

8.1.3 Comparison between the bending stiffness

Figure 8.1 reports the comparison between stiffness of the composite structure for the different approaches. The bending stiffness from the bending tests has been obtained considering the simply supported beam loaded by four lines load.

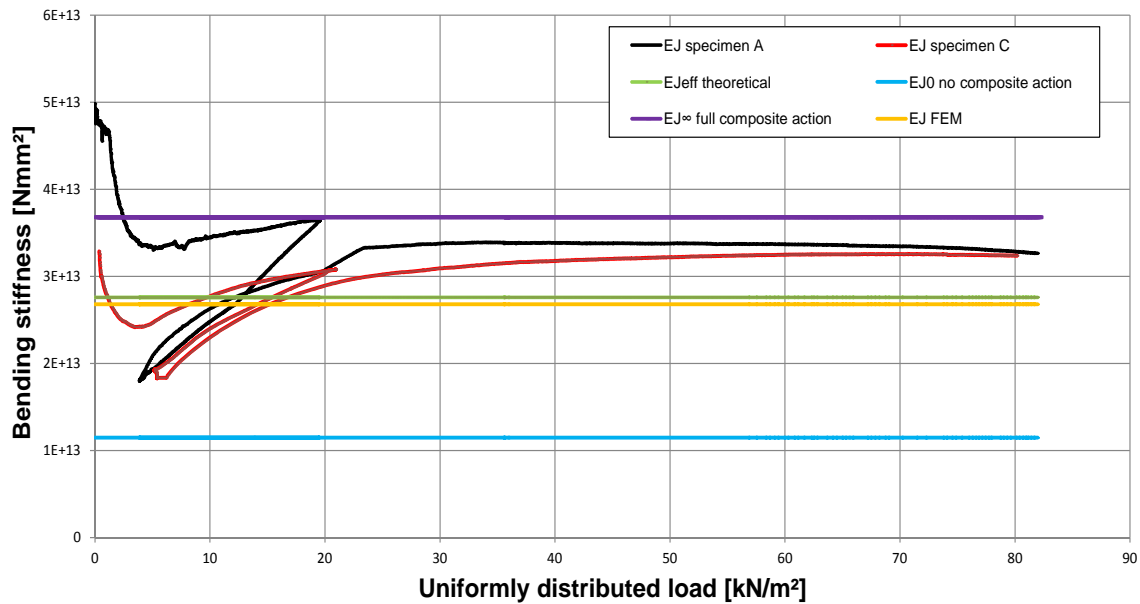


Figure 8.1: Bending stiffness of the specimen A ($EJ_{real,A} = 3,38 \times 10^{13} \text{ Nmm}^2$) and of specimen C ($EJ_{real,C} = 3,24 \times 10^{13} \text{ Nmm}^2$) compared to the theoretical cases of $k = 0$ and $k = \infty$, the effective ($EJ_{eff} = 2,76 \times 10^{13} \text{ Nmm}^2$) and the numerical stiffness ($EJ_{FEM} = 2,68 \times 10^{13} \text{ Nmm}^2$).

Figure 8.1 shows the different bending stiffness evaluated from the different approaches. The real stiffness for both the specimens are higher than the effective one, evaluated on the basis of the stiffness of the shear connectors obtained from the results of the shear tests performed and described in chapter 2. The bending stiffness evaluated from the FE model is a bit lower than the effective one. This could be due to the fact that FE model and analytical calculations does not take into account the contribution of friction. All the approaches have as assumptions elastic and linear behavior of the structure up to the failure.

8.1.4 Comparison between the efficiencies

Figure 8.2 shows the comparison between the efficiencies which has been obtained from the different approaches. For such a purpose, efficiency for each approach has been evaluated by using the formula proposed by Piazza

$$\eta = \frac{EJ - EJ_0}{EJ_\infty - EJ_0}$$

where

EJ_0 is the bending stiffness of the structure with no-composite action;

EJ_∞ is the bending stiffness of the structure with full-composite action;

EJ is the bending stiffness evaluated case by case from the different approaches.

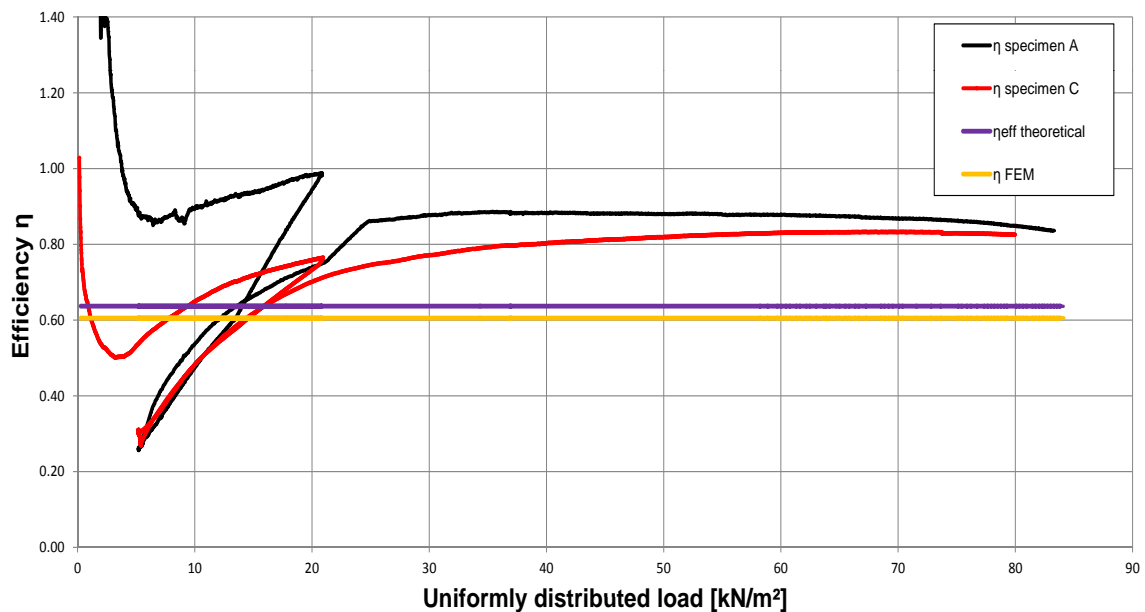


Figure 8.2: Comparison between the real efficiencies ($\eta_{real,A} = 0,88$ and $\eta_{real,C} = 0,82$), the effective efficiency ($\eta_{eff} = 0,64$) and the numerical ($\eta_{FEM} = 0,61$).

Figure 8.2 depicts the comparison of the different efficiencies. The efficiency evaluated by the FE model and the theoretical calculations are very close to each other and as well as this, both are lower than the real one obtained from the two bending tests. As a conclusion, it can be remark that both the system has shown a resistant and rigid behavior if related to normal floor-loads evaluated at SLS. The most important result concerns the huge real bending stiffness of the composite system, whose efficiency is very close to 1.

8.1.5 Comparison between the maximum shear forces on the connector

The maximum shear force acting to the fastener at the supports, for the analytical approach has been obtained with the next expression already presented in chapter 5:

$$F = \frac{\gamma_1 \cdot E_1 A_1 \cdot a_1 \cdot s_{eq}}{EJ} \cdot V$$

determining the parameters γ_1 and a_1 and stiffness EJ related to specific limit state. FE approach provides directly the value of the shear force. The comparison over this values have been reported in Table 8.3:

Uniformly distributed load Approach	Failure load $Q = 80 \text{ kN/m}^2$ Maximum shear force acting on the screw [kN]	Live load $Q = 5 \text{ kN/m}^2$
FEM model	51 kN	3,3 kN
Analytical calculation	72 kN	4,8 kN

Table 8.3: Comparison between the maximum shear force acting on the screw by the different approaches.

By viewing Table 8.3, it can be concluded that for a live load equal to $Q = 5 \text{ kN/m}^2$, the FE model and the theoretical calculation provide very close values of the maximum shear force acting on the screw at the supports. On the other hand, for load close to the failure $Q = 80 \text{ kN/m}^2$, the analytical calculation provides a greater value than the numerical one.

8.2 Conclusions over the three different approaches

In this master thesis timber-to-concrete connections with inclined self-tapping screws were analysed and also a well and quick way to obtain a good level of prefabrication of these types of composite structure has been considered. Short- and long-term bending and even dynamic tests have been performed in order to check the performance of the composite structure, especially the degree of the composite action. Both the two full-scale specimens tested at short-time can be considered highly resistant, by referring to normal floor-loads at SLS. The efficiencies of both the two specimens A and C, were $\eta = 0,88$ and $\eta = 0,82$, respectively. With regard to analytical calculations and FEM results, from the previous comparisons it can be concluded that the results from both the approaches are very close to each other and to the major part provide value to the safe side. Thus, FE model is useful and reliable during the designing phase in order to predict the forces, the mid-span deflections and the frequency for the structure which is designed.

Chapter 9

Future research

The investigations presented in this thesis consider the possibility of full-prefabrication degree in which composite structures are totally produced by moving all the production process to the workshop. The presented studies explore ways to improve the industrial process, to make prefabrication of composite floors more quick and even cheaper. The investigations answered many questions, about the way of production and the way to predict the behavior of the structure by means of theoretical calculations and development of FE models, but raised new questions how can be used these structures for various purposes.

9.1 Experimental investigations

The experimental campaign presented in this thesis is fairly completed and all the parameters have been checked. The self-tapping screws used to join the concrete slab to the glulam beams well responded to their purpose. The composite structures show high level of bending stiffness and degree of efficiency, and a high load-carrying capacity as well. As far as short-term behavior is concerned, it has been catch very well, instead for long-term behavior more analysis have to be conducted. It is here remembered that in this thesis only the results after one month has been reported and discussed, but the experimental campaign still goes on at Lunds Tekniska Högskola for at least six months. Further experimental investigations are needed to draw definitive conclusions regarding the long-term behavior of the proposed composite systems. Creep tests (in variable and conditioned environmental conditions) should be performed on push-out specimens incorporating a few connectors subjected to shear in order to evaluate the reduction in slip modulus of the screws due to relaxation.

As regards durability, the composite system is well working against weathering, since the concrete on the top side ripares the beams. Only special attention must be taken when more of these types of system are placed close to each other in order to realize an horizontal floor by providing a waterproof joint. Last, since the fire

resistance of timber-concrete composite elements is heavily dependent on the effects of fire on the timber and shear connectors, and composite beams will inevitably lose stiffness when subjected to fire, the fire-resistance of the full-prefabricated timber-concrete composite system should be investigated.

9.2 Numerical analysis

The FE model which has been realized is in agreement with theoretical calculations and allows to well predict the behavior of the composite structure for short-term and can be used to extend the experimental results to composite beams with different configurations, geometrical and mechanical properties. Furthermore, FE investigations to improve the analysis on these systems should include parametric studies to identify the optimal cross-sections, numbers and locations of the connectors for systems with different properties. Long-term numerical analysis should be carried out, since the FE model here realized does not contemplate long-term behavior of the materials, which may lead to fail the serviceability limit state deflection criteria.

9.3 Industrial implementation

The choice of using self-tapping full-threaded screws for connecting the two members turns out to be the cheapest and fastest. Further, considering the high degree of prefabrication here proposed, it allows to save money and time. Other ways to develop this type of system completely at the workshop should be investigated.

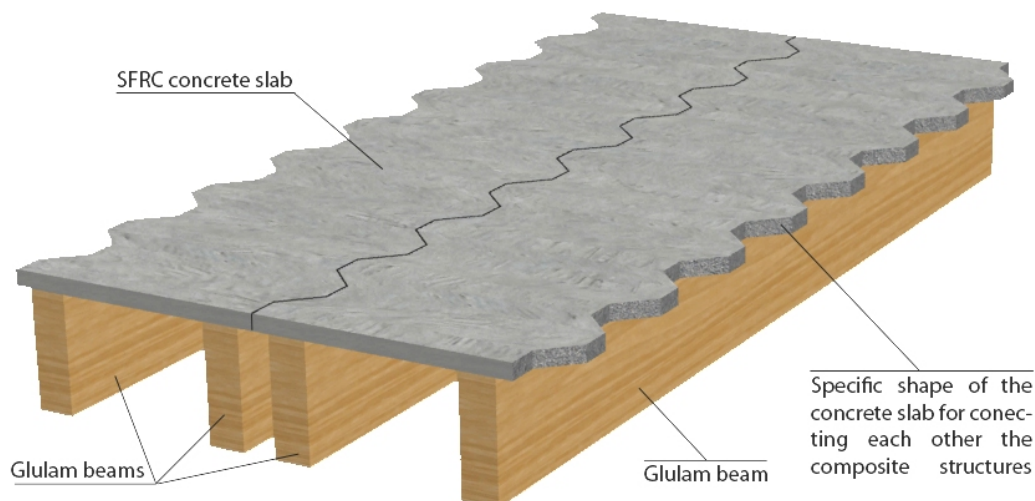


Figure 9.1: Possible interconnection between composite floors for full-prefabricated system.

One aspect of the system which is not discussed in the thesis, but not least from a

manufacturability point of view, is the connection detail between composite floors and vertical element. These aspects need to be considered to ensure that any developed composite floor structure is compatible also for seismic requirements, which need that the horizontal floors for new building must be not deformable in their plane in order to well distribute the horizontal forces.

A possible connection between composite systems, that can be considered for a high degree of prefabrication, is presented in Figure 9.1. In this case, a specific shape of the formwork for the concrete slab is needed.

The proposed prefabricated system should eventually be used to construct a full-scale floor in a real buildings in order to verify its feasibility on-site, especially in case of earthquake, and monitor possible problems during constructions.

Chapter 10

Example of application

This annex presents a calculation example of a particular application for these composite structure based on the theoretical method for composite sections according to Eurocode 5. There have been reported the analytical calculations and verifications for short- and long-term according to Eurocode rules.

10.1 Background

The Strömvasallen is a football stadium in Gävle, Sweden. The stadium holds 7300 people and was built in 1923. Currently, Sweco architects are studying a way to renovate the stadium. One of the main proposal idea is to use timber-concrete composite beam as stands. The composite structures reflect, with the identical dimensions, the composite systems realized and tested at Lund Tekniska Högskola, see chapter 4 and 7. Figure 10.2 shows a plan view of the stadium and the red circles show the stands where the composite structure are used as benches. Figure 10.1 shows a 3D-view of the stands.

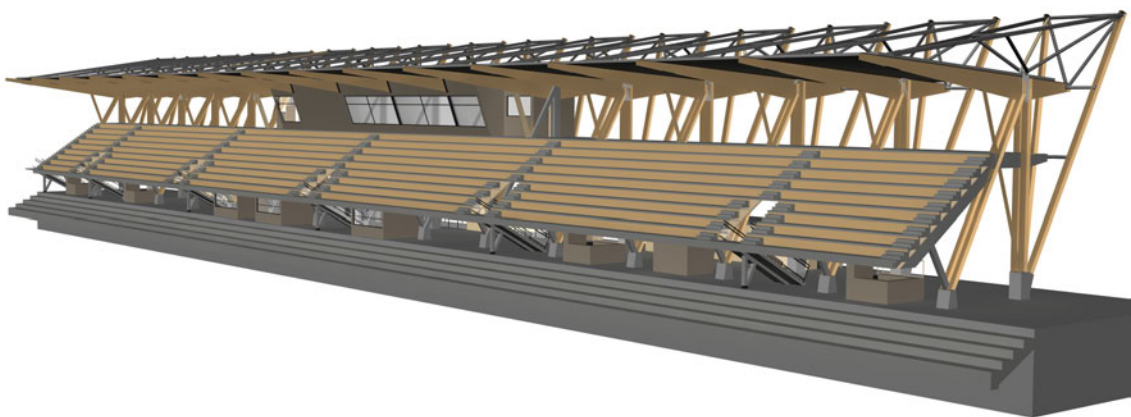


Figure 10.1: 3D-view of the stands.

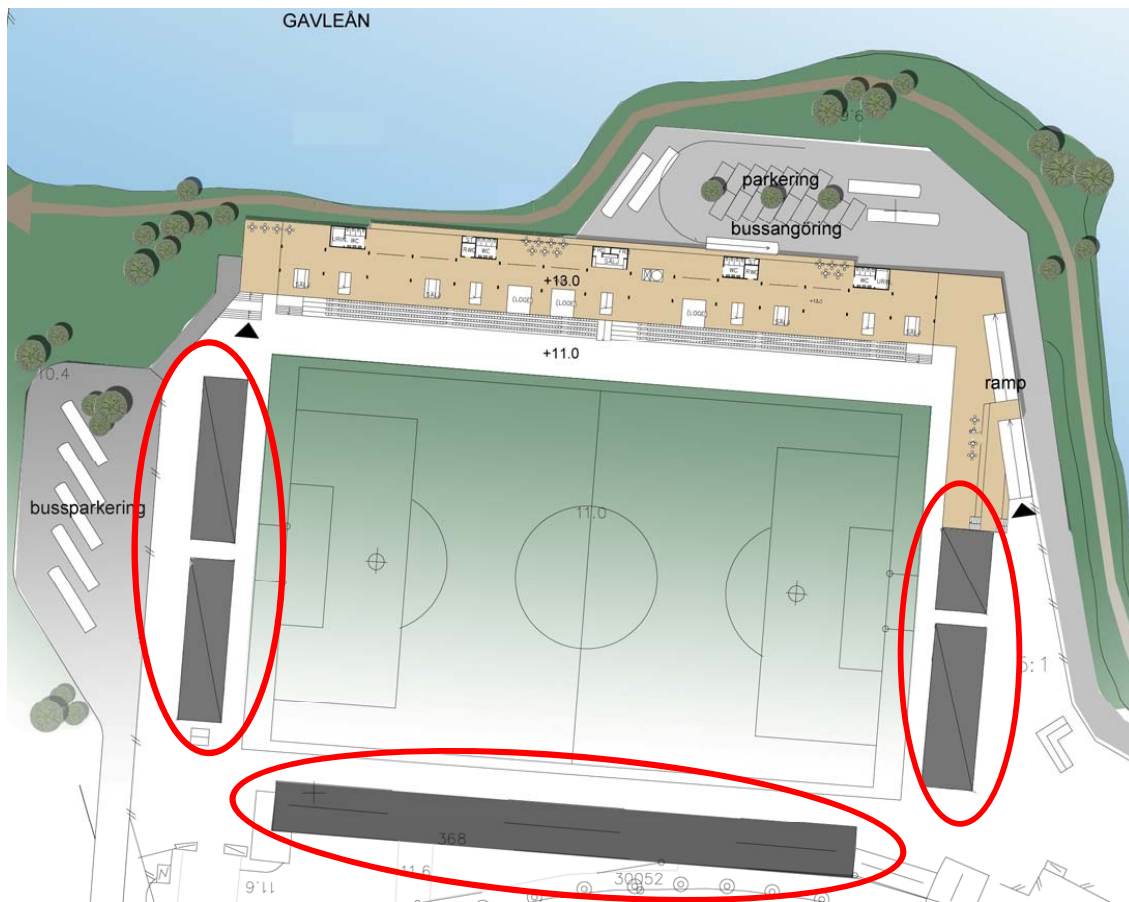


Figure 10.2: Plan view of Strömvasallen stadium.

10.2 Materials

The materials used for the design of the stands are the same used to build out the full-scale specimens and presented in chapter 4 and chapter 7. Anyway, the main properties of materials has been reported in the following paragraphs.

10.2.1 Steel-fibre reinforced concrete

In Table 10.1 are reported the main properties of the concrete which has been used for the design.

Description	Symbol	Value
Characteristic compressive cubic strength	R_{ck}	50, 83 MPa
Characteristic compressive cylinder strength	f_{ck}	42, 19 MPa
Equivalent elastic modulus of the SFRC	E_m	36105 MPa
Specific gravity	γ_c	22, 95 kg/m ³
Design compressive strength of the concrete	$f_{cd} = \frac{\alpha_{cc} \cdot f_{ck}}{\gamma_c}$	23, 91 MPa
Mean value of axial tensile strength	$f_{ctm} = 0, 3 \cdot (f_{ck})^{2/3}$	3, 64 MPa
Mean value of axial tensile strength due to bending	$f_{ctm,m} = f_{ctm} \cdot 1, 2$	4, 36 MPa
Characteristic value at 5% fractile of tensile strength of concrete	$f_{ctk} = f_{ctm,m} \cdot 0, 7$	3, 05 MPa
Design tensile strength of the SFRC	$f_{ctd} = \frac{f_{ctk}}{\gamma_c}$	2, 04 MPa

Table 10.1: Main properties of the concrete.

The partial safety factors reported in the Table 10.1 and required for the design of concrete according to Eurocode 2 are: partial safety factor $\gamma_c = 1, 5$ and the factor for long-time effects $\alpha_{cc} = 0, 85$.

10.2.2 Glulam beams

With regard to the glulam beam, the main properties need for the design phase has been reported in Table 10.2

Description	Symbol	Value
Bending strength	$f_{m,g,k}$	30 MPa
Tensile strength parallel to the grain	$f_{t,0,g,k}$	20 MPa
Shear strength	$f_{v,g,k}$	3, 5 MPa
Specific gravity	$\rho_{g,k}$	390 kg/m ³
Mean elastic modulus perpendicular to the grain	$E_{0,g,mean}$	12500 MPa

Table 10.2: Main properties of the glulam beams.

The project values of general resistance properties (X_d) can be obtained from characteristic X_k values by following relation:

$$X_d = k_{mod} \cdot \frac{X_k}{\gamma_M}$$

where γ_M is the partial safety factor for the material properties, such as recommended from Eurocode 5 and for glued laminated timber assumes the value $\gamma_M = 1,25$. The k_{mod} factor is the modification factor for service class which considers the effect of, on resistances parameters, both the load duration and the moisture content. Since the glulam beam used to realize the stand stay outdoors but protected from the weather such as covered by a roof, it has been referred to the Service Class 2.

Effects must be assigned at one of the load duration categories given in Table 2.1 of Eurocode 5, indicating a class for each known load duration. In this case, it has been referred to two different load duration categories: permanent, in which there are only the elements self-weights, structural and non, and a medium duration category, in which in addition to self-weight there is also the live load. Thus for this factor it has been assumed the following values

$$k_{mod,permanent} = 0,6 \quad k_{mod,medium-term} = 0,8$$

Regarding serviceability checks (SLS), it has to take into account k_{def} factor to estimate viscoelastic deformation, according to the relative service category. In this case, according to Table 3.2 of Eurocode 5, for glued laminated timber and for service class 2 the value of this factor is

$$k_{def} = 0,8$$

The characteristic density of the wood can be estimated as

$$\gamma_{k,GL} = g \cdot 390 = 3,82 \text{ kN/m}^3$$

Successively, it has been calculated and reported in Table 10.3 and Table 10.4 the design strength values with regard to the load duration category as previously shown.

Description	Symbol	Value
Bending strength	$f_{m,d}$	14,4 MPa
Tensile strength parallel to the grain	$f_{t,0,d}$	9,6 MPa
Shear strength	$f_{v,d}$	1,68 MPa

Table 10.3: Design strength values for the glulam beams for permanent load duration ($k_{mod} = 0,60$).

Description	Symbol	Value
Bending strength	$f_{m,d}$	19,2 MPa
Tensile strength parallel to the grain	$f_{t,0,d}$	12,8 MPa
Shear strength	$f_{v,d}$	2,24 MPa

Table 10.4: Design strength values for the glulam beams for medium duration conditions ($k_{mod} = 0,80$).

In order to take into account the load-duration and the moisture influences on deformation at long-term the modulus of elasticity of the wood has to be taken as follow

$$E_{mean,SL5,\infty} = \frac{E_{mean}}{(1 + \psi_2 \cdot k_{def})} = \frac{12500}{(1 + 0,6 \cdot 0,8)} = 8446 \text{ MPa}$$

$$E_{mean,UL5,\infty} = \frac{12500}{(1 + 0,8)} = 6944 \text{ MPa}$$

10.3 Load combinations

For the limit state verifications it has been referred to the following combination rules:

- Basic combination, used for ULS

$$\gamma_G \cdot (G_{k1,slab} + G_{k1,beam} + G_{k2}) + \gamma_Q \cdot Q_k + \dots$$

- Characteristic combination, used for SLS

$$G_{k1,slab} + G_{k1,beam} + G_{k2} + Q_k + \dots$$

- Quasi-permanent combination, used for long-term effects

$$G_{k1,slab} + G_{k1,beam} + G_2 + \psi_{21} \cdot Q_k + \dots$$

For the stand applications only G_{k1} (structural permanent load), G_{k2} (non structural permanent load) and Q_{k1} (leading live load) has been considered. The partial safety factors γ_G and γ_Q and the combination factor ψ_{20} used are reported in Table 10.5. It is worth to point out that in this case it has been considered only the unfavourable case since there is only one span between the supports.

Type of load	Structural permanent load	Non structural permanent load	Live load	Combination factor
Factor	1,2	1,2	1,5	0,6

Table 10.5: Partial safety factor used for the design of the stands.

10.3.1 Structural permanent load

The permanent structural load G_1 is given by self-weight of timber beam and concrete slab above. In accordance with the Figure 7.12, the procedure for calculating the structural load per unit length g_1 and per unit area G_1 is:

$$g_1 = g_{1,c} + g_{1,GL} = \gamma_{k,SFRC} \cdot h_1 \cdot i + \gamma_{k,GL} \cdot h_2 \cdot b_2$$

$$g_{1,c} = 22,95 \cdot 0,05 \cdot 0,4 = 0,46 \text{ kN/m}$$

$$g_{1,GL} = 3,82 \cdot 0,360 \cdot 0,115 = 0,16 \text{ kN/m}$$

$$G_1 = \frac{g_{1,c} + g_{1,GL}}{i} = \frac{0,46 + 0,16}{0,4} = 1,55 \text{ kN/m}^2$$

10.3.2 Non structural permanent load

In addition to structural permanent load there is also a carried permanent action, for such a case of stands, a waterproof membrane is placed over the slab which self-weight can be estimated as $0,2 \text{ kN/m}^2$ or $0,08 \text{ kN/m}$.

10.3.3 Live load

The live load which must be considered for the design load, according to Eurocode 1, belongs to environments susceptible to crowding (category C). The live load which must be considered is a uniformed distributed load equal to 5 kN/m^2 (2 kN/m) which also includes the dynamic effects.

10.3.4 Load combinations and external actions

Checks to consider the different load duration categories and long-term behaviour will be done both at early time (implementation of the system) and at infinite time. In early time ULS checks have been considered two different combinations of actions: one made up by only permanent loads (Combination I) and the other one with all loads, including live load (Combination II). On the other hand, at final time check has been considered with only the second combination, including all loads. By substituting the loads values and considering the load combination rules previously reported it has been obtained:

$$q_{ULS,I} = 1,2 \cdot g_{1,c} + 1,2 \cdot g_{1,GL} + 1,2 \cdot g_2 = 1,2 \cdot 0,46 + 1,2 \cdot 0,16 + 1,2 \cdot 0,08 = 0,84 \text{ kN/m}$$

$$q_{ULS,II} = 1,2 \cdot g_{1,c} + 1,2 \cdot g_{1,GL} + 1,2 \cdot g_2 + 1,5 \cdot q =$$

$$= 1,2 \cdot 0,46 + 1,2 \cdot 0,16 + 1,2 \cdot 0,08 + 1,5 \cdot 2 = 3,84 \text{ kN/m}$$

While the values of actions combined at SLS are equal to:

$$q_{SLS,characteristic} = g_{1,c} + g_{1,GL} + g_2 + q = 0,46 + 0,16 + 0,08 + 2 = 2,70 \text{ kN/m}$$

$$\begin{aligned} q_{SLS,quasi-permanent} &= g_{1,c} + g_{1,GL} + g_2 + \psi_{21} \cdot q = \\ &= 0,46 + 0,16 + 0,08 + 0,6 \cdot 2 = 1,90 \text{ kN/m} \end{aligned}$$

By considering the span length equal to $l = 7200 \text{ mm}$ it has been calculated the design value of bending moment at mid-span (M_d) and shear at the supports the beam (T_d) according to the two significant load combinations at ULS:

$$\begin{aligned} T_{d,I} &= \frac{q_{ULS,I} \cdot l}{2} = \frac{0,84 \cdot 7,2}{2} = 3,01 \text{ kN} \\ M_{d,I} &= \frac{q_{ULS,I} \cdot l^2}{8} = \frac{0,84 \cdot 7,2^2}{8} = 5,42 \text{ kNm} \\ T_{d,II} &= \frac{q_{ULS,II} \cdot l}{2} = \frac{3,84 \cdot 7,2}{2} = 13,81 \text{ kN} \\ M_{d,II} &= \frac{q_{ULS,II} \cdot l^2}{8} = \frac{3,84 \cdot 7,2^2}{9} = 24,86 \text{ kNm} \end{aligned}$$

10.4 Geometry and data

10.4.1 Cross-section

The geometry of the composite beam is the same as the one used for the bending tests. Anyway, Figure 10.3 shows the cross-section of the composite structure, where the length of the span is 7200 mm. The spacing between the glulam beams has been assumed equal to $i = 585 \text{ mm}$.

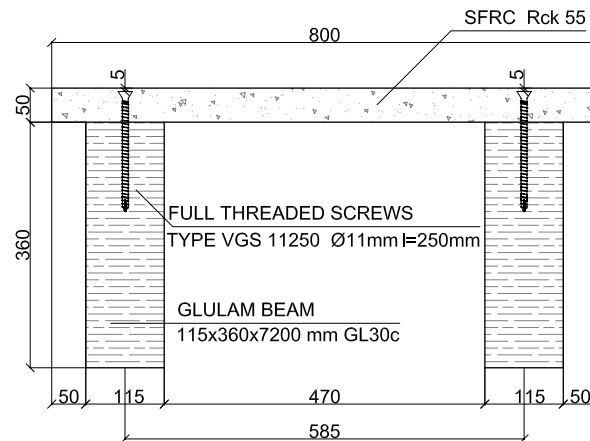


Figure 10.3: Cross-section of the composite structure.

10.4.2 Connection system and its properties

Timber beams are connected to the concrete slab by using self-tapping full-threaded screws as it has been done for the full-scale specimens tested and reported in chapter 7.

Description	Symbol	Value
Inclined angle between the screw axis and the timber plane	$\alpha[^\circ]$	15
Number of screw for connection	n	1
Minimum spacing between screws at the supports	s_{min} [mm]	200
Maximum spacing between screws in the middle part	s_{max} [mm]	300
Equivalent spacing	s_{eq} [mm]	225
Nominal diameter	ϕ_{nom} [mm]	11
Core diameter	ϕ_{core} [mm]	6,6
Shank diameter	ϕ_{shank} [mm]	7,7
Head diameter	ϕ_{head} [mm]	19,3
Effective diameter	ϕ_{eff} [mm]	7,26
Length of the screw	l_b [mm]	250
Penetration depth of the threaded part minus one diameter	l_{ef} [mm]	186
Penetration depth of the screw in the concrete	l_c [mm]	64
Characteristic value for the yielding moment of the screw	$M_{y,k}$ [MPa]	45900
Effective number of screws	n_{ef}	1

Table 10.6: Properties of the connection system with full-threaded inclined screws.

According to Eurocode 5, paper [27], the strength check for the connection system made up by screws loaded both axially and laterally provides the satisfying of the following relation

$$\left(\frac{F_{ax,Ed}}{F_{ax,Rd}}\right)^2 + \left(\frac{F_{v,Ed}}{F_{V,Rd}}\right)^2 \leq 1$$

If it is called α the angle between the screw axis and the longitudinal direction of the beam, previous expression becomes:

$$\left(\frac{F \cdot \cos\alpha}{F_{ax,Rd}}\right)^2 + \left(\frac{F \cdot \sin\alpha}{F_{V,Rd}}\right)^2 \leq 1$$

where F , fastener load, has to be taken as (as suggested at point B.5 of Eurocode 5):

$$F = \frac{\gamma_1 \cdot E_1 A_1 \cdot a_1 \cdot s_{eq}}{E J_{eff}} \cdot V$$

where V is the maximum shear load.

The withdrawal strength $F_{ax,\alpha,Rk}$ has to be taken by using the following expression

$$F_{ax,\alpha,Rk} = n_{ef} \cdot (\pi \cdot d \cdot l_{ef})^{0,8} \cdot f_{ax,\alpha,k}$$

where

$f_{ax,k} = 3,6 \times 10^{-3} \cdot \rho_k^{1,5} = 27,73$ MPa is the characteristic withdrawal strength perpendicular to the grain;

$\rho_k = 390$ kg/m³ is the characteristic density of the timber;

$f_{ax,\alpha,k} = \frac{f_{ax,k}}{\sin^2(\alpha)+1,5 \cdot \cos^2(\alpha)} = \frac{27,73}{\sin^2(45)+1,5 \cdot \cos^2(45)} = 22,18$ MPa is the characteristic withdrawal strength at an angle α to the grain;

drawal strength at an angle α to the grain;

$n_{ef} = n = 1$ is the number of screws acting together in a connection;

$d = 11$ mm is the diameter of each connector (outer diameter of the threaded part);

$l_{ef} = 186$ mm penetration depth of the screws minus one diameter;

Thus, by substituting the single values the characteristic withdrawal capacity of the connections with axially loaded screws has been taken as

$$F_{ax,\alpha,Rk} = 1 \cdot (\pi \cdot 11 \cdot 186)^{0,8} \cdot 22,18 = 24,69 \text{ kN}$$

The characteristic shear strength of screw laterally loaded can be calculated by using expression 8.10 of Eurocode 5, which also considers the rope effect caused by screws withdrawal strength and evaluable, in absence of experimentation, with the quantity $F_{ax,Rk}/4$. The concrete slab can be seen as a thick steel plate as the central member of a double shear connection and thus the formulae to consider are:

$$F_{V,Rk} = \min \left\{ \begin{array}{l} f_{h,1,k} \cdot t_1 \cdot d \\ f_{h,1,k} \cdot t_1 \cdot d \cdot \left[\sqrt{2 + \frac{4 \cdot M_{y,Rk}}{f_{h,1,k} \cdot d \cdot t_1^2}} - 1 \right] + \frac{F_{ax,Rk}}{4} \\ 2,3 \cdot \sqrt{M_{y,Rk} \cdot f_{h,1,k} \cdot d} + \frac{F_{ax,Rk}}{4} \end{array} \right.$$

where

t_1 is the pointside penetration length of the threaded part minus one screw diameter in mm;

$M_{y,Rk}$ is the characteristic value for the yield moment, in Nmm;

$f_{h,0,k}$ is the characteristic embedment strength in MPa.

The connection check imposes to calculate the characteristic embedment strength of the screws (evaluable with expression 8.16 of Eurocode 5):

$$f_{h,0,k} = 0,082 \cdot (1 - 0,01 \cdot d_{eff}) \cdot \rho_k$$

$$f_{h,0,k} = 0,082 \cdot (1 - 0,01 \cdot 7,26) \cdot 390 = 29,66 \text{ MPa}$$

The characteristic value of the yield moment is declared from the producer and its value is 45900 Nmm. It must be considered $d_{eff} = 1,1 \cdot d$ because the previous relation is valid if the screws have not a threaded part.

By substituting the values if the previous equations, the characteristic load-carrying capacity per shear plane per fastener for the different mode of rupture are:

$$F_{v,Rk} = \min \begin{cases} 36,41 \text{ kN} \\ 21,46 \text{ kN} \\ 13,07 \text{ kN} \end{cases}$$

The connection system used to join timber beams with the concrete slab are screw VGS11250 where the outer diameter is $\phi = 11 \text{ mm}$ and the length is equal to $l = 250 \text{ mm}$. These screws are the same used to realize the full-scale specimens presented in chapter 4 and also in previous research as presented in chapter 3. Besides, in order to estimate the slip modulus of the connection specific shear tests have been performed and reported in chapter 2. Anyway, the slip modulus of the connection system for the different checking conditions are:

- for short-term:

$$K_{ser} = 35000 \text{ N/mm}$$

$$K_u = 23333 \text{ N/mm}$$

- for long-term, in order to take into account the load-duration and the moisture influences on deformations an easy way is to reduce the slip modulus by using the following expressions:

$$K_{ser,\infty} = \frac{K_{ser}}{1 + \psi_2 \cdot k_{def}} = \frac{35000}{1 + 0,6 \cdot 0,8} = 23649 \text{ N/mm}$$

$$K_{u,\infty} = \frac{K_u}{1 + k_{def}} = \frac{23333}{1 + 0,8} = 12962 \text{ N/mm}$$

10.5 Stiffness properties of the composite system

In this section it has been assessed the stiffness values, first relative to single items and then relative to composite system. These values have been evaluated both for short-term ($t = 0$) and for long-term ($t = \infty$). Since to report all the calculation takes lot of pages, it has been decided to report before only the equations used (which are actually already presented in chapter 5 and also used in chapter 7) after that the results for each limit state and time checking have been reported in the following table. The symbols whom it has been adopted refers to Figure 10.4.

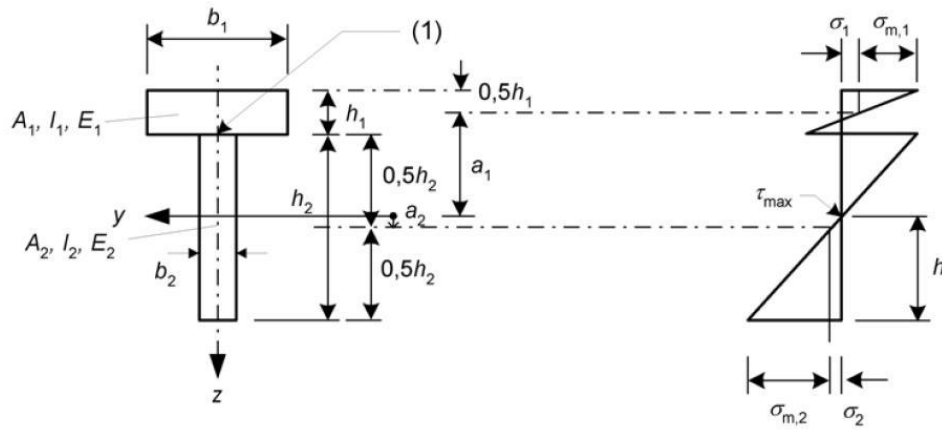


Figure 10.4: Cross-section (left) and distribution of bending stresses (right). All measurements are positive except for a_2 which is taken as positive as shown.

The procedure is:

$$E_1 J_1 = E_{cm} \cdot i \cdot \frac{h_1^3}{12};$$

$$E_2 J_2 = E_{0,mean} \cdot \frac{b_2 \cdot h_2^3}{12};$$

$$E_1 A_1 = E_{cm} \cdot i \cdot h_1;$$

$$E_2 A_2 = E_{0,mean} \cdot b_2 \cdot h_2;$$

$$E J_0 = E_1 J_1 + E_2 J_2;$$

$$E A_0 = \frac{E_1 A_1 \cdot E_2 A_2}{E_1 A_1 + E_2 A_2};$$

$$a = h_1/2 + h_2/2 + t;$$

$$a_2 = \frac{\gamma_1 \cdot E_1 A_1 \cdot a}{\gamma_1 \cdot E_1 A_1 + \gamma_2 \cdot E_2 A_2};$$

$$E J_{ef} = \sum_{i=1} E_i J_i + \gamma_2 \cdot E_2 A_2 \cdot a_2^2 + \gamma_1 \cdot E_1 A_1 \cdot a_1^2;$$

$$E J_{\infty} = \sum_i (E_i J_i + E_i A_i \cdot a_i^2) = E J_0 + E A_0 \cdot a^2;$$

$$\eta = \frac{E J_{ef} - E J_0}{E J_{\infty} - E J_0}.$$

The parameter dimensionless η quantifies the connection efficiency.

Symbol	Value for ULS at		Value for SLS at	
	$t = 0$	$t = \infty$	$t = 0$	$t = \infty$
$E_1 J_1 [Nmm^2]$	$1,50 \times 10^{11}$	$1,50 \times 10^{11}$	$1,50 \times 10^{11}$	$1,50 \times 10^{11}$
$E_1 A_1 [N]$	$7,22 \times 10^8$	$7,22 \times 10^8$	$7,22 \times 10^8$	$7,22 \times 10^{11}$
$E_2 J_2 [Nmm^2]$	$5,59 \times 10^{12}$	$5,59 \times 10^{12}$	$5,59 \times 10^{12}$	$3,78 \times 10^{12}$
$E_2 A_2 [N]$	$2,88 \times 10^8$	$2,88 \times 10^8$	$5,18 \times 10^8$	$3,50 \times 10^8$
$E J_0 [Nmm^2]$	$5,74 \times 10^{12}$	$3,26 \times 10^{12}$	$5,74 \times 10^{12}$	$3,93 \times 10^{12}$
$E A_0 [N]$	$3,01 \times 10^8$	$2,06 \times 10^8$	$3,01 \times 10^8$	$2,36 \times 10^8$
$y_{G\infty} [mm]$	299	327	299	318
γ_2	1	1	1	1
γ_1	0,43	0,30	0,53	0,43
$a [mm]$	205	205	205	205
$a_2 [mm]$	77	87	87	97
$a_1 [mm]$	128	118	118	108
$E J_\infty [Nmm^2]$	$1,84 \times 10^{13}$	$1,19 \times 10^{13}$	$1,84 \times 10^{13}$	$1,38 \times 10^{13}$
$E J_{ef} [Nmm^2]$	$1,39 \times 10^{13}$	$8,40 \times 10^{12}$	$1,50 \times 10^{13}$	$1,09 \times 10^{13}$
η	0,64	0,60	0,73	0,70

Table 10.7: Values of the stiffness and efficiencies for the different conditions.

10.6 Verifications

10.6.1 Strength verifications

Strength verifications regard the glulam beam, the concrete slab and the connection system, and have to be performed both at short-term ($t = 0$) and long-term ($t = \infty$), according to the load duration conditions (short and long-term). It has been referred to the symbols reported in the Appendix of Eurocode 5 and already presented in chapter 5. Verifications that must be checked are:

- Compressive stress of the concrete at the upper side of the slab;
- Tensile stress on concrete at lower side of the concrete slab;
- Combined bending and axial tension in glulam at the lower edge of the glulam beam;
- Shear stress in the glulam beam;
- Combined shear and axial load on the connection system.

Below there are reported the formulations suggested in Appendix B of Eurocode 5, in order to evaluate the stresses in the elements:

$$\sigma_i = \frac{\gamma_i \cdot E_i \cdot a_i}{E J_{ef}} \cdot M$$

$$\sigma_{m,i} = \frac{0,5 \cdot E_i \cdot h_i}{E J_{ef}} \cdot M$$

$$\tau_{max} = \frac{0,5 \cdot E_2 \cdot (a_2 + h_2/2)^2}{E J_{ef}} \cdot V$$

$$\sigma_{c1,c} = \sigma_{1,c} + \sigma_{m1,c}$$

$$\sigma_{t1,c} = \sigma_{m1,c} - \sigma_{1,c}$$

The stresses calculated for each load condition by the previous formulas are reported in the following Table 10.8. The symbols used refers to Figure 10.4. There have been also reported the values of the maximum shear force acting on the screw and the relative component parallel and perpendicular to the shear connector.

Symbol	Permanet load at $t = 0$	All load at $t = 0$	All load at $t = \infty$
$\sigma_{1,c}$ [MPa]	0,78	3,56	3,71
$\sigma_{m1,c}$ [MPa]	0,35	1,62	2,67
$\sigma_{c1,c}$ [MPa]	1,13	5,17	6,39
$\sigma_{t1,c}$ [MPa]	0,42	1,94	1,04
$\sigma_{2,wood}$ [MPa]	0,38	1,72	1,79
$\sigma_{m2,wood}$ [MPa]	0,88	4,03	3,70
$\tau_{max,wood}$ [MPa]	0,1	0,41	0,41
$F_{d,connection}$ [kN]	1,94	8,90	9,29
$F_{ax,Ed}$ [kN]	1,37	6,29	6,57
$F_{V,Ed}$ [kN]	1,37	6,29	6,57

Table 10.8: Stresses in the cross-section for each load condition.

The Ultimate Limit States checking have been conducted by using the formulas provided from Eurocode 5 and below reported:

- Combined bending and axial tension

Formula	Checking for permanent load at $t = 0$	Checking for all loads at $t = 0$	Checking for all loads at $t = \infty$
$\frac{\sigma_{2,wood}}{f_{t,0,d}} + \frac{\sigma_{m2,wood}}{f_{m,d}} \leq 1$	$0,1 \leq 1$	$0,32 \leq 1$	$0,32 \leq 1$

- Shear stress on the glulam beam

Formula	Checking for permanent load at $t = 0$	Checking for all loads at $t = 0$	Checking for all loads at $t = \infty$
$\frac{\tau_{max,wood}}{f_{v,d}} \leq 1$	$0,05 \leq 1$	$0,17 \leq 1$	$0,17 \leq 1$

- Compressive stress on the concrete

Formula	Checking for permanent load at $t = 0$	Checking for all loads at $t = 0$	Checking for all loads at $t = \infty$
$\frac{\sigma_{cl,concrete}}{f_{cd}} \leq 1$	$0,05 \leq 1$	$0,22 \leq 1$	$0,27 \leq 1$

- Tensile stress on the concrete

Formula	Checking for permanent load at $t = 0$	Checking for all loads at $t = 0$	Checking for all loads at $t = \infty$
$\frac{\sigma_{t1,concrete}}{f_{ctd}} \leq 1$	$0,21 \leq 1$	$0,95 \leq 1$	$0,51 \leq 1$

- Connection checks

Formula	Checking for permanent load at $t = 0$	Checking for all loads at $t = 0$	Checking for all loads at $t = \infty$
$\left(\frac{F_{ax,Ed}}{F_{ax,Rd}}\right)^2 + \left(\frac{F_{V,Ed}}{F_{V,Rd}}\right)^2 \leq 1$	$0,01 \leq 1$	$0,30 \leq 1$	$0,32 \leq 1$

Eventually, trend of internal stresses have been reported for the relative load condition in the following Figures. Figure 10.8 shows the comparisons between the short- and long-term internal stresses at Ultimate Llimit States.

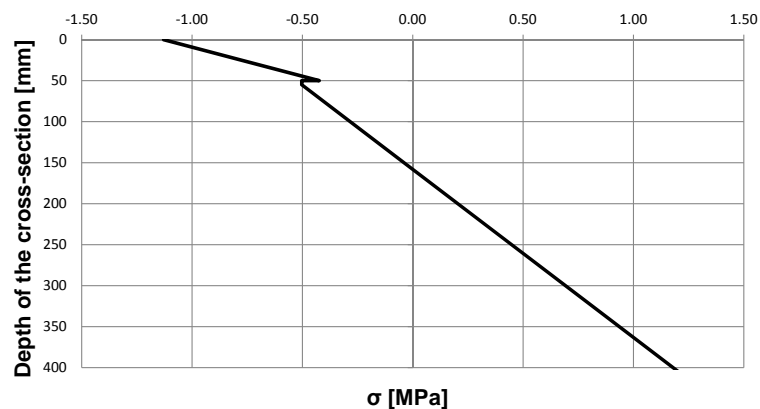


Figure 10.5: Internal trend of the stress on the cross-section with only the permanent load acting, at $t = 0$.

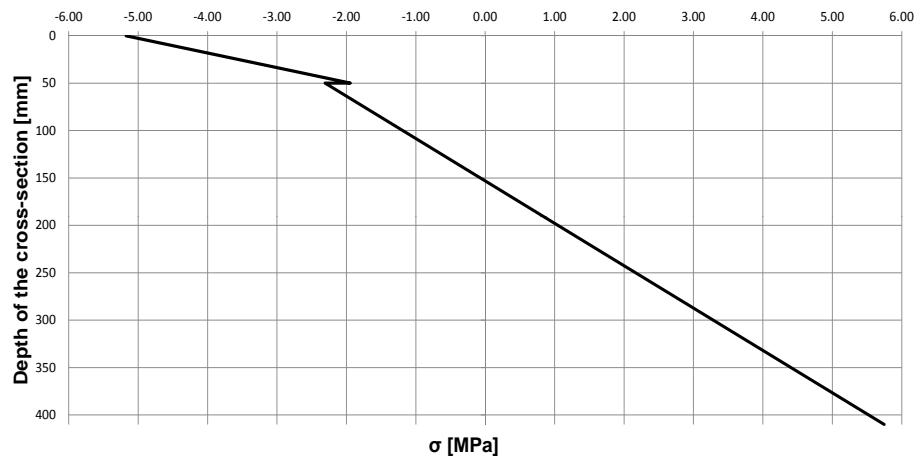


Figure 10.6: Internal trend of the stress on the cross-section with all loads acting, at $t = 0$.

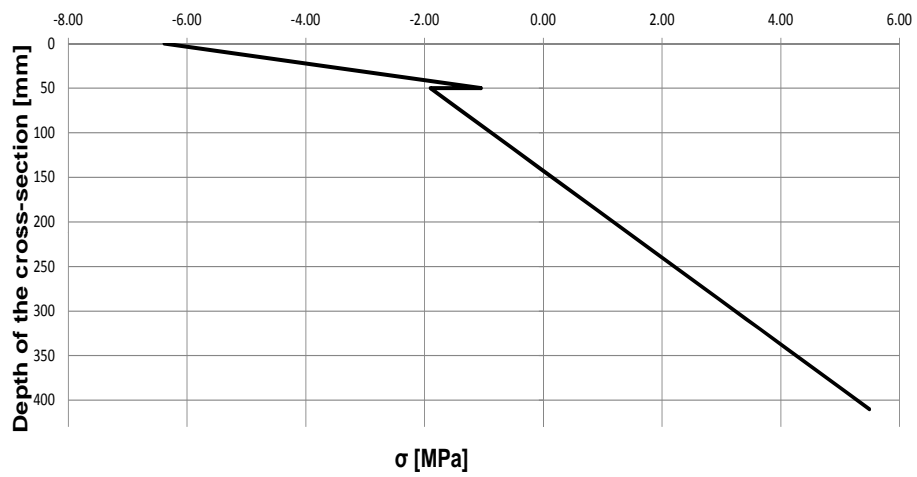


Figure 10.7: Internal trend of the stress on the cross-section with only the permanent load acting, at $t = \infty$.

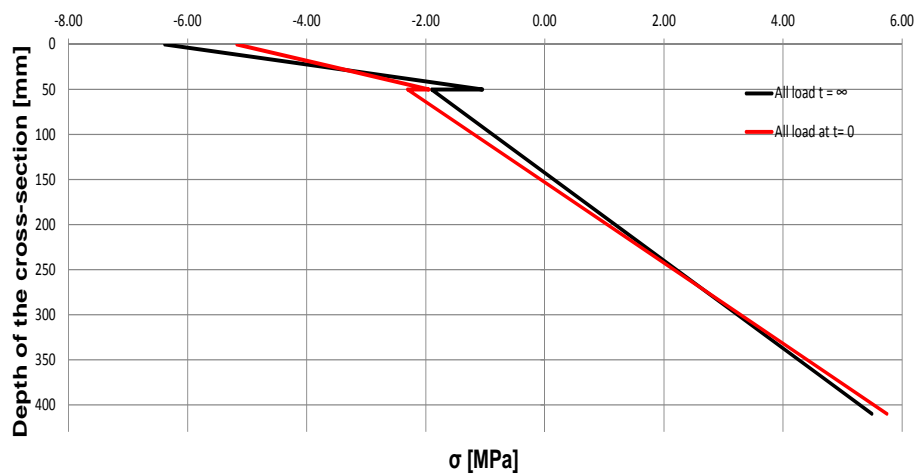


Figure 10.8: Comparison between the internal trend of stresses, for ultimate limit states at $t = 0$ and $t = \infty$.

10.6.2 Verifications of serviceability limit states

Serviceability limit states verifications provide the direct evaluation of the beam mid-span deflection and the checking of the vibrations. The value of the mid-span deflection has to be compared with appropriate limit values:

- Instantaneous mid-span deflection has to be less or equal to $l/400$ (18 mm);
- Net deflection at long-time has to be less or equal to $l/300$ (24 mm).

10.6.2.1 Mid-span deflection check at $t = 0$

The instantaneous mid-span deflection is evaluated on the basis of the characteristic SLS action combination. Conservatively it has been assumed a shear deflection equal to about 10% of the bending deflection. The mid-span deflection has been eventually evaluated by using the following expression:

$$w_{inst,t=0,SLS} = 1,1 \cdot \frac{5}{384} \cdot \frac{q_{SLS,characteristic} \cdot l^4}{EJ_{eff,t=0,SLS}} = 1,1 \cdot \frac{5}{384} \cdot \frac{2,70 \cdot 7200^4}{1,50 \times 10^{13}} = 7 \text{ mm}$$

$$w_{inst,t=0,SLS} = 7 \text{ mm} \leq \frac{l}{400} = 18 \text{ mm}$$

thus the previous check is satisfied.

10.6.2.2 Mid-span deflection check at $t = \infty$

The net final deflection is evaluated on the basis of the quasi-permanent load combination. Conservatively it has been assumed a shear deflection equal to about 10% of the bending action. The mid-span deflection has been eventually evaluated by using the following expression:

$$w_{net,t=\infty,SLS} = 1,1 \cdot \frac{5}{384} \cdot \frac{q_{SLS,quasi-permanent} \cdot l^4}{EJ_{eff,t=\infty,SLS}} = 1,1 \cdot \frac{5}{384} \cdot \frac{1,90 \cdot 7200^4}{1,09 \times 10^{13}} = 7 \text{ mm}$$

$$w_{net,t=\infty,SLS} = 7 \text{ mm} \leq \frac{l}{300} = 24 \text{ mm}$$

thus the previous check is satisfied.

10.6.2.3 Vibration check at $t = 0$

According to point 7.3 of standard reference [27], the fundamental frequency for residential floors has to be higher than 8 Hz. For the particular case of the stands it has been decided that the fundamental frequency has to be higher than 10 Hz. Subsequently, calculations for the vibrations check are reported using the same symbols given in Eurocode 5.

$$m = (22,95 \cdot 0,05 \cdot 0,800 + 2 \cdot 3,83 \cdot 0,115 \cdot 0,360) \cdot \frac{1000}{9,81} \cdot \frac{1}{0,800} = 157 \text{ kg/m}^2$$

$$(EJ)_l = \frac{EJ_{ef,t=0,SLS}}{b_1} = \frac{1,50 \times 10^{13}}{0,400} = 3,75 \times 10^7 \text{ Nm}^2/\text{m}$$

$$f_1 = \frac{\pi}{2 \cdot l^2} \cdot \sqrt{\frac{(EJ)_l}{m}} = \frac{\pi}{2 \cdot 7,2^2} \cdot \sqrt{\frac{3,75 \times 10^7}{157}} = 15 \text{ Hz} > 10 \text{ Hz}$$

$$(EJ)_b = E_{cm} \cdot \frac{h_1^3}{12} = 36210 \cdot \frac{50^3}{12} \cdot 10^{-3} = 3,77 \times 10^5 \text{ Nm}^2/\text{m}$$

$$\frac{w}{F} = \frac{l^3}{48 \cdot EJ_{ef,t=0,SLS}} = \frac{7,2^3}{48 \cdot 1,5 \times 10^{13}} \times 10^{12} = 0,52 \text{ mm/kN}$$

Entering with this value in Figure 10.9 it has been obtained the limit value $b = 150$.

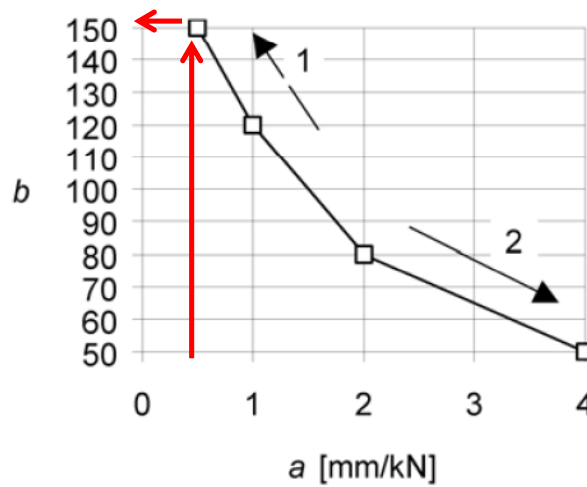


Figure 10.9: Recommended range of and relationship between a and b according to Eurocode 5.

$$b^{(f_1 \cdot \xi - 1)} = 150^{(15 \cdot 0,01 - 1)} = 1,41 \times 10^{-2}$$

where the recommended value for the modal damping ratio of residential floor is $\xi = 0,01$;

$$\eta_{40} = \left\{ \left(\left(\frac{40}{f_1} \right)^2 - 1 \right) \cdot \left(\frac{i}{l} \right)^4 \cdot \frac{EJ_l}{EJ_b} \right\}^{0,25} = \left\{ \left(\left(\frac{40}{15} \right)^2 - 1 \right) \cdot \left(\frac{0,400}{7,200} \right)^4 \cdot \frac{3,75 \times 10^7}{3,55 \times 10^5} \right\}^{0,25} = 0,28$$

$$v = \frac{4 \cdot (0,4 + 0,6 \cdot \eta_{40})}{m \cdot b \cdot l + 200} = \frac{4 \cdot (0,4 + 0,6 \cdot 0,28)}{157 \cdot 0,4 \cdot 7,2 + 200} = 3,48 \times 10^{-3}$$

By substituting the values it can be seen below that the system is verified also with respect to the vibration

$$v = 3,48 \times 10^{-3} < b^{(f_1 \cdot \xi - 1)} = 1,41 \times 10^{-2}$$

10.6.2.4 Vibration check at $t = \infty$

According to point 7.3 of standard reference [27], vibration check for long-term has been done and following reported:

$$m = (22,95 \cdot 0,05 \cdot 0,800 + 2 \cdot 3,83 \cdot 0,115 \cdot 0,360) \cdot \frac{1000}{9,81} \cdot \frac{1}{0,800} = 157 \text{ kg/m}^2$$

$$(EJ)_l = \frac{EJ_{ef,t=0,SL5}}{b_1} = \frac{1,09 \times 10^{13}}{0,400} = 2,73 \times 10^7 \text{ Nm}^2/\text{m}$$

$$f_1 = \frac{\pi}{2 \cdot l^2} \cdot \sqrt{\frac{(EJ)_l}{m}} = \frac{\pi}{2 \cdot 7,2^2} \cdot \sqrt{\frac{2,73 \times 10^7}{157}} = 13 \text{ Hz} > 10 \text{ Hz}$$

$$(EJ)_b = E_{cm} \cdot \frac{h_1^3}{12} = 36210 \cdot \frac{50^3}{12} \cdot 10^{-3} = 3,77 \times 10^5 \text{ Nm}^2/\text{m}$$

$$\frac{w}{F} = \frac{l^3}{48 \cdot EJ_{ef,t=0,SL5}} = \frac{7,2^3}{48 \cdot 1,09 \times 10^{13}} \times 10^{12} = 0,71 \text{ mm/kN}$$

Entering with this value in Figure 10.10 it has been obtained the limit value $b = 140$.

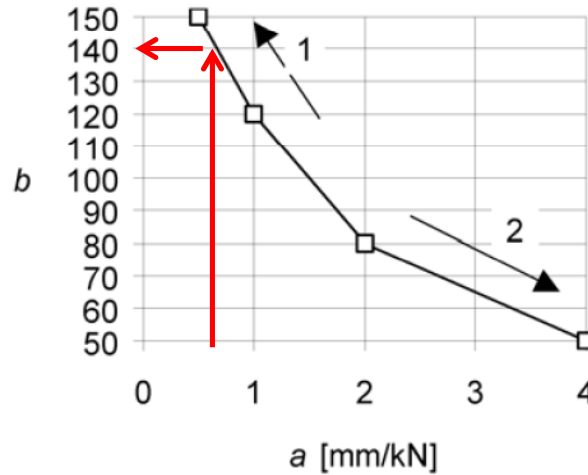


Figure 10.10: Recommended range of and relationship between a and b according to Eurocode 5.

$$b^{(f_1 \cdot \xi - 1)} = 140^{(13 \cdot 0,01 - 1)} = 1,36 \times 10^{-2}$$

where the recommended value for the modal damping ratio of residential floor is $\xi = 0,01$;

$$\eta_{40} = \left\{ \left(\left(\frac{40}{f_1} \right)^2 - 1 \right) \cdot \left(\frac{l}{i} \right)^4 \cdot \frac{EJ_l}{EJ_b} \right\}^{0,25} = \left\{ \left(\left(\frac{40}{13} \right)^2 - 1 \right) \cdot \left(\frac{0,400}{7,200} \right)^4 \cdot \frac{2,73 \times 10^7}{3,55 \times 10^5} \right\}^{0,25} = 0,28$$

$$v = \frac{4 \cdot (0,4 + 0,6 \cdot \eta_{40})}{m \cdot b \cdot l + 200} = \frac{4 \cdot (0,4 + 0,6 \cdot 0,28)}{157 \cdot 0,4 \cdot 7,2 + 200} = 3,48 \times 10^{-3}$$

By substituting the values it can be seen below that the system is verified also with respect to the vibration

$$v = 3,48 \times 10^{-3} < b^{(f_1 \cdot \xi - 1)} = 1,36 \times 10^{-2}$$

Bibliography

- [1] Lukaszewska E. (2009). *Development of Prefabricated Timber- Concrete Composite Floors*. PhD thesis, Luleå University of Technology.
- [2] Lukaszewska E. Johnsson H. Fragiacomio M. (2008), *Performance of connections for prefabricated timber-concrete composite floors*. Materials and Structures RILEM.
- [3] Lukaszewska E. Johnsson H. Stehn L. (2006), *Connections for Prefabricated Timber-Concrete Composite Systems*, Luleå University of Technology.
- [4] Crocetti R. Sartori T. Flansbjer M. (2010), *Timber-Concrete Composite Structures with Prefabricated FRC Slab*. WCTE.
- [5] Bathon L. A. and Graf. M. (2000), *A continuous wood-concrete-composite system*. In: Proc. World Conference of Timber Engineering. Whistler, BC, Canada, University of British Columbia, Vancouver, BC, Canada.
- [6] Gutkowski R., Brown K., Shigidi A. and Natterer J. (2008), *Laboratory tests of composite wood-concrete beams*. Construction and Building Materials, Elsevier.
- [7] Piazza M. and Ballerini M. (2000). *Experimental and numerical results on timber-concrete composite floors with different connection systems*. 6th World Conference on Timber Engineering WCTE 2000, Whistler Resort, British Columbia, Canada.
- [8] Ballerini M., Crocetti R. and Piazza M. (2002). An experimental investigation of notched connections for timber-concrete composite structures. 7th World Conference on Timber Engineering WCTE 2002, Shah Alam, Malaysia.
- [9] Clouston P., Civjan S. and Bathon L. A. (2004). *Experimental behavior of a continuous metal connector for a wood-concrete composite system*. Forest Products Journal.
- [10] Clouston P. and Schreyer A (2006). *Wood-concrete composites: A structurally efficient material option*. Civil Engineering Practice.

- [11] Costa L. (2011), *Timber-concrete composite floors with prefabricated FRC*. Master thesis, Lund University.
- [12] Piazza M. Tomasi R. Modena R. (2005). *Strutture in Legno*. Materiale, calcolo e progetto secondo le nuove normative europee. Ulrico Hoepli Editore, Milano.
- [13] Möhler K. (1956). *Über das Tragverhalten von Biergerträgern und Druckstäben mit zusammengesetzten Querschnitten und nachgiebigen Verbindungsmitteln*. Habilitation, Technische Universität Karlsruhe, Germany.
- [14] Newmark N. M., Siess C. P. and Viest I. M. (1951). *Test and analysis of composite beams with incomplete interaction*. Proc., Society for Experimental Stress Analysis.
- [15] Piazza M. (2007), *Solai composti Approcci normativi, esperienze di ricerca*. CISM - Corso National Advanced Professional Training. Problematiche Avanzate nella Progettazione delle Strutture Lignee, Udine.
- [16] Blass H.J. (1995), *Mechanically jointed beams and columns*, Lecture B11 Timber Engineering, Step 1, STEP/Eurofortech, Centrum Hout, Almere.
- [17] Ceccotti A. (2002). *Composite concrete-timber structures*. Prog. Struct. Engng Mater. 2002. IUAV Univeristy, Venice.
- [18] Ceccotti A. (1995). *Timber-concrete composite structures*. Timber Engineering-STEP 2
- [19] Ceccotti A., Fragiaco M. and Giordano S. (2007). *Long-term and collapse tests on a timber-concrete composite beam with glued-in connection*. Material and Structures.
- [20] Fragiaco M. and Ceccotti A. (2006). *Simplified approach for the long-term behavior of timber-concrete composite beams according to the Eurocode 5 provisions*. 39th Meeting of the Working Commission W18 - Timber Structures, CIB, International Council of Research and Innovation, Florence.
- [21] Schänzlin J. and Kuhlmann U. (2004). *Time dependent behavior of timber-concrete composite structures*. 8th World Conference on Timber Engineering, Lathi, Finland.
- [22] Computers&Structures inc. (2007), *CSI Analysis Reference Manual for SAP2000*. University Avenue Berkeley, California USA.
- [23] Natterer Johannes Weinand Yves. *Modelling of multi-layer beam with inter-layer slips*. Laboratory for timber constructions IBIOS, Ecole Polytechnique fédérale de Lausanne, EPFL, Lausanne, Switzerland.

- [24] Ceccotti A. (2002), *Composite concrete-timber structures*. IUAV University, Venice.
- [25] Kavaliauskas, S., Kvedaras, A. K. and Valiunas, B. (2007). *Mechanical behavior of timber-to-concrete connections with inclined screws*. Journal of Civil Engineering and Management.
- [26] Teng T.L. Chu Y. A. Chang F. A Chin H. S. (2004). *Calculating the elastic moduli of steel-fiber reinforced concrete using a dedicated formula*. Computational Materials Science, Elsevier, Taiwan

Standard references

- [27] Comité Européen de Normalisation (1995-1-1:2009) Eurocode 5. *Design of timber structures. Part 1-1: General-Common rules and rules for buildings*. Brussels (B): CEN
- [28] UNI EN 26891:1991 *Timber structures. Joints made with mechanical fasteners. General principles for the determination of strength and deformation characteristics*. CEN, Brussels
- [29] Comité Européen de Normalisation (1990:2006) Eurocode 0. *Basic of structural design*. Brussels (B): CEN
- [30] Comité Européen de Normalisation (1991:2004) Eurocode 1. *Actions on structures. Part 1-1. General actions - Densities, self-weight, imposed load for buildings*. Brussels (B): CEN
- [31] prEN 14081:2011 *Timber structures - Glued laminated timber and glued solid timber - Requirements*. Brussels (B): CEN
- [32] Comité Européen de Normalisation (1992:2005) Eurocode 2. *Design of concrete structures. Part 1-1. General rules and rules for buildings*. Brussels (B): CEN
- [33] UNI EN 408:2004 *Structural timber and glued laminated timber. Determination of some physical and mechanical properties*. Brussels (B): CEN